Supported Engineered Extracellular Matrices for 3D Cell Culture

by

Stacy Ramcharan

A dissertation submitted in partial fulfillment
of the requirements for the degree of
Doctor of Philosophy
(Chemical Engineering)
in the University of Michigan
2017

Doctoral Committee:

Professor Joerg Lahann, Chair
Professor Ronald G. Larson
Associate Professor Gary D. Luker
Associate Professor Sunitha Nagrath

Stacy Ramcharan

stacyram@umich.edu

ORCID iD: 0000-0001-6509-8158

To my mother,

whose sacrifice was greater than most

Acknowledgements

God. There is no greater acknowledgement to make but to the man upstairs himself. Amongst the list of many other challenges, He has brought me to and through the challenge of graduate studies in, of all disciplines, engineering. He is the reason why, the know-how, the rationale, the capability. By His strength and not by my own have I made it this far, up out of a situation that could have resulted in an unhappy ending, and into a realm of endless joy wrapped in His favor. Where I am the vessel, He is the captain, and I can only ask that any intellect or skillsets I've gained be channeled to do His work in this kingdom He's created on Earth.

My mother. From the early days of frequent trips to the library, to showing me the most efficient order in which to complete homework assignments, and now to making sure I don't go hungry in graduate school, my mother has been behind the scenes, orchestrating through her efforts and prayer the series of successes my life has been. She has remained committed to ensuring her children receive the best available, despite any unfavorable circumstances or sacrifices necessary. I know she sees my life as a manifestation of the opportunities she didn't have for herself, and I hope and pray that God would always enable me to give her the best now that I am for the first time, entering the workforce, and not continuing on as a student.

Professor Joerg Lahann. Coming into graduate school you hear all sorts of wild stories of PhD advisors. Deciding which lab to commit to and which advisor to work for can be a nerve-wrecking process as a first-year graduate student. In my case, I was blessed to have secured two

sources of funding, which I must also acknowledge: the National Science Foundation Graduate Research Fellowship, and the Rackham Merit Fellowship. Having this funding meant I could choose virtually any advisor in the department, and even professors outside of the department had invited me to work for them. After much debate, I decided to go with the Lahann Lab, which believe it or not, I had originally crossed off my list! Today, I can easily say that I could not have made a better decision. Working in the Lahann Lab and with Prof. Lahann has certainly crafted me into who I am today, both technically and non-technically. I feel that I was one of those lucky cases, where a student joins a lab or a project at an opportune time. I truly believe in the commercialization potential of the cell culture system we've developed and I thank Prof. Lahann for placing me on this team from the very beginning. I'm further grateful for his guidance through these years, practical suggestions in group meetings, allowing me to observe his techniques in technical writing, and constructive criticism. Still, beyond this, Prof. Lahann and my experience working in his lab has shaped my mentality and work ethic, taught me professionalism and prioritization, and given me plenty of opportunities to develop basic management skills.

Additionally, the Lahann Lab would not have been the same environment without the people I've met there. When I first joined, I would not have thrived without the advice and mentorship of the Lahann Lab powerhouses, Jaewon Yoon, Asish Misra, Xiaopei Deng, Kenneth Cheng, Sahar Rahmani, and Jake Jordahl. Sahar soon after became more than a colleague, but a dear friend. I can't thank Jake enough, being the main source of training when I joined the lab, and the sole resource on the Lahann Lab 3D jet writing technology. His guidance in the day-to-day lab work quickly enabled me to establish my own research rhythm, and his friendship has developed into a lifelong relationship. After an extravagant proposal, I said yes at the same lab bench where we first met when our professor introduced us five years ago. And I can't begin to acknowledge

Ramya Kumar. There's nothing like starting in a new lab together and working through five years of tears and joys in the journey towards the PhD to produce a best friend. The dynamic of the Lahann Lab incorporates visiting scholars or Masters students, which means the addition of lab members who become friends, but have to leave after only a short period of time. People of note are Hyesun Jun, Kathleen McEnnis, Gokcen Ukuser, Christopher Dunlay, and Ben Neugirg whose friendship and acquaintance will last beyond our shared times in the lab. More recently, the lab has enjoyed the addition of Luis Solorio, Jason Gregory, Stephie Christau, Nahal Habibi, Dylan Neale, and Ayse Muniz. Luis will always be known for expanding the application of our scaffold technology to the cancer space. Jason has brought a good dose of experience and common sense to our lab, and is to be admired for his focus and hard work being both a PhD student and a father of three. Stephie and Nahal have surely made the work environment a happier place, with their boot camp work ethic, and bright smiling faces. I must acknowledge Nahal as more than a lab and office mate, but a companion in my last year here and someone who has repeatedly expressed how much I will be missed. With Dylan and Ayse, our 3D cell culture technology is in good hands. They are both wonderful, capable people, and I am confident that they will continue the work that was started by Jake, Luis, and myself to new applications, cell characterization methods, further validation, and perhaps even push our protein networks towards its commercialization potential. Finally, I must acknowledge the undergraduate students who have helped carry the research to where it is today. Of note are Clark Teeple, Jeffery Noble, and Robert Stinson, who are fairly representative of the beginning, middle, and end of the five-year stretch of my PhD.

I can't end without thanking the many professors who have given their time and dedication to help me get where I am going. Firstly, my PhD committee: Prof. Ron Larson who made fluids class a most entertaining and mind-blowing experience, and whose intuition on molecular-level

phenomena and the complementary nature of science and Christianity is something to aspire towards. Prof. Sunitha Nagrath, whose lab was my first research collaboration in manufacturing microfluidic devices, is always a joy to chat with in the hallways of the NCRC, and is to be admired for her expertise in the cancer space given the breadth of her technical background in chemical, mechanical, and nuclear engineering. She is pure evidence of the interdisciplinary nature of engineering today and demonstrates to me that a career path can take on surprising directions over time. Prof. Gary Luker, whose lab felt like a second home, has been one of our closest collaborators for applications of our 3D cell culture system to cancer. His approach to an academic career is one that had me considering the career path well into my fourth year. I am moved by the example set by Drs. Gary and Kathy Luker and consider them both role models for my own life ahead. Secondly, a number of other outstanding individuals who have extensively supported me along the way: Professors Phil Savage, who was my first research advisor at Michigan, Lola Eniola-Adefeso, who I've consulted for advice and worked under while GSI'ing the course CHE 230, Mark Burns who has taken time to meet with me one-on-one despite his busy schedule as department chair and many others including Bob Ziff, Jingsang Kim, Nick Kotov, Nina Lin, and Susan Montgomery.

Furthermore, as a PhD student and a mini-employee of the university, it takes more than the professors to get the day-to-day work done. I must also acknowledge the hard work of those behind the scenes who keep things running as a well-oiled machine: Julie Gales, Karl Olsen, and Lisa Moran of the Biointerfaces Institute, and Rhonda Jent, Susan Hamlin, Kelly Raickovich, and Mary Beth Westin of the chemical engineering department. Whether it was processing a payment, shipping a package, or getting maintenance work done in the lab, the instances are countless where these key people effectively got things done and got the show on the road.

Finally, although it would take a whole other chapter to do justice to my NCRC friends and supporters who at the very least made my days brighter, I can't end this acknowledgements section without at least mention of a few names: Caymen Novak, Lianette Rivera, Mohit Nahata, Tugba Topal, Paul Dodd, Jeff Lowe, Nina Gasbarro, Kaitlyn Mallett, Ramdane Harouaka, Yasmine Doleyres, Joseph Bazzill, Eric, Jai and Nissa Holt, Molly Kozminsky, Johanna Heureaux, Tao Wei, Catherine Snyder, Liang Zhang, Gleiciani de Queiros Silveira, Kari Nieto, Ana Rioja, Joong Hwan Bahng, Esmeralda Hernandez, Aresha Martinez-Cardoso, Kyle Huston, Karlo Malaga, and all the geese and groundhogs of the NCRC.

Many people compare the journey towards the PhD to running a marathon, and I certainly agree with the analogy. But more than reaching a series of targets, the PhD experience to me, was a development and maturation process. As an incoming first year, you are eager and innocent, like a wildflower ready to take on any adventure as its seed travels in the wind. Slowly you take root and learn to carry on through the four seasons so you can bloom again the next year. You begin to separate wants and needs, get a taste of reality, and learn about yourself and what is most important to you. I thank the people who I have encountered along the way. Every relationship has been a gift, a lesson on someone else's perspective, a recount of an experience to learn something from. By the end of the PhD, you are more like a wilted rose, matured and developed, made to be useful, and thoroughly exhausted. Still there is life in you that is ready to bloom again in fresh soil as you are now as prepared as ever to take on the next journey. I'd like to end on acknowledging the PhD itself for teaching me who I am and who I want to be.

Table of Contents

Chapter 5: Summary and Future Directions

List of Tables

List of Figures

scale view of AT-3 tissue cultured three days on supported ecFn as in *a*. Cells proliferate and fill the 3D space within the protein network across the scaffold. Scale bar 500 μm. (a-b) Channels: cyan, cell nucleus; red, actin. (c) Bioluminescence image of immune-competent mice showing tumor formation 21 days after AT-3 cells were orthotopically implanted (image exposure time 10 seconds). The two mice on the left have had about 30,000 AT-3 cells on supported ecFn implanted into the mammary fat pads indicated by arrows (group 1). The right mammary fat pad received an injection of approximately the same number of cells in the area indicated by circles (group 2). The third mouse on the right is a positive control having received the group 3 supported ecFn in the left mammary fat pad (arrow), and the group 4 injection in the mammary fat pad on the right, each delivering 200,000 AT-3 cells. Previous studies have concluded that a minimum of 200,000 AT-3 cells are required for tumor formation by cell injection[5]. (d) Mason's Trichrome staining of a tumor graft that formed after 21 days at the implant site of the group 1 30,000 AT-3 cells on supported ecFn; AT-3 cells invaded surrounding tissues. Scale bar: 25 μm. (e) Quantification of the $CD29^+/CD24^+$ cells identifying the AT-3 population capable of self-renewal. Cells were cultured three days on TCPS, TCPS with fibronectin conformally adsorbed (Fn on TCPS), or supported ecFn. Single star indicates that the supported ecFn result is statistically different from TCPS and Fn on TCPS; double star indicates that TCPS and Fn on TCPS are statistically similar. $P<0.05$ (f) Quantification of the $CD29^+/CD24^+/CD90.2^+$ AT-3 cells identifying the tumor initiating population after three days of culture on TCPS, TCPS with fibronectin conformally adsorbed (Fn on TCPS), and supported ecFn. Single star indicates that the supported ecFn is statistically different from TCPS and Fn on TCPS; double star indicates that TCPS and Fn on TCPS are statistically similar. *Credits:* The Luker Lab at the University of Michigan conducted all animal studies, and designed and contributed AT-3 cells to this collaboration. Flow cytometry done in the Wicha Lab at the University of Michigan..... 115

Figure 4-2: Supported ecFn promotes a tumorigenic phenotype in AT-3 mouse breast cancer cells (a) LSCM of AT-3 mouse breast cancer cells at the crosshair of the scaffold microfibers after three days of culture on supported ecFn. (b) LSCM image after three days of culture showing *(left)* top view and *(right)* side view of the AT-3s forming multicellular structures as they span up into the open pore of the supported ecFn scaffold. (a-b) Channels: blue, polymer support; cyan, cell nucleus; red, actin. Scale bars 25 μm. (c) Growth curve for AT-3 cells cultured on TCPS (dotted line, criss-cross marker) or supported ecFn (solid line, square marker). (d) Quantification of the $CD90.2^+$ population of AT-3 cells after three days of culture on TCPS, fibronectin conformally coated on TCPS (FN on TCPS), or supported ecFn. Single star indicates that the ecFn network result is statistically different from TCPS and FN on TCPS; double star indicates that TCPS and FN on TCPS results are statistically similar. $P<0.05$ *Credits:* The Luker Lab at the University of Michigan conducted all animal studies, and designed and contributed AT-3 cells to this collaboration. Flow cytometry done in the Wicha Lab at the University of Michigan..... 117

Figure 4-3: Supported ecFn shows successful tumor engraftment in AT-3 mouse breast cancer model throughout the course of three weeks Bioluminescence image of immune-competent mice two, seven, and 21 days after orthotopic implantation of AT-3 cells. Four groups were examined: (1) 30,000 cells on three-millimeter-wide supported ecFn disks (2) 30,000 cells directly injected (3) 200,000 cells on a supported ecFn disk and (4) 200,000 cells directly injected as a positive control being the minimum number of cells required for tumor formation by direct injection[5]. The two mice on the left have group 1 in the left mammary fat pad as indicated by

List of Appendices

Abstract

In the current shift away from 2D tissue culture polystyrene and towards 3D cell culture models, several important design criteria have yet to be considered: (1) provision of large open areas where cells can create their own niche (2) fabrication of a scaffold that is chemically and mechanically tunable and (3) presentation of proteins that mimic native extracellular matrix (ECM). Polymer scaffolds fabricated by 3D jet writing provide extensive void space for maximum cell-cell and cell-ECM interactions. This work expands on such electrospinning technologies to establish a micromanufacturing process that modulates the flow of various polymer solutions through a manifold. The resulting scaffolds contain spatially distinct domains that can be customized to exhibit specific bulk or surface properties. Such tunability is not limited to the synthetic design space. We have discovered that hydrodynamically induced fibrillogenesis can yield remarkably stable networks of protein fibrils suspended across a support or scaffold that recapitulate important structural and functional hallmarks of cell-secreted ECM. These engineered networks of fibronectin serve as a breast cancer microenvironment, making it possible to culture an unfractionated patient sample (n=14), where less than 5% are cancer cells, into a self-selected composition of differentiated cancer cells, stem-like cancer cells, and various stromal cells. An average of 40% increase in the tumor-initiating population and at least a 7-fold increase in the cancer cell population was observed after six days (n=3). This user-defined 3D cell culture platform will enable investigation into the bidirectional relationship between cells and the ECM, not just for breast cancer but a variety of diseased or healthy tissue types.

Chapter 1
The Complete Design Space of 3D Cell Culture

1.1 The problem at hand

In both healthy and pathological states, cell behavior is dictated by chemical and mechanical cues that are derived from soluble signals, and cell-cell or cell-extracellular matrix (ECM) interactions[1, 6-9] as shown in **Figure 1-1**. Physiologically, cells actively remodel the ECM: breaking down existing and secreting new proteins, or changing protein conformation to alter the biological activity of the protein[6]. Fibronectin (Fn), for example, exposes different binding sites as it is restructured from a soluble state (plasma fibronectin or pFn) to an extended fibrillar conformation (cellular fibronectin, or cFn)[3, 10-14]. Furthermore, different tissues and diseased states are characterized by specific ECM compositions[7, 15]. For instance, laminin is primarily found in basement membranes whereas mesenchymal tissues are largely composed of fibronectin[9]. In the case of breast cancer, primary tumors are largely composed of collagen[16], whereas fibronectin has been identified as a major constituent of the pre-metastatic niche[17].

Tissue engineering and 3D cell culture relies on the structural support of a biocompatible scaffold on which cells are grown *in vitro*. The scaffold acts as the ECM otherwise would *in vivo*[1, 8, 18-20]. Given that cells sense and respond to their local environment, the performance of the scaffold is closely correlated with how well it mimics physiological conditions in regards to composition, architecture, protein conformation and mechanical properties[19, 21-23]. For instance, drug response has been shown to be a function of dimensionality, where cells are more sensitive

on 2D than 3D environments[24]. Yet, much of biological research is still conducted on flat polymeric surfaces such as tissue culture polystyrene (TCPS), or proteinaceous mediums such as

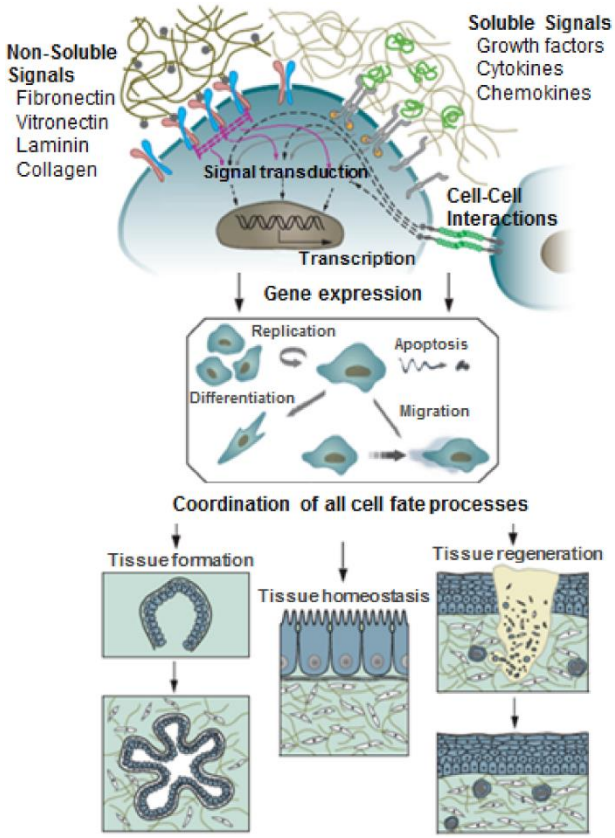

Figure 1-1: Extrinsic factors modulate cell behavior *in vivo* Cells interact with their native environment through soluble and non-soluble signals, and cell-cell interactions. These interactions drive the gene expression that dictates how the cell will behave and ultimate the fate of the cell. Of the various environmental cues, cells rely on the structural environment or extracellular matrix (ECM) for a supply of non-soluble signals. In parallel, when designing an *in vitro* cell culture scaffold, of the various environmental cues, the scaffold is responsible for providing non-soluble signals by presenting proteins in an ECM-like fashion. [Illustration adapted from Lutolf *et al.*[1]]

Matrigel that fail to recapitulate the structure and function of the native cell niche. Poor *in vitro* representations of the environment a cell would encounter *in vivo* can induce an artificial cell response that does not portray how the cell would respond to the same stimulus if in its native cell niche[24, 25]. This can greatly hinder efforts to understand and treat many diseases such as cancer metastasis, where not only the phenotype of the cell, but also the conditions of the microenvironment are what drive tumor cells to home in at a particular site for secondary tumor

formation[16, 26-31]. The need for a scaffold that mimics the structure and function of actual ECM is urgent given the extent of today's biological research and efforts to engineer functioning tissues *in vitro*[24, 32].

Of equal importance when designing a scaffold for research is how well the technology will "drop-in" or readily replace current cell culture models to enable quick and widespread adoption. An ideal culture system will be versatile in regards to compatibility with a diversity of cell types[33], offer a means to independently investigate the effects of different environmental parameters including ECM composition[8, 18] and how cells are remodeling the ECM[19], while remaining amenable to standard culture and characterization techniques[19, 24]. Meeting this need calls for a system with independently tunable processing parameters that can produce a scaffold customized for its intended use. Researchers would select from a library of parameters that include geometries, materials, or ECM protein compositions for the manufacture of scaffolds outfitted to represent various permutations of environmental properties. This ability to decouple otherwise interconnected properties would allow researchers to run the controlled experiments needed to tease out the effect of a specific stimulus on cell response, or design and engineer specific tissues.

1.2 State of the art

Current 3D culture models such as electrospun mats[34] rely on polymeric mimics of ECM that lack the cell binding motifs or proteolytic susceptibility of actual proteins, and allow cells little to no open area for migration[19], endogenous protein secretion[35], or formation of higher-order multicellular structures[1]. Randomly oriented fibers do not allow control of pore size, and pores can be as small as a few microns to nanometers which hinders cell infiltration[22, 35]. Even aligned electrospun fibers are limited in control of pore size and geometry[35]. Another approach is to culture cells in spheroids[8, 36] or within a hydrogel[19, 37], which can be made from common ECM proteins

such as fibrin, collagen or basement membrane extract gels[22] ensuring material biocompatibility and providing cell binding sites. However, integration of cell-secreted protein and cell migration in hydrogels and spheroids are mass transport limited[1]. Hydrogels also offer little to no spatial control of chemical moieties and lack a defined architecture, which in conjunction to being largely composed of water results in poor mechanical properties[38], scalability, and handleability[16]. Systems isolated from animal models or cell feeder layers[1, 19] and decellularized matrices[18] are frequently used. While these products are actual isolated ECMs, they give researchers few independent variables[18], are plagued by a poorly-defined biochemical composition, and may introduce xenogenic or viral contamination[1, 19]. Such batch-to-batch variability and the presence of unidentified factors are particularly disadvantageous when working with cells that are highly sensitive to their environment such as stem cells[39].

Thus, there remains a clear need to design and demonstrate the successful use of a scaffold that: (1) is reproducible, chemically defined, and xenograft-free (2) uses whole proteins that provide binding sites for cell adhesion and are susceptible to proteolysis (3) has an architecture similar to the native cell niche (4) allows cells to secrete endogenous protein and remodel the ECM (5) offers independent definition and customization of environmental parameters (6) allows spatial control of chemical and mechanical properties (7) has a large open area to maximize cell interactions with other cells and ECM proteins, while minimizing cell and protein contact with synthetic material in order to preserve cell phenotype and protein conformation (8) is highly porous with tunable geometries and support of favorable transport properties and (9) is amenable to handling, imaging, and standard cell culture and characterization techniques[1, 19, 21, 22, 40-46].

1.3 A composite solution

Engineering an ECM *in vitro* requires use of whole proteins as opposed to peptides or specific binding sequences. The architecture and protein conformation and composition must be tuned to accurately recapitulate the structure and function of native ECM. At the same time, the ECM protein should be distributed in a way that facilitates cell infiltration, transport of oxygen and nutrients to the cells, and waste products away from the cells[19, 40, 47]. To ensure quick adoption of an engineered ECM into regular practice, it must maintain mechanical integrity at physiological temperatures despite forces exerted by cells,[46] physical handling, or fluid convection in non-static cultures.[19] The solution to meeting these requirements simultaneously is a material composed of both biological elements (ECM proteins) and a rigid scaffold that provides skeletal support to the protein matrix. Biodegradable polymers are an excellent material choice for such a scaffold, offering mechanical stability while ensuring biocompatibility and implantability should the engineered ECM mimic find application in *in vivo* studies or regenerative medicine[6, 19].

Still, fabricating a material that exhibits all the required properties using biological proteins and biodegradable polymers may appear a daunting task. How does one ensure the ECM mimic can be adequately tuned to represent the cell microenvironment of diverse tissue types including skin, muscle, cartilage and bone? Rather than designing a new ECM mimic for each tissue type and experimental study, as has been the current trend in the literature, this study establishes a system for the custom manufacture of a supported engineered ECM (eECM). Instead of designing a single material to meet each of the individual properties outlined in Section 1.2, geometry, material placement, and ECM protein composition will be set during manufacture to produce scaffolds with the chemical and mechanical properties of the cell niche of interest **(Fig. 1-2)**. The first part of the micromanufacturing system is the polymeric skeletal support or scaffold, which

through geometric control, offers a high porosity to facilitate transport, and a tunable mechanical environment. The choice of scaffold can vary, however, in this study 3D jet writing scaffolds[48] were selected not only for precise geometric control, but also for the high percentage of open area, or the ratio of the volume of void space within the scaffold to the volume of the entire scaffold.

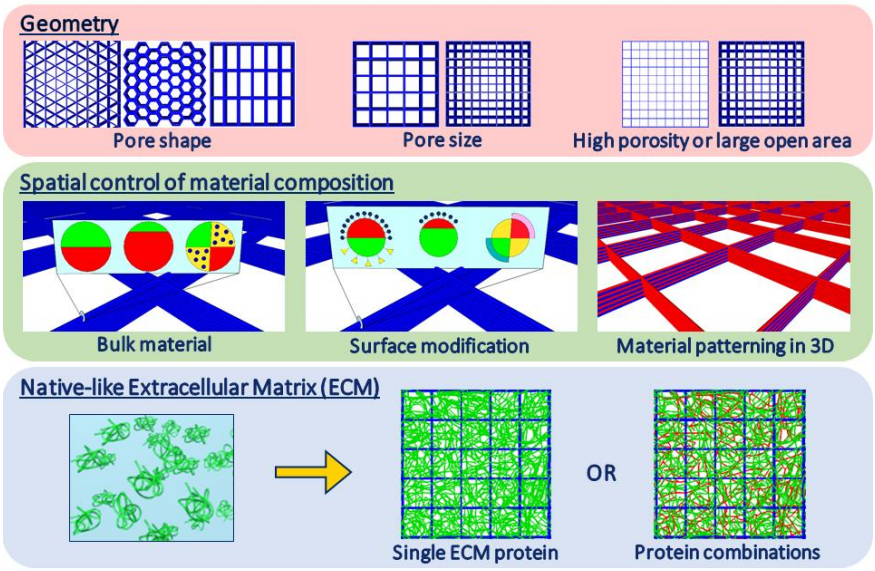

Figure 1-2: Manufacture of a supported engineered extracellular matrix (eECM) via three main manufacturing capabilities A supported eECM is comprised of a porous polymeric scaffold and a network of ECM protein. Three major manufacturing capabilities allow for customization of this 3D cell culture model such that it exhibits features specific for its intended use. Here, the 3D jet writing process is used to fabricate 3D microfiber constructs with tunable pore shape and size. These scaffolds maintain mechanical integrity despite handling in dry or wet conditions while being composed of only ~4% material by volume, leaving the remainder of the volume as void space otherwise referred to as open area. Second is the spatial control of material composition which can be varied across the polymer scaffold in three-dimensional coordinate space. In addition to bulk material, changes in composition include surface functionalities for subsequent chemistries, or embedding of drugs or biomolecules for release. Third is the free suspension of a network of ECM proteins across and within the pores of the polymer scaffold. Proteins fill the open area of the scaffold, limiting contact with the synthetic material surface in effort to preserve protein conformation.

The second part of the micromanufacturing system creates the ability to (1) independently vary one property of the polymer scaffold via bulk or surface composition at a time to observe how one specific change affects cell behavior in a controlled experiment and (2) pattern domains of distinct chemical compositions throughout the polymer scaffold in 3D space. With this development, 3D

jet writing scaffolds will be able to present bulk materials or composites, tethered ligands, or surface functionalities in a spatially selective manner, which can all be used to direct cell behavior much like soluble signaling *in vivo*[6, 7, 19, 49]. The third part of the micromanufacturing process suspends stable bridges of a single or combination of ECM proteins across and within the open pores of the polymer scaffold. This supported eECM serves as an *in vitro* microenvironment where cells are free to create their own cell niche with minimal interference from synthetic material by remodeling or secreting ECM proteins, and forming higher-order multicellular structures such as clusters, ducts or lumens.

The overall goal of this micromanufacturing system is the fabrication of *in vitro* cell microenvironments where the protein composition, cell density and type, polymer scaffold geometry, pore size, pore shape, and three-dimensional distribution of distinct materials are all user-defined parameters. The number of possible permutations of these parameters enable the supported eECM to be tuned to probe specific research questions regarding cell response to a certain stimulus, or to model nearly any *in vivo* cell microenvironment, assuming the defining features of the physiological environment are known. Perhaps in future, this system or variations thereof will be adopted into mainstream cell cultures as a vast improvement over the ubiquitous petri dish.

1.4 Specific aims of this study

This work aims to establish a micromanufacturing system for expansion of the current scaffold design space and suspension of protein networks across scaffolds as a 3D cell culture environment for both *in vitro* and *in vivo* use. In application, the supported eECM serves as a breast cancer niche to observe shifts in cell populations expressing a certain phenotype and for the expansion of primary human cells obtained from breast cancer patients. These three specific aims are illustrated in **Figure 1-3**. Aim 1 focuses on further

development of the synthetic scaffold comprising the supported eECM. Building on previously existing technologies, electrospinning, electrohydrodynamic co-jetting, and 3D jet writing, the addition of a "micro-manifold" allows complete control of the relative amount of each material confined within a single microfiber. Said microfibers are the building blocks for the 3D scaffolds that provide a skeletal support for the suspension of the eECM networks developed in Aim 2. With the manifold, these 3D jet writing scaffolds may now be manufactured with distinct domains controllably localized within the construct. In Aim 2, a process is developed for converting solubilized protein into stable fibrillar networks tethered across the polymer scaffold with a major emphasis on fibronectin. The fibronectin protein network is then shown to be in a bioactive conformation that mimics that of fibronectin secreted by cells, termed cellular fibronectin or cFn. Finally, Aim 3 takes advantage of the supported engineered cFn (ecFn) to expand primary breast cancer cells which are typically difficult to grow *in vitro* and to demonstrate the potential for supported ecFn to promote tumor graft formation. Beyond demonstrating a superior functionality of the scaffold manufactured via Aims 1 and 2, Aim 3 is largely motivated by the continuing need for more physiologically relevant tumor samples for drug screening, and the future promise of precision medicine.

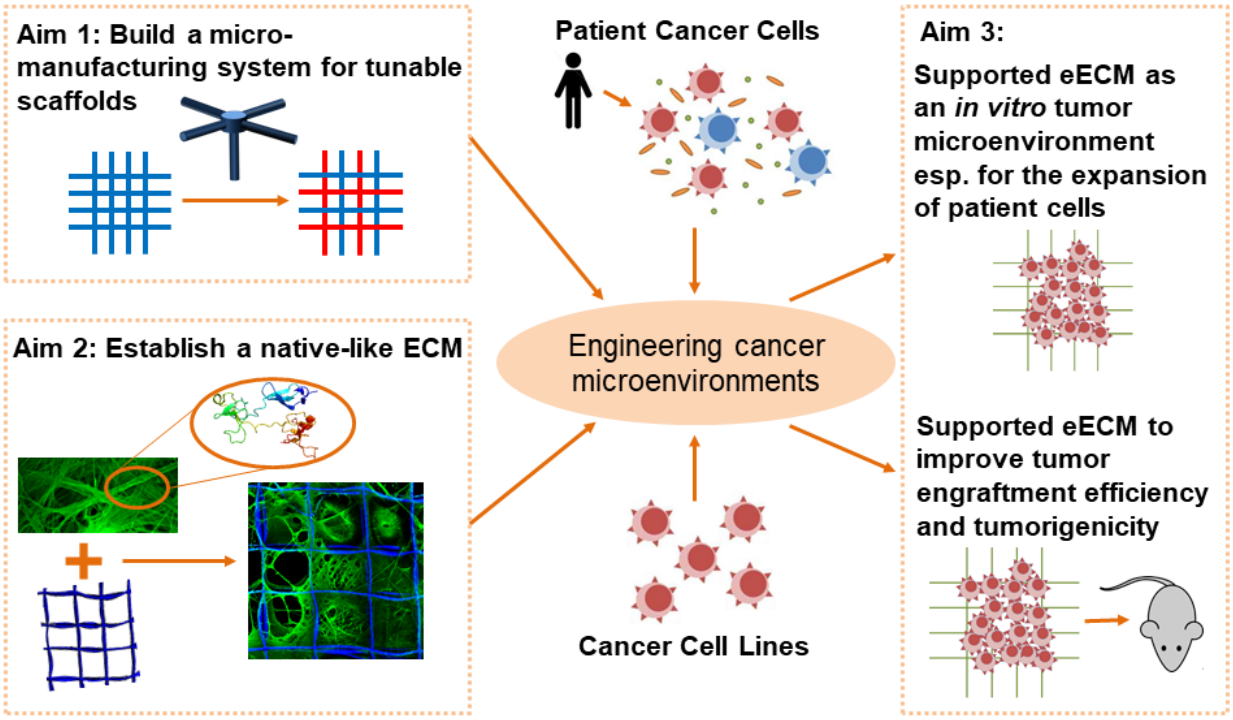

Figure 1-3: Dissertation outline represented as a schematic of three specific aims Aim 1 utilizes a "micro-manifold" to expand the design space of electrospun polymer microfibers and 3D scaffolds. Aim 2 develops a technique for the conversion of solubilized ECM protein into stable networks of fibrillar protein that is tethered to and suspended across the 3D polymer scaffold of Aim 1. Aim 3 demonstrates one of many possible applications of the supported eECM produced via the combination of Aims 1 and 2. Here, the supported eECM serves as a breast cancer microenvironment for the expansion of primary breast cancer patient cells towards ongoing efforts in precision medicine, and tumor graft formation for drug screening, and as a more physiologically relevant 3D cell culture model for fundamental studies.

Chapter 2
Micromanufacturing Customizable Polymer Scaffolds

2.1 Introduction

2.1.1 Electrohydrodynamics and electrospinning

Electrohydrodynamics (EHD) describes the transport of charges within a fluid under an applied electric field. As the charges move, they exert stresses which cause the fluid to move[50]. One of the earliest known investigations of EHD was done by Zeleny in 1917 where a fine jet was formed from a deformed droplet of charged fluid under an electric field[51]. Formhals first used this process to produce plastic fibers and received a patent for it in 1934[50]. A general setup for producing fibers using EHD is shown in **Figure 2-1**. The process begins by pumping a semi-insulating polymer solution through a metal capillary which will serve as the high voltage

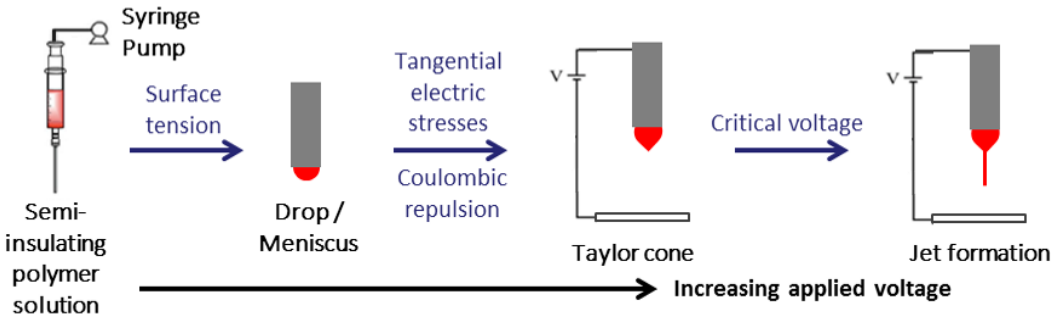

Figure 2-1: Formation of a fluid jet via electrohydrodynamics A semi-insulating polymer solution is driven through a metal capillary using a syringe pump. The droplet that forms at the outlet of the capillary is initially spherical in shape under surface tension. With the application of an electric field, the droplet distorts into a conical shape, known as a Taylor cone. Increasing the voltage past a critical point results in the emission of a fluidized jet from the apex of the Taylor cone. The jet diameter decreases as it propels towards the ground electrode causing rapid evaporation of the solvent and leaving behind a solid polymer fiber.

electrode. A ground electrode is situated a known distance below the high voltage electrode to create a potential difference. This setup allows for the fascinating interplay of a number of driving forces including surface tension, Coulombic interactions, momentum driving forces, and electric stresses[50, 52-54]. Initially, if the potential difference is low or zero, then the surface tension of the fluid dominates and the drop emerging from the capillary at the air-solution interface maintains a hemispherical shape[50]. Electric fields induce fluid flow in dielectric fluids[53]. Since the polymer solution is semi-insulating, there is a potential difference between the top and bottom of the drop which causes a tangential electric field and interfacial electrical shear stresses acting on the drop that drive axisymmetric fluid flow[52]. The drop will remain hemispherical if surface tension dominates over these electric stresses or if the normal electric stress is uniform[54]. However, at a certain critical voltage, the electric stress increases sufficiently to distort the droplet into a conical shape termed a Taylor cone[50]. At this higher voltage, charges in the Taylor cone are strongly attracted towards the ground electrode and move towards the cone apex, increasing the surface charge density until the charge-charge repulsion is relieved by the ejection of excess charge through a fluid jet[50]. Although jet formation is an instability, the cone-jet construct itself remains stable over time due to a balance between the tangential stress and the axisymmetric fluid motion[50].

After a jet has formed, the charges within the polymer solution continue to traverse the distance towards the ground electrode, moving the fluid with it. Hence, the jet is propelled towards the grounded collector reducing the diameter by several orders of magnitude[55]. The fine jet has an increased surface area facilitating the rapid evaporation of the solvent leaving behind a solidified polymer microfiber, which is collected on a grounded electrode[55]. Charges are removed from the fiber during jetting due to corona discharge, humidity, or solvent evaporation, or at the point of collection where the fiber discharges to the ground electrode; however, some residual charges may

remain[50]. In this way, nano- and microfibers are produced from EHD jetting. Typically during jet propulsion towards the ground electrode, a bending or whipping instability develops where the lower end of the jet undergoes a growing oscillatory circular deflection[54, 56]. Whipping results in further thinning of the jet to submicron scales which increases surface area and decreases the time needed for solvent evaporation. The remaining polymer fiber is deposited at the ground electrode as a non-woven mat of interconnected fibers[21] ranging from 20 nm to 5 μm[50]. This process is known as electrospinning and can be used to generate fibers from polymer solutions or melts[50].

2.1.2 3D jet writing

A major drawback of electrospinning is that the fibers are randomly deposited on the grounded collection electrode since the process by which the fiber diameter is reduced to submicron scales, the whipping instability, is inherently unstable[50]. While efforts have been made to control the alignment and orientation of electrospun fibers on the collection electrode[20, 57, 58], repulsive Coulombic forces between the depositing fiber and the fiber mat can make precise fiber deposition[50] and the spinning of a fiber mat thicker than 1.5 - 2 mm difficult[57]. Additionally, failure to modulate the electric field as needed and/or the whipping instability can preclude control over fiber placement. Such problems have been resolved for microfibers in the Lahann Lab by implementing an electrostatic lens to focus the electric field which keeps the depositing fiber directly beneath the Taylor cone. A moving stage is used to reposition a flat plate which serves as the collection electrode during jetting such that a single continuous fiber is patterned into a computer controlled geometry and stacked onto itself to create a third dimension[48]. This process, termed 3D jet writing, allows fabrication of polymer microfiber supports from the FDA approved biodegradable polyester, poly(lactide-co-glycolide) or PLGA[59] (**Fig. 2-2**), and can be extended to include other materials by adjusting process and polymer solution parameters.

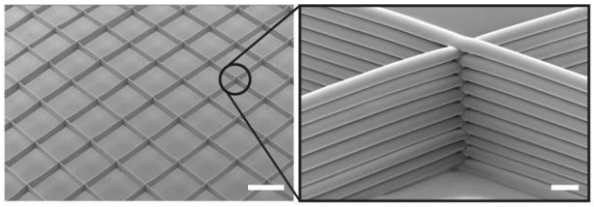

Figure 2-2: 3D jet writing produces three-dimensional microfiber scaffolds By increasing the viscosity of the polymer solution and implementing an electrostatic lens to focus the position of the fiber jet, 3D jet writing affords precise deposition of a single electrospun fiber in a computer-controlled pattern onto a grounded collection plate. The fiber is stacked onto itself to create a third dimension *(inset)*. The scaffold shown here contains square-shaped pores 500 μm wide. Scale bars are 500 μm *(left, zoomed out view)* and 25 μm *(right, inset)*.

Scaffolds fabricated via 3D jet writing enhance transport properties through large open pores of user-defined shape and size, and minimal use of material. 3D jet writing scaffolds feature open areas as large as 96% by volume while maintaining mechanical integrity during handling, under convective fluid flow, and in long term cell culture. Such minimal amounts of synthetic material limits the extent of protein denaturation due to adsorption onto solid surfaces[12], and creates large volumes of space free of synthetic material where cells will only interact with biological compounds such as proteins, growth factors, and other cells. Large synthetic-free voids also provide cells freedom to degrade existing ECM or build their own ECM. Adherent cells have been observed to form "microtissues" or volumes several cell diameters thick that span the open framework. Other cell architectures have also been observed such as clusters and lumens. It is hypothesized that cells residing within the open pores will tend to display a more native or less artificial phenotype, as is often induced by 2D cultures where the entire cell surface is spread out on and in contact with a hard plastic surface[60, 61]. Practically, the control of overall physical geometry afforded by 3D jet writing is convenient for laboratory uses such as fitting into well plates, or to match the size and shape of a patient's defect if implanted for tissue regeneration[19]. When applied as a cell culture matrix, 3D jet writing scaffolds are secured between two metal frames and attached to a spacer such that the physical scaffold is free standing within the cell

media. This ensures easy handling or transfer and maintains the three-dimensionality as opposed to a 2.5D culture where the scaffold sits directly on a hard plastic substrate.

Still, the 3D jet writing system has its limitations in regards to achieving control of where specific materials are localized within the microfiber construct. Such capability would expand the design space by allowing domains with distinct properties (surface functionality, elasticity, degradability, etc.) to be embedded within a single polymer scaffold. It would also further decouple defining features of the material and extend the level of tunability of the final product, empowering researchers with additional tools for probing the effect of changes in the microenvironment on cell behavior. Chapter 2 demonstrates how this limitation is resolved through the design and implementation of a "micro-manifold."

2.1.3 Electrohydrodynamic co-jetting

Electrohydrodynamic (EHD) co-jetting is an electrospinning-based technique developed in the Lahann Lab for the fabrication of multicompartmental electrospun micro- and nanofibers. **Figure 2-3(a)** shows how multiple capillaries, each carrying a distinct polymer solution, are connected in parallel for form a single spinneret[2]. The polymer solutions are driven by a single syringe pump to form a droplet that spans the outlets of all capillaries. Under an applied electric field, the droplet distorts into a Taylor cone where each polymer solution remains in a distinct compartment. In fact, the arrangement of the capillaries is conserved in regards to material placement within the Taylor cone and the ejected fluid jet. The solvent then evaporates from the fluid jet, leaving behind a polymer fiber with a cross section that mirrors that of the bundled capillaries within the spinneret (**Fig. 2-3(d)**)[2]. Increases in solution viscosity and elastic forces, or a decrease in charge density can effectively dampen the instability[20] enabling fiber alignment to produce bundles of fibers as shown in **Figure 2-3(b)**[2]. Two distinct compartments within each

bicompartmental fiber are indicated by red and blue fluorescent dye in **Figure 2-3(c)**[2]. Up to seven compartments have been realized (**Fig. 2-3(d)**)[2].

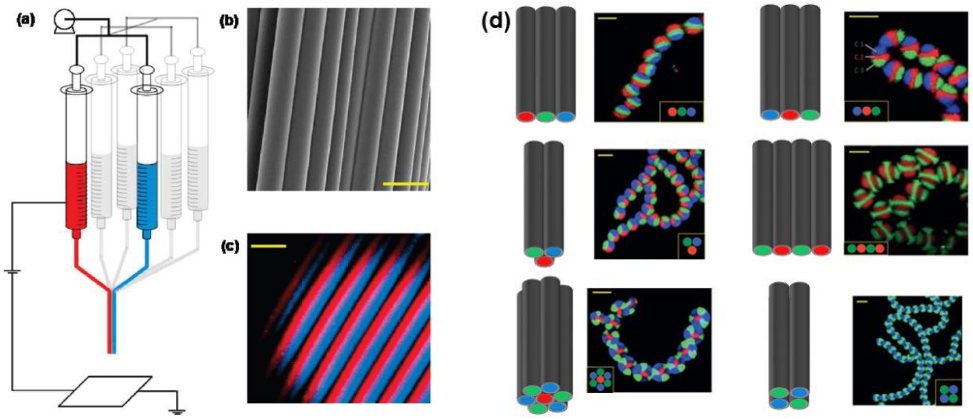

Figure 2-3: EHD co-jetting pioneered in the Lahann Lab enables fabrication of multicompartmental fibers (a) Electrohydrodynamic (EHD) co-jetting setup for production of multicompartmental microfibers showing the connection of multiple capillaries or needles to form a single spinneret. (b) Scanning electron micrograph (SEM) of an aligned bundle of bicompartmental microfibers. (c) Laser scanning confocal micrograph (LSCM) of bicompartmental fiber bundle showing two compartments in each fiber, one labeled in red and the other in blue fluorescent dye. (d) The placement of each needle relative to the other is conserved in compartment placement within each single fiber. Shown are the bundled capillaries used as the spinneret to produce each set of fibers. Scale bars 20 μm. [Figure adapted from Bhaskar *et al.*[2]]

The major advantage of EHD co-jetting is the ability to embed different materials in distinct compartments within the fiber or attribute the surface of each compartment with a distinct functionality. This system affords many possibilities for rationally designed fibers (as well as micro- or nanoparticles) such as the encapsulation of cells, drugs, or biomolecules, or tethering of ligands to select sections of the fiber or particle surface[62-64]. Fiber compartments may be comprised of various polymers and additives by optimizing the properties of the polymer solution in order to stably electrospin the material(s) of interest. Finding the right mix of solvents can be a challenge since the ease with which a polymer solution electrospins is dictated by several process and solution parameters including polymer solubility, solvent miscibility, vapor pressure, viscosity, conductivity, and dielectric constant. Still, a major limitation of EHD co-jetting is the number of capillaries or needles required for control of compartment size. Relative compartmentalization

refers to the relative size of each compartment within a fiber. This is best understood in **Figure 2-4** where to fabricate a bicompartmental fiber where the two compartments are in a size ratio of 60:40, five needles are required, a ratio of 70:30 requires 10 needles, and so on. In addition to a loss of jet stability, a spinneret comprised of such large numbers of needles limits relative compartmentalization to discrete values only. Chapter 2 demonstrates how this limitation is resolved through the design and implementation of a "micro-manifold."

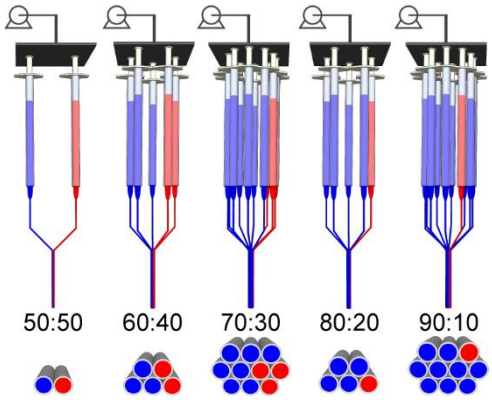

Figure 2-4: Traditional EHD co-jetting has limitations in the relative ratio of compartment size or relative compartmentalization Relative compartmentalization within bicompartmental fibers can only be achieved in discrete ratios with the traditional EHD co-jetting setup. The need for a spinneret comprised of many needles quickly compromises jet stability and fiber quality. Here each of two compartments is represented by either blue or red polymer solution flowing through the bundled capillaries in a way that would theoretically allow fabrication of a fiber with the indicated relative compartmentalization.

Control of compartment bulk composition in EHD co-jetted fibers also allows for control of mechanical properties. This was first seen in bicompartmental fibers comprised of poly(lactide-co-caprolactone) or PLCL in one compartment and PLGA in the other[65]. The Young's modulus of the fiber could then be manipulated by varying the ratio of the two materials within a single fiber by modulating relative compartmentalization. While PLGA is a stiffer polymer, PLCL is considered an elastomer, having greater flexibility than the frequently-used component polymers of PLGA, PLA (polylactic acid) or PGA (polyglycolic acid), and still being biodegradable[66, 67]. Overall, a library of biomaterials exhibiting an array of mechanical properties would greatly

benefit the biomedical community. Mechanical stimuli are frequently employed to regulate cell phenotype[67] or stem cell differentiation[46]. Scaffolds used for 3D cell culture or biomaterials used in clinical applications must be able to maintain mechanical integrity under a range of conditions from material processing to implantation. Furthermore, clinical applications require both flexibility and durability at the same time[66, 67]. Hence developing fibers than can be used as building blocks for textiles or 3D structures via the 3D jet writing process with tunable mechanical properties would prove advantageous in a variety of biomedical applications.

2.2 Materials and Methods

2.2.1 Materials

Poly(D,L-lactide-co-glycolide) or PLGA (85:15 lactide:glycolide, MW 50,000 – 75,000 g/mol, Tg 45-50°C), poly(D,L-lactide-co-caprolactone) or PLCL (DL-lactide 86 mol%, MW ~100,000 g/mol, Tg 16°C) chloroform, and N,N-dimethylformamide (DMF) were purchased from Sigma-Aldrich. Fluorescent polymers are often added to the PLGA solution: (1) Methoxy-polyethylene glycol (PEG)-rhodamine (MW 5,000 g/mol), red dye, was purchased from Creative PEG Works (2) poly[(m-phenylenevinylene)-alt-(2,5-dihexyloxy-p-phenylenevinylene)] (PMPDHPV), blue dye, and (3) poly[tris-2,5-bis(hexyloxy)-1,4-phenylenevinylene)-alt-(1,3-phenylenevinylene)] (PTDPV), green dye, were purchased from Sigma-Aldrich. Tensile tests were performed on the UTM T150 from Keysight Technologies. Laser scanning confocal microscopy (LSCM) was performed on a Nikon A-1 confocal microscope (Nikon Corp., Minato, Tokyo, Japan).

2.2.2 Scaffold fabrication via 3D jet writing

3D jet writing scaffolds are fabricated as previously described[48]. Briefly, a 30 wt% PLGA solution is prepared with chloroform and DMF at a ratio of 93:7. This solution is then driven

through a 20-gauge needle from which it is propelled as a fluidized EHD jet onto a grounded collection plate under an applied electric field. The plate is attached to an x-y stage that makes computerized movements to precisely deposit the electrospun fiber in a prescribed pattern, enabling control of overall geometry, and pore shape and size. Repeatedly stacking the continuously produced fiber onto itself in the same pattern repeatedly creates a third dimension. Process parameters include solution flow rate at 0.4 mL/hr, needle voltage at 15 kV, ring voltage at 9 kV, distance from needle to ground at 4.8 cm, and distance between ring and ground at 2 cm. All process parameters are susceptible to change with environmental conditions, choice of grounded collection electrode, and variations in equipment setup.

2.2.3 Fabrication of single fibers and fiber bundles

In addition to patterning into 3D structures, EHD co-jetted fibers can also be collected as aligned bundles or individual single fibers. Such fibers, when comprised of PLGA, may be produced via the same solution formulation used for 3D jet writing at 30 wt% and a ratio of chloroform to DMF of 93:7. However, PLGA single fibers or fiber bundles presented in this chapter were produced at 35 wt% and the same ratio of chloroform to DMF of 93:7. This is because when producing bicompartmental fibers where one compartment is PLGA and the other is PLCL, this PLGA formulation was found to be more stable; for consistency, the 35 wt% PLGA formulation is used in all single fibers or fiber bundles presented in Chapter 2. Originally, PLCL solution formulation was comprised of chloroform, cyclohexane, and DMF at a ratio of 45:50:5 and 25 wt%. However, better jet stability was achieved when PLCL was prepared at 30 wt% and a chloroform to cyclohexane to DMF ratio of 45:45:10. All fibers containing PLCL presented in Chapter 2 were prepared using this updated formulation. Increasing the polymer concentration of PLGA and the DMF content in the PLCL solution effectively improved the extensibility of the

fiber jet, i.e. how far the jet can stretch without breaking. When PLCL and PLGA were blended into a monocompartmental fiber, appropriate masses of each polymer were combined into the same solution at 37.5 wt% and a ratio of chloroform to DMF of 88:12.

When fabricating bicompartmental fibers of PLCL and PLGA using the manifold, jet initiation was most optimal at an applied needle voltage of ~6 kV whereas fiber collection occurred at ~4.5 kV. Net flow rate was 80 μL/hr. Fibers composed purely of PLGA were prepared at ~10 kV and 40 μL/hr with a 20 gauge needle. Fibers composed purely of PLCL were prepared with an initial voltage of ~6-6.5 kV, and a collection voltage of ~3 kV with a flow rate of 40 μL/hr. Monocompartmental blends of the two polymers, PLGA and PLCL, were fabricated with an initiation needle voltage of ~9 to 10 kV and a variable collection voltage as low as ~3.5 kV with a flow rate of 40 μL/hr. Relative humidity was kept within the range of 20 to 30% and temperature was maintained between 25 and 27°C. Single fibers or fiber bundles for imaging were collected on a glass coverslip attached to a rotating drum covered in aluminum foil. Single fibers for tensile testing were collected on aluminum frames 15.1 cm long, 7.5 cm wide, with a frame thickness of 0.5 cm and a depth ranging from 0.4 to 0.9 cm. A sheet of oak tag with square cutouts 12 mm nominal wide was secured to both sides of the frame, and one single fiber was deposited over each square cutout. Frames were necessary to keep the fiber freely suspended rather than wrapping the fiber around a solid drum where the fiber would contact a hard surface, flatten at the point of contact, and dry in the curvature of the drum. Fibers dried with curvature would undergo pre-stresses as they are straightened for mounting into the tensile testing machine. Fibers freely suspended across the 12 mm square cutouts were directly glued to the oak tag and tensile tested without having to remove the fiber, minimizing fiber damage and pre-stress. After fabrication and

one week of drying at ambient conditions, a drop of epoxy was placed at each end of the fiber to secure the fiber to the oak tag. Epoxy was allowed to cure for 24 hours.

2.2.4 Fiber characterization and tensile testing

Single fibers adhered to and suspended across the 12 mm square cutouts were imaged with a brightfield microscope. Four images were collected for each fiber, one at either end of the fiber, and two more images at different locations along the fiber length. Images were cropped such that the fiber axis was in either a horizontal or vertical orientation and fiber diameters were measured using ImageJ. For each image, two measurements were taken for a total of eight measurements of fiber diameter per fiber. An average fiber diameter was then computed for each fiber over the eight measurements. After two weeks of drying at ambient conditions from the point of fiber fabrication, each square cutout carrying the epoxy-secured fiber was cut from the oak tag sheet. The fiber, now suspended over the square window, was mounted to the tensile tester. ASTM standard C1557 for measuring the tensile strength and Young's modulus of fibers was adhered to as closely as possible. The tensile testing instrument, Keysight Technologies T150 was designed in compliance with ASTM C1557. Actual gauge length was measured with calipers prior to mounting the sample to the tensile tester, and taken as the length of the fiber between the two points of adhesive. ASTM C1557 requires a strain rate sufficiently high to break the fiber within 30 seconds. However, the diversity of fiber compositions being tested did not allow for a single test rate that would apply to all types of fibers. Recognizing that the test rate impacts the mechanical behavior of the polymer fibers, it was preferred to maintain a consistent strain rate amongst all experimental groups. The fibers composed purely of PLGA were selected as the standard test group for which a strain rate was determined that would comply with ASTM C1557. This rate would be low enough to avoid instant breakage of the brittle PLGA fibers, but as high as possible to so break the more elastic

fibers in the least amount of time. Fibers were tested at 0.0015 s^{-1} which resulted in PLGA fiber failure after an average of 11.3 seconds. Young's modulus was calculated from stress-strain curves by inputting gauge length and fiber diameter into the NanoSuite software accompanying the tensile tester from Keysight Technologies.

The relative size of fiber compartments was quantified using 3D volume LSCM images. Surfaces were created over the fiber compartment residing in each channel using Imaris x64 8.3.0 software. The volume encapsulated within each surface was quantified. Relative volumes represented relative compartmentalization.

2.3 Results and Discussion

2.3.1 Manifold device: concept and design

As incorporation of PLCL into a bicompartmental PLGA fiber attributes more elastomeric properties[65], having different polymers in distinct domains within the same 3D construct produces a material with different properties in each spatially separate domain. Conceptually, varying the polymer(s) and/or additives comprising the bulk composition can yield a different stiffness or elasticity, surface texture or topography, degradability, charge density, and functional groups available at the surface for any follow-up chemistries. A single material sporting spatially distinct sets of properties was initially beyond the synthetic material design space of any electrospun fiber scaffold. As such, there was need for a micromanufacturing system that would allow deposition of a specific material into the desired domain within a 3D polymer scaffold.

Since 3D jet writing scaffolds are effectively a single microfiber stacked onto itself, fabrication of scaffolds with distinct material domains requires a fiber that changes in composition along its length. Said fiber would need to be generated simultaneously with the 3D jet writing process so that it may be immediately patterned into the desired three-dimensional geometry. This

can be achieved by preparing a different solution for each bulk composition of interest, and modulating which solution is fed into the Taylor cone at a given time. The idea of several polymer solutions going into a system that has only one outlet, the spinneret from which the Taylor cone would form, describes an already existing device, a manifold. A manifold would have (1) several inlets where different polymer solutions can be fed (2) a single outlet from which a fiber would be electrospun (3) a method of regulating which polymer solutions are outputted at a given time and (4) the ability to create compartmentalized fibers as done with EHD co-jetting. The second property requires that the manifold is sufficiently conductive to propagate charges from a power supply to the polymer solution for Taylor cone and fluid jet formation. Use of the manifold for solution based electrospinning also requires a material resistant to organic solvents.

Since 3D jet writing requires a continuously depositing fiber, the manifold device must have a constant feed of solution from at least one of the inlets to the outlet. Hence, in order to modulate the composition of the depositing fiber along its length, fluid flowing from the inlets to the outlet would have to be switched on or off, or diverted to a collection reservoir when not in use. The number of inlets is determined by the number of distinct materials to be embedded within the polymer support. In this study, the number of inlets was set to four. If fewer inlets are needed, the same solution would be pumped to more than one inlet rather than having an empty inlet that could leak air into the system or provide areas to accommodate fluid back flow. Early manifold design considerations included the size and shape of the inlet and outlet channels, pump arrangements (whether to have one pump applied to all channels and modulate flow on/off by valves, or have multiple pumps – one for each channel), the possible integration of valves to modulate flow, material choice, and the minimization of dead volume or the amount of fluid that is held within the device at a given time. Smaller dead volume would directly lead to shorter time

between switches in outlet solution composition given that the outlet flow rate is constant in the 3D jet writing process. In other words, the solution that occupies the space within the device will be dispensed first, then a new solution carrying a different material composition can enter the outlet line. Ensuring that the outlet was composed of a single channel as opposed to the multi-capillary spinnerets used in EHD co-jetting was expected to maintain unbiased flow from all feeding inlet lines to the Taylor cone. This would minimize risk of (1) the fiber composition differing from that of the outlet flow and (2) instabilities due to a Taylor cone shared unevenly amongst the capillaries. In the end, much of these design considerations were limited by in-house manufacturing capabilities. Hence, the next step was to take the design considerations as a concept and move into prototyping.

2.3.2 Manifold device prototyping

Two major challenges arose in designing and prototyping a manifold: (1) the limited availability of microfabrication methods for prototypes compatible with organic solvents such as chloroform and dimethylformamide and (2) the minimization of "switch time" and therefore dead volume within the device. "Switch time" refers to the amount of time required to "switch" which polymer solution is being delivered from the Taylor cone to the fluid jet at a given moment. This is a direct reflection of the dead volume, or the amount of solution that is contained within the device outlet channel. For example, when switching from solution A to B, all of A must be pumped through the device outlet and out from Taylor cone before the following solution B can take its place in the outlet flow and fluid jet. 3D jet writing of one isotropic PLGA scaffold takes approximately seven minutes, implying that the switch time must be no more than seven minutes to be realized. In an alternative approach, this dead volume can be pumped out of the device by writing a portion of the scaffold, then pausing to write a sacrificial structure expelling unwanted

fluid volume, and returning to the construct of interest after the switch has been made. This alternative approach led to the final successful manifold prototype. In future, switch time can be minimized by using a pump that can dispense as well as retract fluid, so to more quickly alternate which solution is flowing to the manifold outlet. Prior to obtaining a working manifold device, several device iterations were prototyped as described below.

PDMS microfluidic device

In order to quickly generate manifold prototypes testing different microchannel patterns, it was thought that casting polydimethylsiloxane (PDMS) over a mold and bonding the PDMS to a glass slide would give some insight into whether the manifold concept was feasible. Fabrication of PDMS based microfluidic devices is a well-established technique, largely used by the group of Professor Nagrath at the University of Michigan. A collaboration with the Nagrath Lab was initiated to design a couple of prototypes around the conceptual manifold design shown in **Figure 2-5** where four channels are used for inlet flow (A-D) and the center channel, E, will carry the

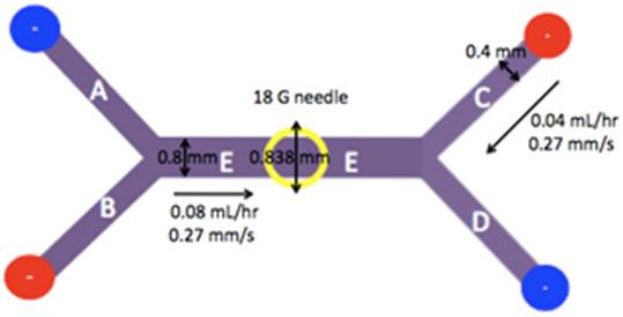

Figure 2-5: First manifold design for manufacture as a PDMS microfluidic device Schematic for manifold with four inlets labelled as channels A, B, C, and D. The outlet is indicated by a yellow ring at the center of channel E where a needle would be inserted in the plane of the page such that it intersects perpendicularly with the channel E flow. Solution would flow from channel E into the needle and be delivered to the needle outlet where it will be electrospun. Red and blue colors represent different polymer solutions.

combined solution flow streams to an outlet indicated by the yellow ring. The inlet flows of A-D would each carry a single electrospinning polymer solution. Multi-solution flow begins where the input channels merge into channel E where they are expected to remain separated under laminar

flow conditions; minimal diffusive mixing is expected at the interface. The output from channel E is a needle, which also serves as the spinneret, intersecting channel E flow perpendicular to the plane of the device itself. Each inlet flow can be driven by a separate syringe pump at different flow rates, or multiple inlets can be simultaneously driven by one pump at the same rate. Currently, 3D jet writing of bicompartmental fiber scaffolds is performed with two 26 gauge needles (one for each compartment) each at a flow rate of 0.04 mL/hr for a total volumetric flow rate of 0.08 mL/hr which was therefore set as the flow rate for output channel E. It was decided that an 18 gauge needle would be used due to previous successful jetting experiences in the Lahann Lab with this size needle. The inner diameter of an 18 gauge needle is 0.838 mm which set the max width of the outlet channel (channel E in **Figure 2-5**), thereafter taken to be 0.8 mm. A standard channel depth (or height) in PDMS microfluidic devices is 0.1 mm, which was set for all channels. With the width and flow rate of channel E set, the respective values for channels A-D were set to half that of channel E since these channels require half the volumetric capacity of channel E for bicompartmental fibers.

Given these constraints on channel geometries, the length of each channel was next to be determined, where a shorter length for channel E was thought to be optimal. Reynolds number was estimated to be on the order of 10^{-4} for channel flow and 10^{-5} for needle flow where the solution viscosity was approximated as that of glycerol, which was sufficiently representative of the viscosity of a PLGA solution, the standard polymer for EHD co-jetting. Some diffusive mixing will occur at the interface of the two flows, but this has not been a problem previously in the Lahann Lab when creating multicompartmental fibers[2]. Nevertheless, diffusive mixing could be limited by reducing the length of the channel E and using the shortest commercially available 18 gauge needle (i.e. reducing the time the different fluid flows spend in contact before reaching the

Taylor cone). Another motivation to minimize the length of channel E was to minimize the dead time of the device, or the time it would take to observing a change in solution within the Taylor cone from switching which inlet channels were in operation (by turning one syringe pump off and another on). Additionally, it was thought that shorter channels would be preferred to minimize pressure drop, but from a simple Poiseuille flow calculation of pressure drop in a rectangular channel it was found that even at relatively large channel lengths, the pressure drop was at most on the order of 1 kPa. This is less than microfluidic channel pressure drops seen in the literature of 10 kPa[68], 40 kPa[69], and 5 kPa[70]. Longer channels, at least for channels A-D, are preferred since the further apart the inlet streams are from each other the less likely are interfering Coulombic interactions to occur between tubing feeding into the device. Also, longer streams will make the device larger and thus easier to handle when setting up the jetting system. Given these considerations, there were no hard constraints on the lengths of any of the device channels. Since the fabrication of PDMS microfluidic devices first requires making a master which can be used to make several different devices at once, it was concluded that devices of varying channel lengths would be made, and the various devices experimentally tested to determine which channel lengths minimized mixing, dead time, and pressure drop while maximizing the overall size of the device (**Fig. 2-6(a-b)**).

Since PDMS is known to swell when in contact with chloroform and many other organic solvents[71, 72], these PDMS devices were prototyped first using glycerin solutions carrying different optical dyes rather than the chloroform-based PLGA solution (**Fig. 2-6(c)**). Glycerin has a similar viscosity to the PLGA solution typically used. Although the glycerin did not readily form a jet sufficiently stable to produce fibers, a Taylor cone formed at the outlet of the needle. This was sufficient to determine as a proof-of-concept that the two solutions were kept separate while

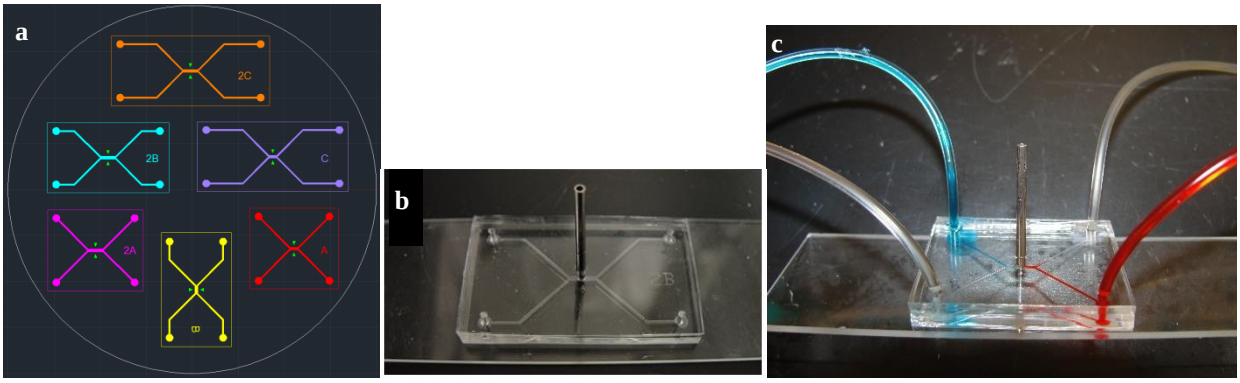

Figure 2-6: Rapid prototyping of various microchannel patterns for manifold manufactured as a PDMS microfluidic device (a) Autocad image of six different schematics drawn for production of a master that would be used to generate PDMS devices. (b) Representative microfluidic device demonstrating how needle is positioned in the middle of the center channel as an outlet flow line and spinneret. (c) Tubing run into the four holes punched out for the four inlet streams using optical dye to trace the movement of fluid in the device. Device orientation is upside-down in (b-c). *Credit:* PDMS devices fabricated in collaboration with Hyeun Joong Yoon of the Nagrath Lab at the University of Michigan.

flowing through the device as shown in **Figure 2-7** where the red and blue compartments are clearly kept unmixed. In the traditional EHD co-jetting setup, a bicompartmental Taylor cone could only be achieved using two needles combined in parallel to form the spinneret. Next, four distinctly colored solutions were loaded into the device: red, blue, green, and yellow. After producing a 50/50 red/blue Taylor cone, the red/blue syringe pump was turned off and at the same instant, the green/yellow syringe pump turned on. After five to seven minutes, the Taylor cone had changed from red and blue, to green and yellow. Several switches back and forth were made successfully, demonstrating as a proof of concept that the device design effectively changes the solution fed to the Taylor cone while keeping distinct solutions partitioned. Finally, to verify that this device design could electrospin fibers, polyethylene oxide (PEO) at 600,000 kDa, a water-soluble polymer, was dissolved into an aqueous electrospinning solution at 7 wt%, and found to produce microfibers from the PDMS microfluidic device (**Fig. 2-8**). Next, the selected PDMS device design A (**Fig. 2-6(a)**), having the shortest channels, will be fabricated out of glass by

etching or aluminum by milling so to achieve the same fluid flow patterns and eliminate solvent compatibility issues.

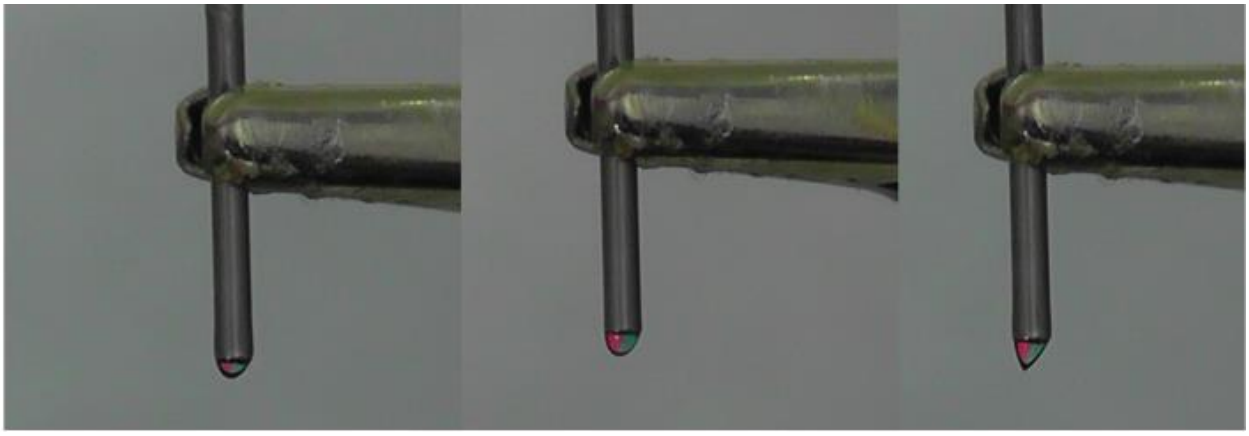

Figure 2-7: First demonstration that the Taylor cone remains partitioned in manifold device Photos show the distortion of the bicompartmental droplet emitting from the single needle of a PDMS microfluidic manifold device. Typically in EHD co-jetting this partitioned cone is achieved through the use of two needles in parallel. Glycerin solutions carrying either red or blue optical dye were pumped into the manifold and flowed in parallel without a solid at the fluid interface. The two fluids moved together through the center channel of the device and through the outlet needle remaining partitioned from droplet to Taylor cone. Bicompartmental separation in the droplet was re-established 5-7 minutes after a compositional switch that changed the outlet droplet through a series of greens and yellows.

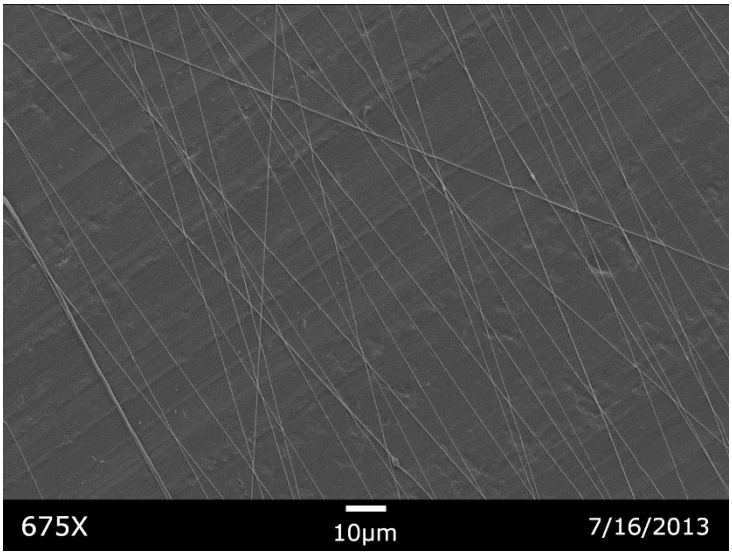

Figure 2-8: Proof of concept that PDMS microfluidic manifold effectively electrospins microfibers Polyethylene oxide (PEO) dissolved in an aqueous solution electrospun from the PDMS microfluidic manifold into microfibers. Fibers are aligned as they are deposited onto a grounded high speed rotating collection electrode.

Aluminum microchannel device

The PDMS device design guided the production of a similar design in aluminum as shown in **Figure 2-9**. Although material-solvent compatibility was no longer a problem, two other major issues arose preventing successful implementation of this manifold. Firstly, making the "world-to-chip" connections necessary to feed electrospinning solution into the device inlets was a challenge.

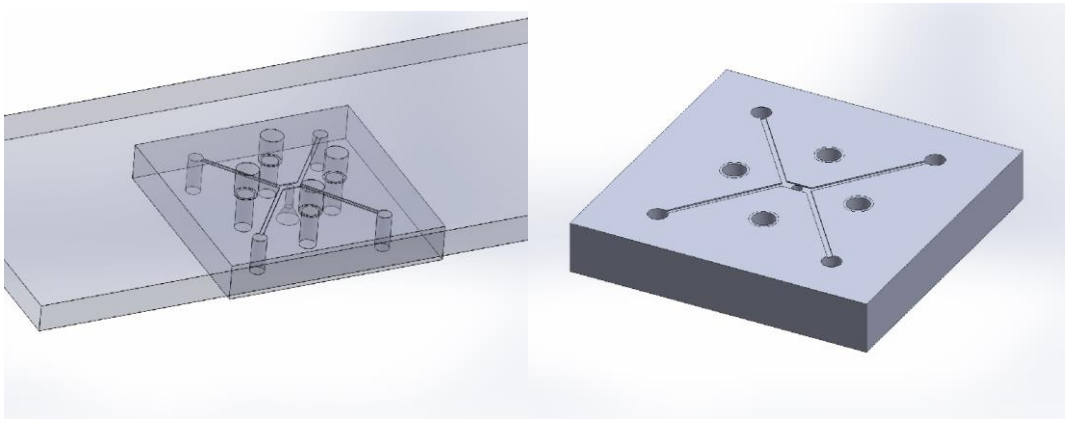

Figure 2-9: CAD drawing of manifold device modeled like the PDMS microfluidic manifold but made from aluminum Computer aided design (CAD) drawing done in Solidworks of assembled aluminum manifold device (left) and engraved channels (right). This device is an aluminum mimic of the PDMS microfluidic manifold device that was effective at switching solution composition and electrospinning microfibers.

For organic solvents, Teflon tubing must be used, in contrast to the Tygon tubing typically used in the PDMS microfluidic devices. Inserting Tygon tubing into holes punched out of PDMS was a secure connection based on friction alone. Teflon tubing is both tougher and smoother, and aluminum being a hard, smooth surface does not exert much frictional force to hold the Teflon tubing in a liquid-tight connection throughout the electrospinning process. Furthermore, fixing the needle into the center channel in a metal-metal connection required an adhesive which would quickly wear out under the use of organic solvents (**Fig. 2-10**). A similar problem arose in the metal-metal connection between the top and bottom parts of the aluminum manifold which were held together by screws. Application of vacuum grease assisted in creating a seal between the two parts and preventing leakages, but this was still insufficient over longer-term use. The second major challenge was charging effects. The applied voltage necessary to charge the electrospinning

solution was often dissipated throughout the aluminum device, reducing the likelihood of droplet distortion into a Taylor cone, and causing a charge build up in the device and any conductive material in the surrounding environment. Fabricating the same design in glass was next attempted so to maintain solvent compatibility, but eliminate device fabrication from a highly conductive material.

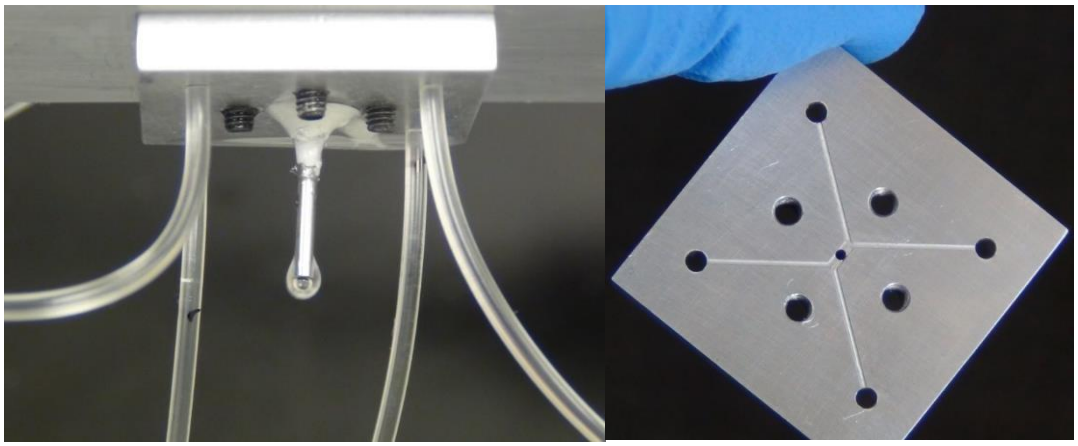

Figure 2-10: PDMS microfluidic manifold device fabricated in aluminum *(left)* Aluminum manifold in operation showing tubing feeding PLGA solution composed of organic solvents into the device and flowing out of the needle that is secured to the device by adhesive. *(right)* One of the two pieces that comprise the aluminum manifold. This part has channels engraved into the aluminum that mimic the pattern of the most successful PDMS microfluidic manifold device. A hole was added to the middle of the center channel where a needle is attached as a spinneret. The four large holes around the center hole are for screws to attach this part to a larger flat plate (as shown in left photo) which acts as the glass slide that the PDMS device would be otherwise bonded to. The four holes at the ends of each of the four channels are for inlets for feed lines.

Glass-etched microfluidic manifold

To create a glass manifold, the same channels designed for molding out of PDMS were etched into a glass wafer as shown in **Figure 2-11**. Each device was diced out of the wafer to obtain the individual devices (six devices were printed on a single wafer). The devices were sealed to a glass slide using a UV-glue and holes were bored into the device for the inlets and outlet using electrochemical drilling. This glass device had great potential to be a success, however, like the aluminum manifold, making world-to-chip connections was difficult, especially with respect to attaching the metal needle to serve as the spinneret in a liquid-tight fashion.

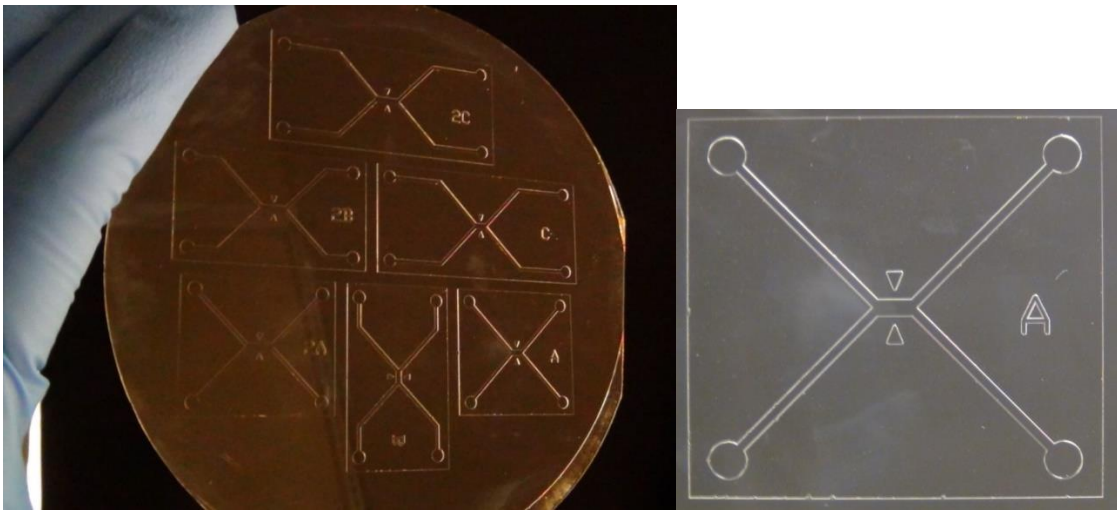

Figure 2-11: Design of PDMS microfluidic manifold device fabricated in glass *(left)* Entire wafer with six devices showing channels that mimic the patterns of the initial PDMS microfluidic manifold devices etched to a depth of 100 µm. *(right)* Zoomed in image of etched channels on a single sheet of glass after etching and dicing. *Credit:* Device fabrication done in collaboration with Brian Johnson of the Burns Lab at the University of Michigan.

Iterating through several more manifold device prototypes

Several more device designs were prototyped shown in **Figure 2-12**. One of the more promising options was to return to the PDMS device, applying sol-gel technology[73], to coat the walls of the microfluidic channels with a solvent resistant layer of silanes that slows the migration of organic solvents out of the channel, delaying the swelling of the PDMS. Although this approach worked, devices could not be re-used, and the time required to fabricate each one would make manifold-based electrospinning impractical (**Fig. 2-12(e)**). With the difficulties in in-house fabrication, the possibility that a device may exist commercially that would serve the purpose of the manifold was explored. It was hoped to find a commercially existing rotary valve manifold, as sketched in **Figure 2-13(a)** that would cut off flow from a given inlet by rotating a knob, thereby minimizing dead time. The flow valve from Hamilton (Reno, NV), shown in **Figure 2-13(b)** was found to be the most similar device to this design on the market. Although much detail was not available on the inner workings and volume within the device from the manufacturer, the device was purchased and prototyped. Shown in **Figure 2-14**, testing this device with PLGA solutions

containing optical dyes revealed the gradient that occurs between switches, but also indicated that a large dead volume was contained within the device itself that would require nearly an hour of sacrificial jetting time for each solution switch, rendering this manifold device impractical.

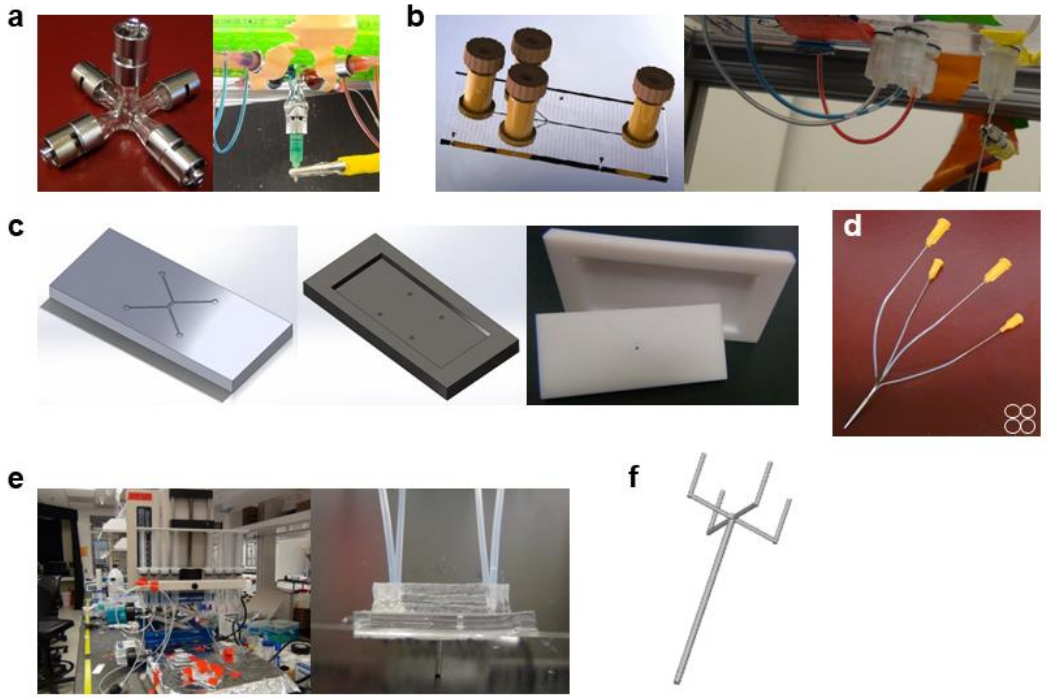

Figure 2-12: Several manifold prototypes (a) (*left*) Glassblown manifold with metal luer-locking connectors (*right*) Glassblown manifold in operation (b) (*left*) Commercially purchased glass microfluidic device from Translume (Ann Arbor, MI) (*right*) in operation (c) PDMS-microfluidic manifold device inspired a similar design in Teflon. CAD drawing of (*left*) top part showing engraved microchannels and (*middle*) bottom part with groove for top part to fit into. (*right*) Photo of top and bottom parts after manufacture. (d) Four-way needle manifold made by connecting four metal capillaries combined to be the manifold outlet and spinneret. Four dispensing tips attached by tubing to the outlet capillaries form the manifold inlets. (e) (*left*) Laboratory setup showing multi-syringe pump required to complete the sol-gel process intended coat PDMS microchannels with a network of silanes for delayed swelling under contact with organic solvents. (*right*) Final sol-gel treated PDMS microfluidic manifold showing PDMS bonded to another piece of PDMS rather than the typical glass slide.

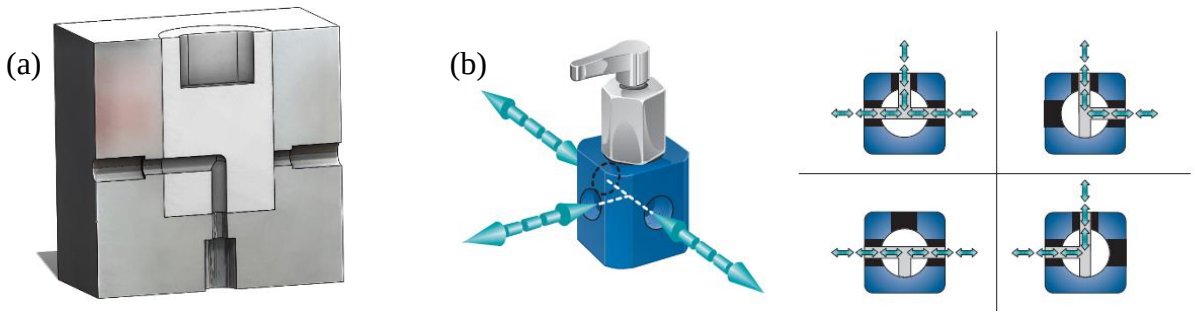

Figure 2-13: First attempts to find a commercially available product that would function as a manifold device (a) CAD design drawn in Solidworks of a cross sectional view of a rotary valve manifold. The center piece (in lighter grey) will rotate to open to the inlet channel desired to flow to the outlet at a given time. *Image credit:* Clark Teeple for CAD drawing. (b) Commercially obtained flow valve from Hamilton (Reno, NV) that is sufficiently similar to the conceptual design in *(a)*.

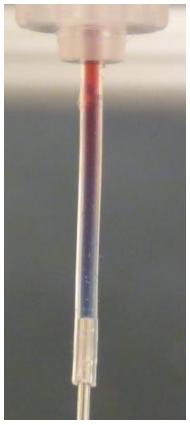

Figure 2-14: Gradient observed switching from blue to red optically dyed PLGA solution in rotary valve manifold Flow valve commercially obtained from Hamilton reveals the gradient that develops in switching from a blue-dyed PLGA solution to a red-dyed. Given the large size of the device (circular channels of diameter 1.5 mm), the dead volume led to a switching time of nearly an hour.

Final successful prototypes

Now, the initial expectations on what a manifold would be capable of in conjunction with the 3D jet writing system were revisited. At the start of this project it was hoped that changes in composition along the length of a fiber could be made in distinct segments under one millimeter. However, this patterning resolution is beyond the limit of electrospinning-based technologies given the "dead" volume within the Taylor cone itself. Estimating the cone to range from approximately one to four millimeters in height, gives a range of cone volumes from 0.1 to 0.4

microliters of polymer solution (based on a 23 gauge bicompartmental needle). This translates to about 15 to 60 centimeters of fiber. Therefore, the original desired patterning resolution for single fibers is infeasible, however, the benefit of the manifold lies in the 3D scaffold design space. Many distinct domains can be embedded within a 3D jet writing scaffold, which on average requires about 660 cm of fiber to produce a 10-stack scaffold with 500 μm wide square pores (including lead-in fiber lengths which are afterwards cut off to obtain the final scaffold as applied for cell culture). As such, use of the manifold for creating changes in composition along a fiber length would most effectively be realized in 3D jet writing microfiber scaffolds.

With new information gained from each manifold prototype, a theoretical design for an optimized manifold was generated, illustrated by the sketch in **Figure 2-15**. This manifold is essentially an assembly of five stainless steel needles welded together around a central cylindrical chamber. The four needles about the larger top cylinder are inlet channels, and the larger single needle positioned perpendicularly to the four inlet needles is both the outlet and spinneret. The entire device would be made of a conductive metal, such as stainless steel, that is compatible with the range of organic solvents that may be of interest for solution-based electrospinning. There would be no need for assembly and no potential for leaks as it is all one piece welded together. Unlike the aluminum manifold, which was also made entirely of a conductive metal, charge buildup is not expected since the channels are made of metal tubing, minimizing the amount of material in contact with the high voltage electrode, in contrast to the etching of microchannels into a larger bulk piece of metal. Conceptual operation of this manifold is demonstrated in the cross-sectional view in **Figure 2-15**. Distinct polymer solutions, represented in blue and red are loaded into individual inlets of the device. Initially, only the blue solution is pumped into the outlet flow channel. Shortly after, the pump driving the blue solution is turned off as that of the red solution

is turned on, allowing red to flow into the outlet channel behind the blue. As this process of switching which solution is driven into the outlet channel is repeated, "plugs" of each solution are

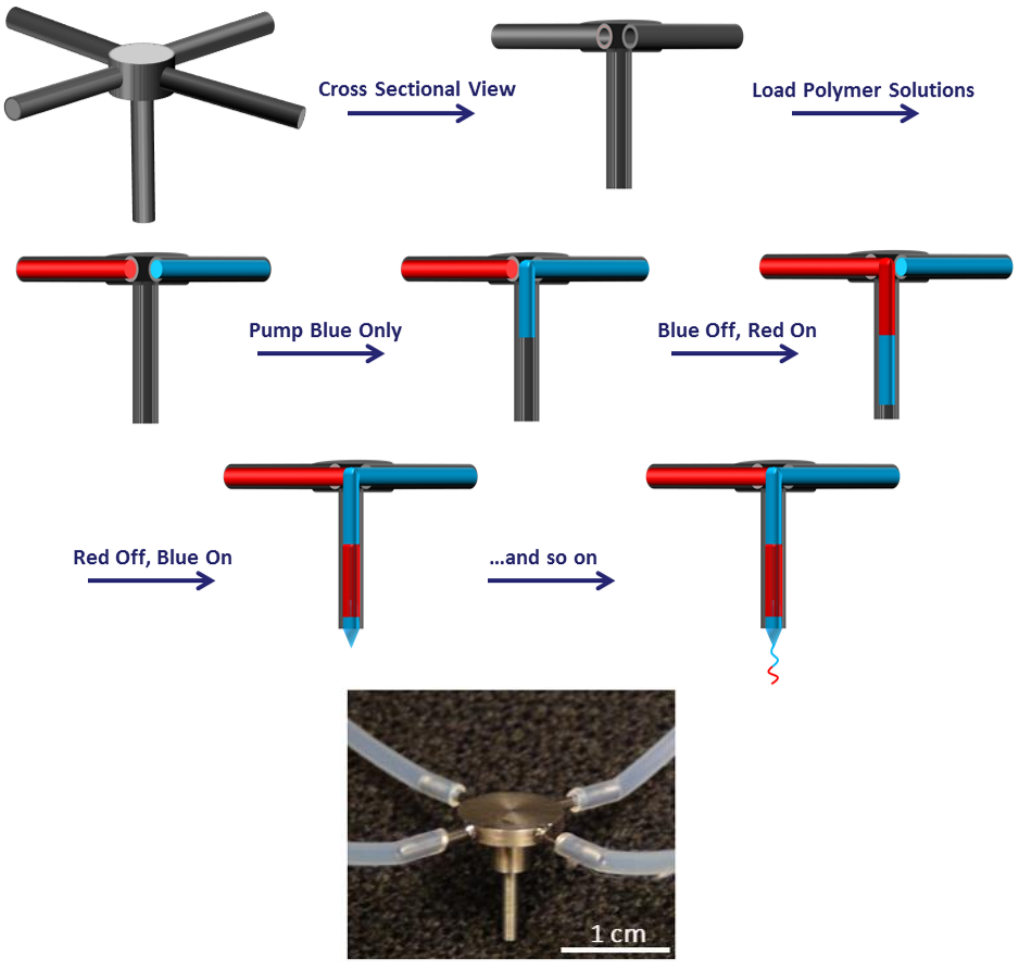

Figure 2-15: Optimized manifold device *(top)* Cartoon schematic showing cross-sectional view of disk manifold in operation to switch the composition of an electrospun fiber along the fiber length where different compositions are indicated in red and blue color. *(bottom)* Photo of successful and most capable, disk manifold. Entirely made of stainless steel, this manifold essentially unites four 20 gauge needles as inlet flows (about the central top-most cylinder) with an 18 gauge needle (the outlet flow and spinneret). Teflon tubing shown fitting air-tight over the four manifold inlet channels. Manifold custom manufactured by Optics Technology (Pittsford, NY).

generated within the outlet channel consecutively. Electrospinning of a polymer fiber directly from the outlet channel which acts as the spinneret will then result in a fiber that changes composition along its length. Of course, this is a conceptual design – in reality, a gradient is expected in between different solutions in the outlet flow as opposed to actual "plugs" of each fluid.

Named the *disk manifold*, this design was custom manufactured by Optics Technology (Pittsford, NY) (**Fig. 2-15**). The first successful switch in polymer solutions at the outlet was realized at an average switch time of 18 minutes. The key features of this manifold that enable its function are the liquid tight connections between the inlet channels and the Teflon tubing feeding the polymer solution into the device. The diameter of each inlet channel was selected to be the size of a 20 gauge needle, after finding a Teflon tubing size that fits over this needle diameter in an air-tight fashion. The outlet flow is the size of an 18 gauge needle and serves as the spinneret, connecting directly to the high voltage electrode without additional parts or wiring. The device is made to be as small as possible while still allowing long enough inlet channels for secure tubing attachment, and an outlet needle that is long enough to connect a power supply. It is also easy to clean after each use. Taking the approach of writing sacrificial structures to dispense excess fluid in between switches, this manifold was successfully used to fabricate 3D jet writing scaffolds where different polymer solutions, annotated by either a blue or red fluorescent dye, could be embedded within the same scaffold in distinct domains as represented in **Figure 2-18**.

The fastest switch time occurs at the theoretical limit of a dead volume of zero. However, irrespective of device design dead volume will always exist within the Taylor cone. This concept led to the final design, the *bicompartmental needle manifold* which was simply two stainless steel tubes, removed from dispensing needles, and bound together by a plastic sleeve as traditionally done in the Lahann Lab for bicompartmental fibers (**Fig. 2-16**). Rather than pumping solution through both needles simultaneously as done in EHD co-jetting, the needle manifold operates by pumping a different solution through each needle separately. The key to operating this device is to carefully ramp down the flow rate of the solution to be switched out while ramping up that of the incoming solution such that a single stable Taylor cone remains spanning the outlet of both needles

during the switch. When turning on a syringe pump, one must consider the startup time required to get the solution pumping at the desired rate. To test the ability of the bicompartmental needle to

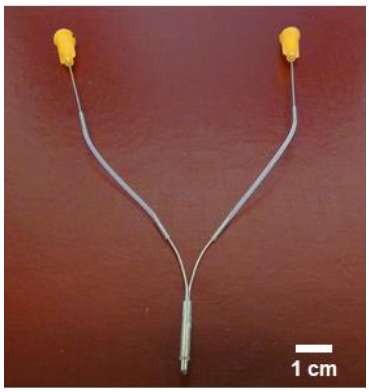

Figure 2-16: Bicompartmental needle manifold An alternative successful manifold design, using simply the combination of two needles as the spinneret, where each needle is connected to a separate syringe pump. This device can function as a manifold, although is limited in its versatility due to the two-needle outlet and the metal interface separating the two polymer solutions that would otherwise be flowing in parallel in the disk manifold.

switch which polymer solution is emitting from the outlet, red and blue fluorescently dyed PLGA solutions were prepared. Electrospinning of fibers onto a grounded rotating collector showed that switching from red to blue and blue to red was possible (**Figure 2-17**). By counting the number of fibers that were jetted during the switch from an all red to an all blue fiber (or vice versa) it was estimated at least in this early study that the switching time is as little as three minutes. This is the fastest switching ever observed in any of the previously tested devices – as is expected since the only dead volume is that of the Taylor cone. In operation, the needle manifold required six minutes safely or a minimum of three to four minutes, of sacrificial electrospinning to fully switch which solution is being fed from the Taylor cone to the fiber jet.

A similar manifold design had been previously prototyped where four needles were combined to form the spinneret, and each of the needles had a separate feed line (**Fig. 2-12(d)**). However, the spinneret, being composed of four round needles, greatly limited the stability of the Taylor cone over time. Polymer solution wicked into the gap formed in between the two needles

dried and hardened, causing greater separation between individual needles, and leading to disturbances in the steady flow of polymer solution to the Taylor cone, and on to the fiber jet.

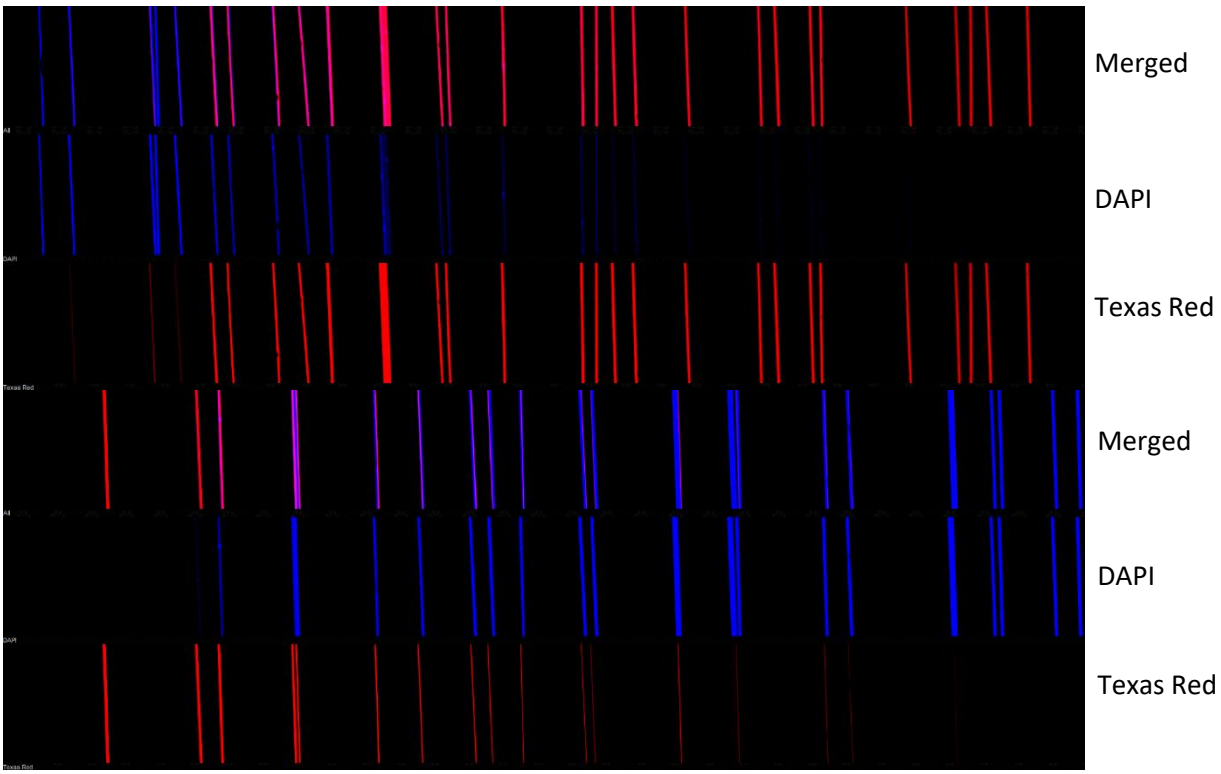

Figure 2-17: Observed switch from blue to red and red to blue in aligned PLGA fibers using bicompartmental needle manifold Switches in which polymer solution was feeding to the fiber jet were observed using fluorescently labelled aligned PLGA fibers collected on a rotating collector and fabricated using the needle manifold. *(top)* Blue fibers were continuously collected as the device switched to red-dyed PLGA solution resulting in the disappearance of blue-dyed fibers and the appearance of red-fibers instead *(bottom)* Continuing from the *top*, fibers were then switched from red-dyed to blue as indicated by the disappearance of red and the appearance of blue fibers. Each switch occurred in three to four minutes.

Another major challenge was maintaining a steady Taylor cone across an outlet that spanned the area and geometry of four combined needles during switches in solution. The most success with this four-way needle prototype was when constantly operating two needles at a time, which limits the capabilities afforded by the conceptual manifold illustrated in the cartoon of **Figure 2-15** since only two distinct domains would be possible within a 3D jet writing scaffold. Two distinct domains require only two inlet feed lines, which is achieved by the bicompartmental needle manifold, shown in **Figure 2-16**. Although the bicompartmental needle manifold is capable of generating

3D jet writing scaffolds containing distinct domains such as those shown in **Figure 2-18** with the lowest switch time possible, the extent of capabilities afforded by this manifold design is vastly limited compared to that of the disk manifold. Firstly, embedding of more than two distinct domains within a scaffold would require more than two inlet flows, in which case the bicompartmental needle manifold is of no use. Secondly, the disk manifold with four inlets allows

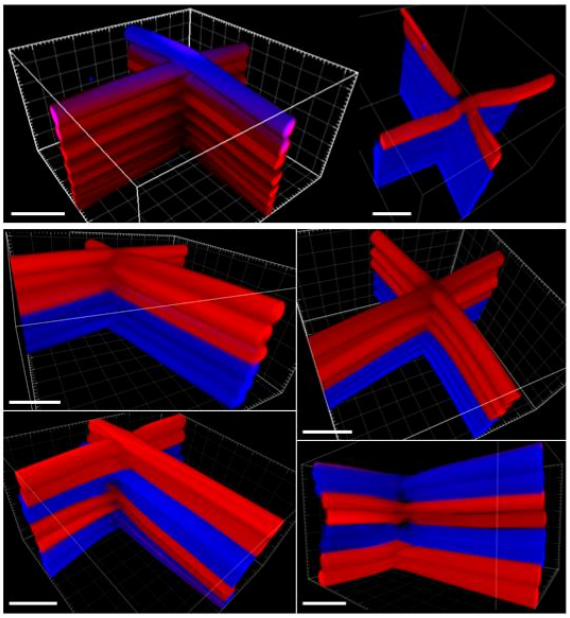

Figure 2-18: Distinct domains realized in 3D jet writing scaffolds with implementation of manifold Switching between a fluorescently red-dyed and blue-dyed PLGA solution by fabrication of sacrificial structures in between switches enables a clean interface between distinct domains patterned into a microfiber construct using the manifold in 3D jet writing.

fabrication of fibers containing compartments in any permutation of four distinct polymer solutions. For example, with four different materials being fed into the device, one into each of the four feed lines, the resulting fiber cross section may contain any one, two, three, or all four of the compartments at a given time. Moreover, the number of compartments within the fiber cross section at any point along the length of the fiber can be tuned with the disk manifold. Thirdly, the prospect of co-jetting different materials may pose challenges in terms of jet stability since different polymer solutions often most stably electrospin under different processing conditions.

Having a single needle outlet as with the disk manifold rather than a dual needle outlet will help minimize the risk of co-jetted polymer solutions splitting the Taylor cone into multiple cones of a single composition instead of the intended single Taylor cone composed of multiple materials. Finally, only the disk manifold allows for changing of the orientation of compartments along the length of a bicompartmental fiber, since four inlets would be required (**Fig. 2-19**). Demonstrating a shift in compartment orientation within a 3D jet writing scaffold is one of many future directions in further characterization of the capabilities of the disk manifold.

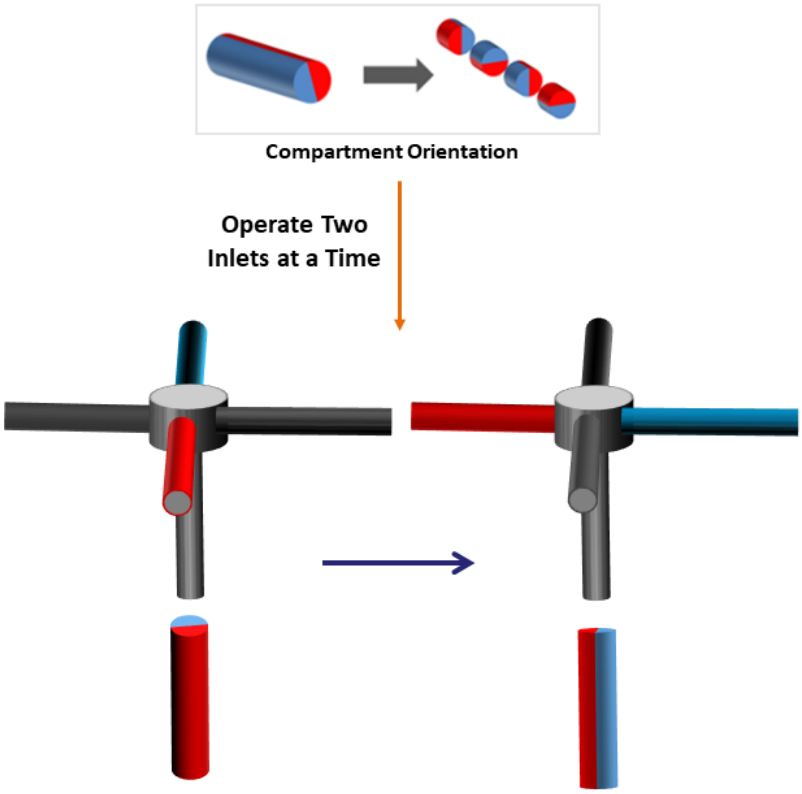

Figure 2-19: Future work to demonstrate changes in compartment orientation within bicompartmental fibers using the disk manifold The next step in demonstrating the capabilities afforded by the disk manifold is to show changes in the orientation of compartments within a bicompartmental fiber as illustrated in the box at the top. To do this, the two materials to become each compartment (represented in red and blue) would be fed into two opposite inlets of the disk manifold and a fiber electrospun. A change in compartment orientation can be realized by then alternating to the other two opposite inlets such that the placement of the red and blue compartments within the outlet flow, Taylor cone, and resultant bicompartmental fiber changes to mimic the orientation of the feed lines. Compartment orientation control requires the use of a longer lead in time in the 3D jet writing scaffold process such that the fiber jet is completely unwound from any prior twisting before entering the area where the desired scaffold resides.

2.3.3 Controlling relative compartmentalization in microfibers

With a successful manifold device, it is now possible to produce multicompartmental fibers where the relative size of each compartment, or relative compartmentalization, is controlled by flow rate. For a bicompartmental fiber, each solution is pumped through independent lines and fed into different manifold inlets. Although the net flow rate is kept constant, the ratio of the two independent flow rates controls the ratio of the compartment size in the resultant fiber. For instance, if the net flow rate is 0.06 mL/hour, then to achieve compartments whose sizes are in a 1:2 ratio, then one solution should be pumped at 0.02 mL/hour while the other is pumped at 0.04 mL/hour. This eliminates the need for large numbers of needles which would compromise jet stability, and enables a continuous spectrum of possible compartment size ratios (**Fig. 2-20**). Whereas with EHD co-jetting a bicompartmental fiber in a compartment size ratio of 7:3 would require ten needles, now with the manifold, the pumps driving each solution can be tuned to a flow rate ratio of 7:3 and the fiber can be electrospun directly from the manifold outlet (**Fig. 2-20(a)**). Certainly, more accurate pumps will correlate with the accuracy in relative compartmentalization. A series of PLGA bicompartmental fibers was electrospun using the manifold, with 10% increments in compartment size, and where each polymer solution was labelled with either a blue or red fluorescent tracer molecule. Representative cross sections of the fibers are shown in **Figure 2-20(b)**, starting from a fiber with a compartment size ratio of red to blue of 1:9 and ending with 9:1. Visually, the steady increase in one compartment can be seen to correlate with the decrease in the other compartment. Using Imaris x64 8.3.0 software, surfaces were generated over the compartment residing in each fluorescent channel. The volume within each surface was quantified to generate the plot shown in **Figure 2-20(b)** where the expected relative compartmentalization or compartment size scales with the fraction of the net flow rate that was driving the corresponding

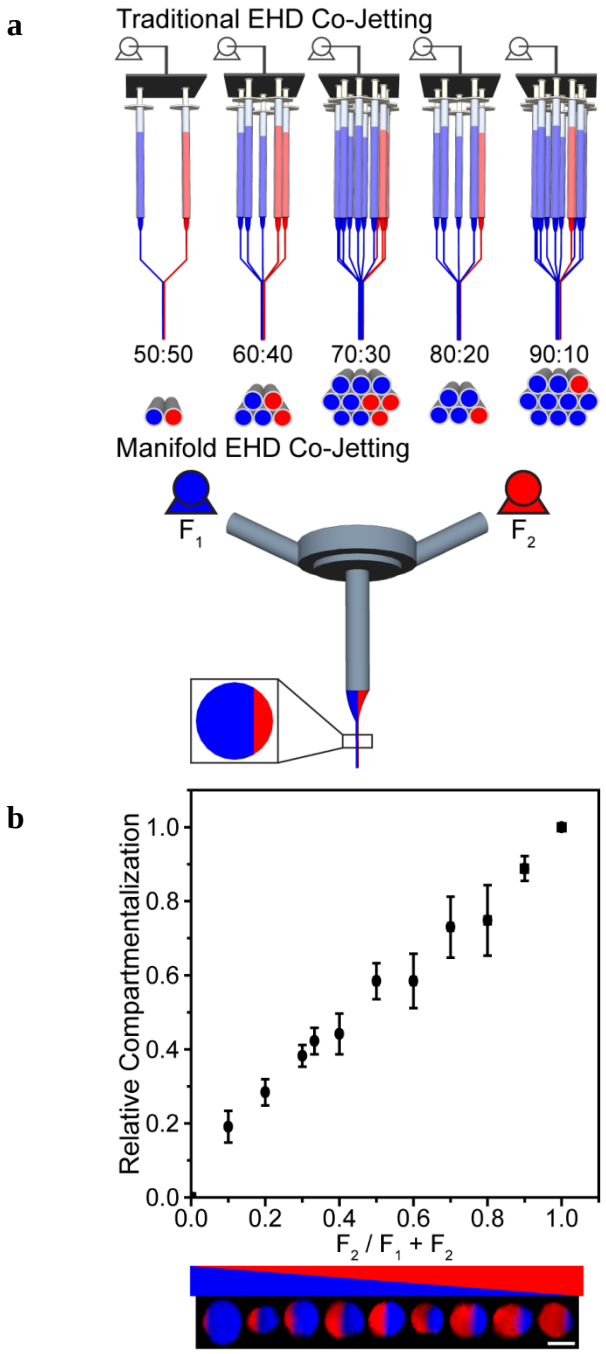

Figure 2-20: Manifold enables non-discrete ratios of compartment sizes with single outflow capillary (a) Sketch contrasting traditional EHD co-jetting with multiple needles combined to form a spinneret to a manifold with two inlets and one outlet. For EHD co-jetting the number of needles required to achieve the indicated compartment size ratios are drawn for bicompartmental fibers. For the manifold setup, two pumps at flow rates F_1 and F_2 are sketched as feed lines to each of the two inlets. The Taylor cone and cross section of the fluid jet are drawn for F_1 greater than F_2. (b) LSCM of bicompartmental fiber cross sections where the flow rate of red compartment increased (and blue compartment decreased) by 10% in each subsequent fiber moving from left to right. Red and blue channels indicate PLGA. Scale bar 10 µm.

polymer solution. This result demonstrates the continuous spectrum of relative compartmentalization now achievable with the manifold.

Moreover, these fibers contribute a new level of tunability to the 3D jet writing scaffold design space where the user can change the bulk fiber composition independently of other scaffold properties. In order to incorporate changes in relative compartmentalization within a 3D jet writing scaffold, the fiber must change composition *in situ* during the electrospinning process. Since 3D jet writing scaffolds are produced by stacking one fiber onto itself, any desired changes in relative compartmentalization must occur at the right time during fabrication. To visualize the ability to continuously change fiber composition and compartmentalization, PLGA was dissolved in a solution including either red or blue optical dye. Starting with a fiber jet of 100% red-dyed PLGA solution, the flow rate of the red solution was steadily reduced by 2.5% while that of the blue was simultaneously increased by 2.5%. Fiber bundles were collected on a grounded rotating collector for about 30 seconds at each flow rate ratio until the fluid jet was comprised of only blue-dyed PLGA solution. The result was a series of aligned fiber bundles that shifted from red to blue in color through a gradient as visible by eye (**Fig. 2-21(a-b)**). With the ability to realize changes in the fiber compartmentalization during the electrospinning process *in situ*, a similar shift from a red fluorescently dyed PLGA to a blue could be realized through a gradient in a 3D jet writing scaffold (**Fig. 2-21(c)**). Furthermore, relative compartmentalization control is not limited to bicompartmental fibers. As shown in **Figure 2-22**, fibers comprised of three and four compartments can be tuned for relative compartmentalization and compartment architecture. These new capabilities can be projected for future use in modulating the outer area of each fiber presenting a certain ligand or surface functionality, the amount of a drug or biomolecule loaded

into a fiber by the relative size of the drug-loaded compartment, or the bulk composition of the fiber – an example of which is presented in the next section.

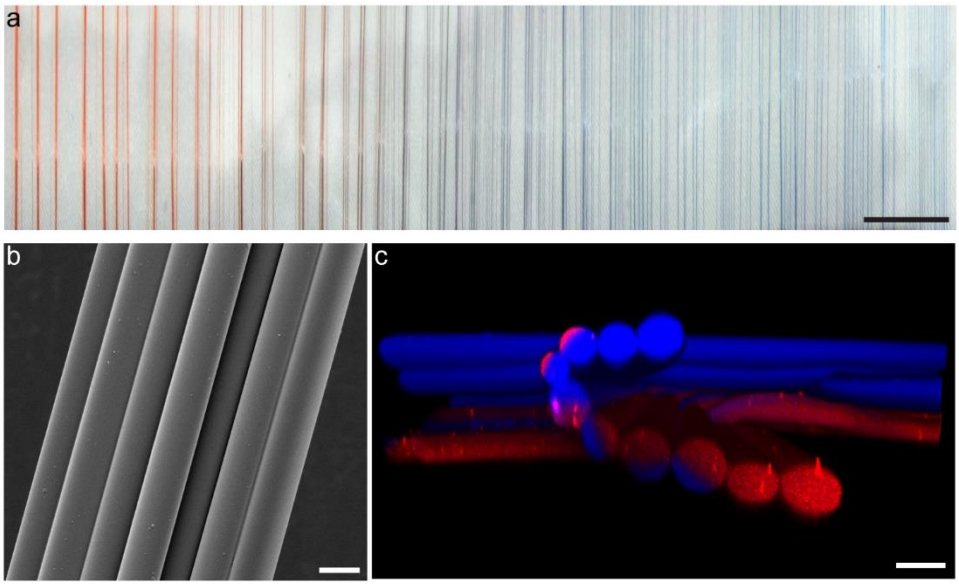

Figure 2-21: Changes in compartmentalization can be made continuously during electrospinning using the manifold (a) PLGA solutions were prepared carrying either a red or blue optical dye. Using the manifold, red fibers were first electrospun and collected on a grounded rotating wheel. By increasing the flow rate of the blue solution and simultaneously decreasing that of the red solution by 2.5%, continuous collection of a fiber revealed a switch from red to blue fibers moving through a color gradient. Scale bar 5 mm. (b) SEM of fiber bundle from *(a)*. Scale bar 10 µm. (c) 3D jet writing scaffold made using the manifold to switch from red-dyed PLGA fibers at the bottom stack to blue at the top stack moving through a color gradient. Red and blue channels are PLGA. Scale bar 25 µm. *Image credit:* Fibers fabricated and imaged by Jeffery Noble.

a

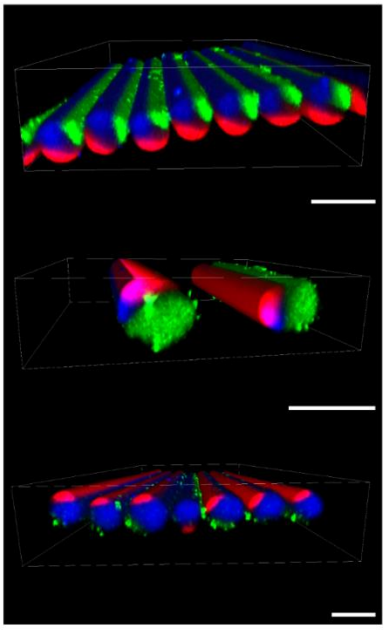

b

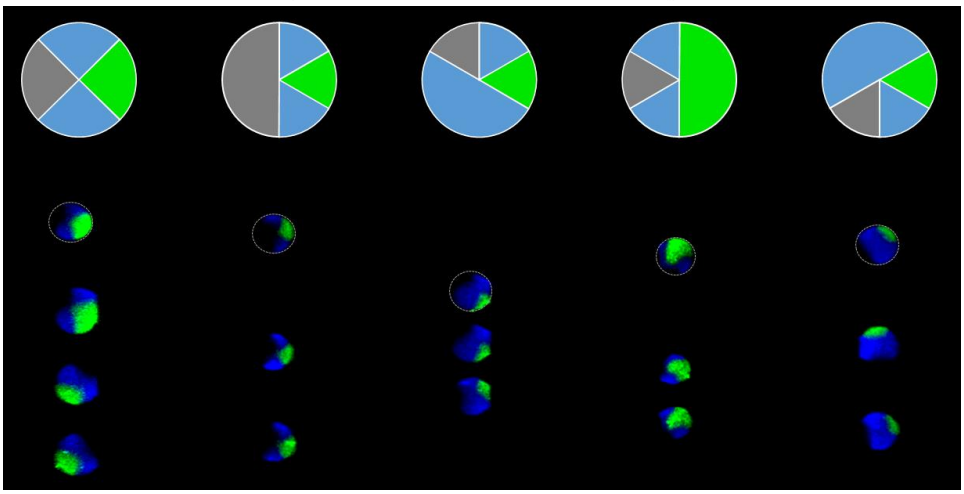

Figure 2-22: Compartmentalization can be controlled via manifold in fibers comprised of more than two compartments Multicompartmental fibers are made using the manifold with (a) three compartments shown in volume view and (b) four compartments shown by fiber cross section where grey compartment marks no dye. Fibers are composed of entirely PLGA but carrying different polymer dyes in each compartment. Green dye is often aggregated due to poor solubility in electrospinning solutions. Scale bar 25 µm. *Image credit:* Fibers fabricated and imaged by *(a)* Jeffery Noble and *(b)* Clark Teeple.

2.3.4 Tuning fiber mechanical properties through bulk composition

Thus far, the capabilities of embedding multiple distinct compartments within a single microfiber, and controllably varying relative compartmentalization has only been shown using different fluorescent dyes mixed within solutions of the same polymer, namely PLGA. However, the ability to tune fiber compartment size yields the ability to tune fiber mechanical properties through the incorporation of different materials into a single fiber. The manifold was used to co-jet bicompartmental fibers at three compartment size ratios, where one compartment was composed of PLGA and a blue fluorescent tracer dye and the other compartment of poly(lactide-co-caprolactone) (PLCL) along with a green fluorescent tracer dye (**Fig. 2-23**). Considered an

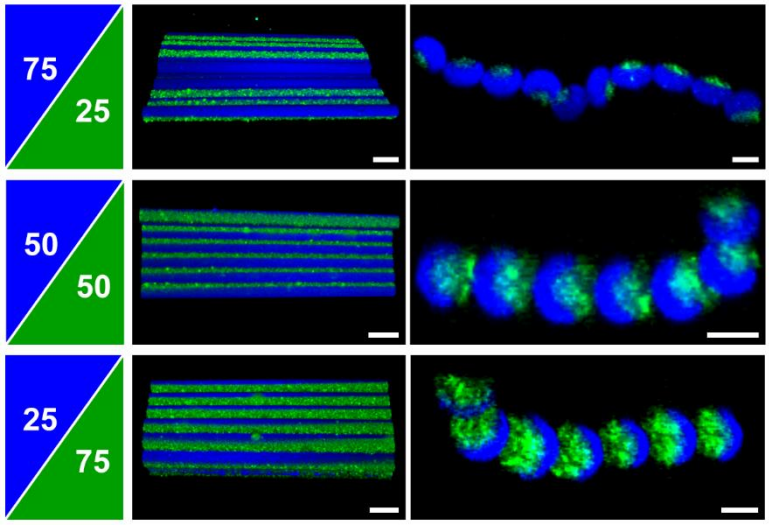

Figure 2-23: Bicompartmental fiber bundles comprised of PLGA and PLCL are fabricated using manifold Bicompartmental fibers having two materials: PLGA and PLCL are produced in bundles at the indicated ratio where the blue channel is PLGA and the green PLCL. Scale bars for images of fiber cross sections 10 μm; scale bars for 3D renderings 25 μm.

elastomer, PLCL is expected to reduce the stiffness of otherwise purely PLGA fibers, as can be quantified by Young's modulus. Five types of fibers were fabricated for tensile testing and determination of Young's modulus: bicompartmental fibers where the ratio of PLGA in one compartment to PLCL in the other were 100:0, 75:25, 50:50, 25:75, or 0:100. Since calculation of Young's modulus requires the sample cross sectional area, single fibers as shown in **Figure 2-**

24(a) were fabricated using the manifold rather than fiber bundles so that a definite cross sectional area could be identified.

Tensile testing of single polymer microfibers is a delicate task. In order to minimize risk of fiber damage, a new grounded electrode setup was designed to collect fibers directly on the substrate where they will be adhered for tensile testing (**Fig. 2-25**). Rectangular frames were individually cut from a hollow cube of aluminum using a horizontal band saw, and sheets of cardstock were attached to each side of the aluminum frame. Windows were cut from each cardstock sheet, and the entire ground electrode was connected to a rotating wheel. The polymer solutions needed to be optimized in order to jet stably on this new ground collector setup since the fluid jet required greater elasticity to span the distance from the spinneret to the bottom of the rotating rectangular frame. The final optimized solutions were PLGA at 35 wt% in a solution of chloroform to dimethylformamide at 93:7, and PLCL at 30 wt% in a chloroform to cyclohexane to DMF ratio of 45:45:10. Finally, fibers were electrospun onto the cardstock, allowed to dry at least a week, and a droplet of epoxy was placed on both ends of the fiber to secure the fiber in place (**Fig. 2-25**). Each window could now be cut out of the cardstock sheet with the single polymer microfiber freely suspended. Brightfield images were collected for each fiber at four different regions along the fiber length. Fiber diameter was measured from each brightfield image using ImageJ. Fiber diameters were found to range from 3.6 to 30.0 μm. After two weeks of drying at ambient conditions, fibers were mounted to the tensile tester, the cardstock windows were snipped, and the fiber was pulled uniaxially from one end at a strain rate of 0.0015 s^{-1}. Since Young's modulus was found to correlate with fiber diameter (**Fig. 2-26**), only fibers with a diameter within the reduced range of 6.0 to 15 μm were selected for the final representation of Young's modulus, as plotted against the fraction of the fiber bulk that is comprised of PLGA in **Figure 2-24(b)**. As

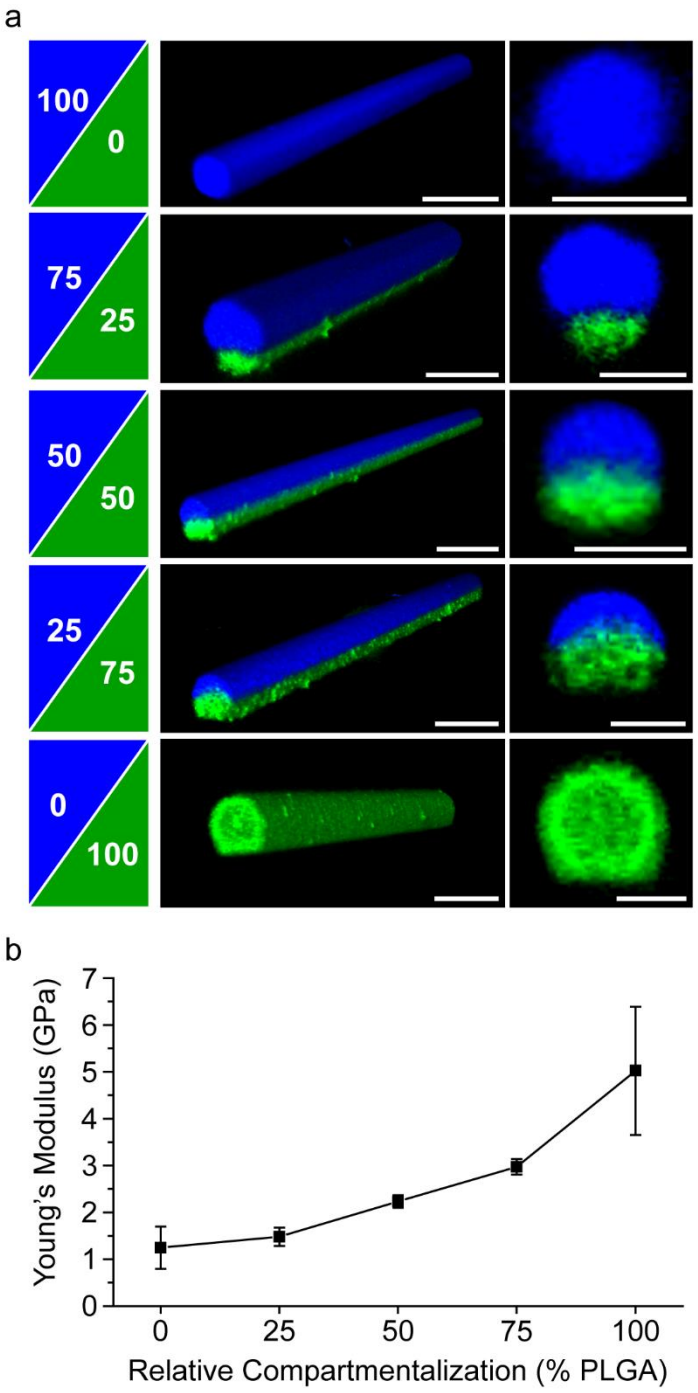

Figure 2-24: Controlled compartment size can be leveraged for tuning of fiber elasticity by incorporating different bulk materials (a) Single fibers fabricated using the manifold consisting of one compartment PLGA (blue) and the other PLCL (green). Single fibers are preferred over fiber bundles for tensile testing and calculation of Young's modulus. 3D render scale bar at 25 μm. Cross section scale bar at 10 μm. (b) Young's modulus scales with the compartment fraction that is PLGA, the remainder PLCL for single polymer microfibers ranging in diameter from 6.0 to 15 μm. Error bars represent a 95% confidence interval.

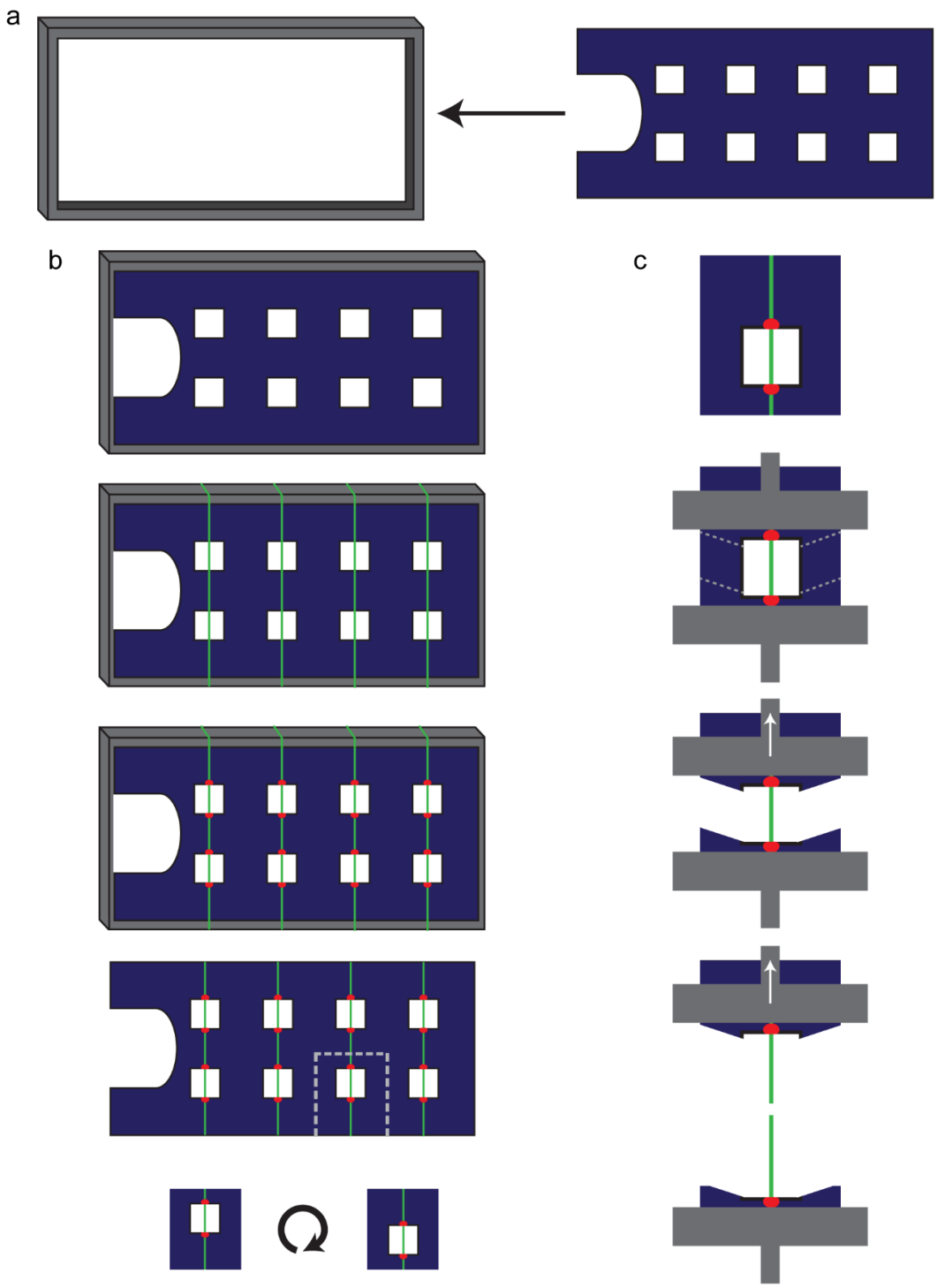

Figure 2-25: New grounded collection electrode setup to minimize risk of damage of single polymer microfibers fabricated for tensile testing (a) Rectangular aluminum frames were cut from a square hollow tube of aluminum. The outline shown on the top right was cut from cardstock and attached to both sides of the aluminum frame. Each square window is nominally 12 mm wide. The large semi-circular cutout is for attachment of the metal frame to a rotator via a split-bolt connector. (b) Fibers, represented in green, were electrospun directly onto the cardstock attached to the frame which acted as the grounded

collection electrode. After at least one week of drying time, fibers were adhered at each end of the 12 mm window to the cardstock using a droplet of epoxy represented in red. Each square window was cut from the cardstock carrying one freely suspended adhered fiber. (c) Each fiber secured to this square oak tag window was mounted to the grips of the tensile tester, represented in grey, such that the larger side of the window cutout was in the top grip. This ensures greatest sensitivity in the Keysight Technologies UTM T150. Uniaxial tension was applied by pulling upward on the fiber to generate stress-strain curves.

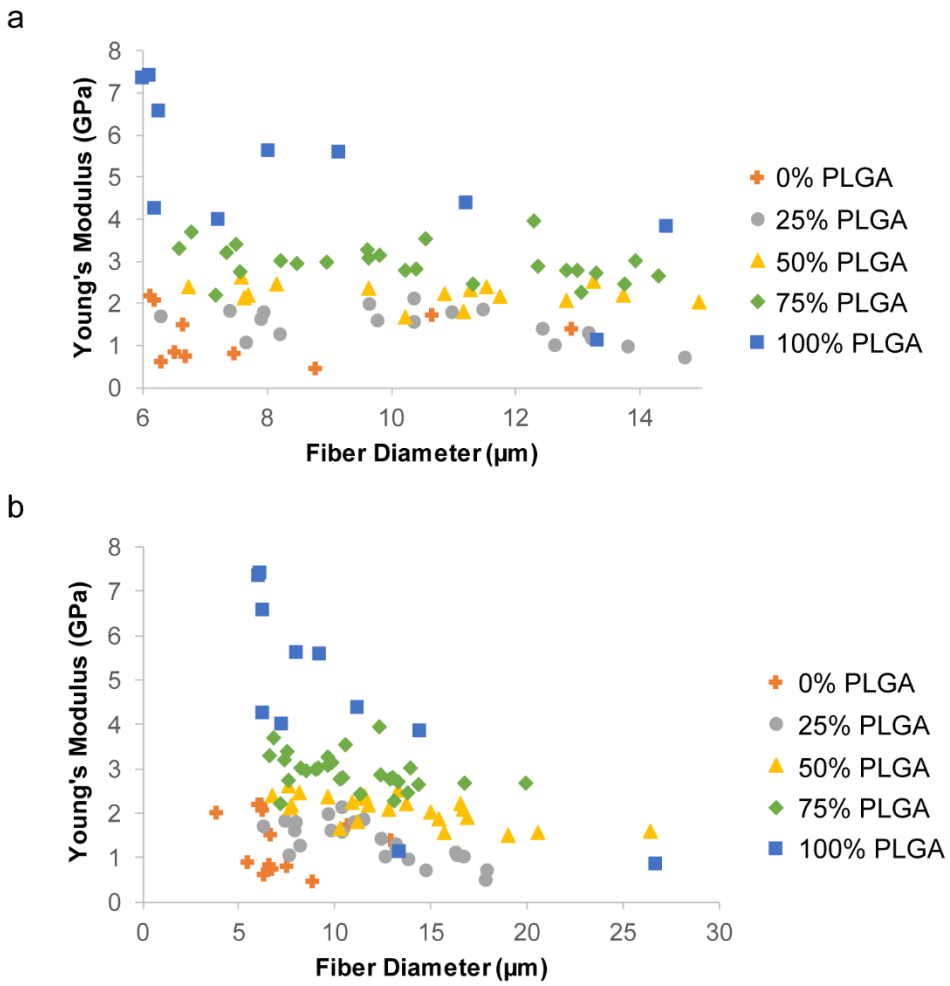

Figure 2-26: Young's modulus inversely correlated to fiber diameter Scatterplot of Young's modulus vs. fiber diameter for (a) fibers within diameter range selected for final calculation and (b) all fibers tested. Legend represents relative compartmentalization with respect to the percentage of PLGA present in the fiber, the remainder being the relative size of the PLCL compartment.

expected, the larger the compartment of PLGA, the higher the Young's modulus and hence, the stiffer the fiber. This result demonstrates the use of the manifold for tuning the stiffness of

electrospin microfibers, and the possibility for custom-designed fibers where the relative compartmentalization in PLCL/PLGA bicompartmental fibers is dictated by a desired elasticity.

With the manifold, fiber stiffness or elasticity is now a user-defined parameter when fabricating single fibers, or constructs composed of single fibers such as fiber bundles or polymer scaffolds. Given a desired Young's modulus, the required compartmentalization of PLCL and PLGA can be determined. In regards to 3D jet writing scaffold design, use of the manifold to produce scaffolds comprised of bicompartmental fibers of PLCL and PLGA will enable tuning of scaffold mechanical properties through bulk composition. However, 3D jet writing of bicompartmental PLCL and PLGA structures has long been plagued by jet instability and poor fiber alignment since the two polymers electrospin at different voltages: ~3-5 kV for PLCL and ~8-10 kV for PLGA. Using the manifold eliminates the metal interface between the two solutions otherwise present in the EHD co-jetting setup. It was hypothesized that flowing the two solutions in parallel along the length of the manifold outlet and into the Taylor cone without a solid surface at their interface would help stabilize the fluid jet. Indeed, the two solutions remained partitioned in the Taylor cone and the bicompartmental fluid jet stability was improved relative to using a two-needle capillary. Although the fluorescent tracer dyes are poor due to recent changes in equipment, **Figure 2-27** illustrates well-aligned fiber stacks within 3D jet writing polymer supports comprised of bicompartmental fibers of PLGA and PLCL at 50:50 and 75:25. The ability to modulate scaffold modulus is a required design feature for 3D cell culture matrices considering that different tissues vary in stiffness[19, 22, 46]. In recapitulating specific cell niches, the mechanical environment must also be matched. Tumors, for example are generally stiffer than healthy tissue[74]. Additionally, the mechanical environment should be modifiable in order to observe stiffness induced cell responses[22, 46, 49]. Important to note is that the Young's modulus measurements reported in **Figure**

2-24(b) are for dry single fibers. Once applied in cell culture, the mechanical properties of these fibers will change upon immersion in aqueous fluids or incubation at physiological temperatures.

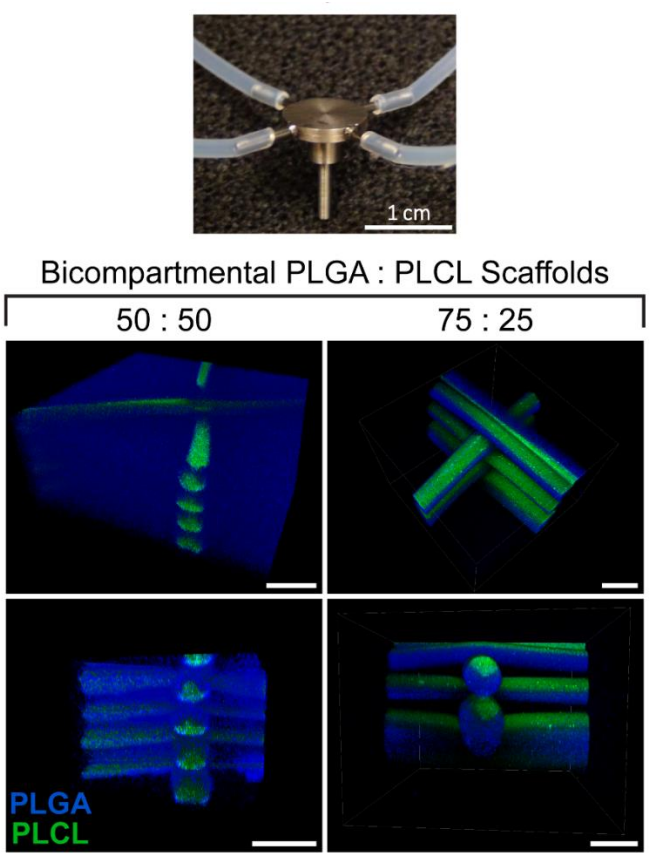

Figure 2-27: Manifold improves jet stability when 3D jet writing bicompartmental structures comprised of PLCL and PLGA Disk manifold, shown above, having a single channel as the outlet (as opposed to a bicompartmental needle) improves jet stability for fabrication of polymer supports made of bicompartmental fibers. Each fiber consists of one compartment of PLGA (blue) and another compartment of PLCL (green). Scale bars 25 μm.

Interestingly, the bicompartmental nature of the single fibers comprised of PLCL and PLGA, and the difference in elasticity between the two materials resulted in fiber curling when stressed to failure as done in tensile testing. Shown in **Figure 2-28**, although the tightness or pitch of the curls varied, the concavity of the loop on the inside consistently remained concave while the outside of the fiber remained convex. Curling was more controllably observed when the fiber was stressed to a fixed strain and relaxed rather than stressed to failure (**Fig. 2-29**). (It is often difficult or impossible to collect the broken pieces of a microfiber after a tensile test to failure.)

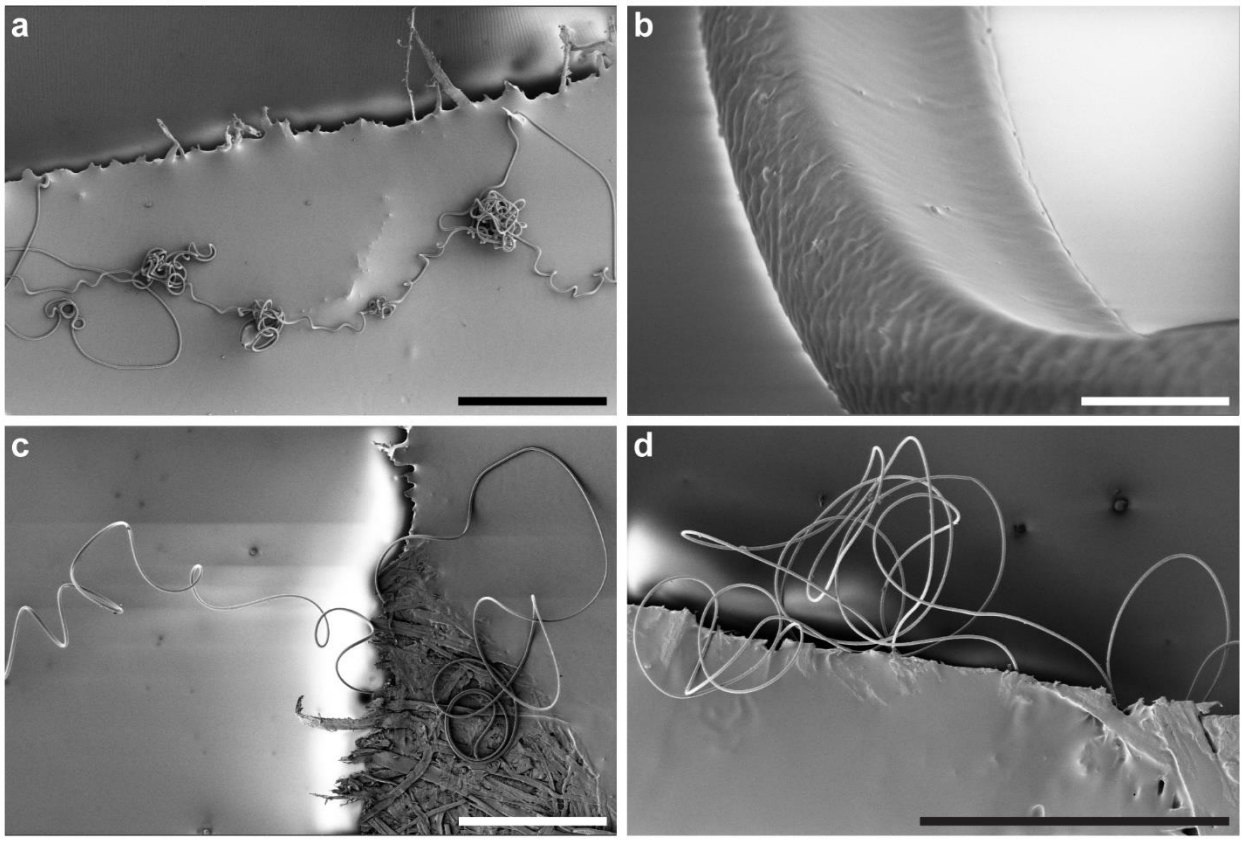

Figure 2-28: Bicompartmental fibers tend to curl after tensile testing Although difficult to collect after tensile testing, the larger broken fiber segments could be located for imaging. Bicompartmental fiber segments consisting of PLGA and PLCL were visualized using scanning electron microscopy. The ratio of compartment size for PLGA to PLCL varied from (a-b) 25:75 (c) 50:50 and (d) 75:25. (a, c, d) Scale bar 500 µm. (b) Scale bar 5 µm.

Fiber curling was restricted to bicompartmental fibers; fibers comprised of a monocompartmental blend of PLGA and PLCL at equal masses or purely PLCL were not observed to coil. Future studies may point towards stress-relaxation of these fibers as a means of fabricating polymer "microsprings." Such springs could be characterized by first stressing the fiber to get the Young's modulus, and allowing the fiber to relax into a coiled morphology. Applying strain to the now coiled fiber would give a spring constant, K_1, rather than a Young's modulus. Continuously repeating this stress-relaxation would yield a spring constant for each stress-strain cycle: K_2, K_3, K_4... Would the value of the spring constant change over time? How many cycles can the coiled fiber withstand without plastic deformation? Are all K values equal or is there any hysteresis in

the force vs. distance curves? Can the properties of the spring be tuned by modulating the relative compartmentalization of the PLGA/PLCL fibers?

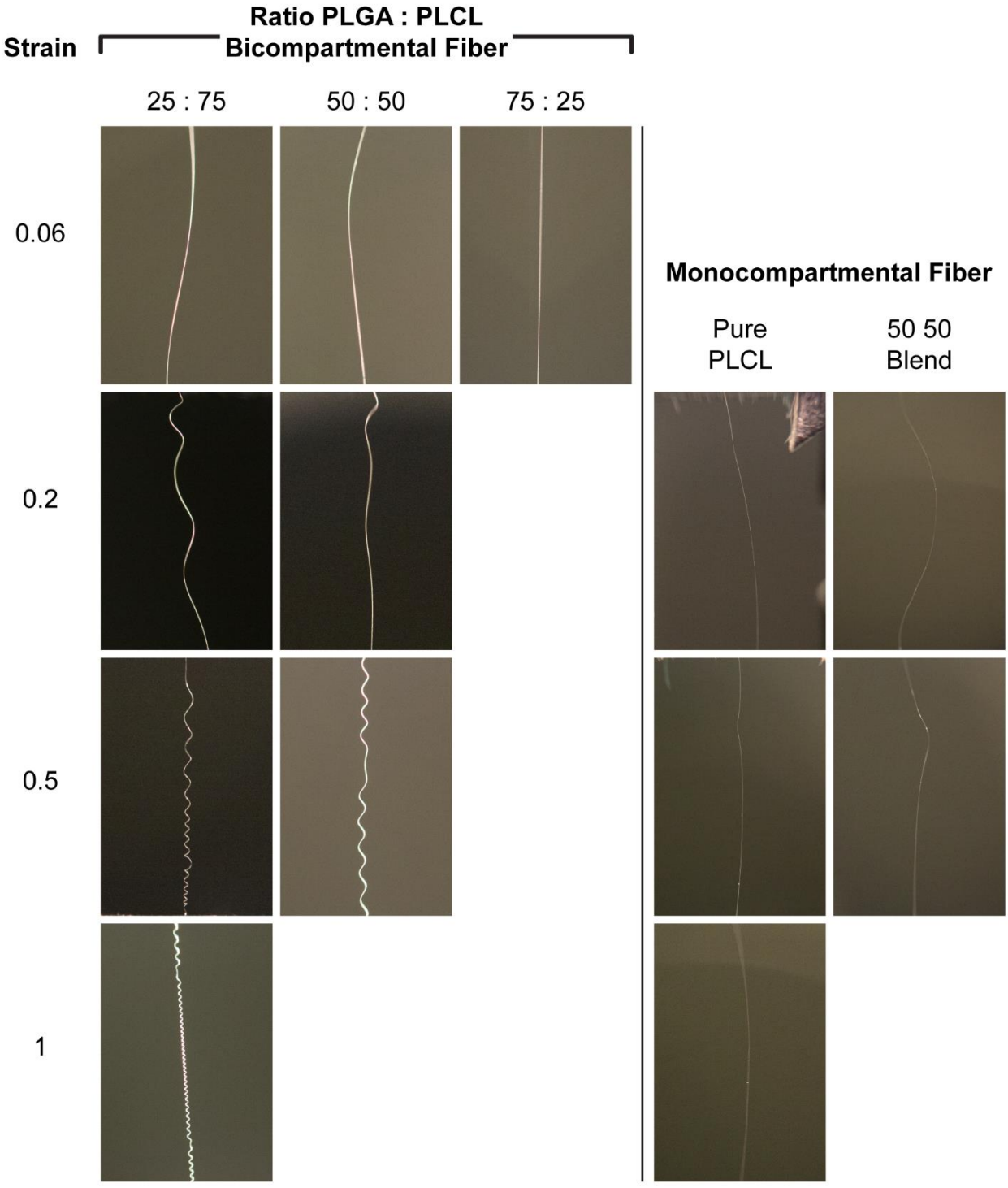

Figure 2-29: Bicompartmental fibers comprised of PLGA in one compartment and PLCL in the other tend to coil after stress-relaxation Bicompartmental fibers were

elongated to the indicated strain values. Compartmentalization was either 25:75, 50:50, or 75:25 PLGA to PLCL. Fibers at 75:25 PLGA to PLCL are too brittle to elongate to strains of 0.2 and above. 50:50 fibers break before reaching a strain of 1. *Image credit:* Stress relaxation and photography completed by Robert Stinson.

2.4 Conclusions and Implications

The advent of the manifold has greatly expanded our electrospinning capabilities for single fibers, fiber bundles, and 3D jet writing scaffolds. Previously EHD co-jetting or 3D jet writing of bicompartmental fibers, where each compartment consisted of a different material has often posed jet stability challenges. In solution electrospinning, solvents are mixed at an optimized ratio to most stably maintain a fiber jet of polymer solution. However, when co-jetting two different materials, in two different solvent systems side-by-side using two needles joined to form a spinneret, instabilities can occur that result in fibers of only one of the two materials, multiple fiber jets simultaneously, or the inability to find a single set of processing parameters effective for both solutions. As in the case of PLGA and PLCL, independently, PLGA requires much higher voltages than PLCL in order to generate fibers. One way around this difference would be to fine tune the solvent mixtures each polymer is dissolved within such that the net properties of the polymer and the solvent allow for electrospinning of each material at the same voltage. Such a highly-designed polymer solution would require extensive experimental iterations, or simulations of polymer-solvent interactions to determine the optimal solution properties including dielectric constant, volatility, and viscosity. A simpler approach to improving jet stability for two dissimilar polymer solutions in parallel is through the use of the manifold with a single needle as the outlet. As was shown for bicompartmental fiber scaffolds comprised of PLGA and PLCL, the disk manifold improved jet stability sufficiently to achieve fiber alignment in 3D jet writing scaffolds. Typically, a co-jet of these two materials results in an unstable jet and poor fiber alignment, leading to a scaffold that more closely resembles a non-woven mat than a 3D jet writing scaffold. With the

elimination of the metal partition between the two solutions, and the two-solution parallel flow through the outlet channel, the disk manifold reduced jet tendencies to split apart into two jets of the pure material.

Furthermore, it has been demonstrated that independently varying the flow rate of each solution pumping into the manifold enables control of the relative compartmentalization within the resultant fiber as follows from the conservation of mass. As polymer solutions fed into the Taylor cone flow into the fiber jet and depositing fiber, relative compartmentalization is conserved. A related phenomenon was reported on by Yoo *et al*. where flow rates were used to mediate the diameter of isotropic alginate fibers[75]. Previously, with the EHD co-jetting system, control of relative compartmentalization was limited to ratios that could be achieved by modulating the number of needles carrying one solution relative to the number of needles carrying another solution in a multi-needle spinneret where all needles were driven at the same flow rate. This meant only discrete compartment size ratios were feasible, and even this was limited by the number of needles that can be combined to form a spinneret without compromising jet stability. Now, the manifold allows for a continuous spectrum of relative compartmentalization where the known limit in resolution is that of the accuracy of the syringe pumps driving each solution flow; this applies not only to bicompartmental fibers, but to three and four compartment fibers, and theoretically could apply to a fiber having as many compartments as there are inlet feed channels on the manifold. Controlling the size of each compartment relative to all other compartment within single fibers, fiber bundles, or 3D jet writing scaffolds does not only mean modulating the bulk composition of the fiber. This capability can be extended to control (1) how much of a fiber surface is functionalized for follow up chemistries such as tethering of ligands onto only a portion of the fiber surface or (2) the rate of degradation of or release from one compartment relative to another

or (3) the presentation of biomolecules at the fiber surface that were directly electrospun into the bulk of the fiber compartment or (4) the mechanical properties of the fiber by co-jetting polymers, elastomers, or composites into variably sized fiber compartments.

Finally, the manifold was also designed to function in conjunction with the existing 3D jet writing technology. As shown, this allows for 3D jet writing scaffolds to be designed to incorporate domains of distinct composition. These domains may differ in bulk composition, surface functionality, loading and release of a drug or biomolecule of interest, degradation rates, and of course, relative compartmentalization, as shown moving through a gradient in **Figure 2-21**. Future work will entail demonstrating these capabilities, which includes expanding the library of materials that electrospin with sufficient stability to form fibers and 3D jet writing scaffolds. Additionally, producing 3D jet writing scaffolds with the current manifold technology is not as high throughput as it could be due to the sacrificial jetting time required to fully switch which feed solution is emitting from the spinneret. In future, this time can be reduced by using the syringe pump to retract the solution that is being switched out while ramping up the flow rate driving the incoming solution. Also, for each specific scaffold design, which syringe pumps are pumping or retracting at a given time, can be coordinated with the position of the x-y stage during both the pattering of the depositing fiber and sacrificial jet writing. The operation of the syringe pumps can be orchestrated with the movement of the x-y stage in order to observe the desired change in fiber composition or orientation at the desired position within the 3D jet writing scaffold. Through a computerized system such as Lab View, such orchestration can be automated, thereby requiring the same level of human interaction as in the 3D jet writing of isotropic scaffolds.

The implications of these manifold benefits are best realized in the field of tissue engineering and 3D cell culture. For example, different tissues are characterized by different

elasticities[19, 22, 46]. Tuning the stiffness of electrospun fibers is one parameter that can be matched in a tissue engineering scaffold to the tissue being recapitulated. Using fibers of tunable stiffness as a building block for 3D jet writing scaffolds allows for tuning of the scaffold stiffness. Control of relative compartmentalization and the fabrication of scaffolds with distinct domains embedded relates directly to the bioactivity and cell signaling properties of the scaffold. For instance, certain domains of the scaffold may be made to resist cell or protein binding by PEGylation to achieve spatially controlled cell or protein patterning in 3D. Or, certain domains of the scaffold can be made to present modalities either covalently bound to the surface or releasing from within the fiber bulk that induce a certain cell behavior in one area of the scaffold but induce another cell response in other areas. In futuristic thinking, perhaps this capability can be adapted to spatially pattern different lineage commitments to stem cells cultured on the same scaffold. Applied as a platform for 3D cell culture *in vitro* or as an implant for *in vivo* use, these highly engineered scaffolds give the researcher a strongly hands-on approach to experimental design where the defining parameters of the scaffold, and hence, the cell microenvironment are independently tunable. For instance, with this technology, the elastic modulus of the skeletal support underlying the cell microenvironment, i.e. the scaffold, can be varied without interfering with other environmental properties. At the same time, 3D jet writing scaffolds provide an open framework that allows cells to experience a hands-off environment where they are free to craft the niche as naturally as possible within an *in vitro* setting. The combination of 3D jet writing and the manifold allows for controlled deposition and patterning of distinct materials in three-dimensional space. The next step in translating our polymer scaffolds into a complete 3D cell culture platform is the addition of a native-like ECM which is explored further in Chapter 3.

Chapter 3
Supported Engineered Extracellular Matrices

Some material from this chapter has been adapted with permission from the following manuscript in preparation:

> S. Ramcharan, L. Solorio, S. McDermott, A. Fox, J.H. Jordahl, C. Dunlay, M. Brown, A. Xiao, M. Wicha, G.D. Luker, J. Lahann. "Engineered 3D cellular fibronectin networks serve as bioequivalent breast cancer tumor microenvironments for patient derived cells" *In Preparation*.

3.1 Introduction

3.1.1 Fibronectin and the extracellular matrix (ECM)

The extracellular matrix (ECM) is the insoluble, proteinaceous, non-cellular component of tissues[7, 76]. It provides a microenvironment for formation of interconnected 3D multicellular structures, and non-soluble signaling cues through dynamically modulated architecture, composition, and protein conformation[10, 77]. Such structural properties of the cell niche guide cellular organization, and provide extrinsic factors that influence cell behaviors such as migration, differentiation, and proliferation[6, 7, 19, 78, 79]. Trans-membrane molecules such as integrins directly bind the cell cytoskeleton to the ECM enabling transduction of environmental parameters into cell signals[7, 22, 46]. Integrins are comprised of α and β subunits which dictate the specific proteins a cell is able to interact with[80]; for instance, 20 known integrins bind to Fn with the most prominent being $\alpha_5\beta_1$ and $\alpha_V\beta_3$[23, 81]. Which integrins a protein can interact with depends, amongst other factors, on which binding sites are exposed and hence the conformation of the protein[81]. The cross

talk between cells and ECM proteins via integrins is bidirectional, meaning binding of the cell to the protein via integrins can lead to events within the cell, or alternatively, lead to restructuring of the protein to regulate its conformation and biological activity[80]. In addition to interacting with cells, an ECM protein may interact with itself, other proteins, growth factors and bacteria as indicated for Fn in **Figure 3-1**[76, 82]. Fn can interact with a number of proteins including collagen, heparin, fibrin, tenascin and decorin[9, 76, 80, 83, 84]. In fact, interactions with Fn is key to the assembly of many ECM proteins including fibrinogen and collagen I and III[3, 76]. As will be seen in Chapter 3, in addition to cell-ECM interactions, supported eECM with its open framework also enables visualization of protein-protein interactions, one of many possible routes for future applications.

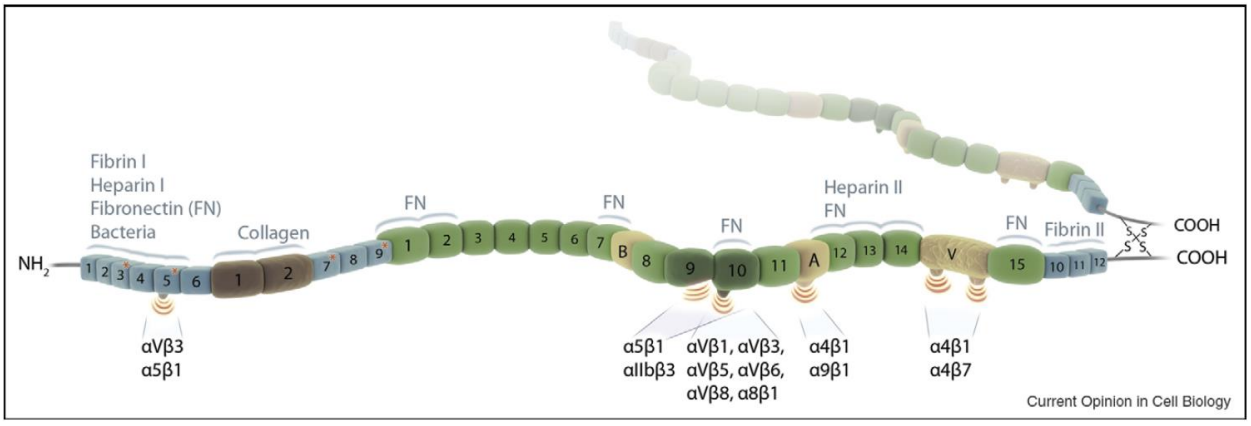

Figure 3-1: Structure and binding sites of fibronectin Leiss *et al*. depict the fibronectin (Fn) dimer distinguishing between the three repeat units, fibronectin-1 (FnI) in blue, fibronectin-2 (FnII) in brown, and fibronectin-3 (FnIII) in green. Two disulfide bonds form at the C-terminus. Sites along the protein that interact with integrins, bacteria, Fn itself, or other proteins are indicated. A, B, and V mark the alternatively spliced extradomains. [Illustration credited to Leiss *et al*.[3]]

Changes in ECM protein structure at molecular or cellular scales can drive biological function in both healthy and diseased states[6, 85]. For example, stiff, unfolded Fn is characteristic of breast tumor stroma and can promote tumorigenesis[85, 86] as well as epithelial to mesenchymal transitions (EMT)[87]. *In vivo*, Fn exists either as (1) a soluble, compact plasma protein (plasma Fn, pFn) typically found at high concentration of ~ 0.3 mg/mL or (2) a detergent-insoluble, extended ECM protein known as cellular fibronectin (cellular Fn, cFn) that exposes cryptic binding domains

not available in pFn[76, 77, 83, 85, 88, 89]. Fn can take on up to 20 different isoforms in humans[90], impacting integrin binding activity and specificity that drive differential cell responses or protein-protein interactions[13, 14, 85]. Although cFn is found in many isoforms, the mechano-sensitive fibronectin-3 domain (FnIII) is consistently exposed, which promotes conversion of the protein into fibrils and ECM assembly[10, 11]. To assemble cFn, cells activate the protein mechanically by translocation of Fn-bound integrins on the cell surface, imparting tension to unfold FnIII. This exposes self-association sites within the protein that mediate Fn-Fn intermolecular interactions which lead to fibrillogenesis[10, 11, 13, 77, 89] (**Fig. 3-2**). Detailed mechanisms underlying Fn fibril assembly and detergent-insolubility are still lacking in the literature[4, 91]. The linkages between

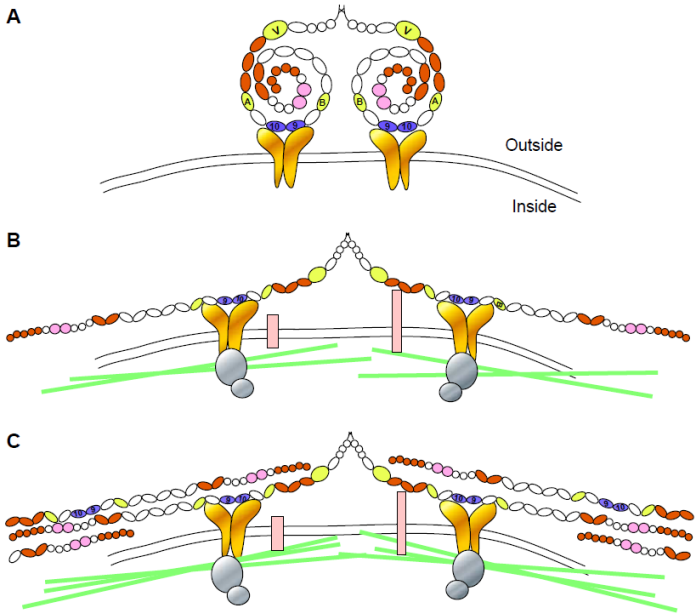

Figure 3-2: Cell-mediated fibronectin fibrillogenesis Mao *et al.* describe the cell-mediated assembly of fibronectin matrix in three steps. The first, shown in (a), is the binding of a solubilized Fn dimer to integrins at the cell surface shown in gold. The red subunits represent self-association sites that mediate Fn intermolecular interactions. The cytoskeleton represented by green lines in (b) begin to reorganize such that the translocation of the integrins at the cell surface imparts tension to the bound Fn dimer causing the protein to unfold and expose the self-association sites. At the same time, signaling activities commence within the cell as a result of its attachment to Fn (represented by silver circles). (c) As neighboring Fn molecules approach the unfolded integrin bound Fn, intermolecular interactions facilitate the assembly of a Fn matrix. [Illustration credited to Mao *et al.*[4]]

individual Fn dimers to form large multimeric structures may be due to covalent disulfide bond formation[92-94] or non-covalent but stable intermolecular forces[95]. In the non-covalent case, partial beta sheet unfolding within FnIII has been seen to promote Fn self-polymerization suggesting the possibility that intermolecular beta sheet formation stabilizes Fn matrix and renders it detergent-insoluble[96]. Although pFn can be assembled into fibrils as in thrombus growth in the case of injury, intramolecular interactions maintain pFn in a soluble form in blood to prevent fibrillar formation and blockage[97-99]. Still, much of the cFn found in ECM originated as pFn[100] as did the cFn networks described in Chapter 3.

Fn (440 kDa) has been observed in its extended form to have a contour length of 120 to 160 nm and an average diameter of 2 nm[101]. Once in an extended fibrillar state, cFn fibrils are initially about 5 nm in diameter, and later cluster to form bundles about 25 nm in diameter[102, 103] though the cFn matrix is continuously remodeled by cells[104]. Fn is a dimeric molecule comprised of distinct repeated domains referred to as fibronectin-1 (FnI), fibronectin-2 (FnII) (**Fig. 3-1**), and the previously mentioned FnIII which can be arranged in tandem within the same molecule and includes the commonly used cell binding domain arginine-glycine-aspartic acid or RGD[83, 105, 106]. FnI and FnII serve to encapsulate the hydrophobic core of the Fn molecule which is exposed when FnIII is unfolded[4, 77, 102]. Certain subunits of FnI and FnIII are known to play a role in fibrillogenesis[4, 107, 108]. However, FnIII in particular is responsible for the extensibility of Fn, as it can be reversibly extended from a folded length of about 4 nm to 29 nm (7-fold extension). Such unfolding takes a theoretical 3.5 to 5 pN of force which is in reasonable range of the force generated by a single kinesin or myosin molecule within a cell[106].

Beyond fibronectin, there are numerous ECM proteins, each making its own contribution to the cell niche, either independently or in concert with other proteins. Different ECM protein

compositions characterize different tissues or disease states[7, 15], making composition control of major importance when designing a versatile *in vitro* cell microenvironment. Contactins, for instance, are strictly found in the nervous system[109]. More common proteins include vitronectin, elastin, osteopontin, thrombospondin, fibrinogen, tenascin, laminin, and collagen[7, 110-112] of which the latter three are explored further in Chapter 3. Although all collagens take the form of a triple helix, there are a number of different types of collagen (types I-III, V, IX, XI, XII, XIV, XVI, XIX- XXII, XXIV and XXVII) that take on different higher order structures as it relates to the molecule serving distinct biological purposes[112]. Collagens I – III are the major fibrillar collagens and are the foundation of connective tissue in mammals[80, 112]; collagen I isolated from rat tails is of focus in Chapter 3 as it is the most significant and abundant[80]. In addition to fibronectin, laminin is one of the most studied noncollagenous ECM glycoproteins, is strictly found in basement membrane, and is a major component of the widely used cell culture medium, Matrigel[9, 60]. Tenascin, on the other hand, and tenascin-C in particular, is a more specialty protein, being most well-known for its role during certain stages of development, and in mediating the effects of other ECM proteins on cell responses such as adhesion and differentiation[9].

3.1.2 Protein adsorption

The spontaneous adsorption of whole proteins to a surface prior to cell culture is a common attempt to present cells with signaling and cell adhesion moieties. Whole proteins are advantageous over peptides alone having more active sites and being susceptible to proteolysis[6]. Establishing a uniform layer of adsorbed protein on 3D scaffolds or 2D surfaces involves a number of different parameters which influence the interactions between the protein and the solvent it is dissolved in, the protein and the solid substrate, and the solvent and the substrate. Whether or not a protein will adsorb to the substrate, remain adsorbed or re-enter solution, or undergo a change in

conformation either in the adsorbed or solvated state depends on these interactions which can include van der Waals forces, hydrogen bonding, hydrophobic and electrostatic interactions.[113, 114] Environmental conditions, contact time, protein solution concentration, and the properties of the protein, solvent, and substrate dictate which interactions are dominant and determine the resulting adsorbed protein morphology, adhesion strength, and the amount, density, and orientation of adsorbed proteins[113-115]. Such characteristics of the protein coat are critical since changes in protein conformation or steric hindrance could lead to denaturation or make binding sites inaccessible[114, 115]. Despite the controls afforded by process conditions, proteins adsorbed onto a solid 2D substrate are not well-suited for cell culture applications due to a lack of porosity and extremely high Young's moduli compared to physiological conditions[66]. Instead, in Chapter 3, a hydrodynamic process is innovated for the free suspension of whole proteins across and within the open pores of polymer supports fabricated by 3D jet writing. Various contact times, incubation temperatures, protein solution concentrations, and fluid-flow patterns were iterated in development of this technology.

In general, the interior of the protein tends to host hydrophobic domains while hydrophilic domains are found on the exterior[116]. Longer contact time is preferred to allow proteins to move interior hydrophobic domains to the exterior for enhanced protein adhesive forces[113, 115]. Longer times also allow the protein coated substrate to reach an equilibrium state; protein adsorption can be reversible although the protein may not necessarily return to its original conformation[115]. Such reversibility implies that the protein solution concentration is another driving force in adsorption. Nakanishi *et al*. report that lower concentrations show no major impact on adsorbed protein conformation. This remains true at higher concentrations initially, but at longer times, a second round of proteins which have undergone conformational change may replace the first round of

weakly adsorbed proteins[115]. This idea is similar to the Vroman effect where smaller proteins rapidly diffuse and adsorb to the surface but are later replaced by larger proteins with more potential binding sites and a stronger binding affinity[116]. Allowing proteins time to unfold increases the molecular footprint and hence, the adhesion strength. Nakanishi *et al*. also state that higher temperature generally favors larger amounts of adsorbed proteins[115] which is probably due to enhanced protein flexibility enabling the protein to make the conformational changes necessary for adsorption. Hence, in developing a process to suspend proteins across a porous 3D scaffold, higher solution concentration, longer contact time, higher temperature, and incubation under convective fluid flow are preferred in order to maximize the amount of adsorbed protein, and ensure that the protein morphology and conformation has equilibrated prior to the introduction of cells.

3.1.3 Cell-free fibronectin fibrillogenesis

When cells form fibrillar cFn matrix *in vivo*, the protein is first put under mechanical tension, which stretches the protein and exposes self-association sites that facilitate the intermolecular interactions necessary for fibrillogenesis. *In vitro*, a range of different stimuli including electrical, chemical, mechanical and interfacially active denaturants have been used to expose the same self-association sites needed to form Fn fibrils from pFn without the use of cells[77, 117-119]. For example, the drawing of fibers by skimming a pointed tip across the surface of a pFn solution[12, 120], or formation of Fn fiber mats about the shaft of a stirrer at the air-pFn solution interface[120].

Interestingly, in both these examples, fibrillogenesis occurs at a three-phase interface of air, pFn solution, and a solid object. In fact, Fn has been shown to accumulate as a sheet of soluble protein at the air-solution interface[13]. Forcing the interface through a micropillared substrate

resulted in insoluble fibronectin fibrils suspended within the interpillar space[13]. In this sheet-to-fiber transition, shear force serves as a protein denaturant, exposing the binding sites responsible for the Fn-Fn interactions that facilitate fibrillogenesis[14]. We sought to take a similar approach to engineering networks of Fn fibrils. Because of the reversibility of the FnIII domain unfolding[121], a heterogeneous interface containing a scaffold support was required where extended fibronectin fibrils could be permanently secured for the time-scales of a cell culture experiment (**Fig. 3-3**). Interfacial forces at the air-water interface induce pFn deformation which facilitates self-association amongst protein molecules[13, 14]. The scaffold will then promote intermolecular interactions between partially unfolded protein molecules by locally confining the protein within the pores. Additionally, the large open pores minimize denaturation of the protein due to contact with synthetic surfaces, maximizing the likelihood that the deposited protein remains in a native, biologically active conformation[12]. While being comprised of minimal synthetic material, the ideal scaffold must maintain mechanical integrity both at ambient and cell incubation conditions.

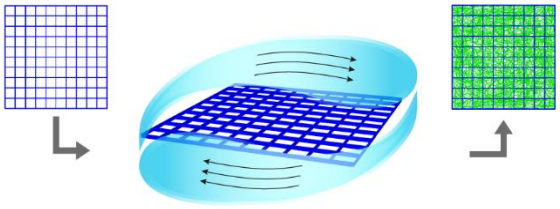

Figure 3-3: Hydrodynamically induced fibronectin fibrillogenesis Schematic illustrating the process of hydrodynamically induced fibronectin fibrillogenesis. A membrane or textured substrate, represented by a blue grid, is secured at the interface of a three-phase system with air and a solution of plasma fibronectin. Although a variety of membranes or substrates can provide the solid support needed to create supported engineered cFn (ecFn), 3D jet writing scaffolds are of focus. As the scaffold is exposed to repeated shearing of the air-solution interface (achieved using a rotisserie rotator), fibrils of fibronectin suspend across the scaffold pores resulting in the final product, a network of cFn fibrils termed supported ecFn.

Such a scaffold is best achieved by poly(lactide-co-glycolide) (PLGA) microfiber constructs fabricated by 3D jet writing[48]. 3D jet writing scaffolds consist of approximately 4% material by volume while ensuring structural integrity. Scaffold size and geometries are tunable,

but those reported here are 5.8 mm by 6 mm, made by stacks of ten fibers (8-12 μm in diameter), patterned into a grid array of square pores 500 μm wide unless otherwise noted. Each pore offers large open areas that can contain upwards of 35,000 cells, allowing cells to secrete their own ECM and form multicellular structures, while limiting interference from synthetic material on cell behavior and protein conformation. Although the biodegradable PLGA scaffolds fabricated by 3D jet writing are most optimal and of focus throughout this dissertation, the technique described in Chapter 3 for cell-free formation of supported engineered ECM (eECM) is versatile and can be applied to any roughed, textured, or porous substrate or membrane.

3.2 Materials and Methods

3.2.1 Materials

Human fibronectin (Corning, Corning, NY), rat tail Collagen Type I (Corning, Corning, NY), mouse laminin (Life Technologies, Carlsbad, CA), Dulbelco's Modified Eagle Medium (DMEM), non-essential amino acids (NEAA), antibiotic-antimycotic, Micro-BCA kit, anti-cellular fibronectin clone FnIII (Abcam, Cambridge, MA), and Dubelco's Phosphate Buffered Saline (DPBS) were obtained from Fisher Scientific and used as received. Siliconized low-retention microcentrifuge tubes by Biotix were purchased from VWR. Stainless steel frames were custom fabricated by Microphoto, Inc. (Roseville, MI).

3.2.2 Formation of supported eECM

A 3D jet writing scaffold was first secured in a custom-made stainless-steel frame. The framed scaffold was then placed at the center of a 2-mL microcentrifuge tube containing 900 μL volume of a 110 μg/mL solution of human fibronectin such that the air, scaffold, and solution formed a three-phase interface when the tube was laid on its side. The tube was placed on a rotisserie rotator at 30°C and 8 rpm (for an interface velocity of 10.4 mm/s) for a period of 2 h.

The protein-loaded scaffold was then washed 3 times in DPBS and stored at 4°C up to one week until use. The same process was applied for laminin at a temperature of 26ºC and concentration of 400 µg/mL. For collagen, 900 µL of collagen I dissolved in 33 mM acetic acid at 2.7 mg/mL was combined with 100 µL of DMEM and 140 µL of 0.34 N NaOH in a 2-mL microcentrifuge tube. The solution should turn from yellow to pink with the addition of base. All collagen preparations were performed on ice. The framed scaffold was then secured in the 2-mL tube to form a three-phase interface and rotated for four hours at 27ºC. See Appendix C for detailed protocols.

3.2.3 Characterization of supported eECM

Proteins were fluorescently labelled using standard primary and secondary antibody staining protocols, and were imaged using a Nikon A-1 confocal microscope (Nikon Corp., Minato, Tokyo, Japan). SEM micrographs were taken with a Helios 650 Nanolab SEM/FIB by FEI of Thermo Fisher Scientific at voltages ranging from 2 to 5 kV. Prior to SEM, samples of cells or proteins were dehydrated by soaking for 20 minutes in a series of ethanol solutions increasing in concentration. The sample was then transferred to a microcentrifuge tube and tertbutanol was added to cover. The tube was placed in liquid nitrogen for two minutes then lyophilized overnight. (See Appendix B for detailed protocol.) A µBCA assay (Pierce Biotechnology, Rockford, IL) was used to measure the mass of protein deposited onto the scaffolds. First, the PLGA was degraded in a 0.9 M NaOH solution for 1 h, and then the solution was neutralized in a 0.9 M HCl solution. The mass of protein was determined by measuring the absorption at 562 nm after a 1 h, 60°C incubation, in the µBCA working reagent and referenced to a standard curve of known masses.

3.2.4 Culturing cells on supported eECM

The desired number of cells to be seeded were suspended in a 100 µL droplet and carefully pipetted onto the supported eECM within a 24-well plate. The plate was placed in an incubator at

37ºC and 5% CO_2 for four hours for cell adhesion. Cell media was then added for a final volume of 1 mL followed by an overnight incubation. The supported eECM, now seeded with cells, was transferred to a clean well with 1 mL of media for the remainder of the culture time. Immunohistochemical analysis was performed as previously described[48]. Briefly, cells on the supported eECM were fixed with a 2% paraformaldehyde overnight. Cells were then permeabilized with a 0.1% Triton X-100 solution for 5 minutes. The fixed cells were then exposed to a 5% BSA blocking solution for 1 h before application of the antibodies. Cells were imaged using a Nikon A-1 confocal microscope (Nikon Corp., Minato, Tokyo, Japan).

If cells were removed from supported cFn networks to visualize the remaining protein matrix, samples were decellularized in a protocol adapted from Lu *et al.*[122]. Samples were washed with PBS, then DI water, and immersed in a solution of 0.1% Triton X-100 with 1.5 M KCl in 50 mM Tris buffer at 4ºC on a slow-moving shaker for two hours. Samples were washed in 10 mM Tris buffer, followed by DI water for one hour each. See Appendix A for detailed protocol.

3.3 Results and Discussion

3.3.1 Developing and characterizing supported eECM

Adherent cells must anchor to the insoluble proteinaceous environment surrounding them to survive requiring cell binding sites when culturing cells on synthetic material[6, 46, 115]. Laminin, collagen I and IV, and fibronectin are major ECM proteins[37, 115] which each contain recognition sites or particular peptide sequences such as arginine-glycine-aspartic acid (RGD) that cells are able to bind to through integrin receptors[7]. This phenomenon was seen in an early attempt to adsorb fibronectin and laminin onto the PLGA microfiber scaffolds fabricated by 3D jet writing. These polymer scaffolds either contained no protein, fibronectin, laminin, or a 1:1 ratio of both, and were subsequently seeded with cells expressing green fluorescent protein (GFP). As shown in **Figure**

3-4, polymer scaffolds on their own did not facilitate cell adhesion, but cell adhesion was observed on the first day to the fourth and last day of culture for polymer scaffolds with fibronectin and/or laminin. This confirms the need to incorporate protein elements into the synthetic polymer scaffold in order to create an *in vitro* 3D cell culture model.

Although systems exist in the literature that incorporate specific peptide binding sequences into a polymeric support, we chose instead to focus on whole ECM proteins. Many cells are able to remodel the ECM through proteolysis and secretion of new proteins[6, 19, 22, 123]. Incorporating whole ECM proteins onto the polymer scaffolds would give cells the freedom to customize the protein environment in contrast to peptide sequences which are less susceptible to proteolysis and remodeling. However, simply adsorbing whole proteins to the surface of the scaffold is a poor mimic of native ECM morphology, which is characterized by more fibrillar or spongy structures of interconnected pores. Building on previous studies demonstrating cell-free fibrillogenesis, several experimental conditions governing the hydrodynamically induced fibrillogenesis sketched in **Figure 3-3** were tested to find the most optimal process. Using fibronectin, the effect of contact time, temperature, protein solution concentration, and static versus dynamic incubation conditions were examined for the formation of a web-like network of protein suspended across and within the scaffold pores. However, the mode of fluid flow proved to be the most crucial to achieving complete coverage of the scaffold with fibrillar protein networks (**Fig. 3-5**). Two modes of fluid flow were employed during incubation, orbital shaking (**Fig. 3-5(a)**) and rotisserie rotation (**Fig. 3-5(b)**) at for either 2 hours or 24 hours. Rotisserie rotation consistently resulted in more uniform protein networks across the open pores of the polymer scaffold. This result further confirms the criticality of the three-phase interface in hydrodynamically induced fibrillogenesis of Fn. In orbital shaking, the scaffold is first entirely submerged within the bulk pFn solution in a well-plate. As

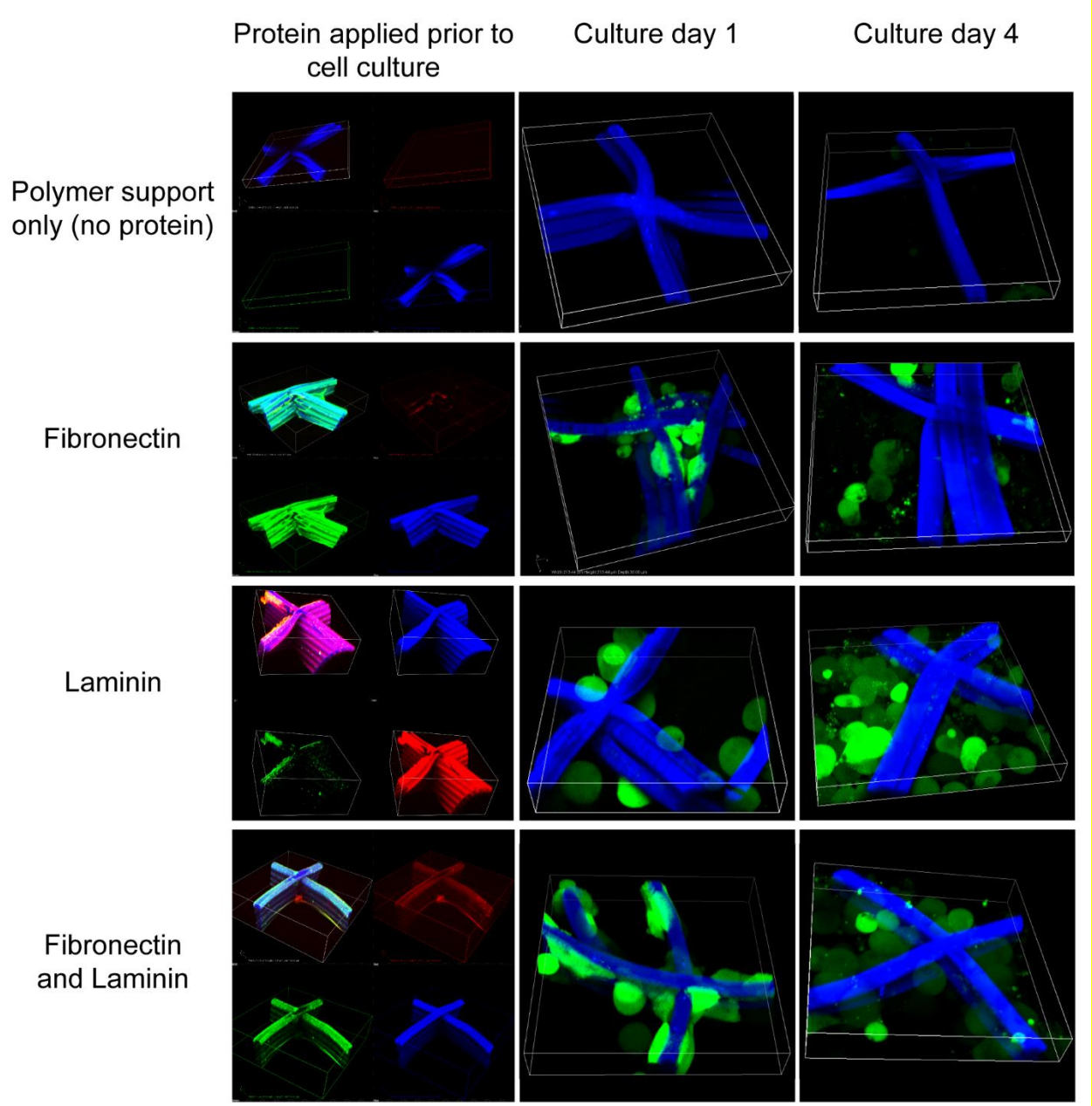

Figure 3-4: Protein is required for cell adhesion to polymer scaffolds The first column verifies the adsorption of fibronectin (green), and/or laminin (red) onto the surface of the polymer scaffold (blue) prior to the seeding of cells. The second column shows GFP expressing cells (green) adhered to the polymer scaffolds (blue) only when containing protein whether it is fibronectin alone, laminin alone, or a 50:50 mixture of both after only one day of culture time. The third column shows the same scaffolds in culture with the GFP expressing cells adhered to the polymer scaffolds after four days of culture. Note that in the second and third columns, the protein was not stained for and is therefore not visible in the LSCM images. The length and width of each 3D volume bounding box is 213.44 µm.

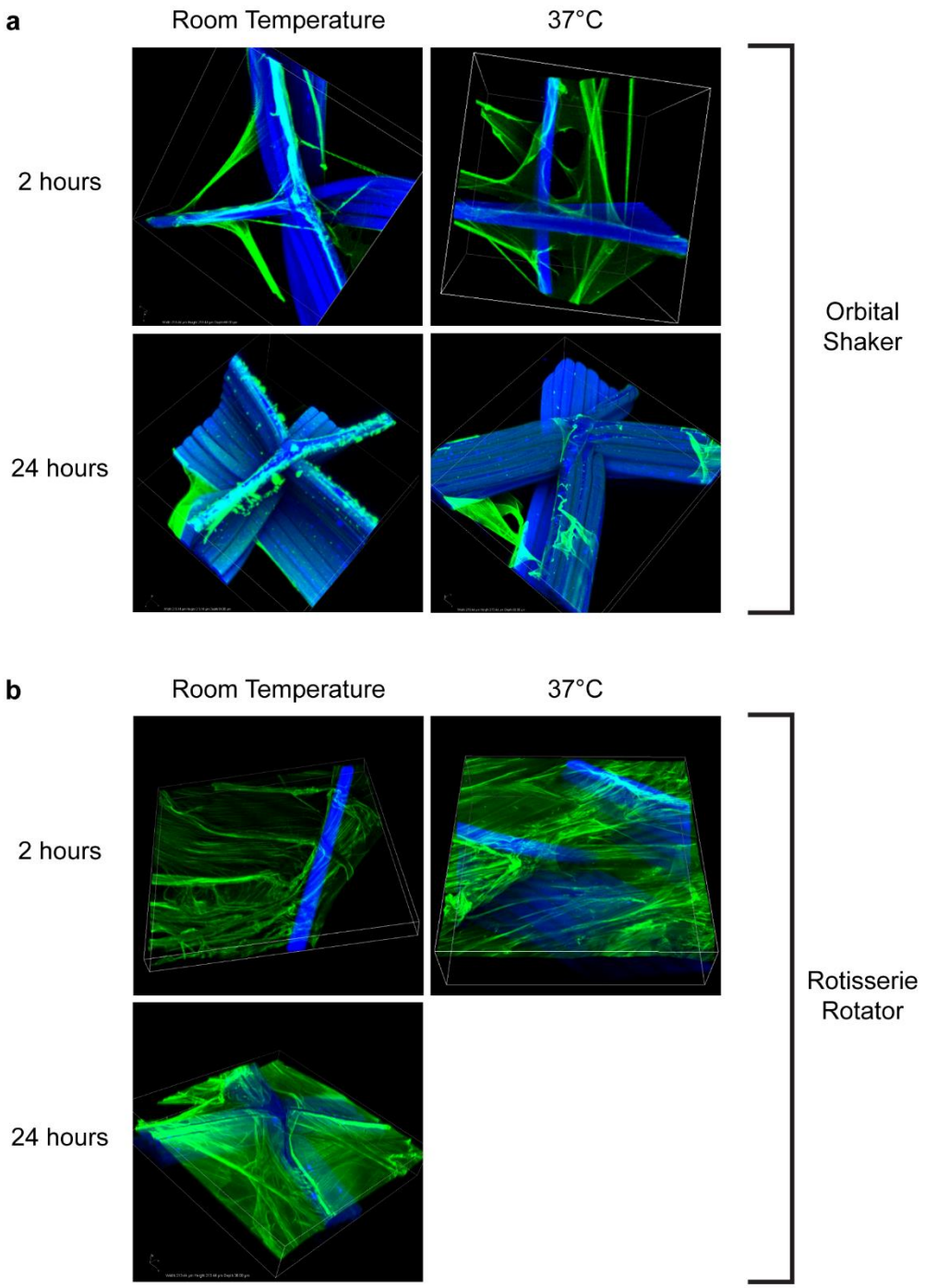

Figure 3-5: Determining optimal conditions to achieve hydrodynamically induced fibrillogenesis (a) Representative sections of the polymer scaffold (blue) and tethered fibronectin (green) show some fibril formation using an orbital shaker to create fluid flow during either a 2 hour or 24 hour incubation at either room temperature or 37ºC. (b) Webs of fibronectin fibrils (green) are far more apparent using a rotisserie rotator compared to the orbital shaking motion as a means of fluid flow during either a 2 hour or 24 hour incubation of the polymer scaffold (blue) in fibronectin solution. Little to no difference was observed with respect to the protein network at either room temperature or 37ºC. (a-b) 3D volume bounding box in all images is a square of length 213.44 µm.

movement commences, the fluid is circled around the well while the scaffold remains submerged. At sufficiently high orbit speeds, the air-pFn solution interface may form on the scaffold as fluid is centripetally thrusted to the outer edges of the round well. In these instances, a three-phase contact line is formed with the scaffold, air, and the pFn solution; it is most likely that in these instances some fibrils of Fn are observed on the resulting scaffold. In contrast, the rotisserie rotator consistently shears the air-pFn solution interface along the scaffold from on end to the next repeatedly during the course of the incubation time. As shown in **Figure 3-5**, the rotisserie rotator results in far fuller coverage of the Fn fibrils across the scaffold, further evidencing the integrality of the three-phase interface in hydrodynamically induced fibrillogenesis. Continuing with rotisserie rotation as the mode of fluid flow, and given that longer time and warmer temperatures promote stronger protein adhesion and allow establishment of an adsorption equilibrium, we attempted protein network formation for 24 hours but at 30ºC. The lower temperature was preferred to keep the PLGA scaffold well below the reported bulk glass transition temperature of 45-50ºC (Sigma-Aldrich). This penultimate iteration, shown in **Figure 3-6**, resulted in extensive

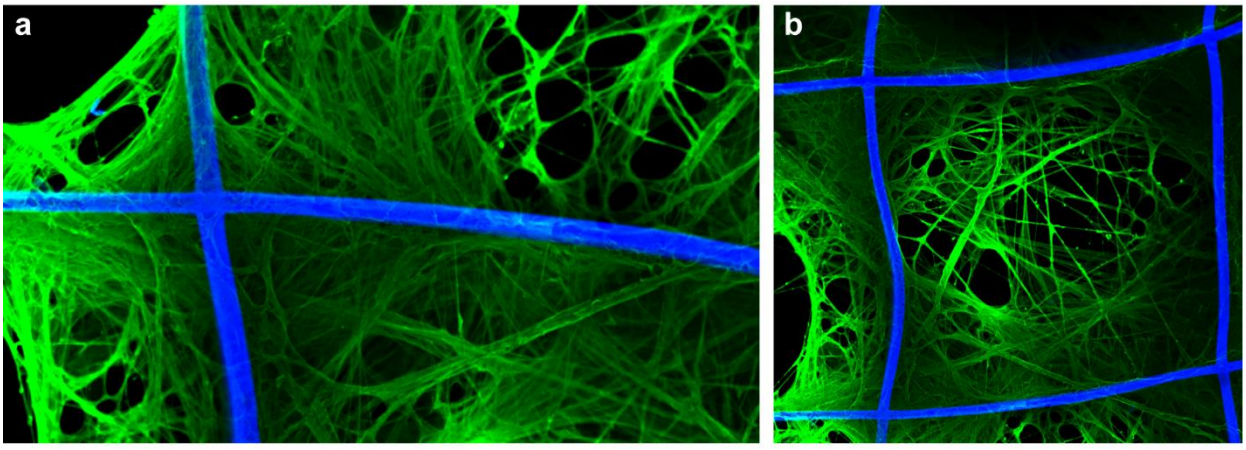

Figure 3-6: Optimal fluid motion and temperature determined as rotisserie rotation at 30ºC Prior to this time optimal conditions were two hours of incubation under rotisserie rotation at 37ºC. However, extensive fibrillar networks of Fn (green) resulted at 30ºC. This lower temperature was preferred to keep the PLGA scaffold (blue), well below the glass transition temperature of 45-50ºC.

engineered cFn networks (**Fig. 3-6(a)**) that spanned across entire 500 µm wide square pores of the polymer scaffold (**Fig. 3-6(b)**). Optimal pFn solution concentration was found to be 100 µg/mL (data not shown).

Although the process conditions used to achieve the supported eECM shown in **Figure 3-6** suffice for formation of uniform fibrillar webs of protein, it was unknown whether 24 hours of incubation time was necessary. To understand the amount of time required to reach an equilibrium in regards to protein loading onto the scaffold, the hydrodynamically induced fibrillogenesis process was run for 15, 30, 60, 120, and 240 minutes. **Figure 3-7(a)** shows that after 15 minutes of hydrodynamic shearing at the three-phase interface at 30ºC, networks of insoluble cFn fibrils had freely-suspended across the entire polymer scaffold. With increasing time, the mass of protein loaded onto the scaffold increased until 120 minutes as shown by the plateau in the curve in **Figure 3-7(c)**. Submerging the scaffold in pFn-solution of the same concentration and temperature for the same length of time (two hours) but without fluid flow resulted in a conformal coating as this technique lacks hydrodynamic shearing and the three-phase interface (**Fig. 3-7(b)**). Relative to statically adsorbed Fn, the supported ecFn contained at least 12 times more protein irrespective of scaffold pore size (**Fig. 3-7(d)**). Supported ecFn consistently spanned across and within the entire area of the scaffold at a large scale of 5.8 by 6 mm. Supported ecFn was formed using a pFn solution at 0.11 mg/mL, in contrast to hydrogel matrices that take much higher concentrations: 1-5 mg/mL of protein[111]. The ability to prepare supported eECM of various shapes and sizes enhances the versatility of this technology whether as an *in vitro* scaffold in a specific cell culture chamber or well plate, or to fit a certain shape or sized defect for tissue regeneration. Furthermore, pore sizes were found not to influence the hydrodynamically induced fibrillogenesis process, leaving scaffold pore size as another degree of freedom for rational supported eECM design (**Fig.**

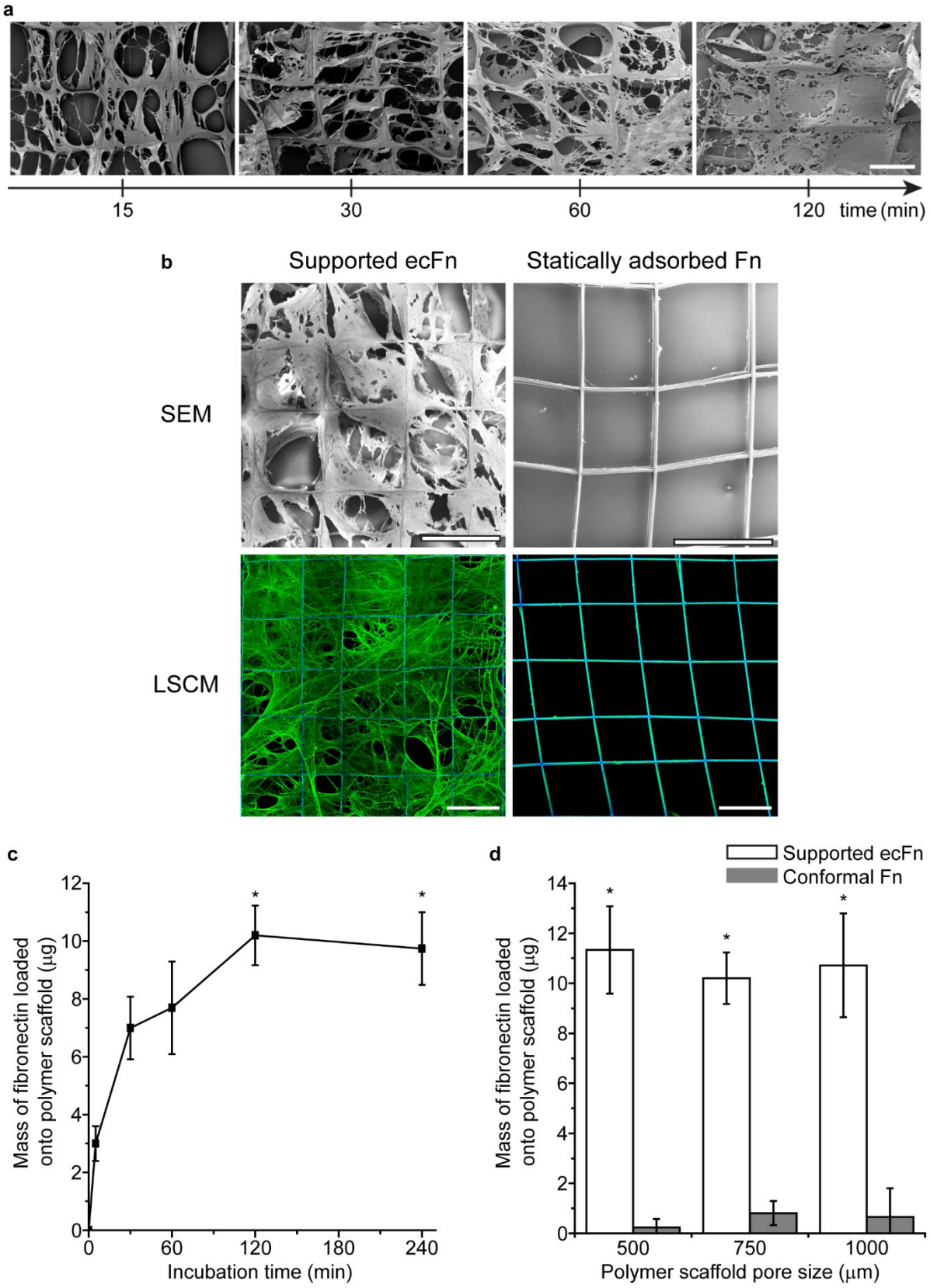

Figure 3-7: Dynamic incubation conditions are necessary for hydrodynamically induced fibrillogenesis (a) Time sequence characterized by SEM showing increasing

amounts of Fn tethered to the polymer scaffold with time. (b) SEM and LSCM images showing large scale view of supported ecFn *(left)* produced by hydrodynamically induced fibrillogenesis in contrast to *(right)* the scaffold after a static incubation in pFn solution. The solution concentration, incubation time, and temperature are consistent between the supported ecFn and the statically adsorbed Fn at 100 μg/mL, 2 hours, and 30ºC. Fluorescence images show Fn in the green channel and the polymer scaffold in blue. (a-b) Note defects in SEM images may be due to the dehydration process which occurs during SEM sample preparation. (c) Quantification of the mass of Fn loaded onto the polymer scaffold under hydrodynamically induced fibrillogenesis indicating that equilibrium is reached after 120 minutes, i.e. max protein loading is achieved after two hours. These time points correlate to the images shown in *(a)*. (d) Mass of protein loaded onto polymer scaffold is at least 12 times higher for supported ecFn (white bars) compared to the conformal coating (grey bars) that results from a static incubation of the polymer scaffold in pFn solution of the same concentration, for the same amount of time, and at the same temperature. Moreover, mass loading onto the scaffold is not a function of pore size. (c-d) Quantification of protein mass conducted by μBCA assay.

3-7(d)). Varying pore sizes will impact the mechanical environment cells experience when cultured on a supported eECM.

The support used in this study is a poly(lactide-co-glycolide) (PLGA) microfiber scaffold fabricated by 3D jet writing[48], consisting of approximately 4% material by volume[48]. While 3D jet writing affords widely tunable scaffold sizes and geometries, all scaffold used in this study fit an area of 34.8 mm^2 and were comprised of ten stacked fibers (fiber diameter: 8-12 μm) (as was shown in **Fig. 2-2**). The large open pores ensure mild denaturation of the protein due to limited contact with synthetic surfaces, maximizing the likelihood that the deposited protein remains in a biologically active state[12]. In addition, the scaffold maintains mechanical integrity both at ambient and cell incubation conditions. However, to verify that the hydrodynamically induced fibrillogenesis process is not limited to 3D jet writing scaffolds, mesh screening that was also of a porous grid pattern geometry was exposed to the same process. Although this study was performed prior to the final optimization of the hydrodynamically induced fibrillogenesis process conditions, the result clearly shows a webbed protein morphology resulting from hydrodynamic shearing at the three-phase contact line as opposed to a conformal coating produced by static submersion of the mesh in a pFn solution (**Fig. 3-8**). This confirms that the technique is not limited to 3D jet

writing scaffolds and further reinforces the requirement of hydrodynamic shearing of the three-phase contact line formed by the solid support, air or perhaps another hydrophobic medium such as oil, and the aqueous pFn solution.

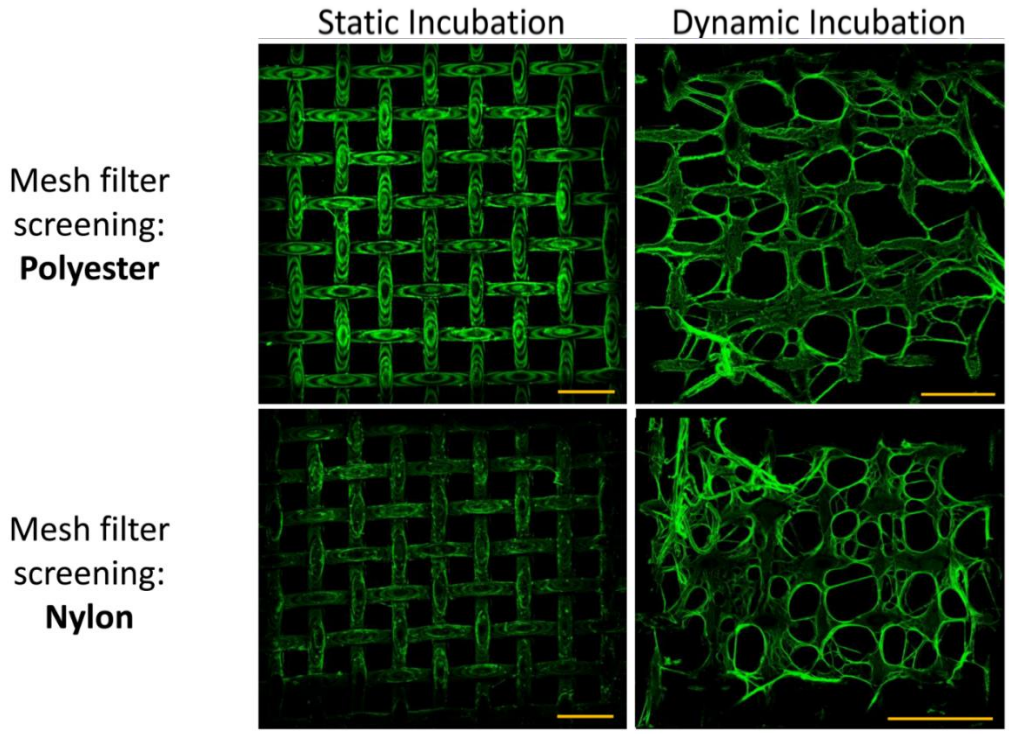

Figure 3-8: Hydrodynamically induced fibrillogenesis is not limited to 3D jet writing scaffolds Mesh screening made of either polyester or nylon were exposed either to static incubation in pFn solution or the hydrodynamically induced fibrillogenesis process (dynamic incubation). In contrast to 3D jet writing scaffolds characterized by square pores 500 μm wide with a wall diameter of 8-12 μm and an open area greater than 95%, the polyester mesh screening had square pore openings of 530 μm, wall diameter of 220 μm, and an open area of 50%, and the nylon mesh screening carried square gap openings of 500 μm, wall diameter of 225 μm, and an open area of 47%. Still, results are consistent with *Fig. 3-6(b)* indicating that whether the support is a 3D jet writing scaffold, polyester mesh or nylon mesh screening, static incubation results only in a conformal coating of Fn whereas supported ecFn require hydrodynamic shearing. Scale bars 1000 μm. Note this study was conducted prior to final optimization of the process conditions for hydrodynamically induced fibrillogenesis.

To further understand the criteria of substrates or membranes that can be applied as a support in the hydrodynamically induced fibrillogenesis process, and as a further control experiment, tissue culture polystyrene (TCPS) was exposed to three-phase hydrodynamic shearing, or static incubation in pFn-solution, both resulting in conformally adsorbed protein (**Fig.**

3-9(a-b)). This suggests that either porosity or topographical features are necessary to locally confine the protein, promoting intermolecular interactions as FnIII domains unfold under tension. To represent a non-porous but textured substrate, TCPS was roughed with sand paper to produce the surface shown in **Figure 3-9**. Roughened TCPS, although non-porous, was able to facilitate fibrillogenesis, forming networks of protein, but with a more sheet-like morphology (**Fig. 3-9(c)**) relative to 3D jet writing scaffolds (**Fig. 3-9(d)**). These results indicate that porosity is not necessary to draw cFn fibrils from pFn solution, but rather a non-smooth topography such as surface roughness is needed to nucleate the formation of cFn networks. Additionally, the stark

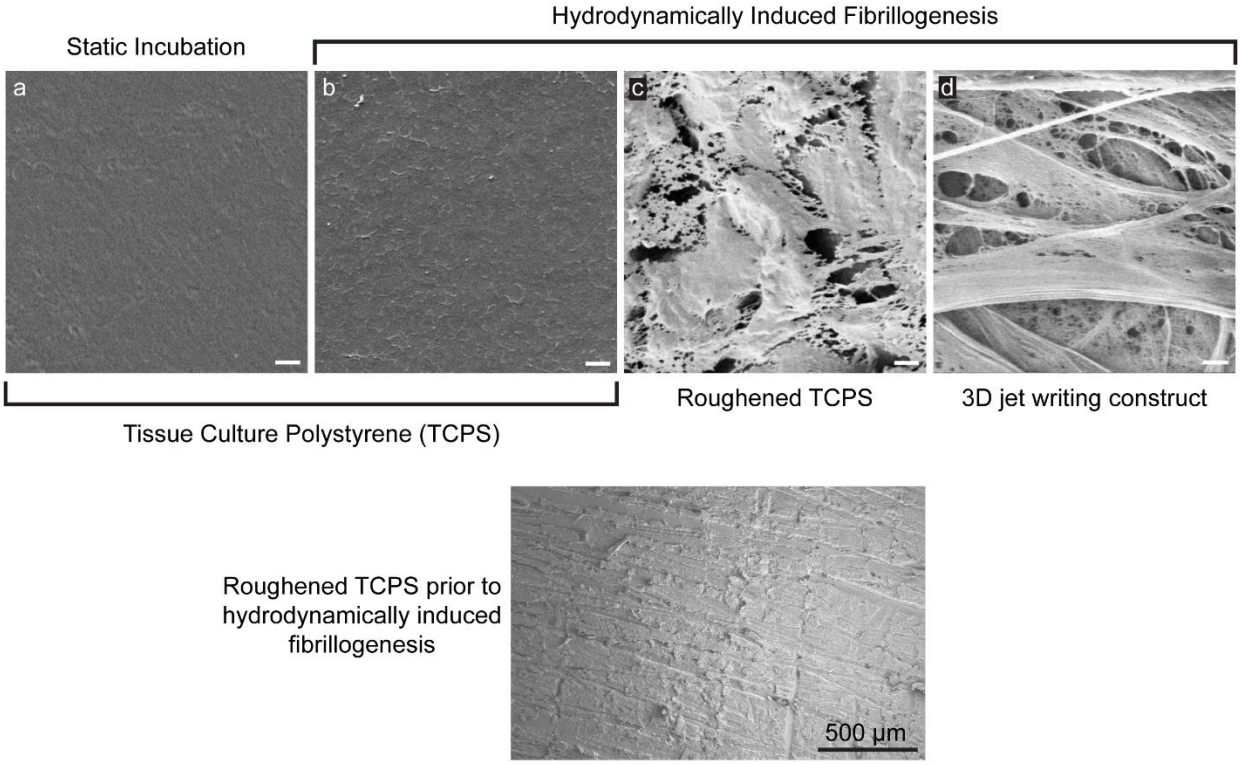

Figure 3-9: Textured but not porous surface is required for hydrodynamically induced fibronectin fibrillogenesis SEM of fibronectin conformally coated onto tissue culture polystyrene (TCPS) via (a) static adsorption in contrast to (b) hydrodynamic deposition of Fn using the same method as when producing supported ecFn. (c) Representing a textured but non-porous substrate, sanded TCPS was exposed to the hydrodynamically induced fibrillogenesis process resulting in protein deposition of a different morphology. SEM of sanded TCPS prior to hydrodynamic shearing is shown. (d) For comparison supported ecFn at the same scale as *(a-c)* is shown after hydrodynamic deposition of Fn onto a 3D jet writing scaffold. (a-d) Scale bars 1 µm.

contrast in Fn morphology on roughened TCPS compared to 3D jet writing scaffolds suggests a potential avenue for regulating the protein network architecture by modulating pores or surface features. More recently, Dylan Neale of the Lahann Lab has demonstrated the formation of supported ecFn using grids fabricated by photolithography out of the photoresist, SU-8 having similar geometric parameters as a 500 μm square pore 3D jet writing scaffold. This further demonstrates that the membrane or substrate used to form the three-phase contact line in hydrodynamically induced fibrillogenesis can be made of various materials, in addition to the array of possible surface or pore features.

3.3.2 Validating cellular nature of supported ecFn

The overarching goal of Chapter 3 is to engineer an ECM that accurately mimics physiological ECM. Hydrodynamically induced fibrillogenesis successfully converts pFn into a webbed network of protein suspended across a polymer scaffold. The question remains whether this protein network is actually representative of native ECM, where fibronectin is known to (1) have a fibrillar architecture, (2) exist in an unfolded conformation that exposes the FnIII domain, and (3) be detergent-insoluble[4, 76, 89, 107, 124, 125]. Supported ecFn was therefore analyzed for these three characteristics. High resolution SEM of dehydrated supported ecFn reveals a 3D web-like matrix of fibronectin (**Fig. 3-10(a)**). To compare this structure with that of cell-secreted Fn, human mammary fibroblasts were cultured on glass substrates to confluency. The substrates were subsequently decellularized, and in parallel with supported ecFn, stained for human fibronectin. The cell-secreted Fn and supported ecFn both exhibited a fibrillar, porous morphology ((**Fig. 3-10(b)**). Supported ecFn were also found to remain intact following treatment with deoxycholate or Triton X-100 detergent, rendering the protein network detergent-insoluble (**Fig. 3-10(d)**). In addition to being insoluble and having a fibrillar architecture as is that of ECM *in vivo*[89, 124],

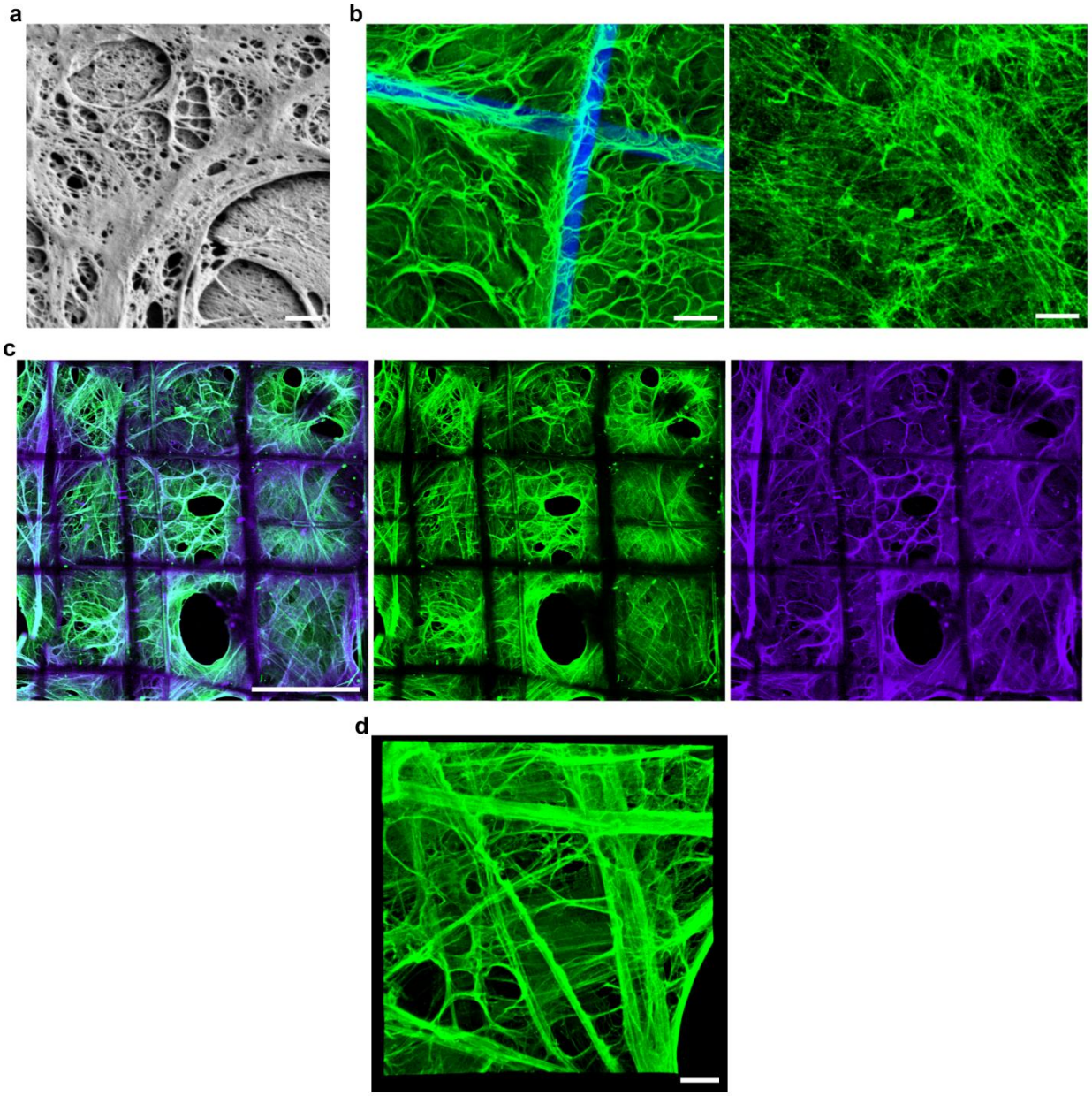

Figure 3-10: Protein morphology, conformation, and insolubility validates the cellular nature of supported ecFn (a) High resolution SEM of Fn as it appears from the top surface of supported ecFn. Scale bar 1 µm. (b) Comparison of supported ecFn (green) as it is suspended on the polymer scaffold (blue) shown on the left to Fn secreted by human mammary fibroblasts cultured to confluency on a glass slide and subsequently decellularized. Scale bars 25 µm. (c) Split channel view of supported ecFn, irrespective of conformation (green) and specifically the FnIII domain (purple) across the large scale of the 3D jet writing scaffold, indicating that the ecFn is in an unfolded, extended conformation as it is *in vivo*. Overlay image of the two channels shown on the left. Scale bar 500 µm. (d) Supported ecFn remains intact despite treatment with Triton X-100 detergent, showing detergent-insolubility. Scale bar 25 µm.

exposure of the FnIII domain would confirm, not by morphology but rather biochemically, the cellular nature of supported ecFn. We adopted positive staining of the FnIII domain as a direct indication that hydrodynamically induced fibrillogenesis indeed transformed pFn into cFn[10, 85, 126, 127]. We found that FnIII stained positively on supported ecFn throughout the large-scale area of the polymer scaffold as shown in **Figure 3-10(c)**. As a control, the same trend was observed for decellularized human mammary fibroblast-secreted matrix (**Fig 3-11(a-b)**). Little to no FnIII signal was observed on glass or 3D jet writing scaffolds that were conformally coated with pFn via static adsorption, indicating that conformal coatings lack exposed FnIII domains and the associated biological activity[10, 11, 94, 128] (**Fig. 3-11(c-d)**). The fact that static incubation does not present the protein in an unfolded conformation where the FnIII domain is exposed implies that hydrodynamic shearing at the three-phase interface effectively unfolds the protein and suspends it across the pores of the polymer scaffold in an extended, physiological conformation. Importantly, the impact of this result goes beyond asserting the ECM-like nature of supported ecFn. The procedure of static incubation is commonly used in the literature for coating TCPS dishes or glass substrates prior to cell culture in an attempt to expose cells to a more native environment, for cell anchorage, and to achieve desired signaling via integrin binding to the specific protein. However, the desired binding sites may remain sequestered within the protein when adsorbed conformally onto a solid surface as was FnIII after static incubation in pFn solution. Assuming full bioactivity of conformally adsorbed Fn may lead to inaccurate experimental conclusions, where a cell response is attributed to the protein or protein-induced cell signaling rather than another feature of the artificial environment.

It is well known that protein structure is strongly correlated to functionality[85, 111]. In fact, varying degrees of protein unfolding impacts not only the availability of binding sites such as the

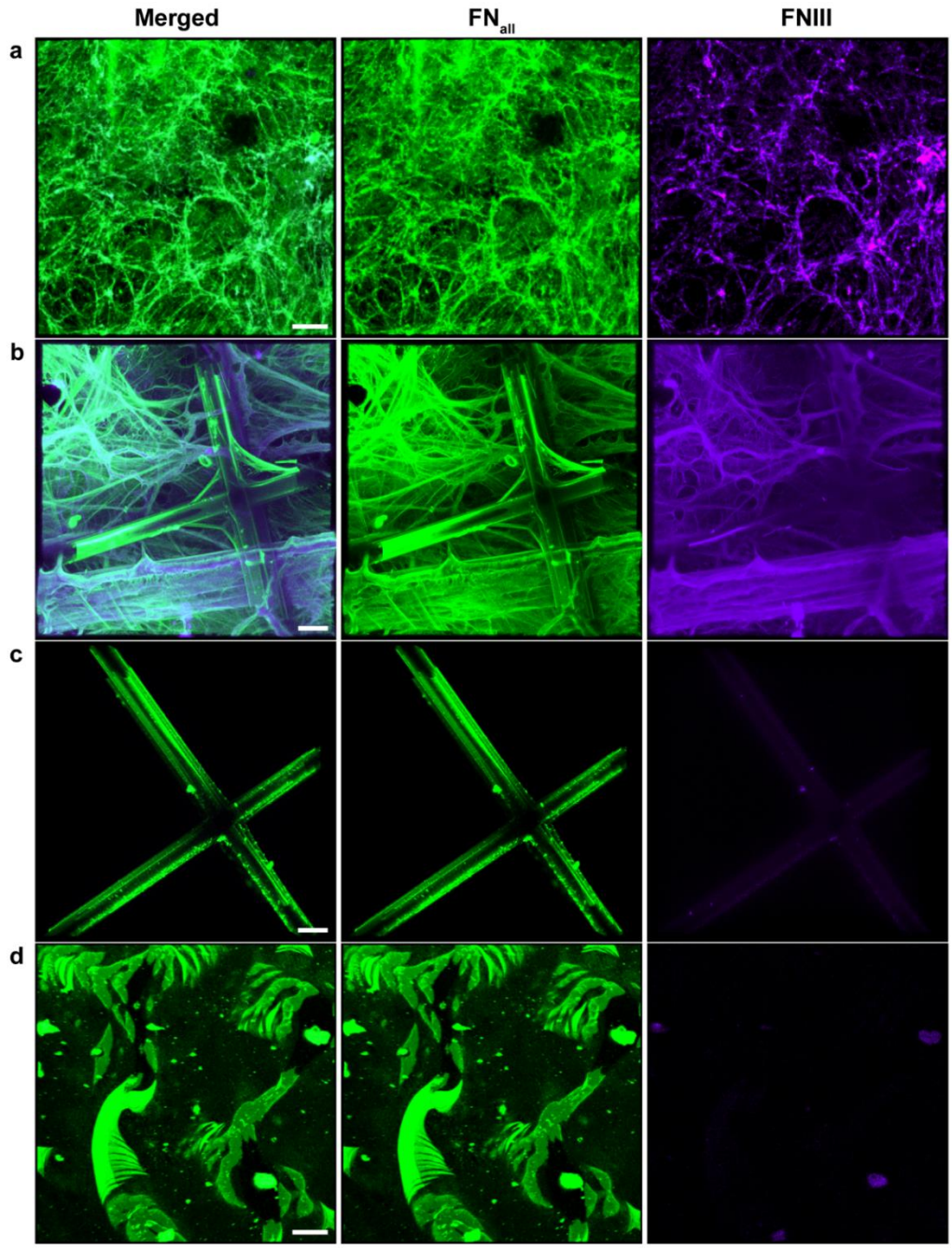

Figure 3-11: FnIII domains exposed on supported ecFn as it is in cell-secreted Fn Fibronectin (green) as secreted by human mammary fibroblasts cultured on glass and subsequently decellularized showing exposure of FnIII domains (purple). Overlay of the two channels shown in left column. (b-d) Overlay of channels (left), Fn stained irrespective of exposed domains (green, center), and specifically the FnIII domain (purple, right) for plasma fibronectin: (b) suspended as ecFn across a 3D jet writing scaffold to form supported ecFn, (c) conformally coated onto a 3D jet writing scaffold and (d) conformally coated onto glass via static adsorption. Scale bars 25 μm. All images taken at the same laser power and imaging settings via LSCM. Strong overlap of green and purple appear white in overlay image *(left images in (a) and (b))*. Saturated pixels in the FnIII channel of *(a)* appear pink in color.

mechano-sensitive α5β1, but also the stiffness of the protein coated surface which can be mechanotransduced to cause specific cell responses[129]. For example, matrix stiffening by means of protein unfolding mediates integrin activity, increasing vascular endothelial growth factor secretion and decreasing cell adhesion – supporting breast tumor development[42, 86]. Moreover, different tissues or diseased states are often characterized by the extent to which cFn is unfolded. Partially unfolded cFn was identified in obese tissue from mice[129]. With the extreme flexibility and possible conformations of proteins, a best-case solution is to allow cells to remodel or restructure the protein matrix of their *in vitro* environment. Such a "hands-off" approach is achieved by supported eECM, where the bulk of the deposited protein is kept within the large pores of the 3D jet writing scaffold rather than adsorbed onto the walls. This design firstly keeps the majority of the protein freely suspended, surrounded only by cell media when in culture, and free from artificial restructuring due to contact with a solid surface. Secondly, the unconfined protein network is accessible only by cells in culture and therefore any remodeling of the protein structure or composition is governed only by cell activity. Cells seeded on supported eECM will eventually generate their own protein matrix promoting the natural bidirectional signaling between cells and ECM.

Of course, in addition to a native-like architecture and conformation, a required feature in designing an *in vitro* ECM-mimic, is compositional control. Not only is hydrodynamic shearing effective for converting pFn to cFn, but it also successfully deposits 3D matrices of laminin (LAM) and collagen I (COL) onto the polymer scaffold as shown in **Figure 3-12(a)**. LAM and COL within the matrix secreted by human mammary fibroblasts was found to be comparable to that of supported eECM but for the formation of thicker bundles in the shear-deposited protein than that of the decellularized matrix (**Fig. 3-13(a)**). The SEM images provide better resolution of the finer

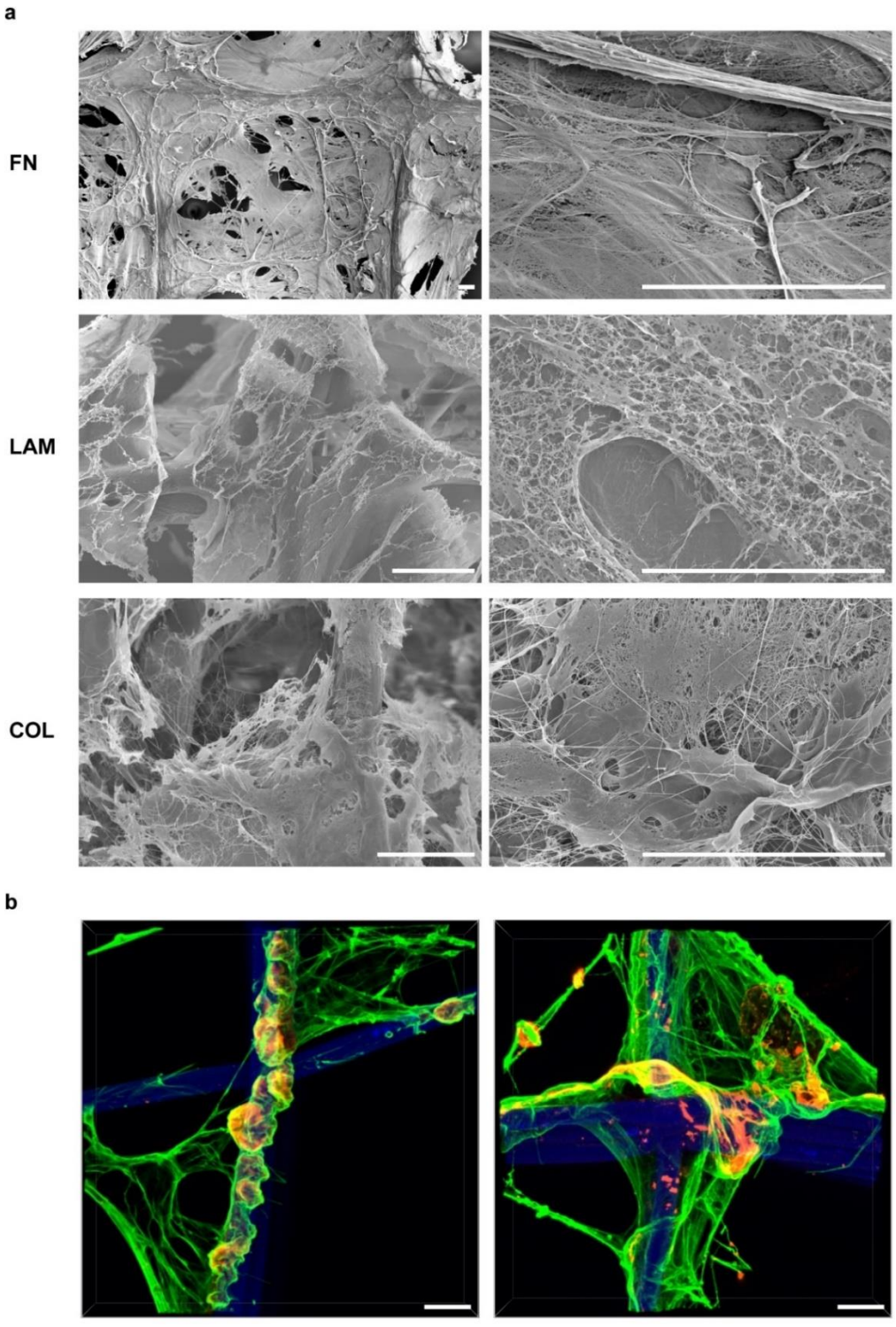

Figure 3-12: Shear-driven hydrodynamic deposition is not limited to fibronectin (a) Fibronectin (top), laminin (middle), and collagen I isolated from rat tail (bottom) hydrodynamically deposited onto 3D jet writing scaffolds. SEM images of protein either at the crosshairs of the polymer microfibers or within the 500 µm open square pores. (b) Fibronectin (green) and laminin (orange) combined to form a supported eECM. (a-b) Scale bars 25 µm. Blue channel indicates polymer scaffold. *Credit:* Collagen I isolated from rat tail and generously donated by the Chun Lab at the University of Michigan.

features of the supported eECM revealing a porous and fibrillar architecture (**Fig. 3-13(a)**). In an early experiment prior to protocol optimization, it was also shown that proteins can be deposited onto the polymer scaffold in binary combinations as with Fn and LAM in **Figure 3-12(b)**. A more specialty protein, tenascin-C, which is known to bind to Fn[130, 131], could also be distributed throughout the supported eECM in combination with Fn at a ratio of only 5:95 tenascin-C:Fn (**Fig. 3-13(b)**). Tenascin-C plays a major role in certain physiological phenomena including bone and cartilage development, secondary lung tumor formation in breast cancer[132], and invasiveness, angiogenesis, and cancer cell viability in metastasis[133]. As such, including tenascin-C in the library of proteins that can be suspended across polymer scaffolds opens a new door to explore the effect of tenascin-C in various cell cultures or co-cultures. Practically, the ability to create a large-scale niche ECM that incorporates tenascin-C at amounts as low as 5% loading is cost effective given the higher prices of such specialty proteins (10% shown in **Fig. 3-14**). Combinations of more than two proteins has not been experimented with, but is a promising avenue for future engineered ECM design. The ability to visualize both proteins and their interactions with one another prior to seeding cells is yet another demonstrated advantage of supported eECM. For instance, Fn appeared to surround LAM in clusters (**Fig. 3-12(b)**) in contrast to the uniform distribution of Fn with tenascin-C (**Fig. 3-13(c)**). Interestingly, the two antiparallel beta sheets that form FnIII in Fn, is conserved in tenascin where it is folded identically to the FnIII of Fn[105]. Such similarities in protein structure between Fn and tenascin may explain why the two proteins disperse together throughout the supported eECM while Fn and LAM remained more separated. The interplay between tenascin-C and Fn is particularly interesting in the context of tumorigenesis where tenascin-C inhibits cell adhesion to and assembly of cFn matrix[131]; the effect of Fn with and without tenascin-C on cancer cell behavior is one of many future applications of supported eECM.

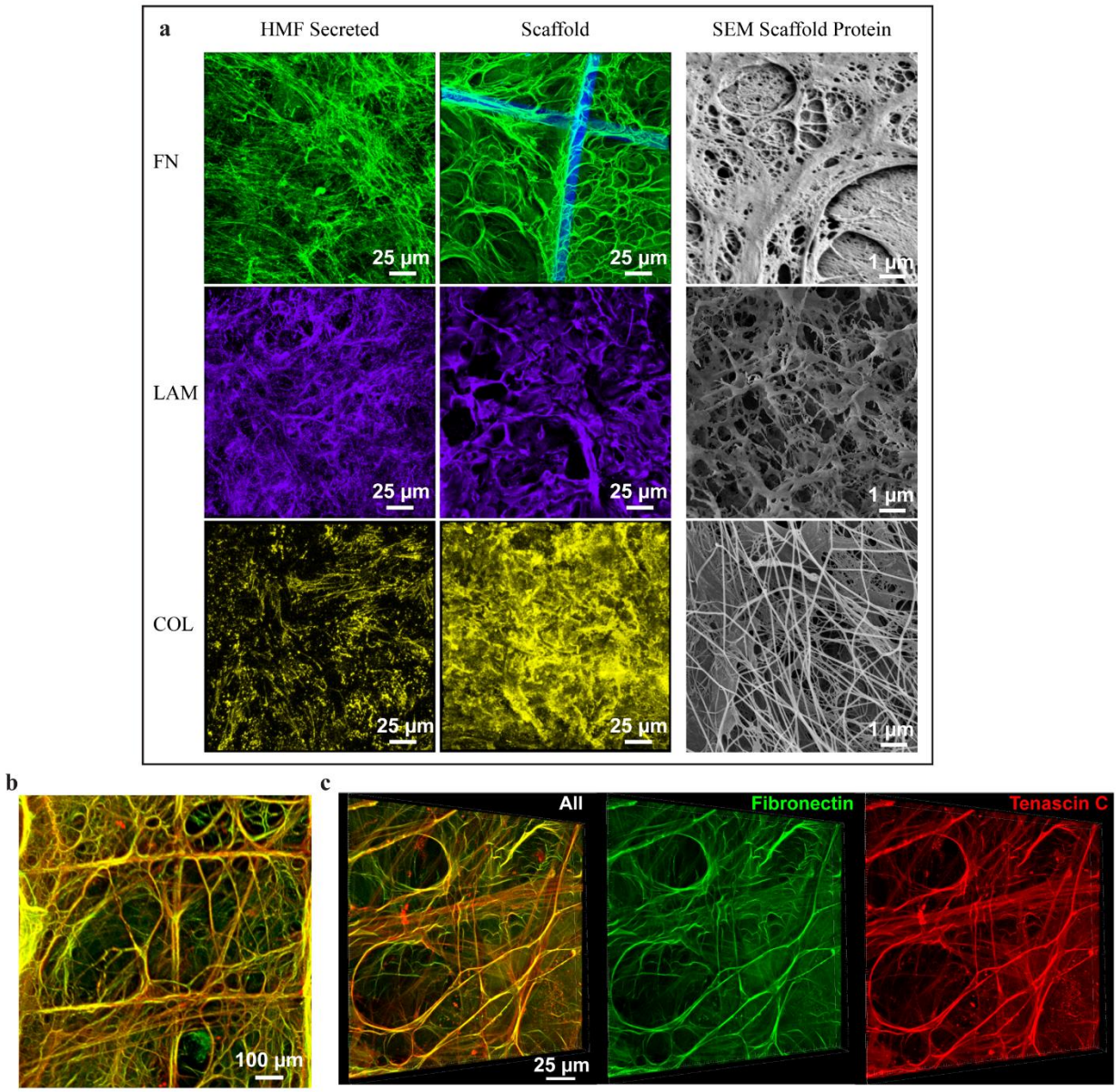

Figure 3-13: Expanded library of proteins for supported eECM include niche protein tenascin-C (a) (left column) Fibronectin (FN), laminin (LAM), and collagen I (COL) as secreted by human mammary fibroblasts when cultured on tissue culture polystyrene. (middle column) FN, LAM, and COL as suspended on 3D jet writing scaffolds to form supported eECM. (right column) SEM images of supported eECM comprised of either FN, LAM, or COL at 10,000x magnification. (b) Zoomed out view showing larger scale visualization of FN (green) in combination with tenascin-c (red) on a supported eECM at a ratio of 5:95 tenascin-C to Fn. (c) Higher magnification of sample shown in *(b)* with split channel view of Fn (green) and tenascin-C (red) including the overlay image on the left. *Credits:* Collagen I isolated from rat tail and generously donated by the Chun Lab at the University of Michigan. Tenascin-C contributed by the Lawlor Lab at the University of Michigan in a collaborative project including students Elizabeth Pedersen and Allegra Hawkins.

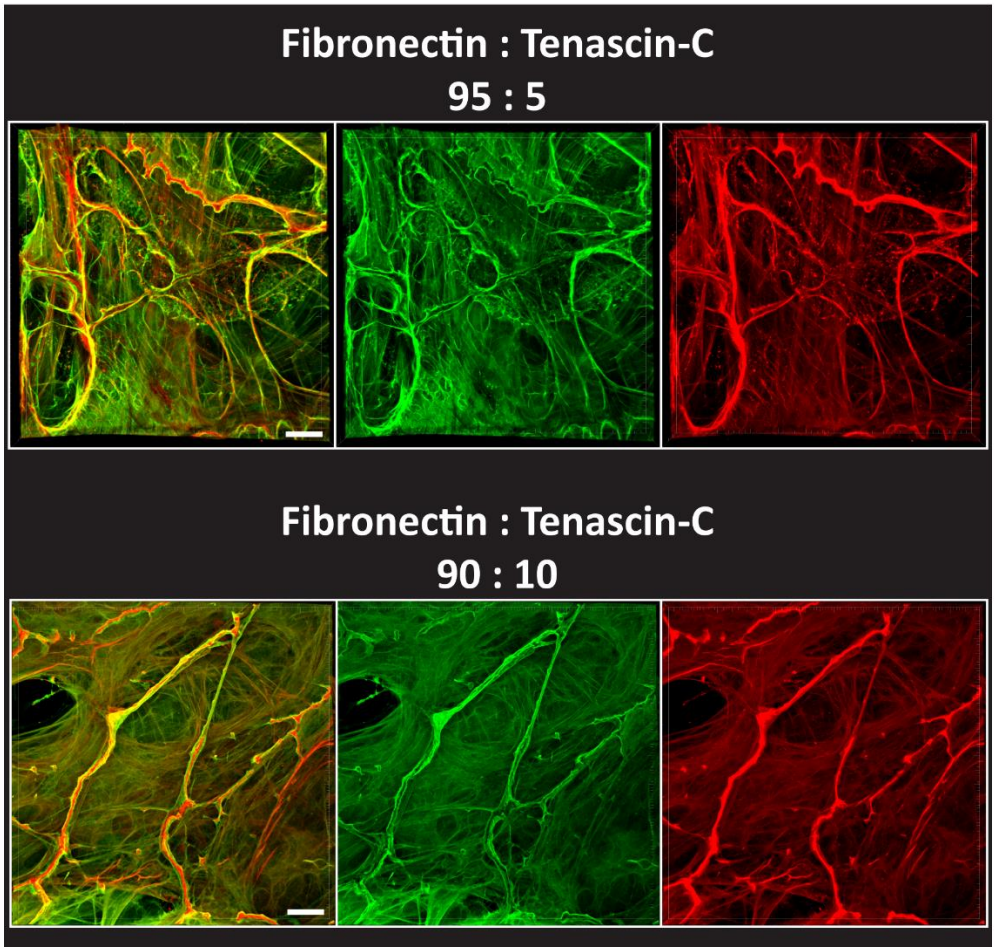

Figure 3-14: Small loadings of tenascin-C are sufficient to distribute the protein across the open pores of the polymer scaffold Distributions of fibronectin and tenascin-C at ratios of 95:5 or 90:10 provide sufficient tenascin-C to the system for hydrodynamically induced fibrillogenesis to carry the tenascin-C along with the fibronectin to form fibrillar structures spanning across the open pores of the polymer scaffold. Fibronectin in green channel, tenascin-C in red, overlay image shown on the far left in both cases shown. Scale bars 25 µm. *Credit:* Tenascin-C contributed by the Lawlor Lab at the University of Michigan in a collaborative project including students Elizabeth Pedersen and Allegra Hawkins.

3.3.3 Functionality of supported ecFn in various cell cultures

The final validation of the supported eECM technology is to observe it in use for various cell culture applications. As a first baseline experiment, NIH-3T3 mouse fibroblasts were cultured on supported ecFn (**Fig. 3-15(b)**). In parallel for comparison, Fn statically adsorbed onto the same polymer scaffold (**Fig. 3-15(a)**) was also seeded with the same number of cells. After three days of culture, the fibroblasts had expanded across the entire area of the supported ecFn, forming a 3D

volume of cells or microtissue several cell diameters thick (**Fig 3-15(d-f)**). In contrast, cells had simply adhered to the surface of scaffolds with a conformal layer of protein with little to no cell bridging across pores (**Fig. 3-15(c)**). The suspension of ecFn across and within the large square pores of the polymer scaffold act as highways for cells to migrate away from the polymer microfibers and towards the softer proteinaceous matrix found in the pore as was evidenced by a live-cell time lapse video of GFP NIH-3T3 fibroblasts seeded onto supported ecFn; note that each 500 μm wide pore of the polymer scaffold provides sufficient volume for cell numbers upwards of 60,000 cells. Cells can therefore embed themselves amongst the suspended webs of protein within 3D space, as opposed to forming a monolayer atop a conformal protein coating on a 2D substrate. Furthermore, the supported ecFn enabled rapid cell proliferation and expansion relative to the same polymer scaffold statically incubated in pFn solution. At the same three day timepoint, the coverage of cells across the supported ecFn far supersedes that of the statically adsorbed Fn. Even after 22 days, 57% of scaffold pores were not fully covered with cells when only statically incubated in pFn solution (**Fig. 3-16(a)**). To verify that this ability to rapidly generate cell volumes is due to the protein network and not the 3D jet writing scaffold, a similar study was done using polyester and nylon mesh screening as the membrane (**Fig. 3-16**). Again, static Fn adsorption onto either polyester or nylon mesh screening left nearly all pores with incomplete cell coverage, even after 22 days of culture time (**Fig. 3-16(b-c)**). At the same time, three days were sufficient to form cell volumes spanning nearly the entire area of the mesh screening when Fn was deposited via hydrodynamically induced fibrillogenesis for both polyester and nylon mesh screening (**Fig. 3-16(d-g)**). Hence, the hydrodynamically induced fibrillogenesis technique is effective for forming 3D cell culture matrices regardless of the source of solid support. This will be important in mass production of supported eECM should the technology transition from bench scale to commercial,

as we move towards the overarching goal of updating the most ubiquitous cell culture substrate, flat TCPS surfaces.

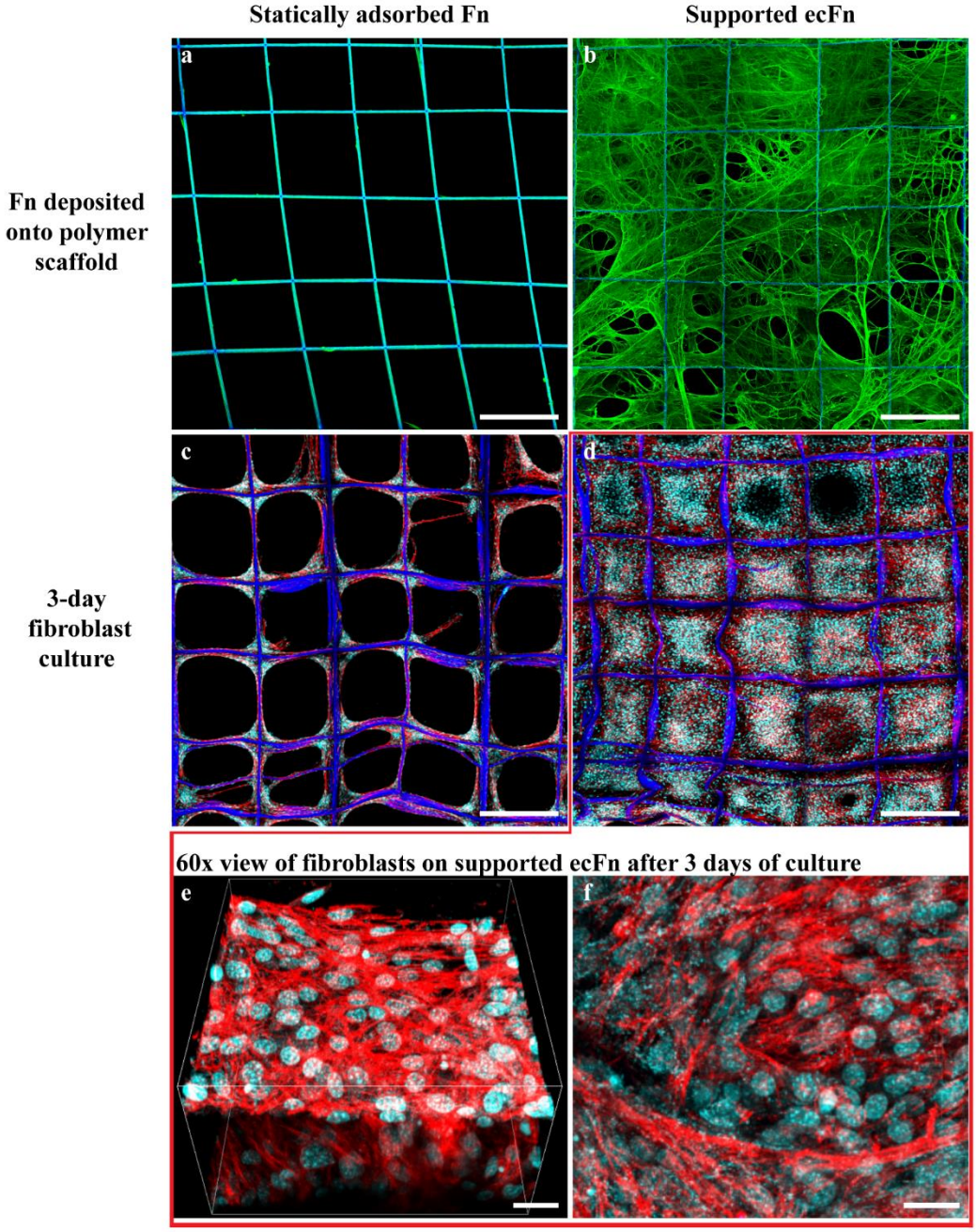

Figure 3-15: Supported ecFn facilitates formation of 3D cell volumes (a) Conformal protein coat that results from static incubation of the polymer scaffold in pFn solution. Fn adsorbs only onto the microfibers with little to no bridging of Fn across or within the pores of the scaffold. (b) In contrast to *(a)*, supported ecFn is an array cFn fibrils bridging across the open pores of the polymer scaffold. (c) After three days of culturing NIH-3T3 mouse fibroblasts on statically Fn coated polymer scaffolds, cells only tend to adhere along the polymer fibers. (d) However, three days on supported ecFn was sufficient for fibroblasts

to fill all scaffold pores to depths several cell diameters thick indicating the supported ecFn yields superior cell proliferation and rapid microtissue formation. (e) 3D volume view showing depth of tissue created by cells in culture 3 days on supported ecFn. (f) Top view showing interconnectivity of cells and cell-cell contacts on supported ecFn. Channels: blue, polymer microfibers; green, fibronectin; red, actin; cyan, cell nucleus. Scale bars: (a-d) 500 μm (e-f) 25 μm.

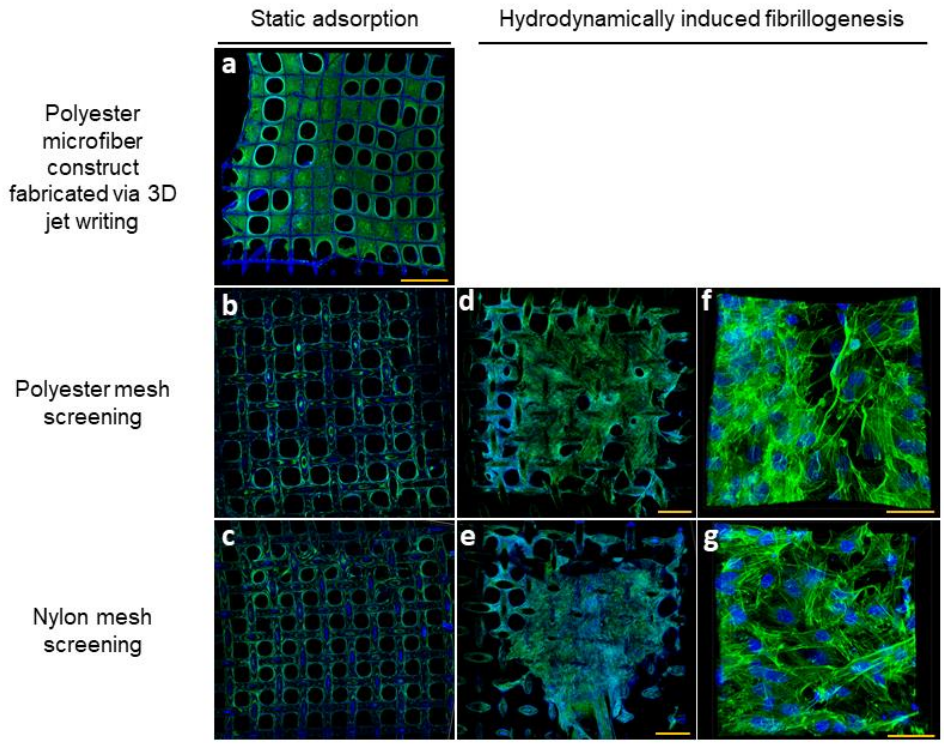

Figure 3-16: Protein network facilitates formation of 3D cell volumes irrespective of the choice of scaffold (a-c) NIH-3T3 fibroblasts after 22 days of culture on polymer scaffolds statically incubated in pFn solution to form a conformal layer of Fn on all surfaces prior to cell seeding. Polymer scaffolds are (a) 3D jet writing microfiber construct, (b) polyester mesh screening, (c) nylon mesh screening. (d-g) NIH-3T3 fibroblasts form extensive 3D cell volumes after three days in culture on supported ecFn produced via hydrodynamically induced fibrillogenesis on both (d, f) polyester and (e, g) nylon mesh. All cell nuclei stained blue, and actin stained green. (a-e) Scale bars 1000 μm. (f, g) Scale bars 50 μm.

Protein bridges suspended across the open pores of the polymer scaffold have now been shown to facilitate cell outgrowth away from the polymer fibers and into the void spaces free of synthetic material. Once residing in the void spaces, cells can choose to remodel the deposited protein network by secreting new ECM proteins, and/or lysing or restructuring the existing ECM that was pre-deposited. In addition to visualizing protein synthetically deposited onto the polymer

scaffold, supported eECM allows researchers to visualize changes in the protein network due to cell activity. To demonstrate detection of specific cell secreted protein using supported eECM, MDA-MB-468 breast cancer cells were cultured four days on supported ecFn (**Fig. 3-17(a)**). The scaffolds were decellularized, and Fn and any endogenous LAM were fluorescently labelled and imaged to show that the MDA-MB-468s had secreted small amounts of LAM (**Fig. 3-17(b)**). In addition to endogenously secreting proteins, cells may also lyse the pre-deposited protein. This

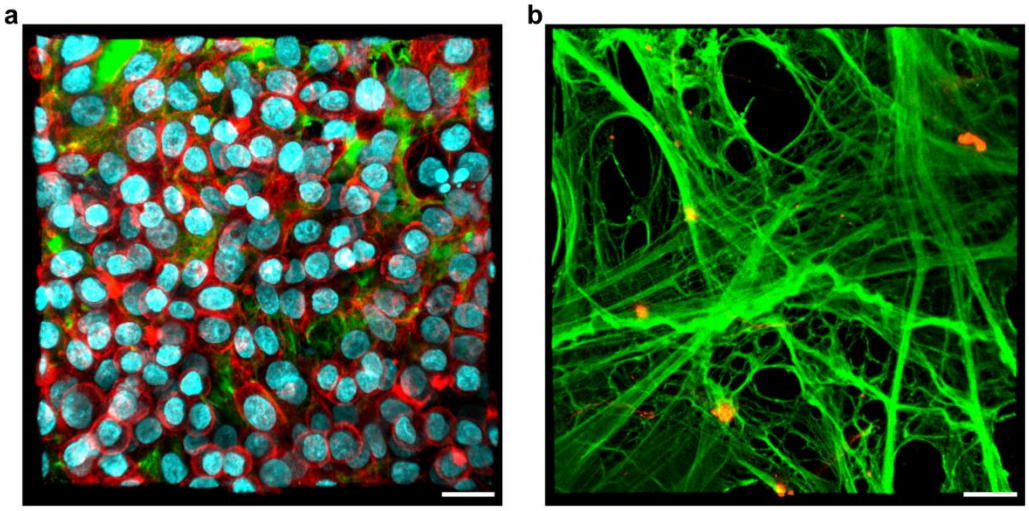

Figure 3-17: Supported ecFn enables observation of protein secreted by cells during culture (a) MDA-MB-468 breast cancer cells cultured four days on supported ecFn form cell-cell and cell-ECM contacts. Fn shown in green and cell-secreted laminin in orange. Scale bar 25 µm. (b) After four days of culture, MDA-MB-468 cells were removed from the supported ecFn, and the remaining protein was stained for all fibronectin (green) and endogenously secreted laminin (orange). Scale bar 25 µm. (a-b) Channels: green, fibronectin; orange, laminin; cyan, cell nucleus; red, actin.

behavior was seen with the human breast cancer cell line, MDA-MB-231 (231s). 231s were cultured on TCPS (**Fig. 3-18(a)**) and supported ecFn (**Fig. 3-18(b)**). Supported ecFn fostered a higher degree of cell-cell contacts compared to the same culture on TCPS for the same amount of time. Cells cultured on TCPS also displayed a flattened morphology. After six days of culture on supported ecFn, 231s had formed confluent volumes within each pore of the polymer scaffold as shown in **Figure 3-18(c)**. However, by the tenth day in culture, the cells had migrated off the scaffold, where the only cells remaining were adhered to the microfibers of the 3D jet writing

construct (**Fig. 3-18(d)**). The cells had also aggressively broken down the pre-deposited ecFn. The same behavior was quantified by observing the number of 231 cells adhered to the supported ecFn over time. The growth curve, shown in **Figure 3-19(a)**, highlights that the 231s were proliferative until about the eighth day in culture when they transitioned to a more migratory phenotype such

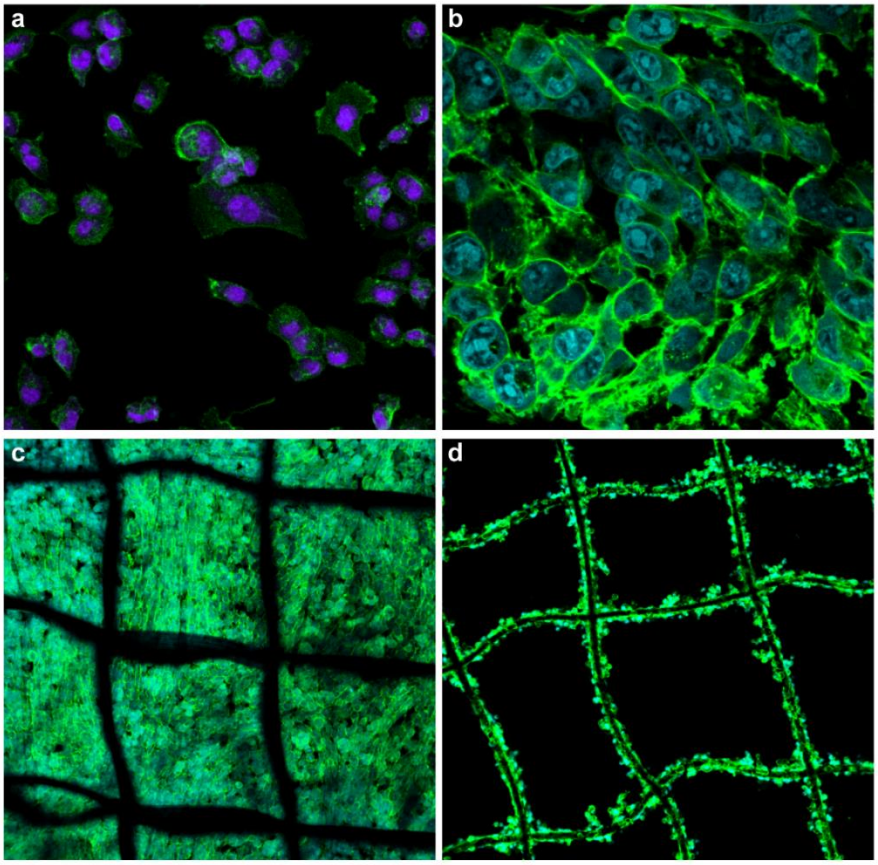

Figure 3-18: MDA-MB-231 human breast cancer cells break down protein of supported ecFn (a) MDA-MB-231 (231s) human breast cancer cell line cultured on tissue culture polystyrene (TCPS). Cells cultured on TCPS have a more artificial flattened morphology and make fewer cell-cell contacts. Cell nucleus in purple, actin in green. Laser scanning confocal microscope (LSCM) image at 60x magnification. (b) 231s cultured and imaged on supported ecFn at 60x magnification on LSCM. Cell nucleus in cyan, actin in green. Supported ecFn promote cell-cell contacts in 3D space to form a thriving microtissue *in vitro* (b-c) compared to the same cell type cultured on TCPS for the same amount of time in *(a)*. (c) 231s after six days of culture form a confluent volume of tissue on supported ecFn. (d) After 10 days of culture on supported ecFn, 231s are no longer tethered to the protein but rather migrate off the scaffold into solution. (Subsequent experiments show that these cells are still 98% viable in solution.) At 10 days, the ecFn is no longer visible indicating that the cells have broken down or remodeled the proteinaceous environment as they move off into solution.

that by the 10th day, the number of cells still adhered to the supported cFn network is only slightly higher than the number of cells initially seeded. Follow up studies indicated that the 231s that had left the supported ecFn and found suspended in solution had remained 98% viable. Were these 231s attempting to begin the metastatic cascade? Could supported ecFn also serve as a model of metastasis as illustrated in **Figure 3-19(b)**? Certainly, this is a topic for future studies.

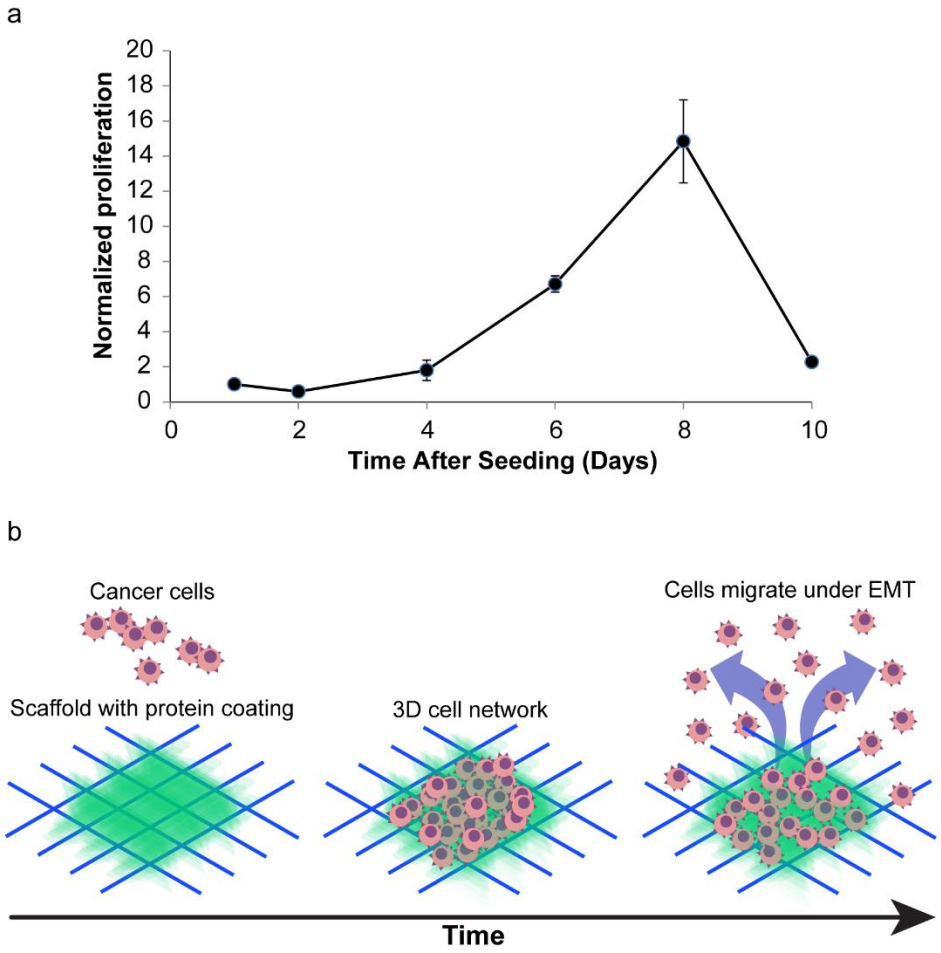

Figure 3-19: Supported ecFn may be a potential model of breast cancer metastasis (a) Bioluminescence was used to quantify the relative number of MDA-MB-231 breast cancer cells adhered to the supported ecFn at various time points during a 10-day culture. Initially, cells are proliferating but at day-8 the cells transition to a migratory state leaving few cells adhered to the supported ecFn by day-10. (b) Schematic of the hypothesis regarding the possibility of supported ecFn to serve as a model of metastasis. Cancer cells are first seeded onto the supported ecFn where they form 3D cell volumes. Upon reaching a critical confluency, cells become more aggressive and migrate off into solution, remaining viable. This is a topic for future investigation.

In addition to observing cell activity in matrix remodeling, supported eECM also allows ECM protein composition control. In designing a 3D cell culture matrix, a tunable ECM composition is required in order to recapitulate specific cell niches and tissues in both healthy and diseased states, and experimentally important in regards to probing the effect of a certain protein or combination of proteins on cell behavior. For instance, the protein breakdown observed when MDA-MB-231s were cultured on supported ecFn (**Fig. 3-18–19(a)**) was not observed when the same cells were cultured on supported eCOL. When cultured on collagen I, these cells did not migrate off the scaffold, nor did they lyse and break down the protein. Instead, 231s cultured on supported eCOL remained within the microenvironment in a proliferative phase. To exhibit the versatility of ECM composition in supported eECM, in addition to Fn, 231s were grown on LAM, COL, and a combination of Fn and LAM (**Fig. 3-20(a-d)**). Growth curves for 231s on LAM alone and the combination of Fn and LAM reveal the dependence of cell proliferation on the composition of the supported eECM. When cultured on suspended eECM of Fn and LAM, the number of 231s adhered to the scaffold grew up to about three times higher than that of LAM alone (**Fig. 3-20(e)).** This demonstrates the applicability of supported eECM in elucidating the impact of different protein compositions on cell behavior while providing a more physiologically relevant *in vitro* 3D culture environment.

The ability to tune the protein composition of supported eECM is largely beneficial for recapitulating specific cell niches, as with the combination of Fn with tenascin-C. Tenascin-C is found in the stroma of most solid tumors, and has been considered an oncogene i.e. having the ability to transform a cell into a tumor cell[132, 134]. The Lawlor lab at the University of Michigan has found that tenascin-C plays a role in the childhood disease, Ewing sarcoma, where tenascin-C is required for tumor formation in a mouse model. Tenascin-C also facilitates migration and

invasion[135], impacts cell colony formation, and promotes cell adhesion (data not shown). Observation of such cell behaviors is critical to understanding Ewing sarcoma which is not easily characterized by markers commonly used in cancer to identify cells of epithelial or mesenchymal phenotypes[136]. Supported eECM offers the ability to probe cell response to incorporation of tenascin-C into the synthetically deposited protein microenvironment. In parallel, cells cultured on supported eECM can be engineered to have either a tenascin-C knockdown, or normal expression

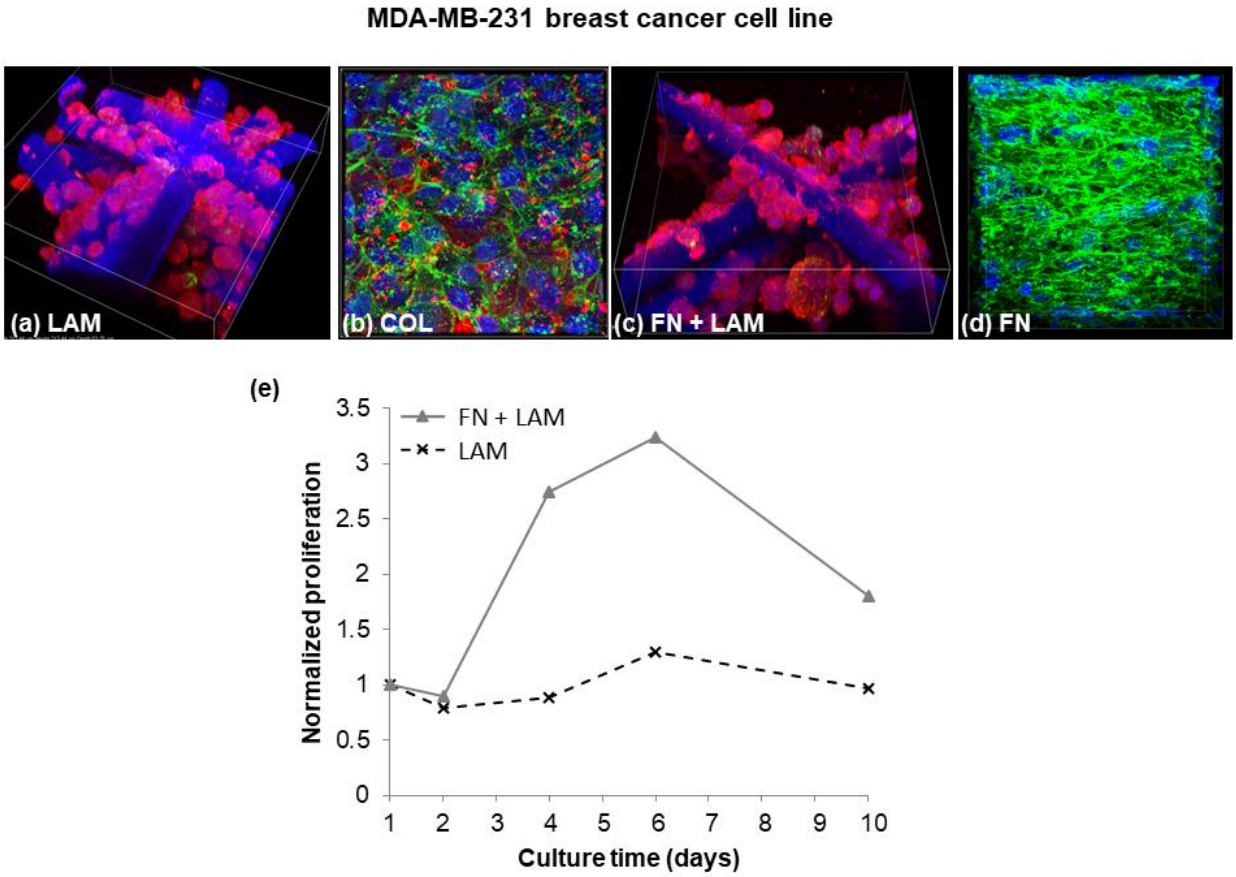

Figure 3-20: Supported eECM provides a means to probing the effect of different ECM composition on cell response Demonstration of culture of MDA-MB-231 human breast cancer cells on supported eECM of varying composition: (a) laminin (LAM) only (cell nucleus in purple; actin in red; polymer microfibers in blue; protein not stained), (b) collagen I (COL) only (cell nucleus in blue; actin in green; collagen I in red), (c) Fn and LAM in combination (cell nucleus in purple; actin in red; polymer microfibers in blue; protein not stained), and (d) Fn only (cell nucleus in blue; actin in green). (e) Growth curves plotting normalized cell proliferation against time for a 10-day culture of 231s on supported eLAM in contrast to Fn and LAM combined. *Credits:* Collagen I isolated from rat tail and generously donated by the Chun Lab at the University of Michigan.

of tenascin-C termed non-silencing cells. This gives researchers the advantage of elucidating the effect of tenascin-C both intra- and extracellularly. Extracellularly, whether or not tenascin-C was combined with Fn to form the supported eECM did not appear to have any effect on TC32 Ewing sarcoma cell morphology (**Fig. 3-21 and 3-22**). TC32s were cultured nine days on either ecFn, or supported networks of both cFn and tenascin-C. Although no difference in cell morphology was observed, with both protein compositions, cells had restructured the morphology of the ecFn by day seven (**Fig. 3-21 and 3-22**). Some degradation of the tenascin-C within the protein matrix was also observed by day nine (**Fig. 3-22**). Future studies will aim to understand whether these cells are indeed of a migratory or invasive phenotype as would be indicated by ECM breakdown. Notably, no differences in cell proliferation were found between the two protein matrix compositions (**3-23**). In a separate assay focused on intracellular differences in tenascin-C expression, the cell type varied between non-silencing cells or tenascin-C knockdown cells and the supported eECM composition was fixed to fibronectin only (**Fig. 3-24**). After four days of culture, the non-silencing cells had largely degraded the ecFn network which is characteristic of a migratory phenotype. In contrast, without intracellular tenascin-C, the tenascin-C knockdown cells left the protein matrix relatively intact (**Fig. 3-24 and 3-25**). This example serves as another demonstration of some of the key advantages of the supported eECM: (1) cells are freely able to breakdown the deposited protein which is susceptible to proteolysis and (2) the technology is amenable to microscopy techniques allowing visualization of the entire polymer scaffold, the presence or degradation of deposited protein, and higher magnification views of cultured cells. Future directions in this study will probe the bidirectional relationship between tenascin-C and cell response by toggling expression of intracellular tenascin-C and incorporation of tenascin-C extracellularly into the protein matrix.

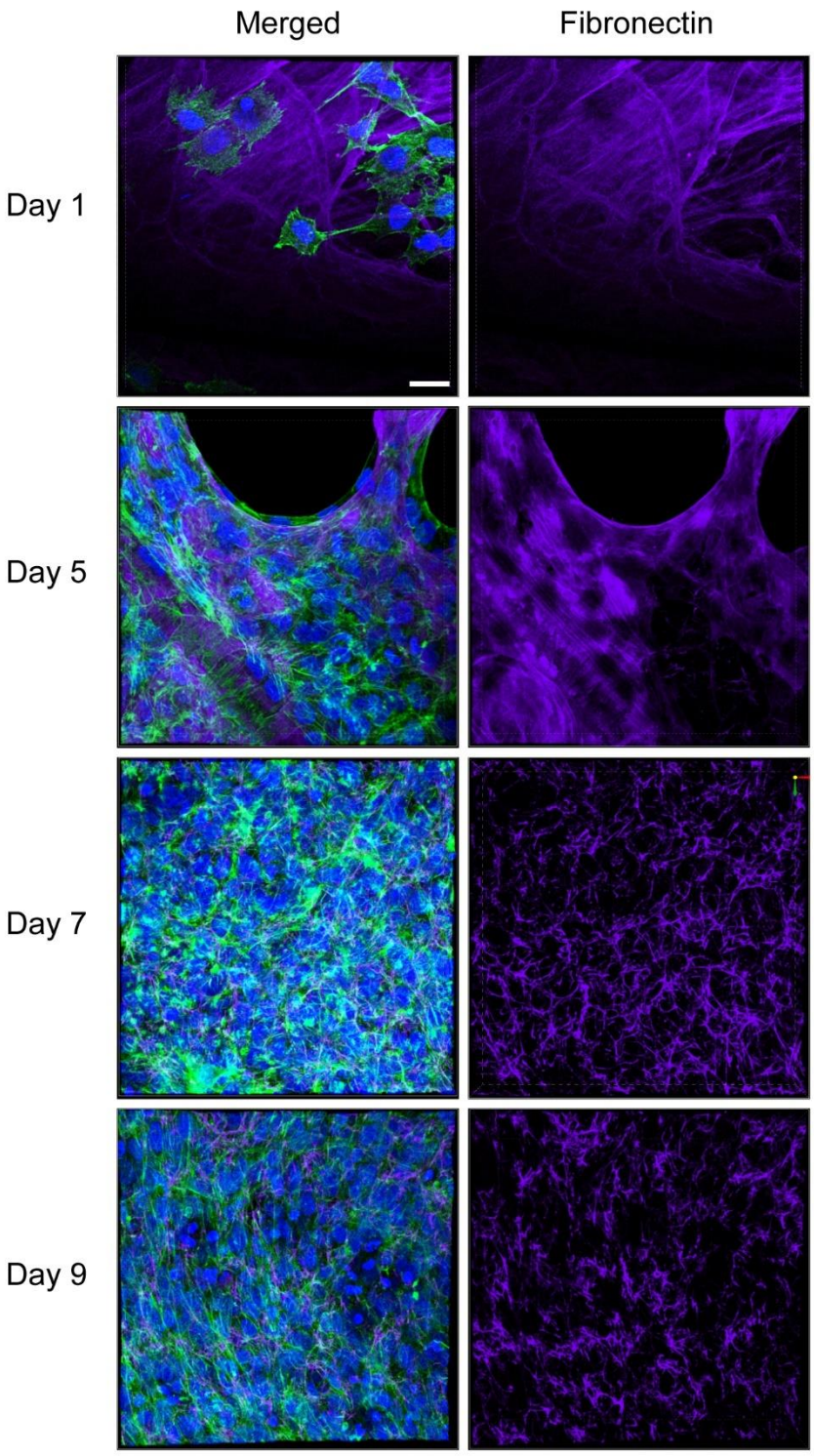

Figure 3-21: Ewing sarcoma cells restructure supported ecFn matrix TC32 Ewing sarcoma cells were cultured on supported ecFn for nine days. Fn adopted a different morphology after cells resided within the matrix for seven days. All images at the same scale. Scale bar 25 µm. Channels: cell nucleus (blue), actin (green), fibronectin (purple). *Credit:* TC32 cells contributed by the Lawlor Lab at the University of Michigan in a collaborative project including students Elizabeth Pedersen and Allegra Hawkins.

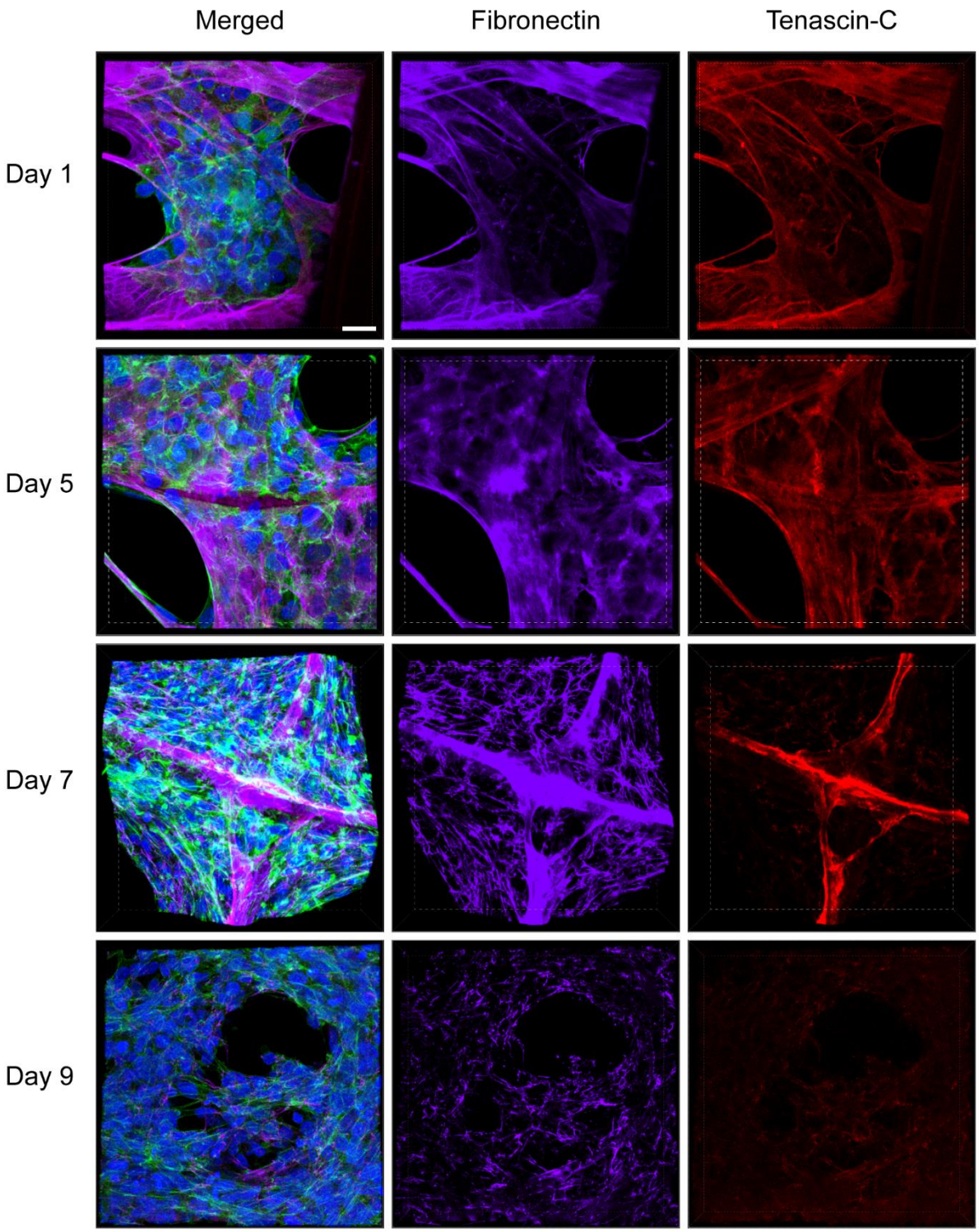

Figure 3-22: Ewing sarcoma cells restructure ecFn and appear to degrade tenascin-C when cultured on supported eECM comprised of both proteins TC32 Ewing sarcoma cells were cultured on supported ecFn either without (*Fig. 3-21*) or with the addition of tenascin-C for nine days. Cells grew confluent on both types of microenvironments. Fn adopted a different morphology after cells resided within the matrix for seven days. All images at the same scale. Scale bar 25 µm. Channels: cell nucleus (blue), actin (green),

fibronectin (purple), tenascin-C (red). *Credit:* Tenascin-C and TC32 cells contributed by the Lawlor Lab at the University of Michigan in a collaborative project including students Elizabeth Pedersen and Allegra Hawkins.

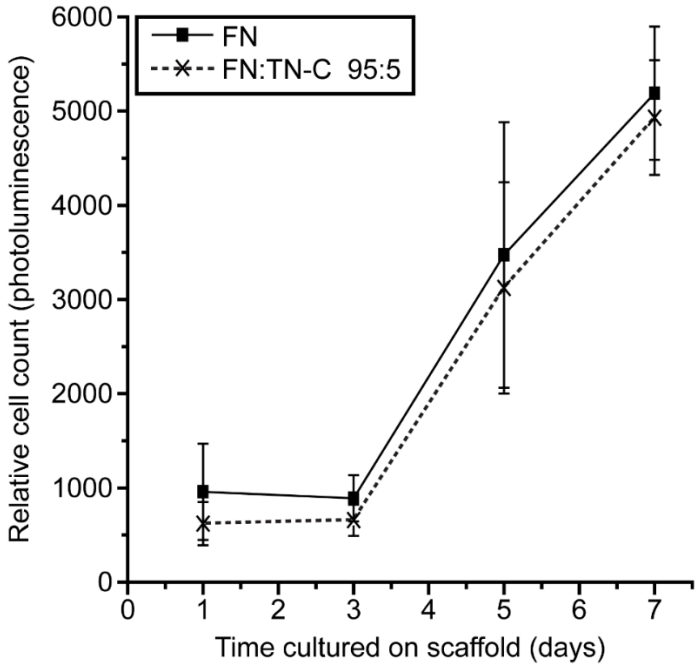

Figure 3-23: Proliferation of TC32 Ewing sarcoma cells is not affected by incorporation of tenascin-C into supported ecFn TC32 Ewing sarcoma cells were cultured seven days on supported ecFn (blue line) or supported eECM comprised of both cFn and tenascin-C (red line). Fibronectin and tenascin-C were incorporated at a mass ratio of 95:5 in solution to form the supported eECM. Luminescence measurements were collected over time to represent a relative cell number adhered to the supported eECM. No difference between the two types of microenvironments were observed. *Credit:* Tenascin-C and TC32 cells contributed by the Lawlor Lab at the University of Michigan in a collaborative project including students Elizabeth Pedersen and Allegra Hawkins.

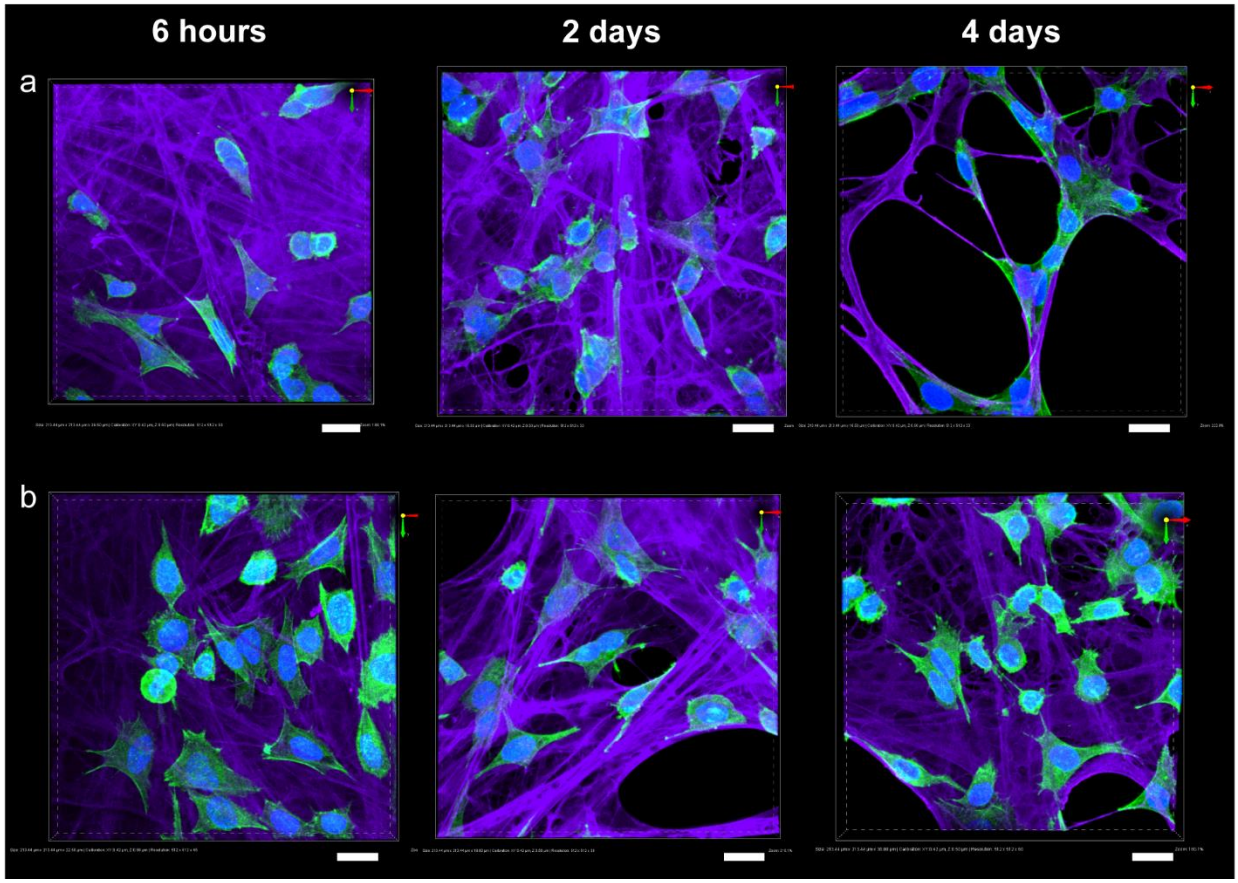

Figure 3-24: Time sequence of Ewing sarcoma cells either expressing or knocked down for tenascin-C cultured on supported ecFn TC32 Ewing sarcoma cells that were either (a) expressing tenascin-C i.e. non-silencing or (b) under a tenascin-C knockdown were cultured four days on supported ecFn. Scaffolds were imaged 6 hours after seeding, two days, and four days as indicated. Non-silencing cells, having tenascin-C expression, had more drastically degraded the protein matrix relative to the tenascin-C knockdown cells by the fourth day. *Credit:* TC32 cells contributed by the Lawlor Lab at the University of Michigan in a collaborative project including students Elizabeth Pedersen and Allegra Hawkins.

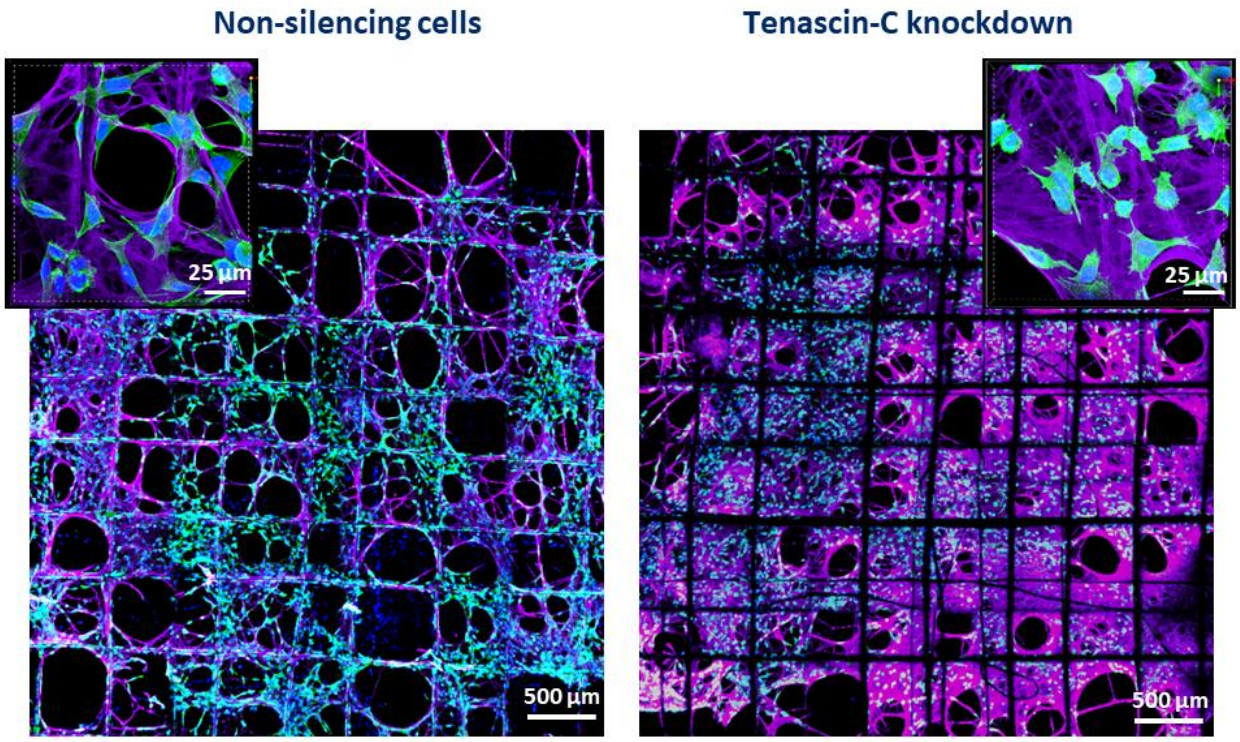

Figure 3-25: Supported eECM provides a means of visualizing cell-induced protein matrix breakdown *in vitro* Two groups of TC32 Ewing's sarcoma cells were cultured on supported ecFn, one group expressing the oncogene tenascin-C (non-silencing cells shown on the left) and the other having had a tenascin-c knockdown (shown on the right). Shown are zoomed out views, and in the insets zoomed in views of the scaffolds after four days of culture. Channels: fibronectin in purple; cell nucleus in blue; actin in green. *Credit:* TC32 cells contributed by the Lawlor Lab at the University of Michigan in a collaborative project including students Elizabeth Pedersen and Allegra Hawkins.

In addition to Ewing sarcoma and breast cancer cells, supported ecFn has maintained successful *in vitro* cultures of a variety of cell types across projects in the Lahann Lab including endothelial cells, human epithelial keratinocytes, human mesenchymal stem cells, induced pluripotent stem cells, human embryonic stem cells, pancreatic and prostate cancer cells. Shown in **Figure 3-26(a-c)**, MDA-MB-231 breast cancer cells have been cultured on collagen I, and Fn to form confluent cultures that can span across entire 3D jet writing scaffold, an area approximately 5.6 by 6 mm. Various time points were imaged for a Sum159 human breast cancer cell culture on supported ecFn. **Figure 3-26(d-f)** exhibits how these cells proliferated from the adhesion of only a few cells at day one to a mass of cells occupying and spanning across each pore of the polymer

scaffold by the fourth day. Two types of pancreatic cancer cells were also expanded on supported ecFn, enabling analysis of distinct phenotypes in parallel: the UM53 epithelial patient-derived cell (**Fig. 3-26(g)**) and the ASPC1 mesenchymal cell line (**Fig. 3-26(h-i)**). Beyond cancerous cells, another interesting cell type are endothelial cells as the need to vascularize engineered 3D tissue constructs persists. Human umbilical vein endothelial cells (HUVECs) were found to require the combination of laminin and fibronectin in order to thrive (**Fig. 3-26(j-k)**). In other studies, HUVECs required a fibrillar form of Fn to proliferate and migrate[137-139]. Unlike the cancer cells which form confluent volumes across and within the pores of the polymer support, HUVECs remain in lower density bridges (**Fig. 3-26(l)**). The array of cell types that have been successfully maintained *in vitro* on suspended eECM further validates its versatility and implies that it is a technology that can be widely adopted into mainstream biological research across disciplines if pushed towards commercialization.

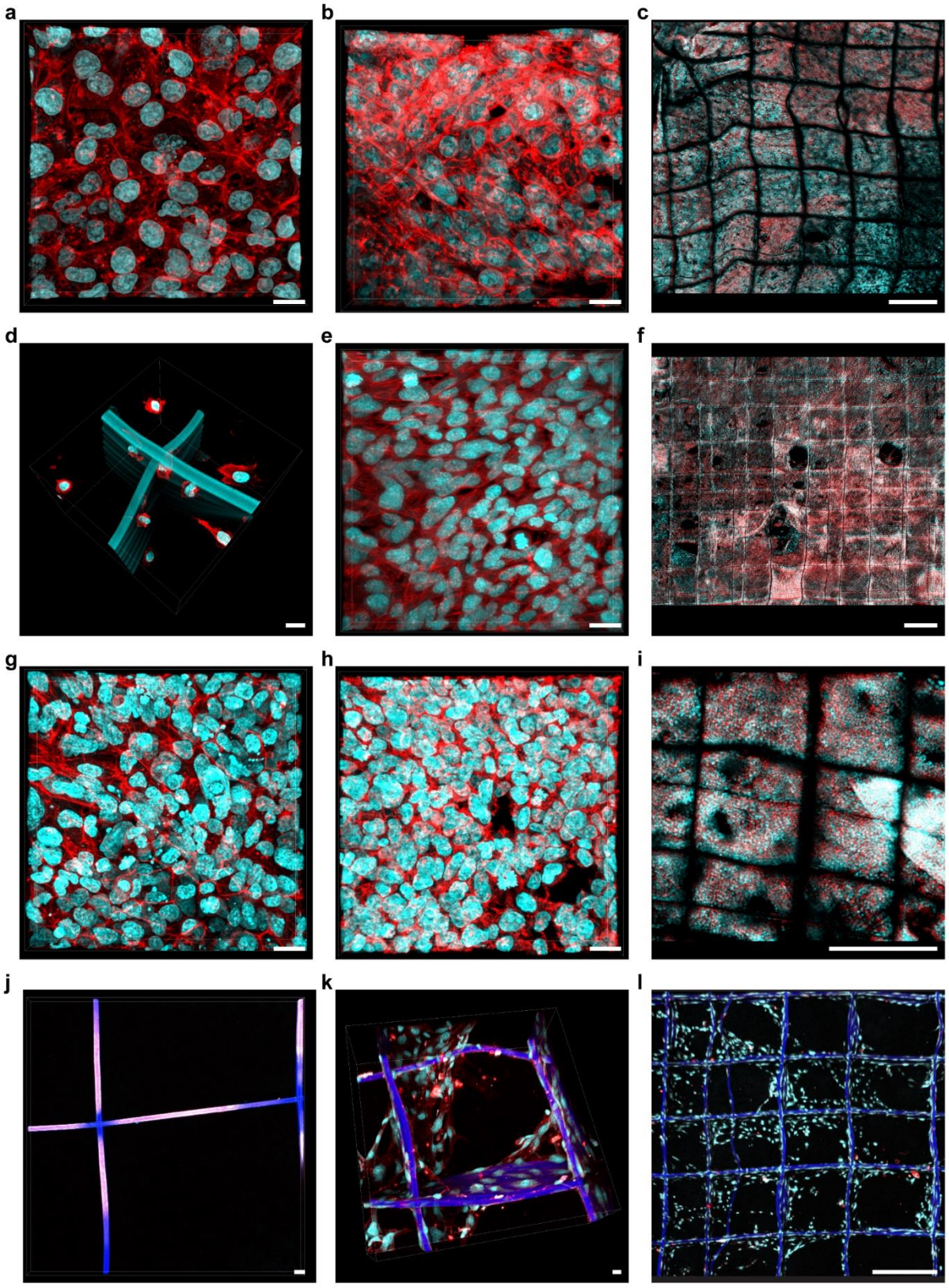

Figure 3-26: Cell type versatility of supported ecFn (a-c) MDA-MB-231 breast cancer cells on supported eECM of (a) collagen I and (b, c) fibronectin at six days. (d-f) Sum159

breast cancer cells on supported ecFn after (d) one day and (e, f) four days of culture. (g-i) Pancreatic cancer cells on supported ecFn. (g) Pancreatic cancer cells from the UM53 epithelial patient-derived cell line after two-day culture. (h, i) ASPC1 mesenchymal pancreatic cancer cell line cultured four days. (j-l) Human umbilical vein endothelial cells cultured for seven days do not grow on supported eECM composed of (j) laminin only (nor fibronectin only – data not shown) but cells thrive well when (k, l) laminin and fibronectin are combined. Whereas cancer cells form confluent volumes across the scaffold (c, f, i) HUVECS remain in lower density bridged structures as shown in (l). (a, b, d, e, g, h, j, k) Scale bars 25 µm. (c, f, i, l) Scale bars 500 µm. (a-l) Channels: cyan, cell nucleus; red, actin. (j-l) Channels: blue, polymer scaffold; cyan, cell nucleus; red, actin. *Credits:* Collagen I isolated from rat tail and generously donated by the Chun Lab at the University of Michigan. Pancreatic cancer cells generously donated by the Simeone Lab at the University of Michigan.

3.4 Conclusions and Implications

A successful 3D cell culture platform will aim to controllably supply cells with the environmental signals it would otherwise receive from the native cell niche *in vivo*. Of these, non-soluble signals in particular are solely provided by the culture substrate or scaffold. In this regard, and considering that the primary purpose of a scaffold is to provide solid structure to the cell microenvironment[140], the ECM is the key feature of the native cell niche to be recreated on a scaffold. Furthermore, for research purposes, a well-designed 3D culture system will offer a means to observe how cells are remodeling the ECM[19], while preserving the biological activity of matrix proteins[128]. At the same time it should be easily handled, and remain amenable to standard culture and characterization techniques[19, 24]. We have found that gentle shearing (interface velocity: 10.4 mm/s) of a concentrated pFn solution at the three-phase contact line defined by air, aqueous solution, and a tessellated scaffold comprised of 500x500 µm square pores can yield extended networks of fibrillar cFn. The ideal scaffold is characterized by a high percentage of open area i.e. the ratio of void to total volume. Large open areas not only allow cells to freely migrate and secrete their own ECM, but also limit interference from synthetic material on protein conformation, cellular function, and formation of cell-cell or cell-ECM contacts. ecFn had suspended within and across the square pores of the 3D jet writing scaffold irrespective of pore size (500 µm, 750 µm,

and 1000 μm pores tested). ecFn fibrils, like cell-secreted matrix, was characterized by a fibrillar architecture, resisted dissolution in detergent, and maintained expression of FnIII. Use of whole proteins in this system not only provided cells with non-soluble signals, but also made the protein matrix susceptible to remodeling and proteolysis as in the MDA-MB-231 human breast cancer culture. Such matrix remodeling was directly observable by microscopy as seen in the TC32 Ewing sarcoma cell culture. As will be seen in Chapter 4, supported ecFn is also readily applicable to other cell characterization techniques such as flow cytometry, and can be implanted into mice. These scaffolds are mechanically stable throughout long term cultures – at least six to eight weeks, as longer cultures have not yet been tested – and fit conveniently into a 24-well plate freely suspended off the plastic surface for a true 3D culture as opposed to a 2.5D culture. All in all, supported eECM advances current cell culture technologies towards greater physiological relevance, which is one step closer to ensuring that biological studies are not plagued by artificial cell behaviors in response to unintentional external signals. Patent protection has been filed for supported eECM, as it is a technology that may be crucial to more reliable cell-based outcomes in applications such as cancer biology, fundamental studies of both diseased and healthy states, and screening of pharmaceuticals where 3D cell culture has potential to bridge the gap between benchtop and animal experiments.

Based on experimental observations, and a review of literature, the mechanism underlying hydrodynamically induced fibrillogenesis is hypothesized as a multi-step process. Submerging the scaffold fully into the pFn solution eliminates its contact with the air-solution interface failing to result in fibrillogenesis, but securing the scaffold at the interface under hydrodynamic shearing consistently induces fibril formation, suggesting that the air-pFn solution interface is required for this technique. We have seen in the literature that Fn molecules in a pFn solution forms a sheet of

aggregated protein at the air-pFn solution interface[13]. Interaction between the Fn and both the hydrophobic and hydrophilic mediums simultaneously is likely to destabilize the solubilized protein which is known to have a hydrophobic core consisting of FnIII which is surrounded by FnI and FnII domains[4, 77, 102]. Hence, the pFn at the interface is expected to have a more open structure than that of the bulk solution. Now, the destabilized pFn should require less force to achieve further extension and opening of the Fn molecule under applied tension or fluid shearing. As FnI domains initiate Fn-Fn interactions[4, 107], and FnIII domains are revealed making more self-association sites available[3, 4, 141], stretched Fn dimers are bound together to form multimers, resulting in the final fibril assembly[96]. Whether dimers are bound by non-covalent intermolecular interactions or covalent disulfide bonds is still unclear in the literature[4, 91, 142]. Although this process is largely described for Fn, it is possible that laminin may also undergo a similar process since its *in vivo* assembly within the basement membrane resembles that of Fn where cells assemble the protein via required integrin receptors and laminin self-interactions[108, 143-146].

The structure, and therefore function, as well as protein composition of the ECM varies depending on the tissue type and should be taken into consideration when recapitulating specific tissues on scaffolds[22]. Researchers need the ability to independently investigate the effects of various ECM compositions as the impact of non-soluble signals on cell response is increasingly realized across disciplines[8, 18, 26, 30]. Supported eECM is not limited to fibronectin alone, but includes collagen, laminin, and with minor protocol optimizations, can include other protein mediums such as Matrigel which is of particular interest to the cancer community. This gives researchers the ability to tune the composition of the protein microenvironment, either by addition of individual proteins, or combinations of proteins as seen with fibronectin and laminin or tenascin-C. Hydrogels are commonly used to culture cells *in vitro* in a proteinaceous environment.

However, hydrogels lack mechanical stability, are difficult to handle and transfer, and are not easily adaptable to current cell characterization techniques. Additionally, hydrogels couple the support of a scaffold with protein composition, implying that if cells were to completely degrade the protein matrix, they would be left suspended in solution rather than adhered to a polymer scaffold as seen in the MDA-MB-231 human breast cancer culture example. Supported eECM also expedites cell expansion as was seen with the fibroblast culture on scaffolds either conformally coated with Fn or after hydrodynamically induced fibrillogenesis. Fibroblasts are able to use fibrillar suspensions of protein to access the large pores of the polymer scaffold providing extensive area for cell adhesion and proliferation. Rapid cell expansion is another advantage of supported ecFn, since shorter culture times are more conducive to aggregating results whether in a research context or precision medicine. The concept of cell migration along Fn fibrils has more recently opened a new focus area in the Lahann Lab where supported eECM is applied in a cell migration assay. Since the entire scaffold can be visualized, live cultures of fluorescent cells have been maintained under a microscope where migration of single cells and cells in bulk can be observed. Current technology for migration assays are largely limited to physiologically inaccurate platforms or 2D cultures[147], bringing to light yet another possible commercial application of supported eECM that is currently under development by students in the Lahann Lab.

Chapter 4

Engineered Fibronectin Networks Applied as a Cancer Microenvironment

Some material from this chapter has been adapted with permission from the following manuscript in preparation:

> S. Ramcharan, L. Solorio, S. McDermott, A. Fox, J.H. Jordahl, C. Dunlay, M. Brown, A. Xiao, M. Wicha, G.D. Luker, J. Lahann. "Engineered 3D cellular fibronectin networks serve as bioequivalent breast cancer tumor microenvironments for patient derived cells" *In Preparation*.

4.1 Introduction

4.1.1 The epithelial-to-mesenchymal transition (EMT)

The dissemination of tumorigenic cells from a primary to a secondary tumor has been found to be accompanied by changes in phenotype between a proliferative epithelial state and a migratory mesenchymal state through a process known as the epithelial-to-mesenchymal transition (EMT) and its reverse, MET[29, 148]. Cells within the primary tumor proliferate until they undergo EMT and become ready to migrate[29, 148]. Upon reaching the metastatic site, these cells can remain dormant, undergo apoptosis, or resume a proliferative, tumor-forming state through MET[29, 148]. This phenotypic plasticity has been considered as a means by which a cancer may resist treatment[149, 150]. Several markers have been proven effective in identifying whether a cancer cell is of an epithelial or mesenchymal phenotype. CD44, a transmembrane hyaluronan receptor, is important to cell migration and cancer invasion as it functions in the degradation of hyaluronan[149]. CD44 is frequently employed as an EMT marker in cancers such as breast and colon[149]. Fibronectin and vimentin expressions are also increased in EMT[149]. If simultaneously expressed with a lack of

CD24, a $CD44^+$ cancer cell is known to have self-renewal properties and is often considered a cancer stem cell (CSC) of a mesenchymal phenotype[150]. In fact, it has been hypothesized that EMT may be the mechanism by which differentiated cancer cells are converted into CSCs[151]. In breast tumors, the mesenchymal CSCs are largely found at the edge of the tumor where they can easily migrate away from the tumor and become invasive. The opposite phenotype, the epithelial CSCs are typically located within the central bulk of the tumor, and are positive for aldehyde dehydrogenase (ALDH)[150]. Although both the $CD44^+/CD24^-$ and the $ALDH^+$ phenotypes are considered tumor-initiating, cells expressing both phenotypes simultaneously were found to have the greatest tumor-initiating potential in a patient derived xenograft model[152]. In addition to strong implications in cancer metastasis, EMT also occurs in development[153] and in the case of injury[154].

4.1.2 Tumor-initiating cells and the pre-metastatic niche

Amongst current breast cancer therapeutics are effective strategies against primary tumors, but little success has been realized in the prevention of recurrence or metastases. Several studies point to a particular subpopulation of cancer cells that have a unique tumor-initiating capability as a possible root cause of secondary tumor formation[148, 155-157]. This subpopulation, considered CSCs, is not targeted by conventional therapies[150, 158, 159], and further understanding of the mechanisms underlying their role in tumor initiation is stunted by the lack of physiologically relevant *in vitro* models[24, 156]. As with cells in general, the surrounding microenvironment is a major regulator of CSC cell fate including self-renewal and differentiation potential[160]. One of the main challenges in cancer research is understanding what are the defining characteristics of the pre-metastatic niche, or a specific site within the target organ prepared for the invasion of migrating tumor cells and secondary tumor formation[28, 132]. The concept of a pre-metastatic niche has previously been metaphorically described through the soil-seed hypothesis where the niche acts as

soil, providing the appropriate microenvironment for the growth of the seeds, or invading tumor cells[26]. ECM composition, tissue stiffness, level of oxygen supply, soluble factors, and the assortment of stromal cells are just some features that may be tuned to make the pre-metastatic niche a suitable environment for the settlement of invading tumor cells and expansion of tumor-initiating cells[28-31]. Fibronectin is a known pre-metastatic niche protein[149, 161] and its expression has been shown to be upregulated in primary human breast cancer cells of the $CD44^{+}/CD24^{-}$ phenotype[162]. It is the hope that supported eECM can provide a fully-defined *in vitro* 3D cell microenvironment with independently tunable properties for co-cultures of cancer cells with stromal cells, probing the effects of various ECM compositions, and possible future combination into a bioreactor system where supply of oxygen and soluble factors can be regulated.

4.1.3 Current in vitro cancer models and expansion of patient-derived cells

Cancer research and drug screening has largely relied on the physiologically irrelevant 2D culture of cancer cell lines leading to results that cannot be directly translated to the treatment of cancer *in vivo*[36, 163, 164]. Each cancer cell line represents the genetics and biology of only a single patient, and even this is unreliable after years of preservation on 2-D plastic[165, 166]. Furthermore, these systems provide no way to accurately model key features of cancer such as metastasis, patient-to-patient variability, and inherent tumor heterogeneity[165-167]. In fact, Vargo-Gogola *et al*. refer to breast cancer as a "collection of diseases" arguing that the diversities observed in different breast cancers cannot be captured in a single model requiring a versatile "multi-system" approach[168]. Hence, the development of a cancer microenvironment that faithfully recreates the tumor biology of human patients remains a critical task. Towards this challenge, Chapter 4 demonstrates the application of supported ecFn as a breast cancer microenvironment for cell lines and primary patient cells.

Tumor grafts are a major component of the current state-of-the-art for patient specific models, where tissues removed from a patient's tumor are implanted in immune-deficient mice for cultivation[165]. In the event that a patient's cancer cells are obtained from fluids such as a pleural effusion, these cells are instead injected into the xenograft[166]. However, this approach has endured extremely low grafting efficiencies, especially in the case of breast and prostate cancer due to the hormone dependency of these diseases[165, 169]; the difficulty in growing tumor grafts from estrogen receptor positive (ER^+) breast cancers is widely known[170] yet about 80% of breast cancers are ER^+[166]. DeRose *et al*. demonstrated the highest currently known breast tumor take rate (the ratio of patient implants that formed tumors to all tumor grafts attempted) at 37% irrespective of receptor status (whether the cancer is positive or negative for ER, human epidermal growth factor receptor 2 or HER2, and progesterone receptor or PR)[165]. Despite the difficulty, developing patient-specific models is imperative, especially in the case of breast cancer, where the success of current therapies is largely stunted by the diversity of treatment responses observed in patients[165, 170] leading to an estimated clinical failure rate for new drugs of 90%[165]. Chapter 4 discusses an alternate approach to recreating patient-specific tumor samples *ex vivo* where rather than relying on a mouse to provide a culture microenvironment, supported ecFn is applied as a breast cancer microenvironment for expansion of patient-derived cells *in vitro*.

4.2 Materials and Methods

4.2.1 Materials

Triton X-100, Tox-8 mitochondrial activity kit, and 4'6-diamidino-2-phenylindole (DAPI) were purchased from Sigma Aldrich and used as received. Dulbelco's Modified Eagle Medium (DMEM), non-essential amino acids (NEAA), antibiotic-antimycotic, and the following antibodies were purchased through Fisher Scientific and used as received: PE-EpCAM clone EBA-1 (BD

Bioscience, San Jose, CA), APC-CD44 clone G44-26 (BD Bioscience, San Jose, CA), PE-Cy7-CD24 clone ML5 (Biolegend, San Diegeo, CA), mouse Pe-IgG1 clone X40 (BD Bioscience, San Jose, CA), mouse Pe-Cy7-IgG1 clone X40 (BD Bioscience, San Jose, CA), mouse APC-IgG1 clone X40 (BD Bioscience, San Jose, CA), Biotin-CD45 clone HI30 (eBioscience, San Diego, CA), Biotin-HLA-DR clone LN3 (eBioscience, San Diego, CA), Biotin-CD14 clone 61D3 (eBioscience, San Diego, CA), Biotin-CD31 clone WM59 (eBioscience, San Diego, CA), Biotin-CD41 clone MEM-06 (Abcam, Cambridge, MA), Biotin-CD19 clone HIB19 (eBioscience, San Diego, CA), Biotin-CD235a clone HIR2 (eBioscience, San Diego, CA), Biotin-CD56 clone CMSSB (eBioscience, San Diego, CA), Biotin-CD3 clone UCHT1 (eBioscience, San Diego, CA), Biotin-CD16 clone eBioCB16 (eBioscience, San Diego, CA), Biotin-CD140b clone 18A2 (Biolegend, San Diego, CA). Aldehyde dehydrogenase activity assay kit was obtained from Cayman Chemicals (Ann Arbor, MI) and used as received.

4.2.2 Mouse breast cancer tumor engraftment assay

All animal studies were approved by the University of Michigan Institutional Animal Care and Use Committee. Briefly, 6-8-week-old female C57BL/6J mice (Charles River Laboratories Inc., Wimington, MA) were anesthetized using 1-2% isoflurane at a flowing oxygen rate of 1 L/min (EZ150 Isoglurane Vaporizer, EZ Anesthesias), and an incision was made to expose the mammary fat pad. AT-3 cells cultured on supported ecFn was placed directly into the fat pad[5] and the incision was closed with wound clips. The number of AT-3 cells on the scaffold was verified using luminescence. 15 mg/mL D-luciferin was added to the cell medium at a ratio of 1:100 and incubated for 10 min before the relative light intensity was measured using a luminometer (Perkin Elmer MLD2300-000), and compared with a standard curve. Tumor engraftment was evaluated using bioluminescence imaging[5]. Tumor histology was evaluated by first fixing the tissue with 4%

formalin for 24 h. Then the tissue was prepared for histology by dehydrating in ethanol, sealed with paraffin, and sliced for staining with hematoxylin, eosin, and Masson's trichrome.

4.2.3 Cell culture and characterization

Breast cancer patient cell samples were seeded in 1 mL onto supported ecFn with square pores 500 μm wide at a concentration of $2x10^6$ cells/mL. Cells were cultured in DMEM containing 10% FBS, 1% NEAA, 2 mM L-glutamine, and 1% Antibiotic-Antimycotic. Cells were seeded and cultured in low adhesion 24 well plates (Corning Inc., Corning, NY) and maintained at 37˚C in 5% CO_2 as previously described. AT-3 mouse breast cancer cells, and human breast cancer cell lines T47D and Sum159 were firefly luciferase expressing. Proliferation was tracked over time by administering 15 mg/mL D-luciferin to the cell medium at a ratio of 1:100 and incubating for 10 min before the relative light intensity was measured using a luminometer (Perkin Elmer MLD2300-000). The growth rate of the primary patient samples and the MDA-MB-468 cell line were evaluated by measuring changes in the mitochondrial activity using a resazurin based assay kit (Tox-8, Sigma Aldrich, St. Louis, MO) following the manufacturer guidelines. The initial signal was recorded after seeding, and then subsequent mitochondrial activity measurements were normalized to the initial time point. If cells were removed from supported ecFn to visualize the remaining protein matrix, samples were decellularized in a protocol adapted from Lu *et. al.*[122]. Samples were washed with PBS, then DI water, and immersed in a solution of 0.1% Triton X-100 with 1.5 M KCl in 50 mM Tris buffer at 4ºC on a slow-moving shaker for two hours. Samples were washed in 10 mM Tris buffer, followed by DI water for one hour each. See Appendix A for detailed protocol.

4.2.4 Evaluating cell tumorigenicity by flow cytometry

Cells were stained following a previously established protocol[152, 157]. Cells were removed using 0.25% trypsin, which was neutralized using a 3:1 volume of complete medium. Cells were then counted using a Luna-FL dual fluorescence cell counter (Logos Biosystems, Dongan-gu, Anyang-si, Gyueonggi-do, South Korea), and re-suspended in aldefluor buffer. Antibodies were added and incubated for 30 minutes, and then rinsed with aldefluor buffer. For primary patient sample analysis, the cells were first incubated in the lineage cocktail for 30 minutes, before staining for EpCAM, CD44, CD24, and ALDH activity. MDA-MB-468 cells were used to establish single color channels. Isotype controls were used to establish gating for the CD44, EpCAM, lineage$^-$ cells, and CD24[152, 157]. DEAB was used to establish gating for the aldefluor activity assay[152].

4.3 Results and Discussion

4.3.1 Improving mouse breast tumor engraftment efficiency

Fibronectin is a major ECM protein of the pre-metastatic niche and has been identified in micro-metastasis[17, 171, 172]. As a validation of the bioactivity of supported ecFn, we investigated its potential to induce phenotypic changes by enhancing tumorigenicity in an established mouse breast cancer tumor graft model. AT-3 firefly luciferase expressing mammary cancer cells, a cell line derived from the primary mammary gland tumor of MMTV-PyMT mice[5], were cultured on supported ecFn. After three days, the AT-3s formed 3D multicellular networks of cell-cell contacts (**Fig. 4-1(a) and Fig. 4-2(a-b)**) at large scale (**Fig. 4-1(b)**) and were still in a proliferative phase (**Fig. 4-2(c)**). Four groups of AT-3 cells were then orthotopically implanted across three immunocompetent C57BL/6 mice for tumor engraftment: (1) 30,000 cells on three-millimeter-wide disks punched out of supported ecFn (2) 30,000 cells directly injected (3) 200,000 cells on a supported ecFn disk and (4) 200,000 cells directly injected. Group 4 is a positive control, being

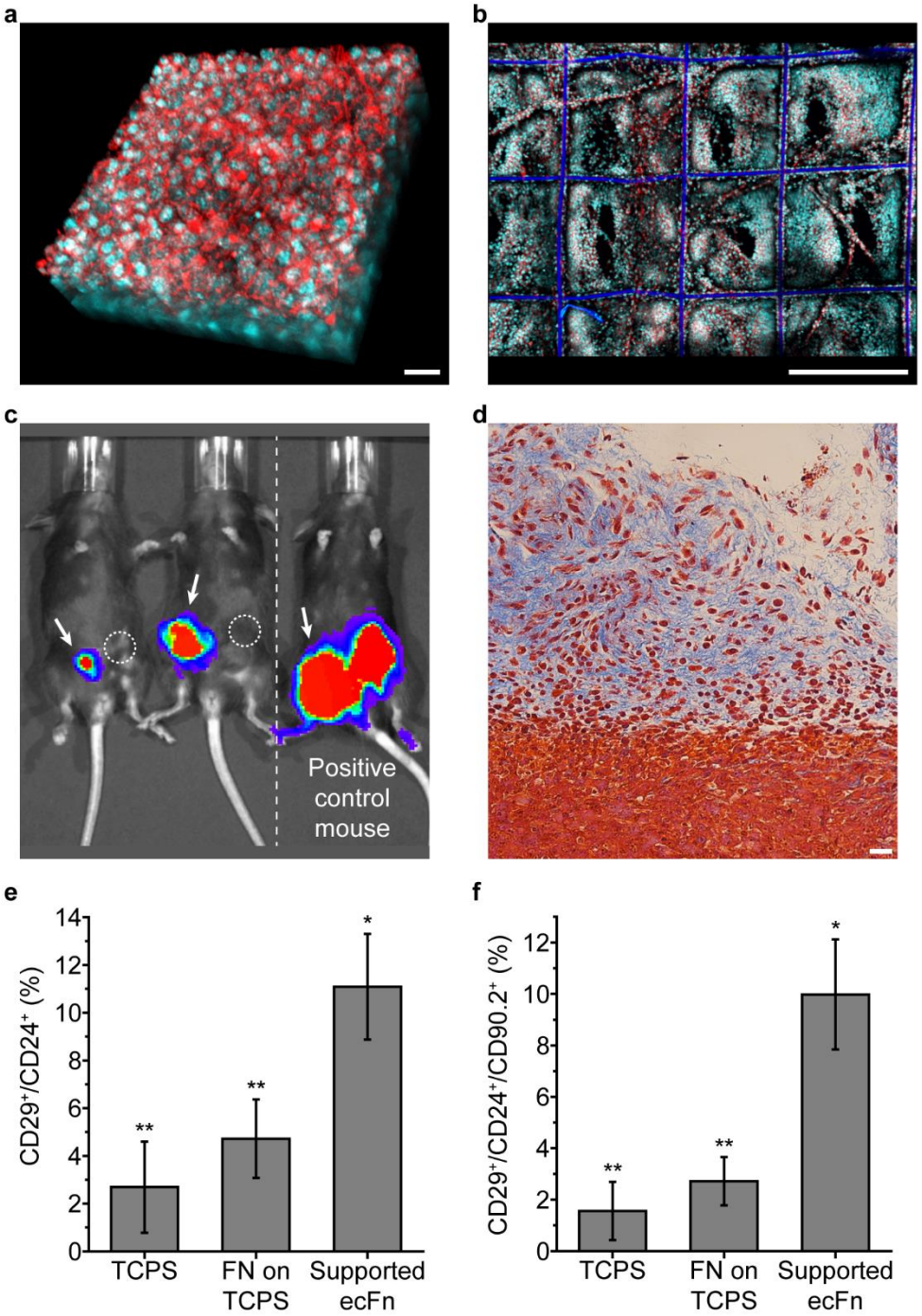

Figure 4-1: Supported ecFn enhances tumor engraftment efficiency in a mouse breast cancer model (a) Representative 3D CLSM of AT-3 mouse breast cancer tissue formed *in vitro* after three days on supported ecFn. Section thickness is approximately 70 µm. Scale bar 25 µm. (b) Large scale view of AT-3 tissue cultured three days on supported ecFn as in *a*. Cells proliferate and fill the 3D space within the protein network across the scaffold. Scale bar 500 µm. (a-b) Channels: cyan, cell nucleus; red, actin. (c) Bioluminescence image of immune-competent mice showing tumor formation 21 days after AT-3 cells were orthotopically implanted (image exposure time 10 seconds). The two mice on the left have

had about 30,000 AT-3 cells on supported ecFn implanted into the mammary fat pads indicated by arrows (group 1). The right mammary fat pad received an injection of approximately the same number of cells in the area indicated by circles (group 2). The third mouse on the right is a positive control having received the group 3 supported ecFn in the left mammary fat pad (arrow), and the group 4 injection in the mammary fat pad on the right, each delivering 200,000 AT-3 cells. Previous studies have concluded that a minimum of 200,000 AT-3 cells are required for tumor formation by cell injection[5]. (d) Mason's Trichrome staining of a tumor graft that formed after 21 days at the implant site of the group 1 30,000 AT-3 cells on supported ecFn; AT-3 cells invaded surrounding tissues. Scale bar: 25 μm. (e) Quantification of the $CD29^+/CD24^+$ cells identifying the AT-3 population capable of self-renewal. Cells were cultured three days on TCPS, TCPS with fibronectin conformally adsorbed (Fn on TCPS), or supported ecFn. Single star indicates that the supported ecFn result is statistically different from TCPS and Fn on TCPS; double star indicates that TCPS and Fn on TCPS are statistically similar. $P<0.05$ (f) Quantification of the $CD29^+/CD24^+/CD90.2^+$ AT-3 cells identifying the tumor initiating population after three days of culture on TCPS, TCPS with fibronectin conformally adsorbed (Fn on TCPS), and supported ecFn. Single star indicates that the supported ecFn is statistically different from TCPS and Fn on TCPS; double star indicates that TCPS and Fn on TCPS are statistically similar. *Credits:* The Luker Lab at the University of Michigan conducted all animal studies, and designed and contributed AT-3 cells to this collaboration. Flow cytometry done in the Wicha Lab at the University of Michigan.

the minimum number of cells required to form a tumor by direct injection[5]. Pre-culture of cells *in vitro* on scaffolds has been shown to enhance cell delivery and engraftment compared to injection of free cells in myocardial tissue[173, 174], and is essential in bone regeneration[33]. Injections of free cells[173, 174] or hydrogel suspensions[175] typically result in reduced cell survival, engraftment, and retention at the delivery site. Attributes of a successful cell-delivery vehicle include (1) high cell density (2) anchorage and integration into a protein matrix and (3) the provision of space for cells to spread into their natural morphology, form cell-cell contacts, and secrete endogenous matrix proteins[33, 175], all features of supported eECM.

Bioluminescence readings two days after AT-3 implantation indicated that group 1, supported ecFn carrying only 30,000 cells, had resulted in the start of tumor formation, whereas no signal was detected at the group 2 injection of an equivalent number of cells into the contralateral mammary fat pad (**Fig. 4-3**); this result remained consistent for the 21-day duration of the study (**Fig. 4-1(c)**). As expected, group 4 resulted in tumor formation in the positive control

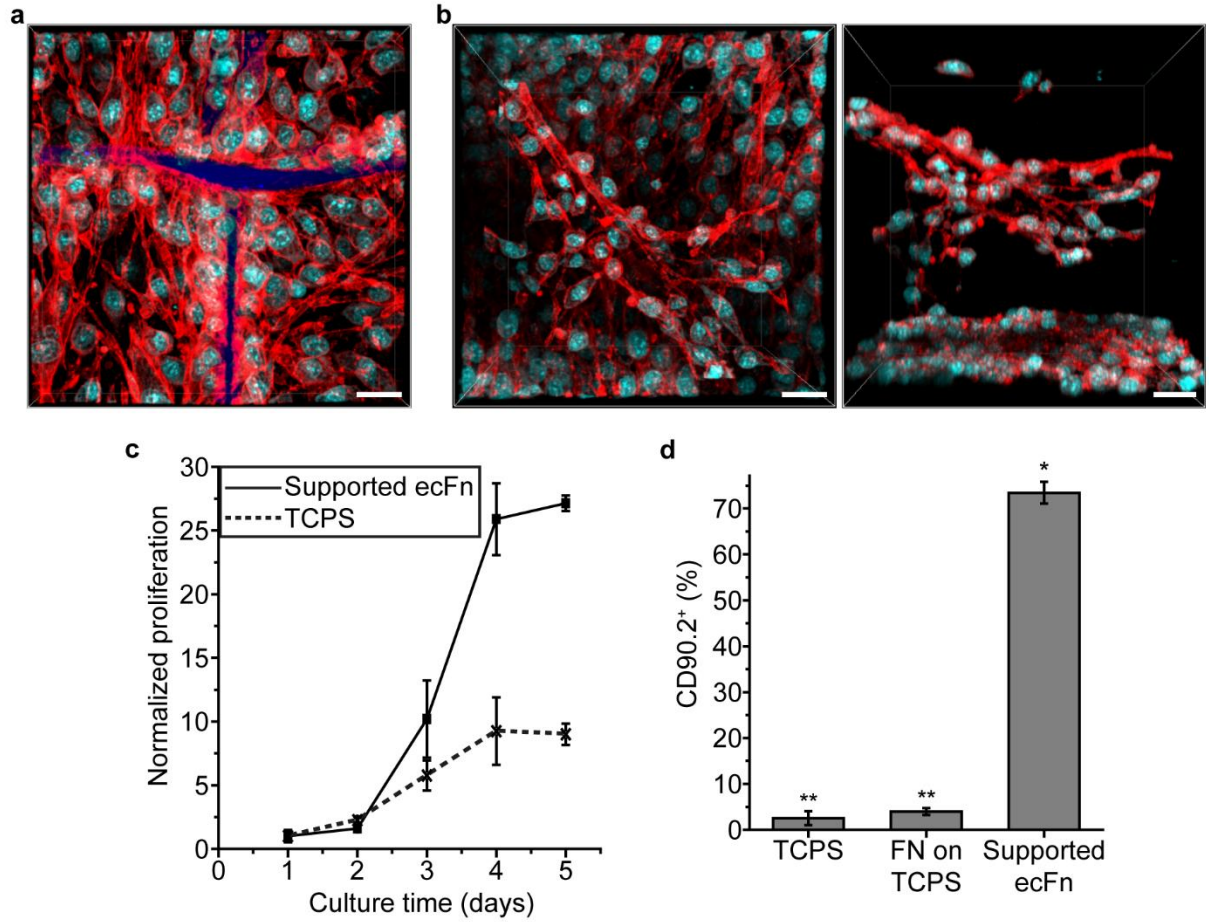

Figure 4-2: Supported ecFn promotes a tumorigenic phenotype in AT-3 mouse breast cancer cells (a) LSCM of AT-3 mouse breast cancer cells at the crosshair of the scaffold microfibers after three days of culture on supported ecFn. (b) LSCM image after three days of culture showing *(left)* top view and *(right)* side view of the AT-3s forming multicellular structures as they span up into the open pore of the supported ecFn scaffold. (a-b) Channels: blue, polymer support; cyan, cell nucleus; red, actin. Scale bars 25 µm. (c) Growth curve for AT-3 cells cultured on TCPS (dotted line, criss-cross marker) or supported ecFn (solid line, square marker). (d) Quantification of the $CD90.2^{+}$ population of AT-3 cells after three days of culture on TCPS, fibronectin conformally coated on TCPS (FN on TCPS), or supported ecFn. Single star indicates that the ecFn network result is statistically different from TCPS and FN on TCPS; double star indicates that TCPS and FN on TCPS results are statistically similar. $P<0.05$ *Credits:* The Luker Lab at the University of Michigan conducted all animal studies, and designed and contributed AT-3 cells to this collaboration. Flow cytometry done in the Wicha Lab at the University of Michigan.

mouse, as did group 3, supported ecFn with 200,000 cells (**Fig. 4-1(c)**). In addition to improved tumor engraftment, this study demonstrates the cell-delivery capabilities of supported ecFn. We hypothesize that the *in vitro* formation of 3D cell-protein structures prior to implantation enables supported ecFn to serve as an effective cell delivery vehicle. We expect enhanced cell survival and

engraftment upon implantation since the cells have pre-formed a thriving tissue element. This is in contrast to injection of freely floating cells that may disperse from the target upon injection, fail to survive delivery, or fail to integrate into the existing matrix in the target area. The presence of the protein matrix on supported ecFn improves localization of cells within the scaffold and target implant region as previously reported in other systems[176, 177].

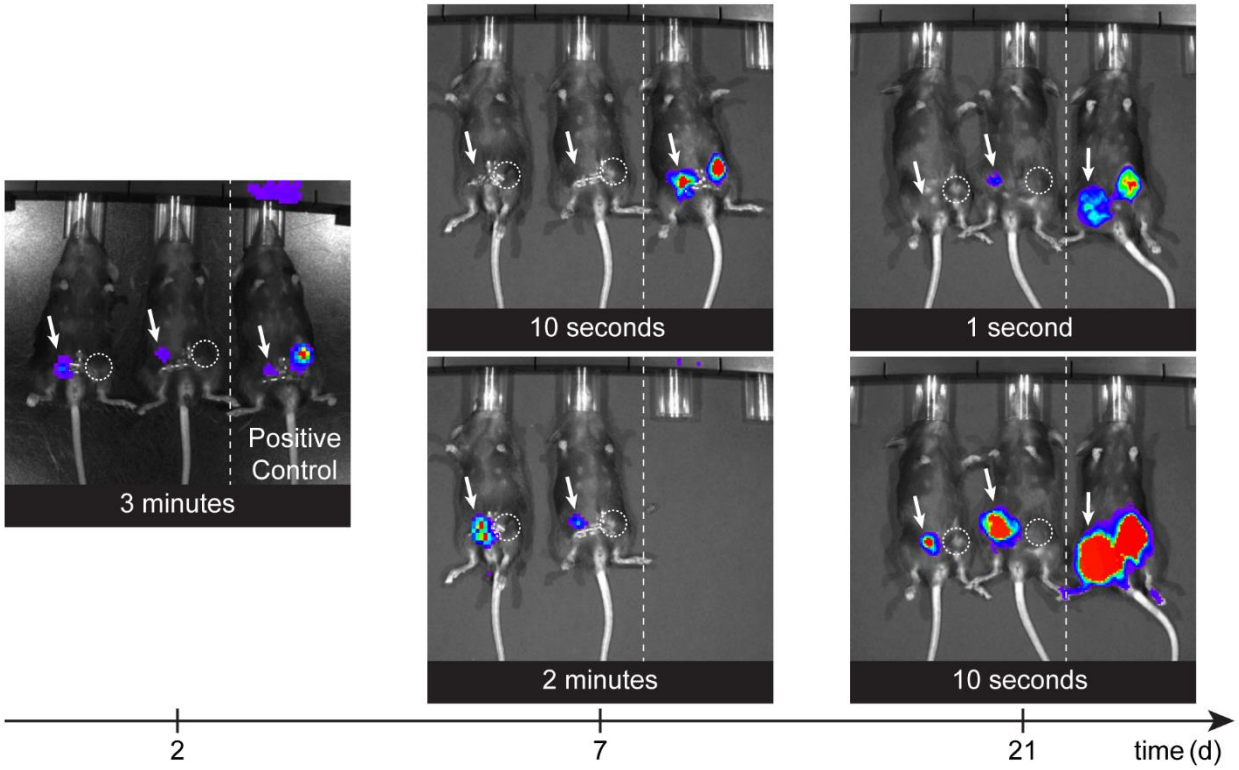

Figure 4-3: Supported ecFn shows successful tumor engraftment in AT-3 mouse breast cancer model throughout the course of three weeks Bioluminescence image of immune-competent mice two, seven, and 21 days after orthotopic implantation of AT-3 cells. Four groups were examined: (1) 30,000 cells on three-millimeter-wide supported ecFn disks (2) 30,000 cells directly injected (3) 200,000 cells on a supported ecFn disk and (4) 200,000 cells directly injected as a positive control being the minimum number of cells required for tumor formation by direct injection[5]. The two mice on the left have group 1 in the left mammary fat pad as indicated by arrows and group 2 in the contralateral mammary fat pad on the right indicated by dashed circles. The third mouse on the right is a positive control carrying group 3 in the left mammary fat pad indicated by an arrow and group 4 in the contralateral right mammary fat pad. Exposure time for each bioluminescence image is indicated. *Credits:* The Luker Lab at the University of Michigan conducted all animal studies, and designed and contributed AT-3 cells to this collaboration.

Follow up histological analyses of tumor grafts resulting from group 1 implants of supported ecFn showed that AT-3 cells were of an invasive character as seen in **Figure 4-1(d)** where cancer cells are seen invading into the adjacent collagenous tissue. We further investigated the tumorigenicity of AT-3s cultured three days on TCPS, fibronectin conformally coated onto TCPS (FN on TCPS), or supported ecFn (**Fig. 4-1(e-f) and Fig. 4-2(d)**). The population of AT-3s positive for CD29 (β1 integrin) and CD24 (heat shock protein) retain their capacity for self-renewal and tumor initiation[178, 179]; and was found to be significantly increased on supported ecFn relative to TCPS and FN on TCPS (**Fig. 4-1(e)**). Most of these $CD29^{+}/CD24^{+}$ cells were epithelial and metastatic in nature, being also positive for CD90.2 (**Fig. 4-2(d)**)[179-182]. In fact, $CD90.2^{+}$ marked the largest phenotypic difference between supported ecFn and TCPS or FN on TCPS; almost a 30-fold increase was observed for cells cultured on supported ecFn relative to TCPS (**Fig. 4-2(d)**). Given the stark increase in tumorigenicity of the AT-3s on supported ecFn, we next sought to explore any similar effects on human breast cancer cells with the MDA-MB-468 cell line.

4.3.2 Enriching the tumor-initiating cell population

The increased tumorigenicity observed in **Figure 4-1(e-f)** for the AT-3 mouse breast cancer cells after culture on supported ecFn was also seen for human in the triple negative breast cancer cell line, MDA-MB-468. Because of the low percentage of cells that express the mesenchymal $CD44^{+}/CD24^{-}$ tumor initiating phenotype (less than 3%)[156, 170, 183], MDA-MB-468s were selected as a model human cell line in which to observe upregulations in the mesenchymal population. MDA-MB-468s were cultured four days on supported ecFn, forming a microtissue across the entire volume of the polymer scaffold (**Fig. 4-4(b) and 4-5(a)**) and exhibiting extensive cell-cell and cell-Fn contacts (**Fig. 4-4(a)**). MDA-MB-468s were also cultured on TCPS, and Fn on TCPS. The $CD44^{+}/CD24^{-}$ population was highest on supported ecFn with the most significant enrichment

on the sixth day (**Fig. 4-4(c)**). We also quantified the population positive for aldehyde dehydrogenase (ALDH), a known marker of mammary stem cells and epithelial-like proliferative behavior[152, 156, 159, 170], that has been considered a superior indicator of tumor-initiating cells

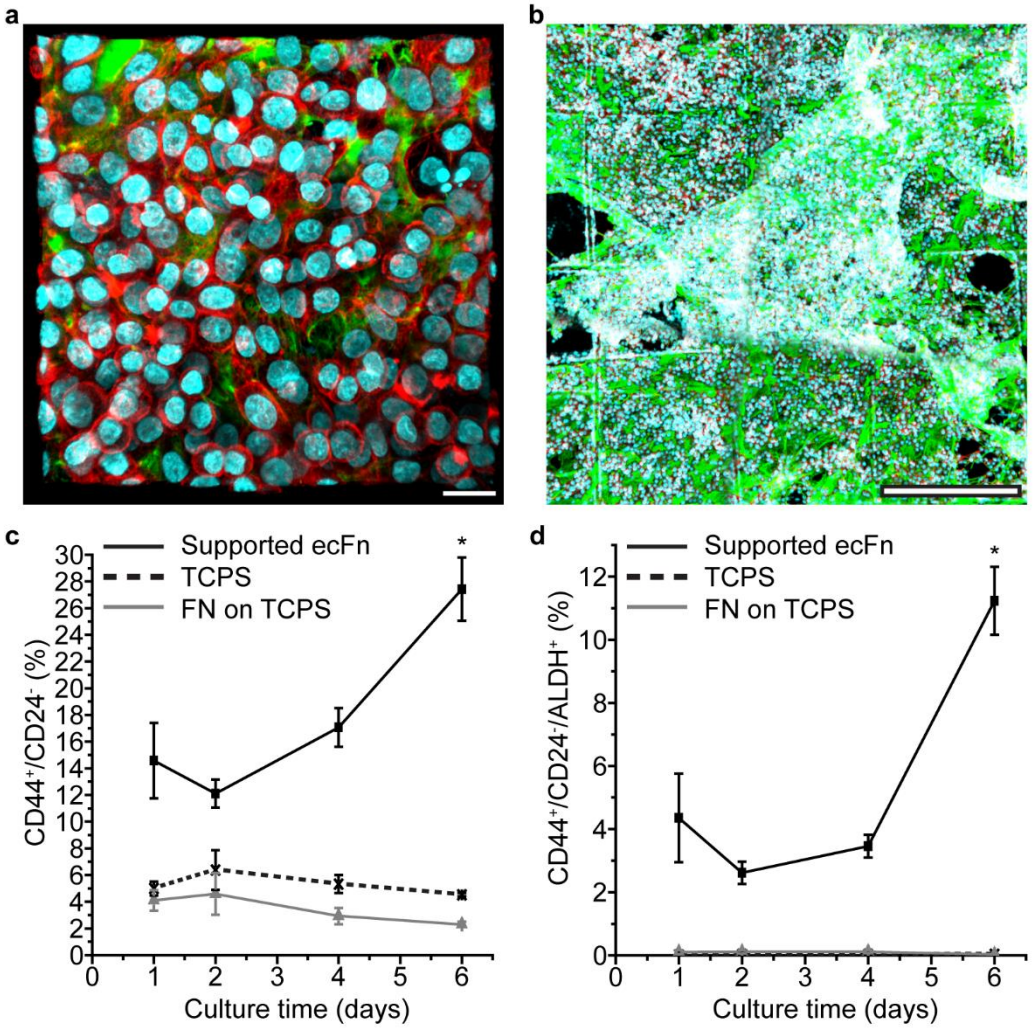

Figure 4-4: Supported ecFn increases the tumor-initiating population in MDA-MB-468 human breast cancer cells (a) MDA-MB-468 breast cancer cells cultured four days on supported ecFn form cell-cell and cell-ECM contacts. Scale bar 25 µm. (b) MDA-MB-468 cells form confluent volumes at large scale across supported ecFn scaffolds after four days. Scale bar 500 µm. (a-b) Channels: green, fibronectin; orange, laminin; cyan, cell nucleus; red, actin. (c-d) Population of MDA-MB-468s on supported ecFn (black solid line and square marker), TCPS (black dotted line and criss-cross marker), or fibronectin adsorbed conformally onto TCPS (grey line and triangular marker) that are (c) $CD44^+/CD24^-$ and (d) $CD44^+/CD24^-/ALDH^+$ measured over time via flow cytometry. The starred time point is statistically different from the other three time points within the supported ecFn dataset. *Credits:* Flow cytometry done in the Wicha Lab at the University of Michigan.

relative to $CD44^+/CD24^-$ alone[155, 159]. Interestingly, after four days in culture, the difference in the $ALDH^+$ sub-population was diminished between supported ecFn and TCPS or Fn on TCPS (**Fig. 4-5(b)**) suggesting that the increasing $CD44^+/CD24^-/ALDH^+$ trend shown in **Figure 4-4(d)** is largely driven by mesenchymal tumor-initiating cells. Furthermore, the MDA-MB-468 population expressing the epithelial cell adhesion molecule ($EpCAM^+$) was greater than 99% for all three culture systems (data not shown). Taken together this data suggest that supported ecFn induced an epithelial to mesenchymal transition in the MDA-MB-468 cells. Further studies aimed at understanding the effect of supported ecFn on EMT/MET in breast cancer cells will look at additional human cell lines, such as the epithelial T47D and the mesenchymal Sum159 for any shifts away from the respective well-known characteristic phenotypes[151, 153, 184, 185] (**Fig. 4-6**).

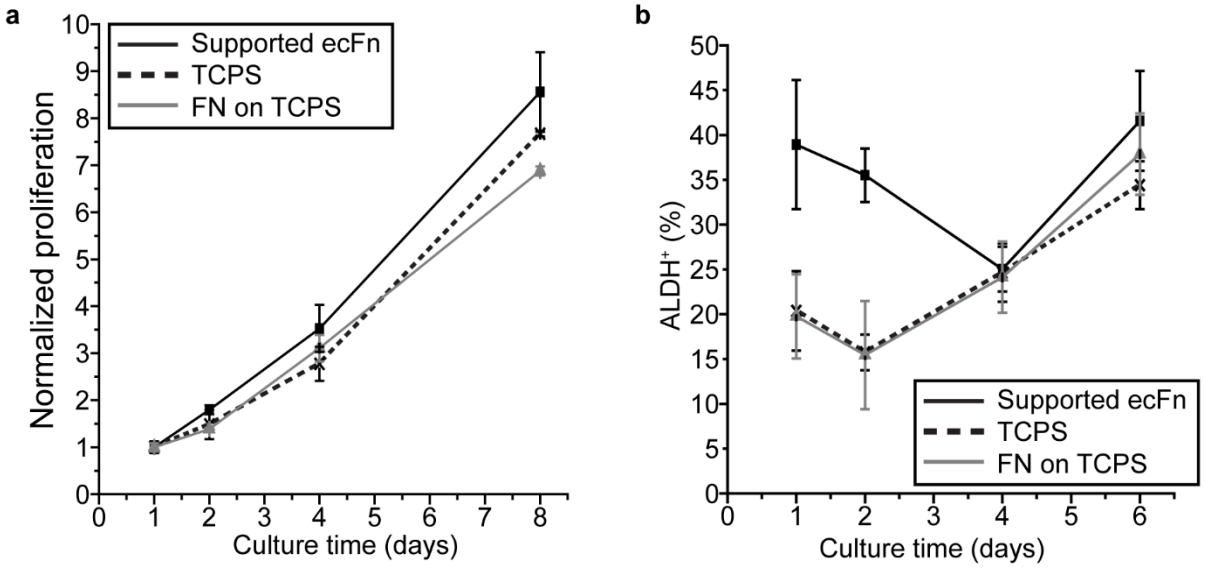

Figure 4-5: Proliferation trends and ALDH expression for MDA-MB-468 cells are similar across different cell culture substrates (a) Normalized proliferation measured by net mitochondrial activity of MDA-MB-468 cells shows little to no difference amongst supported ecFn and control substrates despite observed changes in tumorigenicity. (b) Early timepoints show increased fractions of $ALDH^+$ (aldehyde dehydrogenase) cells on supported ecFn relative to TCPS, and FN on TCPS, but ALDH populations across the three cell culture substrates converge and increase together from the fourth to sixth day in culture. (a-b) Supported ecFn (black solid line and square marker), TCPS (black dotted line and criss-cross marker), and TCPS conformally coated with fibronectin or FN on TCPS (grey line and triangular marker). *Credits:* Flow cytometry done in the Wicha Lab at the University of Michigan.

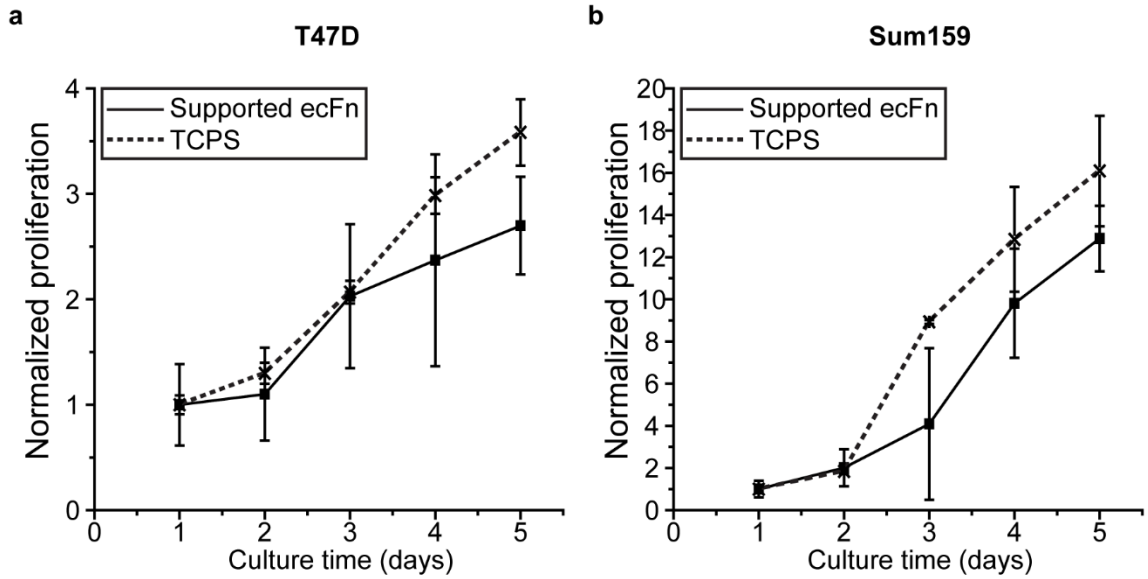

Figure 4-6: T47D and Sum159 human breast cancer cells proliferate on supported ecFn Normalized proliferation gives fold increase in cell number over the course of five days in culture on either supported ecFn (black solid line and square marker) or TCPS (black dotted line and criss-cross marker). Supported ecFn is able to support growth of human breast cancer cells as with (a) T47d and (b) Sum159 cell lines. As with MDA-MB-468s in Figure 4-5(a), the growth profile on TCPS is similar to that of supported ecFn.

4.3.3 Expanding patient-derived cells and inducing EMT

With the observed increases in tumor-initiating potential in the mouse AT-3 and human MDA-MB-468 breast cancer cell lines, we hypothesized that supported ecFn would provide patient-derived cancer cells a sufficiently tumorigenic environment to enable *in vitro* expansion. Malignant pleural effusion or ascites samples were collected from 14 women representing a diverse array of metastatic breast cancers (**Table 4-1**) and were successfully cultured on supported ecFn without prior fractionation (**Fig. 4-7(a-c), 4-8(a-d)**); of this 8 out of 12 were estrogen receptor positive (2 patients had unknown receptor status), a breast cancer subtype that is significantly less likely to form a tumor graft[169, 170]. All 14 patient samples proliferated on supported ecFn but not on TCPS or Fn on TCPS as represented in **Figure 4-7(c)** and **Figure 4-10(b)**. Ki67 staining further confirmed that the cells were in a proliferative state[150, 169] on supported ecFn but senescent on TCPS (**Fig. 4-7(c)**). This observed ability of supported ecFn to maintain cultures of cells that are

Table 4-1: Breast cancer patient data

Patient*	Sample type**	Patient age	Receptor status***			Detected metastases
			ER	PR	HER2	
A - IDC	AC	47	-	-	-	Lymph node, Bone
B - ILC	AC	76	+	+	-	Peritoneum, Bone
C - ILC	AC	54	+	+	+	Peritoneum, Bone
D - ---	AC	73	----	----	----	Renal, Omental, Peritoneum
E - IDC	AC	61	+	+	-	Endometrial, Uterine cancer
F - IDC	AC	51	-	-	+	Chest wall, Skin, Left axilla, Lymph node
G - IDC	PE	51	+	+	+	Skin, Pleura, Bone
H - IBC	PE	44	-	-	+	Pleura
I - IBC	PE	53	+	+	-	Chest wall, Ovaries, Bone
J - IDC, ILC	PE	57	+	-	-	Liver, Bone
K - IDC	PE	56	+	+	-	Skin, Liver, Lung, Pleura, Lymph node
L - IDC	PE	42	+	+	-	Leptomeningeal, Eye, Bone
M - IDC	PE	40	-	-	+	Lymph node
N - ---	PE	62	----	----	----	Bone

*Patient: Patient sample as arbitrary letter name followed by cancer type. Invasive ductal carcinoma (IDC), invasive lobular carcinoma (ILC), inflammatory breast cancer (IBC)
**Sample type: ascites (AC), pleural effusion (PE)
***Receptor status: estrogen receptor (ER), progesterone receptor (PR), human epidermal growth factor receptor 2 (HER2)

otherwise difficult to grow *in vitro* may be interpreted as another confirmation of superior physiological relevance compared to other cell culture substrates. A worthy direction of future study therefore is to apply supported eECM to the expansion of other cell types that are difficult to culture such as other primary cells[186, 187], human embryonic stem cells[188], and neurons[189]. Supported ecFn maintained cell proliferative capacity such that patient cell count had increased 7-fold after eight days in culture (**Fig. 4-7(c)**). Patient samples could expand throughout the entire 34.8 mm^2 polymer scaffold in under 10 days (**Fig. 4-7(b)**). Rapid *in vitro* expansion of patient derived cancer cells either for achieving greater cell numbers or formation of a representative patient tumor graft *ex vivo* will prove advantageous in regards to precision medicine and quickly attaining personalized drug response results. Interestingly, Patient E cells (patient samples arbitrarily named) that were first cultured on supported ecFn for one day, removed and re-seeded

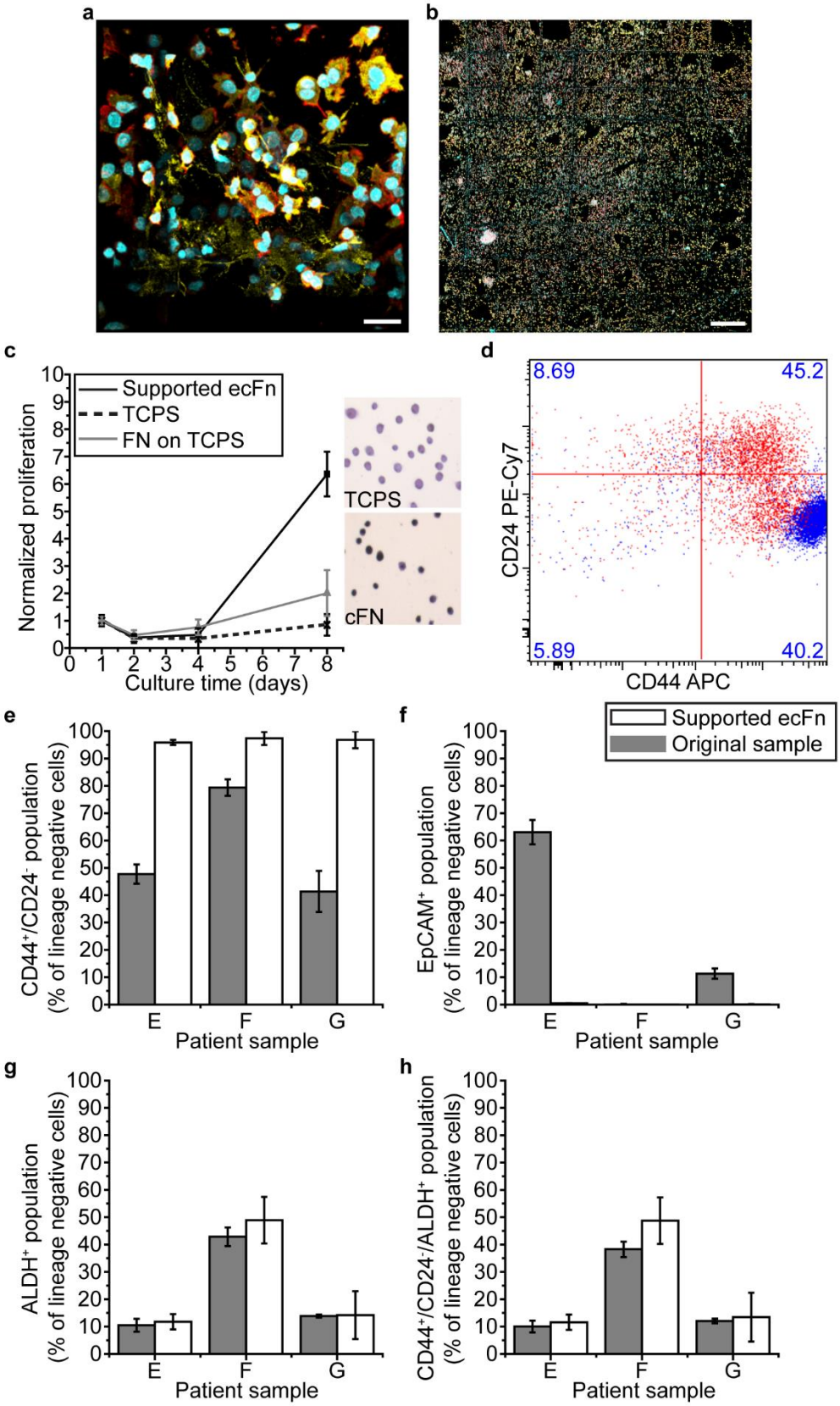

Figure 4-7: Supported ecFn enables expansion of patient breast cancer cells and enrich the tumor-initiating cell population in an epithelial to mesenchymal transition

(a-b) Supported ecFn maintains culture of heterogenous cell populations taken from Patient E ascites sample. LSCM volume views taken after four days of culture. Channels: cyan, cell nucleus; red, actin; yellow, cytokeratin 5. (a) 3D cell structures form within the pores and along the microfiber walls of the scaffold. Scale bar 25 μm. (b) Patient E cells fill supported ecFn scaffold at large scale across many 500 μm square pores. Scale bar 500 μm. (c) Proliferation measured via mitochondrial activity for ascites sample from Patient A is far increased on supported ecFn (black solid line and square marker), with little to no growth on fibronectin adsorbed conformally onto TCPS (grey line and triangular marker), or TCPS (black dotted line and criss-cross marker). Inset shows representative images of Ki67 staining of Patient B cells cultured on either TCPS or supported ecFn. Darker color indicates that the cells are in a proliferative state on supported ecFn but senescent on TCPS. (d) Flow cytometry measurement of CD24 and CD44 in the ascites sample from Patient E where the original sample is shown in red and the same sample after six days of culture on supported ecFn is shown in blue. Original spread in cell phenotype concentrated towards $CD44^+/CD24^-$ status after culture on ecFn networks. (e-h) Flow cytometry measurements of the percentage of lineage negative cells that are (e) $CD44^+/CD24^-$ (f) $EpCAM^+$ (epithelial cell adhesion molecule) (g) $ALDH^+$ (aldehyde dehydrogenase) and (h) $CD44^+/CD24^-/ALDH^+$ within ascites samples from Patients E and F, and a pleural effusion sample from Patient G. Grey bars represent the original patient sample and white bars indicate result after cells were cultured on supported ecFn *in vitro* for six days. *Credits:* Patient cells were obtained through the Luker Lab and Hayes Lab at the University of Michigan. Flow cytometry done in the Wicha Lab at the University of Michigan.

onto TCPS, thrived on TCPS thereafter (**Fig. 4-10(a)**). Although further studies are necessary to understand this phenomenon, it leaves open the possibility for various uses of supported eECM in expansion and propagation of patient samples starting from a single tissue source. For example, supported eECM can provide a culture substrate where patient cells are directly seeded, expanded, and formed into a 3D tumor graft representative of a specific patient, as similarly done here. Alternatively, the supported eECM can act as a pre-culture system that first conditions cells from a patient's body to make the transition to surviving on any other cell culture matrix of interest *in vitro* where it would otherwise be difficult to culture primary human cells.

Supported ecFn enabled the co-culture of cell populations that were heterogeneous with respect to cell morphology or cytokeratin 5 (CK5) expression (**Fig. 4-7(a) and Fig. 4-8(a-d)**), and had increased specifically the number of cancer cells, represented by the lineage negative population, at least 7-fold relative to the original patient sample after only six days in culture (**Fig. 4-9(a)**). This shift was also observed by microscopy as shown in **Figure 4-8(d)** where after five

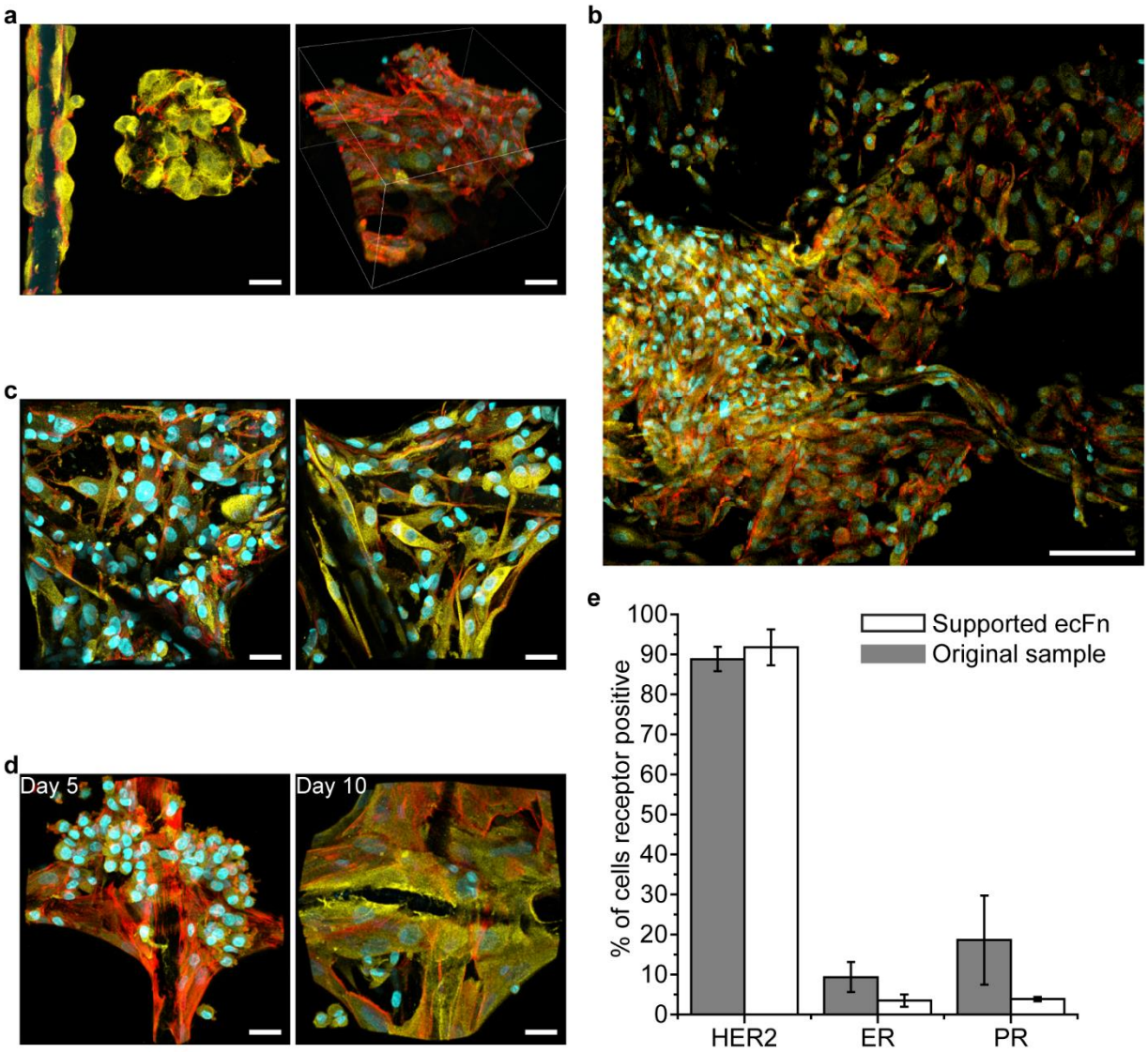

Figure 4-8: Supported ecFn provide a microenvironment for the expansion of patient pleural effusion and ascites samples *ex vivo* while maintaining receptor status (a-c) Pleural effusion samples from (a-b) Patient I and (c) Patient H cultured on supported ecFn and imaged via LSCM showing heterogeneity, scalability, formation of 3D cell structures, and separation of cells by cell type into different areas of the same scaffold. (d) Population shifts in favor of cancer cells marked by cytokeratin in ascites sample from Patient J cultured either five days or ten days on supported ecFn. Representative LSCM images taken at the microfiber crosshair of the 3D jet writing polymer scaffold. (a-d) Channels: cyan, cell nucleus; red, actin; yellow, cytokeratin 5. Scale bar (a, c, d) 25 µm, (b) 100 µm. (e) Pleural effusion sample from Patient F was made into a cytospin, stained, and quantified for positive signals of human epidermal growth factor receptor 2 (HER2), estrogen receptor (ER), and progesterone receptor (PR). This analysis was performed on cells from the original patient sample (grey bars) and after six days of culture on supported ecFn (white bars). Hospital data reported that this patient's receptor status was $HER2^{+}ER^{-}PR^{-}$. Error bars represent standard deviation of % of receptor positive cells measured from three to four microscope fields of view. *Credits:* Patient cells were obtained through the Luker Lab and Hayes Lab at the University of Michigan.

days of culture, the $CK5^+$ cells remained in small clusters. By day 10, $CK5^+$ cells had increased in population and formed a cell network spreading into the open pores of the polymer scaffold. Different cell types were found to spatially separate on the same scaffold as seen in **Figure 4-8(a)** where $CK5^+$ cells formed tight clusters on the supported ecFn while actin-rich cells of a spindle-like morphology adhered first to the scaffold microfibers and proliferated outwards. Culture on supported ecFn inherently removed some cells such as platelets and blood cells which are non-adherent. These results address several challenges typically faced in breast cancer cell culture. Firstly, as previously mentioned, the tumor microenvironment is largely composed of heterogeneous cell populations on both the cancer and stromal cell front. The culture of different cell types, i.e. co-cultures are known to be more challenging to maintain *in vitro*, however, supported ecFn has successfully expanded all 14 patient samples which always consist of a mixture of cell types. The large volume available for cell spreading allows cells to freely assemble into distinct 3D cell structures such as clusters or sheets, and to spatially segregate by cell type in different areas of the same scaffold. In regards to observing heterogeneity, supported eECM can be directly visualized by standard microscopy techniques (**Fig. 4-8**), or the cells can be removed and sorted by flow cytometry (**Fig. 4-9**). Secondly, as with any patient sample, there always lies a challenge in collecting sufficient amounts of material or being able to propagate patient material *in vitro* to have enough samples for experimental or patient treatment purposes. Although the amount of patient material collected in the pleural effusions and ascites was relatively substantial, the population of cells that are actually cancer can be far less than 5% (**Fig. 4-9(a)**). Supported ecFn helps in concentrating down patient samples to the cells of interest, in this case, the cancer cells, by inherently sorting out non-adherent cells through media changes and enriching the cancer cell population (**Fig. 4-9(a)**). This naturally occurring enrichment of the cancer cell population

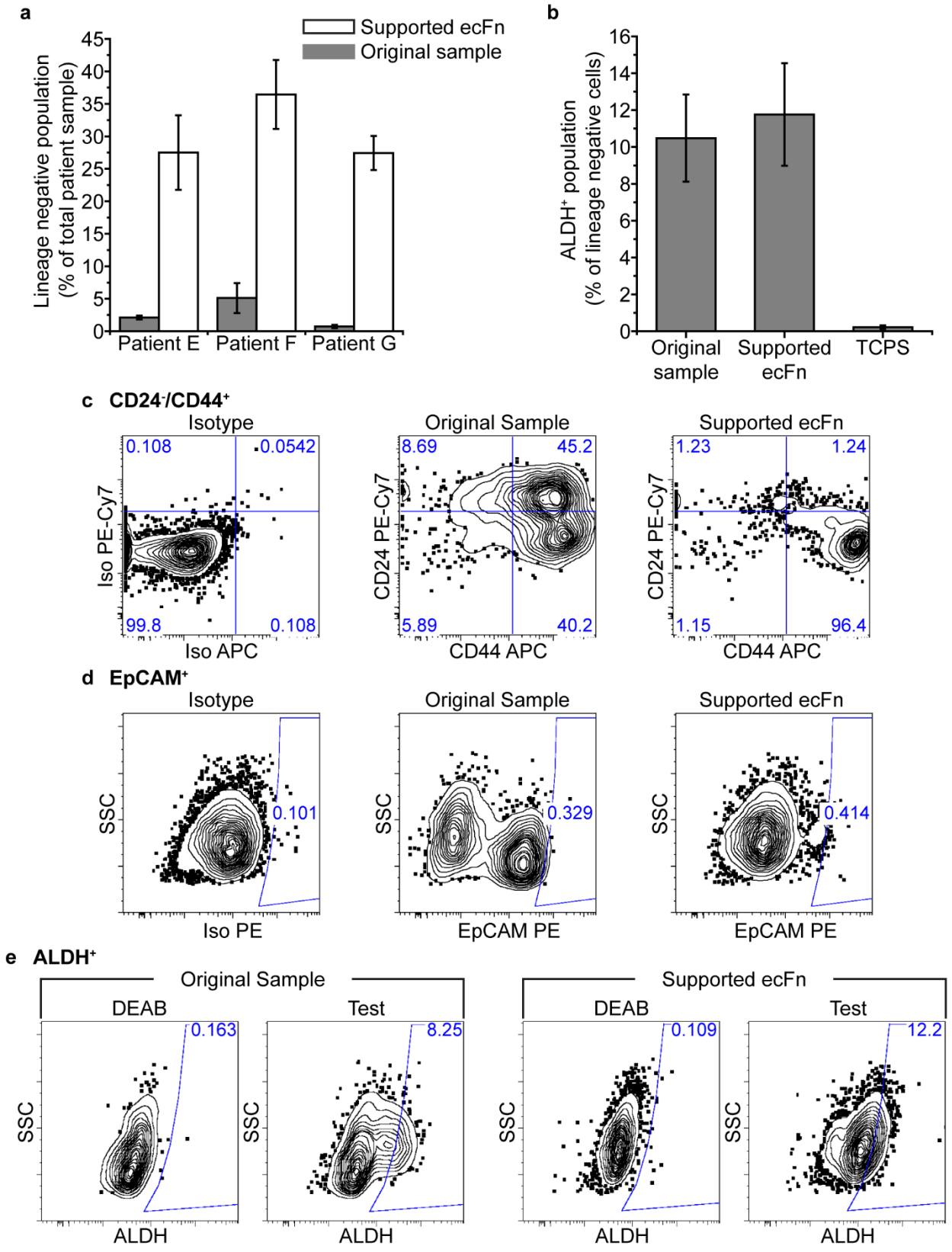

Figure 4-9: Six-day culture on supported ecFn enriches breast cancer cell population in patient pleural effusion or ascites samples (a) Percent of total sample that are cancer

cells indicated by the lineage negative population as measured directly from the patient (grey bars) and after six days of culture on supported ecFn (white bars). (b) Percent of Patient E lineage negative cells that are $ALDH^+$ (aldehyde dehydrogenase) after culture on supported ecFn or TCPS as compared to the original ascites sample. (c-e) Representative flow cytometry scatterplots for Patient E comparing the original ascites sample to cells cultured on supported ecFn for six days. The (c) $CD24^-/CD44^+$ (d) $EpCAM^+$ (epithelial cell adhesion molecule) and (e) $ALDH^+$ cells within the lineage negative population were quantified. *Credits:* Patient cells were obtained through the Luker Lab and Hayes Lab at the University of Michigan. Flow cytometry done in the Wicha Lab at the University of Michigan.

after culture on supported ecFn requires future studies of shifting cell populations to be fully understood. Are the originally present cancer cells outcompeting the non-cancer cells and proliferating at a faster rate? Are the non-cancer cells proliferating more slowly or dying out? Does the presence of Fn, being a pre-metastatic niche protein, have any effect on how conducive the scaffold is to cancer cell growth and tumor formation?

Having distinct receptor statuses, patient samples E, F, and G were selected to evaluate cell phenotype and tumorigenicity after a six-day culture on supported ecFn. As was seen with the MDA-MB-468s in **Figure 4-4(c)**, within the patient cancer cell population, culture on supported ecFn enriched the mesenchymal self-renewing $CD44^+/CD24^-$ subpopulation relative to the original patient sample (**Fig. 4-7(e) and Fig. 4-9(c)**). Shown in **Figure 4-7(d),** CD24 and CD44 expression was disperse across the original patient sample (red) but concentrated towards the $CD44^+/CD24^-$ phenotype after culture on supported ecFn (blue). At the same time, the epithelial-like tumor-initiating subpopulations indicated by expression of ALDH (**Fig. 4-7(g) and Fig. 4-9(b,e)**), and the overlapping immunotype $CD44^+/CD24^-/ALDH^+$ (**Fig. 4-7(h)**) were maintained on supported ecFn relative to the original patient sample. A similar result was observed for the ALDH expression of the MDA-MB-468s in **Figure 4-5(b)**. For comparison, while the population of $ALDH^+$ patient cells was maintained on supported ecFn, after culture on TCPS it had dropped dramatically compared to the original patient sample. Finally, when present in the original patient sample, the

percentage of cancer cells expressing EpCAM dropped to nearly zero after culture on supported ecFn (**Fig. 4-7(f) and Fig. 4-9(d)**). As determined for the human breast cancer cell line, MDA-MB-468, these results suggest that supported ecFn induced EMT in patient derived breast cancer cells. Still, despite this shift towards a mesenchymal character, the breast cancer receptor status of the original sample was maintained (n=1) (**Fig. 4-8(e)**). Maintaining patient receptor status is important to ensure that the *ex vivo* tumor graft accurately represents the cancer of the patient and allows for testing of hormone based therapies such as letrozole or lapitinib on supported ecFn.

EMT has been linked to cancer metastasis, CSCs, and resistance to therapeutics and apoptosis, but much is still unknown regarding the relationships between these concepts and the governing cell/ECM mechanisms[150, 153, 190]. Chapter 4 has shown that supported ecFn has great potential to serve as a model in which to study EMT *in vitro*. Future studies will also explain some of the outcomes thus far observed such as the consistent increase in the mesenchymal stem-like cell population in the mouse AT-3s, the human MDA-MB-468s, and the patient derived breast cancer cells. Are the stem-like tumor-initiating cells seeded from the patient sample proliferating faster than the differentiated cancer cells? Or are the differentiated cancer cells de-differentiating on the supported ecFn contributing to the enriched tumor initiating cell population? In any case, the observed increase in tumor-initiating cell populations suggests another possible application of supported ecFn as a pre-culture system, where patient cells are first cultured for about a week, removed from the scaffolds, and flow sorted to collect a concentrated fraction of tumor-initiating cells. These tumor-initiating cells can then be expanded either directly on scaffolds, or injected into a mouse for xenograft formation. The odds of forming a patient derived xenograft (PDX) using this concentrated sample of tumor-initiating cells is expected to be significantly higher than the original patient sample as collected. Once grafts are developed, they can be serially propagated

to generate enough patient-representative samples for personalized or high-throughput drug screening, fundamental cancer biology studies, or patient prognoses.

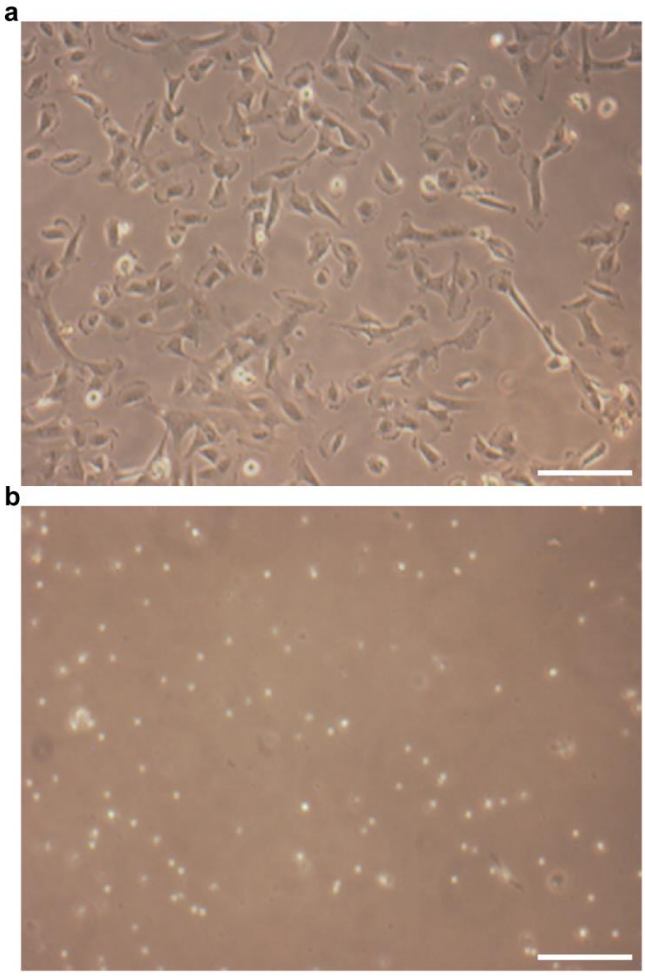

Figure 4-10: Patient ascites cells grow on tissue culture polystyrene if first expanded on supported ecFn (a) Ascites sample from Patient E cultured first on supported ecFn for two days then trypsinized and re-plated onto tissue culture polystyrene (TCPS) dish. (b) Brightfield microscope image of cells from the same patient sample as in *(a)* plated directly from the patient onto TCPS. Image taken after one day of culture showing cells do not survive. Scale bars 25 µm. *Credits:* Patient cells were obtained through the Luker Lab and Hayes Lab at the University of Michigan.

4.4 Conclusions and Implications

Supported ecFn consistently increased the tumor-initiating potential across a mouse model, human cell line, and breast cancer patient samples. AT-3 mouse tumor engraftment efficiency was improved in parallel with an enrichment of the tumor-initiating population after *in vitro* culture. Notably, the three mice used for this study were mice were immunocompetent – a critical factor that is of increasing interest as we begin to understand the role of the immune system in tumor progression[191]. When cultured on supported ecFn for six days, primary human breast cancer cells from pleural effusions or ascites showed a distinct upregulation of the mesenchymal stem cell phenotype, $CD44^+/CD24^-$, which coincided with a downregulation of EpCAM, and maintenance of the $ALDH^+$ population compared to the original sample. Cumulatively, these results characterize an epithelial to mesenchymal transition, thought to be a pathway for metastasis[150]. Therefore, one possible explanation of the elevated population of $CD44^+/CD24^-$ cells present in the original patient sample is the cell source (**Fig. 4-7(e)**). All patient samples were collected from ascites or pleural effusions, in which case cancer cells have already migrated away from the primary breast tumor as if traveling to a metastatic site. Also, CD24 and CD44 have been shown *in vitro* to play a role in anchorage to several ECM proteins including fibronectin[192, 193]. Could integrin activation and cell signaling through CD44 impact cell behavior on supported ecFn? This possibility further reiterates the importance of using whole proteins rather than peptides in scaffold design and maintaining Fn in its extended state complete with exposure of critical binding sites for cell interaction. Going forward, supported ecFn may be used to unravel current uncertainties regarding the full effect of CD44, CD24, or ALDH expression on tumor cell behavior, understanding cancer cell dormancy, and in the search for additional markers of the tumor-initiating phenotype. Therapeutic targeting of this elusive subpopulation of cancer cells will largely

benefit from a reliable set of identifying characteristics. In addition, as we move towards precision medicine, generating a tumor from patient-derived material alone is insufficient. To harness the true value of patient specific tumor models, patient cell phenotype must be conserved over time[166]. This implies that the tumor graft should maintain the gene and receptor expression,[165, 170] drug response,[166] and tumor-to-stroma ratios[165] of the patient, and if grafted in a mouse, demonstrate metastasis to the same sites as those of the patient[165]. Future work will be aimed at determining the bioequivalency of patient tumor grafts generated on supported ecFn to the patient's tumor. Here it has been showed for an n = 1, that the patient's breast cancer receptor status is conserved after a six-day culture on supported ecFn (**Fig. 4-8(e)**). Therefore, it is hypothesized that the scaffold platform herein described reduces phenotypic drift, particularly given the minimization of interactions between cells and synthetic material, three-dimensionality, and native-like protein matrix.

It is well known that extrinsic factors play a major role in modulating the phenotype and fate of both healthy[1] and malignant cells[194, 195]. Time and resources poured into current cancer research can have a far bigger impact if a shift is made to a more physiologically relevant system in which environmental parameters can be independently varied; this would enable the decoupling of the vast array of cellular and acellular mechanisms underlying cancer[32, 167]. Studies have shown that varying the stiffness[194] and both non-soluble[196, 197] and soluble factors[198, 199] within the cancer microenvironment results in cellular phenotypic changes and EMT. This goes beyond breast cancer. For example, in adenocarcinoma the specific combination of laminin and fibronectin are characteristic of metastatic sites whereas collagen I and IV are more prevalent within the primary tumor[196]. Looking to the future, 3D model microenvironments that faithfully recapitulate the key distinguishing features of breast and other cancers will be indispensable in the understanding of

metastasis, the identification of cells of a more stem-like or tumor-initiating phenotype, and the development of therapeutics and treatment strategies[24, 167]. Supported eECM can make a major contribution to this effort as further studies are done to demonstrate and characterize the capability of our scaffold platform to tune protein matrix stiffness, co-culture feasibility, and incorporation into bioreactor systems for complete spatio-temporal control.

Chapter 5
Summary and Future Directions

5.1 Summary

As research shifts away from 2D monolayer cultures, we believe supported eECM is one potential solution to address the current need for a new standard, fully defined, 3D cell culture system. Supported ecFn has been shown to be a biophysically and biochemically relevant 3D cell microenvironment for maintenance of both immortalized and primary cells *in vitro*, and can serve as an implantable tissue engineering scaffold as shown in the AT-3 tumor graft assay. Furthermore, the polymer scaffold providing a skeletal structure to the supported eECM are highly tunable microfiber constructs fabricated by 3D jet writing. The composition and spatial positioning of each microfiber within the construct are now independently tunable properties due to the development of the manifold. Together, 3D jet writing, flow control as governed by the manifold, and the native-like ECM produce a micro-manufacturing platform for customizable supported eECM with independently tunable properties.

The innovation of the manifold has expanded the design space of electrospun fibers. Now, relative compartmentalization can be controlled within single fibers and 3D jet writing scaffolds. This means the user can dictate how much of each fiber surface presents a certain ligand, or what percentage of the bulk material is loaded with a biomolecule or composed of a faster degrading material. With the manifold, distinct domains can now be embedded within 3D jet writing scaffolds, establishing a complete micro-manufacturing system where different materials are

deposited within a single scaffold with spatial control. The applications of this capability are endless from cell and protein patterning to spatially targeted cell signaling. Finally, the manifold improves jet stability for co-jetting of dissimilar materials. With future work, the library of materials optimized to be processed into fibers and scaffolds will be expanded, further extending the design space of the synthetic component of supported eECM. Overall, the manifold affords intelligently designed, customizable scaffolds with high resolution control of all environmental parameters while allowing cells to redefine the cell microenvironment and create an *in vitro* cell niche that mimics the native cell niche as closely as possible.

Many published studies where cell response is measured against an environmental factor must first begin not with the cell culture, but with inventing a 3D culture system that enables the researcher to toggle the environmental variable of interest. Not only can inventing a culture system pose major challenges such as fabrication and validation prior to conducting the intended cell work, but results in a lack of standardization in scientific reports across the biomedical community. TCPS remains a ubiquitous benchmark, serving at least as a control in many studies since it is the only *in vitro* culture platform that is widely known and well characterized. The need for a replacement that is mindful of the actual *in vivo* cell microenvironment is critical in order to more efficiently utilize resources and progress biomedical research. Reticker-Flynn *et al.* state that there is currently no satisfactory platform to specifically observe cell-ECM interactions *in vitro*[16]. Supported eECM can be scaled to fit the size of the polymer scaffold, can be made with less than 5% by volume synthetic material, and unlike any other currently known 3D cell culture systems, presents protein in an insoluble fibrillar ECM-like network. Until now, such an *in vitro* culture environment has only been secreted by cells which limits matrix thickness, is bound to a hard substrate, and is compositionally undefined. This work reports on the first fully defined freely-

suspended protein network manufactured in a cell-free system. The free suspension is key to maintaining three-dimensionality, ensuring that the scaffold is surrounded only by cell media when in culture rather than sitting atop a hard glass or plastic surface (i.e. 2.5D). Finally, cells are able to readily infiltrate the scaffold, tethering to and remodeling the protein matrix *in vitro* as it would the ECM *in vivo*.

The general need for a physiologically relevant *in vitro* cell niche persists in bridging the gaps between benchtop, animal studies (particularly reducing the number of animals needed) and clinical trials for drug screening irrespective of the specific disease[8, 200]. In the case of cancer, tumor grafts can provide a thriving tissue sample representative of a human tumor for preclinical drug screening and development[165, 169], to serve as a model for fundamental studies[165], or as a platform for precision medicine[170]. Unfortunately, expanding patient-derived tumor cells *ex vivo* has been difficult whether *in vitro* in cell culture or *in vivo* as in a patient derived xenograft. Hypothesized to be due to the more native-like environment and presence of pre-metastatic niche protein fibronectin, supported ecFn has allowed for expansion of 14 out of 14 breast cancer patient samples collected from pleural effusions or ascites directly on the scaffold. Six-day culture enriched the mesenchymal self-renewing cell population while inducing a reduction in EpCAM indicative of a possible EMT. This ability of supported ecFn to enrich the tumor-initiating cell population was also seen in mouse and human breast cancer cell lines. These studies put supported eECM to extensive use in cell culture, serving as a further validation of its utility and commercial potential. Practicality must be considered if a 3D cell culture model is to be a competitive choice for widespread use in laboratories. Each polymer scaffold is made to fit into the well of a 24-well plate, secured to a metal frame with a spacer to keep it off the plastic surface. Supported eECM meets scaffold requirements as outlined in literature being biocompatible, biodegradable, easily

handled and transferred, transparent and amenable to current imaging and cell-based characterization techniques[19, 46]. It is the hope that future work will further develop and validate this platform technology as it moves towards realizing its commercial potential.

5.2 Future Directions

5.2.1 Expanding 3D jet writing material library and design space

The ultimate goal of this work is to establish a fully functional cell culture system that can provide a vast array of independently tunable parameters which can be defined by the user as needed for a specific experiment or application. Our scaffolds can be decomposed into synthetic and biological elements: the polymer scaffold and the eECM respectively. As further work is done to give the user more freedom to assign values to each defining parameter within both elements, the more utility will be gained from our 3D cell culture model. This also creates a single controlled cell environment for investigation of the effect of nearly any parameter on cellular response rather than having to re-invent a new system for each different environmental condition of interest. Thus far, capabilities added to the existing 3D jet writing and EHD co-jetting systems include control of relative sizes of fiber compartments, elastic modulus of bicompartmental fibers, and deposition of distinct materials within certain domains of a microfiber construct. The next steps in developing the synthetic element within the supported eECM include expanding the library of possible materials, and demonstrating various applications of the capabilities newly established in this work. Currently, PLGA both with and without various functionalities is the least challenging polymer to process into micro- and nano-fibers whether by EHD co-jetting or 3D jet writing. In this study, PLCL was also optimized to co-jet with PLGA in a side-by-side configuration. What are the governing parameters that lead to a fluid jet sufficiently stable to produce fibers or 3D microfiber scaffolds without defects or unwanted surface features? Although this is a grander

challenge, it would be well worthwhile for expanding the polymer library to take a physical science approach to modeling and understanding how to intelligently design polymer solutions for jet stability. Typically, our polymers are dissolved in mixtures of solvents, where the ratio of one solvent to the others is determined through an experimental iterative process. Estimating viscosity, dielectric constant, volatility, and conductivity of solvent mixtures requires more than simply a weighted average of each individual solvent property, especially when polymer molecules are introduced to the solvent.

As far as applications of the manifold-produced scaffolds, the possibilities are seemingly endless. Firstly, the use of biodegradable polymers in scaffold production opens an avenue for controlled release, much like soluble signaling *in vivo*, and degradation. With the manifold, various portions of the scaffold can be made to degrade at a faster or slower rate, either by patterning the faster and slower degrading material into distinct 3D domains or by modulating relative compartmentalization within each fiber. One could imagine a validation experiment where the tunability of fiber compartment size is directly proportional to degradation rate. A similar phenomenon has been previously reported for polymer particles[201]. The ability to controllably degrade or release a biomolecule of interest from the polymer scaffold would create another independently tunable environmental parameter. Thus far, microfibers with a core-shell architecture have been fabricated with a shell comprised of PLGA and a core loaded with stromal cell-derived factor 1α (SDF-1α) (**Fig. 5-1**). Secondly, the ability to pattern materials either within single fibers or 3D scaffolds thereby allows for patterning of surface functionalities. This would allow for tethering of certain ligands onto only designated areas or make cell and protein patterning possible across 3D constructs[62]. Thirdly, gradients across 3D scaffolds are now feasible, as was shown for two PLGA solutions carrying different tracer dyes in **Figure 2-21**. Future work

implementing such a gradient can be manifested in many ways such as increasing a non-fouling effect across the scaffold by PEGylation or changing the fiber elastic modulus. These developments would enable our 3D microfiber constructs to exhibit bulk materials, tethered ligands, or surface functional groups in a spatially designed manner, which can all be used to direct cell behavior much like cell signaling *in vivo*[6, 7, 19, 49].

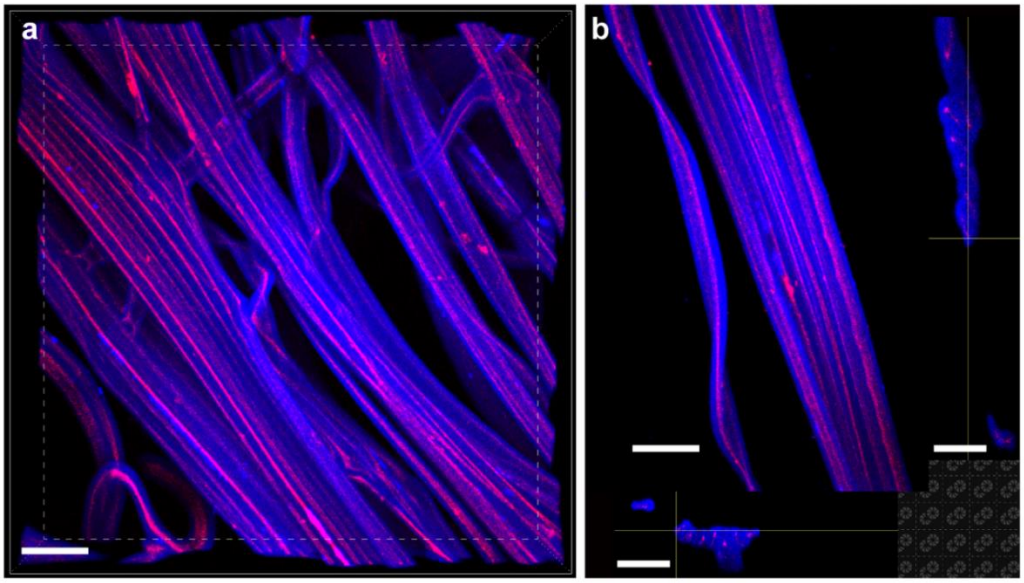

Figure 5-1: Stromal cell-derived factor 1α (SDF-1α) loaded into core of core-shell PLGA microfibers SDF-1α-Cherry fluoresces red in the core of microfibers comprised of a PLGA shell labelled blue. (a) Volume view of aligned fibers collected on a rotating wheel during the electrospinning process. (b) Single fiber bundle collected on a rotating wheel indicating cross sectional views to emphasize the SDF-1α-Cherry core within the PLGA shell. All scale bars 25 μm. *Credit:* Fiber fabrication done by Gokcen Ukuser. SDF-1α-Cherry generously donated by the Luker Lab at the University of Michigan.

5.2.2 Confirming bioequivalency of supported eECM

Supported eECM allows cells to enact behaviors that they typically would *in vivo* such as forming multicellular structures with many cell-cell contacts, and depositing and degrading ECM protein[36]. It has been shown that supported ecFn made it possible to culture breast cancer patient cells that do not thrive on TCPS. Furthermore, with less than 5% by volume being comprised of the polymer scaffold, the remaining volume is occupied by a protein matrix that mimics the architecture, detergent insolubility, and in the case of Fn, conformational state of native ECM.

Nevertheless it is a continuous effort, as ongoing and future experiments are carried out, to consider how supported eECM may be further validated for bioequivalancy to native ECM. For example, cell-cell and cell-ECM contacts can be quantified for cells cultured on supported eECM as compared to the corresponding protein hydrogel by identifying focal adhesions or adherens junctions (cell-cell contacts) and integrin activation due to protein binding. A gene array of cells cultured on supported eECM can also be compared to those cultured on TCPS and a decellularized matrix, where the decellularized matrix represents a physiological ECM. Finally, of course, the ability to culture other "hard-to-culture" cell types such as primary patient cells, neurons, and human embryonic stem cells will not only contribute new capabilities to the field, but also serve to further validate the physiological nature of supported eECM.

5.2.3 Ex vivo patient-specific tumor grafts

Without the risk of xeno-contamination, lower costs, higher-throughput, and having thus far a "tumor-take rate" of 100%, supported ecFn could provide not only a patient-specific tumor element, but by serial propagation, a more physiologically relevant model representing human patients at large for screening of pharmaceutical compounds; this could curtail the need for animal models[8, 19]. The next step towards this goal is to ensure that the tumor biology of the patient is accurately represented by the tumor graft formed on the scaffold. Here it was shown in **Figure 4-8** that the breast cancer receptor status was maintained on supported ecFn for a sample size of one patient; additional patient samples are needed in order to get a statistically significant result. While gene and protein arrays are the ultimate techniques for verifying the maintenance of patient phenotype, less costly approaches such as histology, flow cytometry, and polymerase chain reaction (PCR) can provide valuable information. Histology reveals cell morphology, tumor structure, and how stroma is integrated into the tumor[169]. Epithelial or mesenchymal phenotypes

can be quantified by PCR and flow cytometry. However, all of these techniques require access to patient specific data beyond receptor status. Any histology of an excised tumor could be used to compare to that of a tumor graft formed via supported eECM culture. Observed EMT or MET may be explainable by understanding the patient's prognoses. Finally, knowing the patient's response to various therapeutics will determine whether a similar response was observed when patient cells grown *in vitro* are exposed to the same drugs.

Aside from generating patient-representative tumor grafts *in vitro* directly on supported eECM, these cell microenvironments can alternatively serve as a pre-culture system. As shown, patient cells did not survive when directly seeded onto TCPS, but grew on TCPS after culture on supported ecFn (**Fig. 4-10**). Future work will determine whether this implies that patient samples which would not otherwise form a PDX or survive *in vitro*, are able to do so after a "pre-culture" on supported ecFn. It would also be interesting to investigate the mechanism by which supported ecFn is enabling primary cell growth *ex vivo*. Is it due to the observed enrichment in tumor-initiating cells after culture on supported ecFn? Or are the cells better able to adapt to surviving *ex vivo* if first cultured on a more native-like ECM? After enrichment of the tumor-initiating cells on supported ecFn, a next logical step is to remove these cells, flow sort to obtain the tumor-initiating fraction, and either re-seed this fraction onto scaffolds for implantation in mice, or directly inject these cells into mice for PDX development. Once implanted, tumor take rate, tumor growth rate, serial transplantability, and maintenance of patient phenotype would be evaluated. If direct implantation of tumor-initiating cells on supported ecFn improves the odds of PDX formation relative to direct injection, this may serve as evidence of enhanced cell-delivery capabilities in support of hypotheses that cell integration into a matrix of cell-cell and cell-ECM interactions prior

to implantation increases cell survival after implantation and maintains cells until integration with surrounding endogenous tissue.

5.3 Further Applications

5.3.1 Cell response to varying protein matrix compositions

In addition to expanding the array of possibilities on the synthetic front, future efforts to expand the protein library available for suspension on our 3D jet writing scaffolds will also aid in probing cell responses to certain protein matrix compositions and in modeling specific cell niches. For example, healthy mammary tissue growth is mediated by an ECM primarily composed of laminin-1, collagen IV, and nidogen[29], therefore a scaffold that mimics mammary epithelia should include these three proteins. Much of cancer research involves culture on a basement membrane extract known by the trade name Matrigel, making this protein mixture an important addition to the scaffold protein library for future cancer studies. In fact, utilizing supported eECM to further understand EMT is a major application of interest going forward. In Chapter 4 it was shown that supported ecFn appeared to be inducing an EMT for mouse and human cell lines, and primary patient cells. What are the mechanisms underlying this shift in phenotype? Does the protein composition play a role? Shown in **Figure 5-2**, for cultures of the MCF7 human breast cancer cell line on supported eECM, laminin resulted in an increase in the $ALDH^+$ population at 2.34% relative to fibronectin at 1.48%; cultures on supported eECM were also imaged for differences in cell morphology. This agrees with a previously done study showing laminin-1 promoting E-cadherin expression, indicative of adherens junctions formation connecting neighboring cells, implying an epithelial phenotype[29]. Another cell type, Sum159, showed a unique affinity towards fibronectin where from day one of culture, cells seeded preferentially on the ecFn in the pores of the polymer scaffold where they proliferated to form thicker volumes by the fourth day of culture

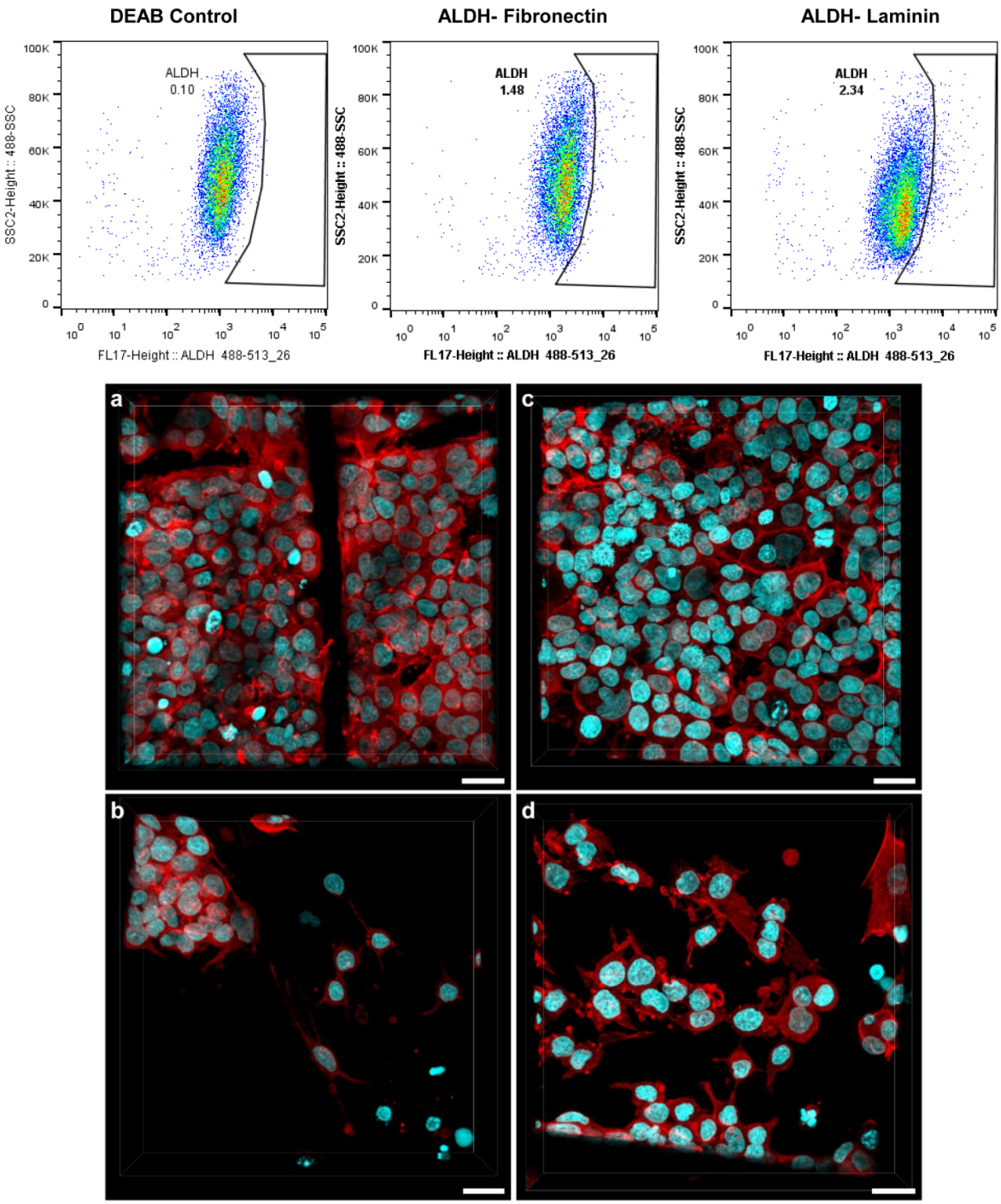

Figure 5-2: MCF7 breast cancer cells show increased ALDH positive population when cultured on supported eECM of laminin relative to fibronectin (top) ALDH expression increased from 1.48% on fibronectin to 2.34% on laminin for MCF7 human breast cancer cells cultured on supported eECM. **(bottom)** MCF7 human breast cancer cells cultured 10 days on supported eLAM and imaged in an area of (a) high cell density and (b) low cell density. MCF7s were also cultured 10 days in parallel on supported ecFn and imaged in an area of (c) high cell density and (d) low cell density. (a-d) Scale bar 25 µm. Cell nucleus in cyan, and actin in red. *Credits:* Flow cytometry done in the Wicha Lab at the University of Michigan.

(**Fig. 5-3**). This is in stark contrast to nearly every other cell type thus far observed where cells first anchor to the microfibers and over time migrate into and proliferate within the ecFn-rich pores; the result shown in **Figure 5-3** also reiterates the benefit of a scaffold with large open area. Future work with Sum159s may seek to investigate if this cell type has a similar affinity to proteins other than Fn.

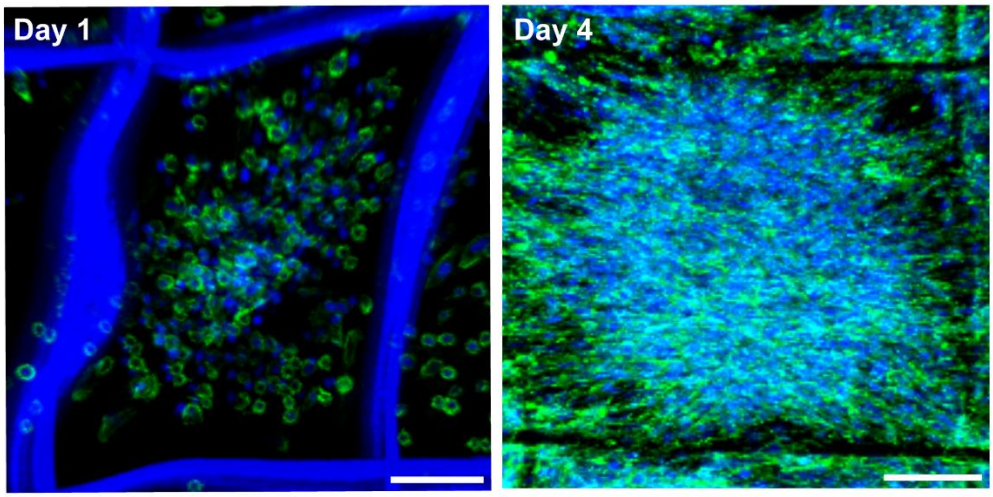

Figure 5-3: Sum159 human breast cancer cells show strong affinity towards fibronectin immediately upon seeding Sum159 human breast cancer cells preferentially seeded onto supported ecFn within scaffold pores rather than the polymer microfibers. Cells formed thick volumes within the pore by the fourth day in culture. Volume thickness reduced in areas on or near the polymer microfibers. This is a phenomenon was uniquely observed with this cell type. Scale bars 100 μm.

Still, to better understand the effect of the microenvironment on shifts between epithelial and mesenchymal phenotypes, additional readouts are necessary. For example, markers other than CD24, CD44, and ALDH have been used to identify mesenchymal or epithelial phenotypes (**Table 5-1**). Of these, matrix metalloproteinase 2 (MMP2) was briefly considered for its role in the behavior observed of MDA-MB-231 human breast cancer cells on supported ecFn. Illustrated in **Figure 3-18 and 3-19**, these cells may be undergoing EMT as they transition from a proliferative phase to a state where most of the cells have migrated off the scaffold remaining 98% viable in solution. In support of this hypothesis, MMP2 was not expressed in 231s at early timepoints, but

did appear at the 10th day in culture (**Fig. 5-4**). However, E-cadherin was constantly expressed (**Fig. 5-4**). Future work in understanding 231 behavior on supported ecFn will seek to elucidate whether this system serves as a true model of metastasis. As done in this brief study and a previous study in colon cancer[149], epithelial markers such as E-cadherin should be analyzed in parallel with mesenchymal

Table 5-1: Epithelial to mesenchymal transition markers of interest

Several Epithelial to Mesenchymal Transition Markers of Interest	
Downregulated	
E-cadherin	Enhances cell-cell adhesion decreasing motility
Cytokeratin (cytokeratin 5, 6, 18)	Keratin directs E-cadherin to the membrane
Upregulated	
SNAIL	Transcription factor involved in activating EMT in cancer
TWIST	Transcription factor represses E-Cadherin and induces N-cadherin independently of SNAIL
N-cadherin	Facilitates pathway for cancer cell migration
α-smooth muscle actin	Facilitates cell movement and acts as sensory extensions
Matrix metalloproteinases (MMP2, MMP9)	ECM protein degradation enables invasion

markers such as N-cadherin. In the 231 study, EMT markers should be analyzed at initial seeding, middle of the culture, end of the culture when cells migrate off, and migrated cells should be re-seeded onto a second scaffold to see whether these cells invade the new environment, reverting to an epithelial phenotype as they "form the secondary tumor." Repeating this series of experiments with different protein compositions will shed light on the role of fibronectin in what may be a metastatic process. Finally, beyond quantification of various EMT markers, supported eECM allows the investigator to observe the physical proteinaceous microenvironment. Observation of how cells are degrading protein, or reconfiguring protein conformation can reveal how motile a cell is, or what kind of cell niche it is creating. Recent work in the Lahann Lab has led to fluorescently labelled Fn, which is then processed into supported ecFn to create an inherently fluorescent protein network. Future developments can take advantage of FRET (fluorescence

resonance energy transfer) to get a fluorescent indication of cell-induced changes in Fn conformation[12, 202, 203]. Lastly, the versatility of supported eECM is extended theoretically to cultures of all adherent cells. **Figure 5-5** shows that these cancer studies need not be limited to breast cancer. Pancreatic cancer cells, including a patient-derived cell line, have been successfully expanded on supported ecFn.

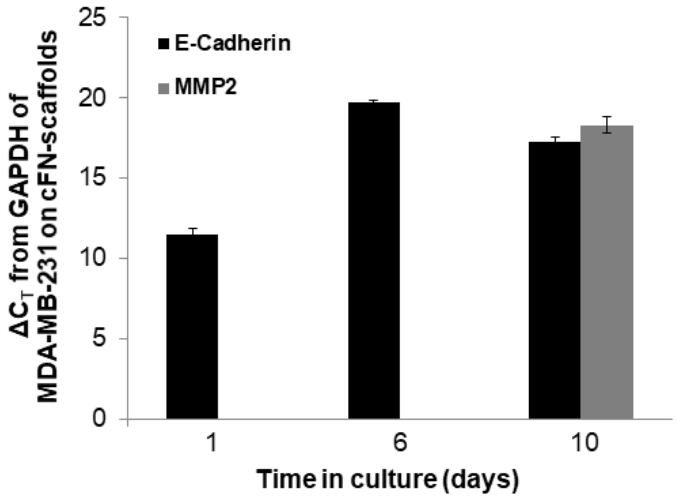

Figure 5-4: Matrix metalloproteinase expression increases at a later timepoint in MDA-MB-231 culture when cells have migrated off the scaffold remaining viable in solution Matrix metalloproteinase 2 (MMP2) was quantified alongside E-cadherin for MDA-MB-231 human breast cancer cells on supported ecFn. MMP2 indicates proteolytic activity characteristic of invasive cells and a mesenchymal phenotype. E-cadherin expression results from formation of cell-cell contacts, known to be downregulated in EMT.

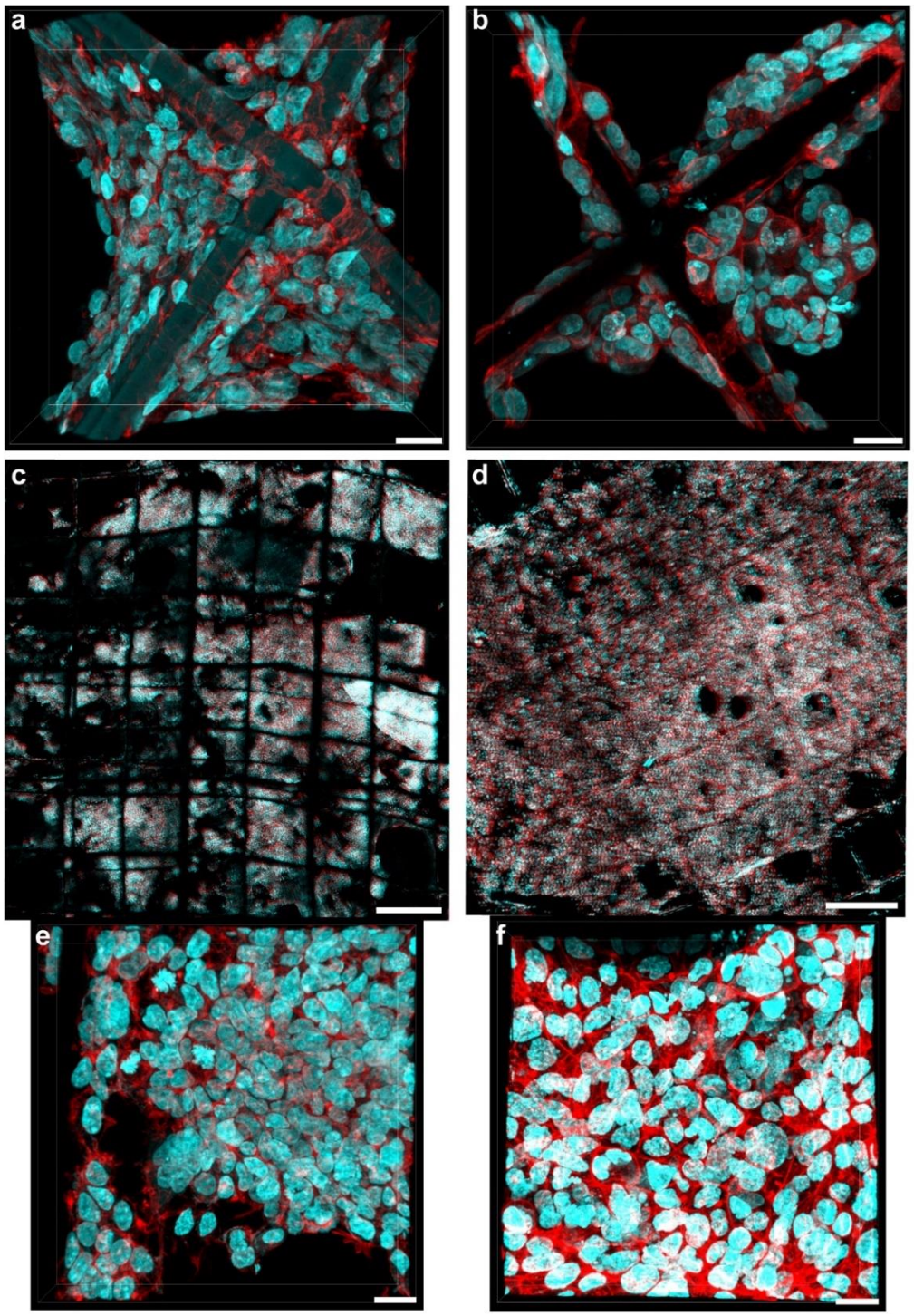

Figure 5-5: Study of EMT and MET is not limited to breast cancer – cells cultured on supported ecFn for a pancreatic cancer model system (a) ASPC1 pancreatic cell line, mesenchymal by nature and (b) UM53 patient-derived pancreatic cells, epithelial by nature, at a low cell density area of the scaffold showing how cells proliferate and shirt off the polymer microfibers and into the open pore areas at the six-day culture timepoint. Large scale scaffold at low magnification showing (c) ASPC1 after four days and (d) UM53 after two days of culture on supported ecFn. (e) Zoomed in view showing individual cells from *(c)*. (f) Zoomed in view showing individual cells from *(d)*. (a-b, e-f) Scale bars 25 μm. (c-

d) Scale bars 500 µm. Cell nucleus in cyan, actin in red. *Credits:* Pancreatic cancer cells generously donated by the Simeone Lab at the University of Michigan.

5.3.2 Cell-sheet stacking and co-cultures

The need for flexibility in scaffold ECM composition was demonstrated in **Figure 3-26** where human umbilical vein endothelial cells (HUVECs) showed very minimal adhesion to supported eECM of laminin or fibronectin, but when cultured with both proteins combined, the HUVECs were able to adhere and proliferate, even forming possible lumen-like structures (**Fig. 5-6**). HUVECs and other endothelial cells are of great interest with respect to vasculogenesis. In an ongoing collaboration with the Levenberg Lab (Technion Israel Institute of Technology), growth of human adipose microvascular endothelial cells (HAMECs) is supported by a co-culture system with human dermal fibroblasts (HNDF) on either supported ecFn or Fn conformally coated onto 3D jet writing scaffolds (**Fig. 5-7**). Next steps involve determining how to quantify differences in structures formed by the HAMECs in order to identify the microenvironmental conditions (stromal cell and protein) that best support formation of tubules or cell alignment. Vasculogenesis is becoming increasingly important with the growth of the tissue engineering field[204]. Diffusion limitations in thick engineered tissues can be overcome by functioning vasculature. Supported eECM is easily amenable to cell-sheet stacking, or the culture of different cell types on independent scaffolds that are then "sandwiched" together to form a thicker 3D co-culture. Stacking sheets of fibroblasts and endothelial cells has proven effective in promoting vascularization as well as the introduction of angiogenic factors[204-209]. Future directions may entail similar sandwiching of sheets of endothelial cells between sheets of fibroblast first individually cultured on supported eECM.

Establishing a native-like ECM is crucial for creating an *in vitro* cell niche for the study of cancer, EMT, and other areas. Still, physiologically, much of cell signaling is derived from other

cells. Future application of supported eECM will incorporate co-cultures of both cancer cells and stromal cells. An early attempt at a co-culture of NIH-3T3 mouse fibroblasts with GFP-MDA-

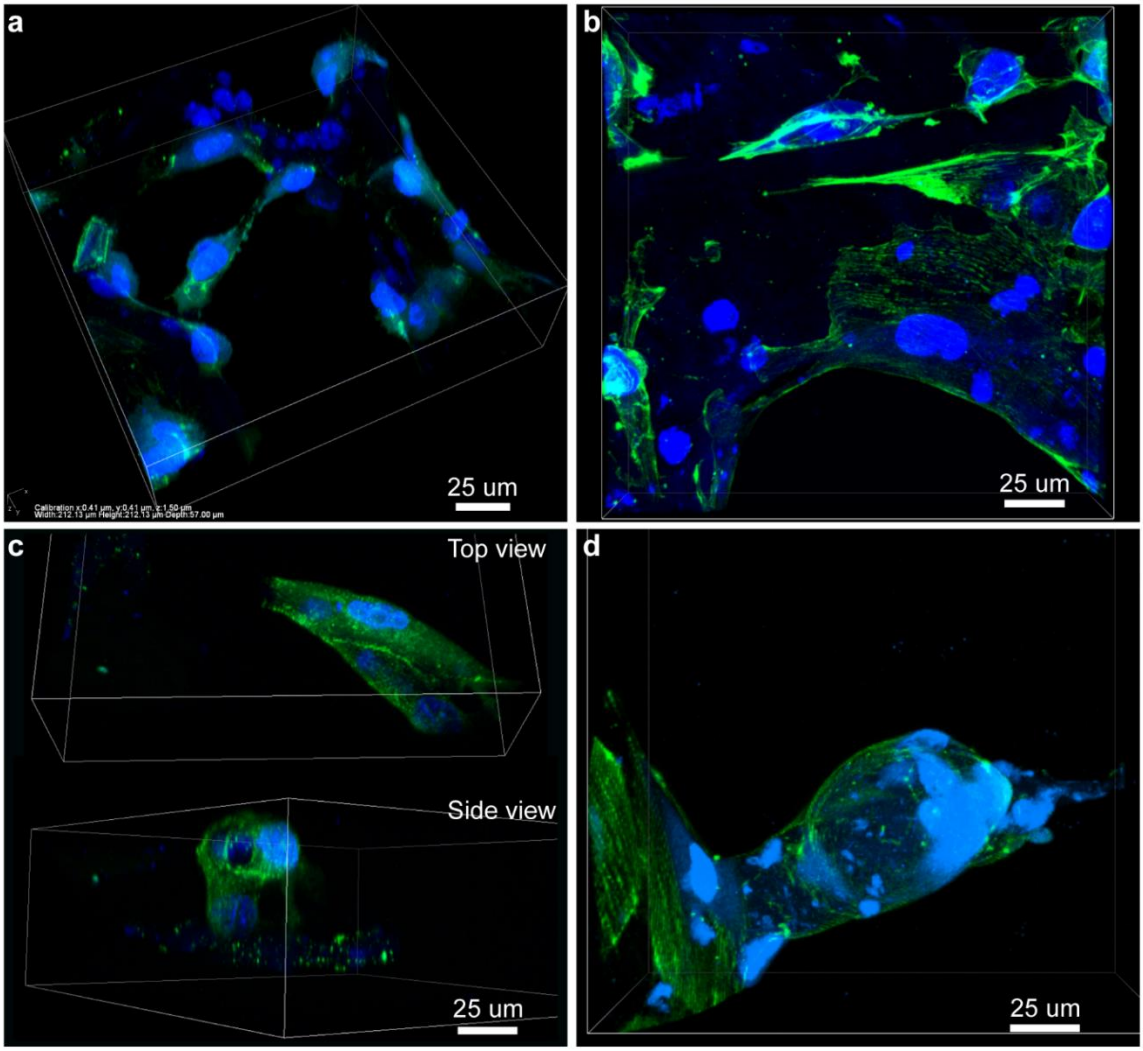

Figure 5-6: Supported eECM provides cells large open area for formation of 3D cell structures demonstrated by endothelial cells (a) HUVECs (human umbilical vein endothelial cells) starting to branch out into the center of the scaffold pore. (b) Area of scaffold showing higher cell confluency as opposed to low cell density areas shown in (c) and (d) where formation of tubular structures are more easily visualized. All scale bars 25 µm. All supported eECM comprised of fibronectin and laminin. Cells cultured one month. Cell nucleus shown in blue; actin shown in green.

MB-231 human breast cancer cells was done in a similar fashion to the stacking of cell sheets seen in the literature for vasculogenesis. Three supported ecFn scaffolds were prepared, two were used for fibroblast culture, and the third for 231s. The 231s were sandwiched between the two fibroblast

sheets. Imaging was done on a confocal microscope in an attempt to visualize the three sheets of cells, however distinguishing individual cell types was difficult, and the thickness of the three scaffolds combined far superseded the imaging depth afforded by the microscope working distance

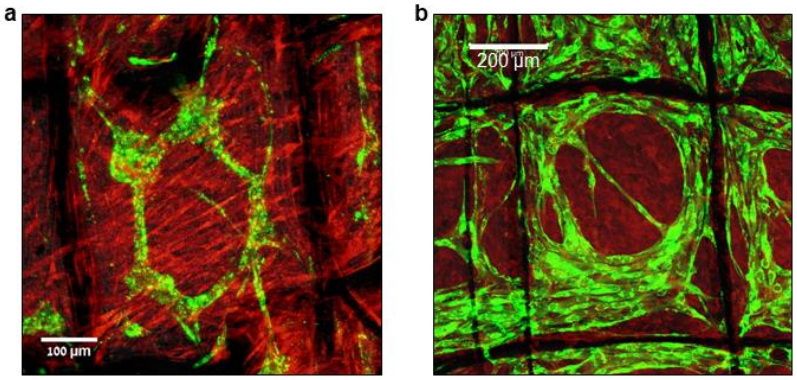

Figure 5-7: Supported ecFn demonstrates potential for vasculogenesis in a co-culture system of endothelial cells and fibroblasts HAMEC (human adipose microvascular endothelial cells) and HNDF (human dermal fibroblasts) cultured on (a) supported ecFn and (b) 3D jet writing scaffolds coated conformally with Fn. (a) Both cell types seeded onto scaffold at the same time. Image taken after 14 days of co-culture. Scale bar 100 µm. (b) HAMECs seeded first onto scaffold and cultured three days before HNDFs were seeded. Image taken after eight days of co-culture or 11 days of total culture time. Scale bar 200 µm. Endothelial cells (HAMEC) in green, and fibroblasts (HNDF) in red. *Credits:* Fabrication of 3D jet writing scaffold done by Lahann Lab at University of Michigan. All other procedures including protein deposition, cell culture, and imaging done by Ariel Szklanny of the Levenberg Lab at Technion Israel Institute of Technology.

(**Fig. 5-8**). When repeating this study in future, confluency of individual cell sheets at the time of stacking, and a histological protocol for imaging should be considered. Furthermore, this study combined mouse fibroblasts with human cancer cells. Future work should look to more applicable stromal cell populations, including an analysis of the impact of stromal fibroblasts obtained from healthy patients in contrast to breast cancer patients (**Fig. 5-9**). Stromal cells are a necessary component in modeling the breast cancer cell niche and should be considered for supported eECM cultures going forward. Previous studies have recapitulated mammary tissue using healthy patient fibroblasts, HUVECs, and the breast cancer cell line MCF10 where the addition of HUVECs induced an invasive cancer cell phenotype[210]. In other systems, contact with stromal fibroblasts increased MMP expression[30] and invasive potential[211] in malignant cells. In fact, oncogenic signals

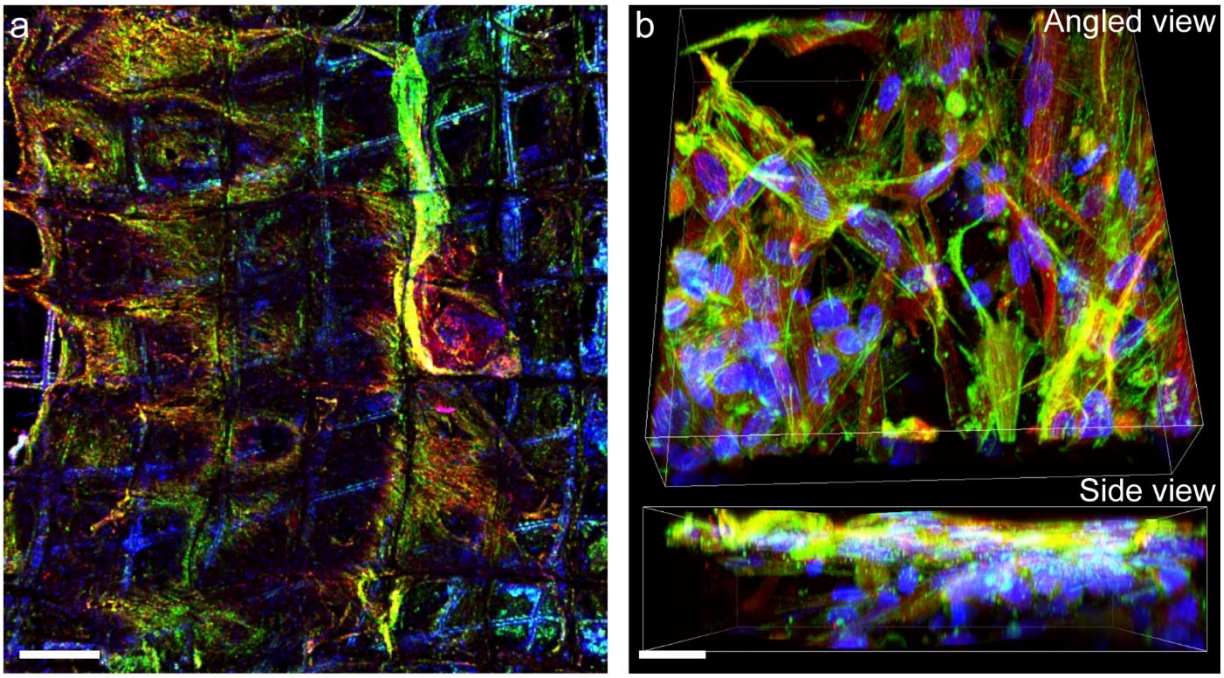

Figure 5-8: Co-culture of fibroblasts and human breast cancer cells by layering three scaffolds (a) Full top view of three scaffolds stacked onto one another. The two outer scaffolds were seeded with NIH-3T3 mouse fibroblasts, which should appear blue under the nuclear stain. The center scaffold carries GFP-MDA-MB-231 human breast cancer cells which fluoresce green but also contain a red stain for cytokeratin. Scale bar 500 µm. (b) Zoomed in angled and side view of scaffold stack shown in *(a)* at a depth of only 53 µm which does not encompass the entire thickness of the sample. All cells are marked in a blue nuclear stain, while the cancer cells are labelled in both green and red (GFP and cytokeratin). All cultures done on supported ecFn. Scale bar 25 µm.

from tumor derived fibroblasts can change non-malignant epithelial cell populations to malignant resulting in tumor progression[8]. Consulting published studies such as these for guidance on future experiments using supported eECM is sure to reveal new information on the effect of various stromal populations on cancer cell behavior. Thus far, we have observed the self-assembly of T47D breast cancer cells and NIH-3T3 fibroblasts into segregated structures when co-cultured at a ratio of 4:1 on supported ecFn at both a five-day and 10-day timepoint (**Fig. 5-10**). Although the T47Ds had formed a confluent volume of cells on the scaffold at five days, by the 10th day, they had largely migrated off the scaffold. Any remaining T47Ds on the scaffold by the 10th day had also experienced a loss of EpCAM expression. These observations are a start towards future work in co-cultures of cancer and stromal cells on supported ecFn.

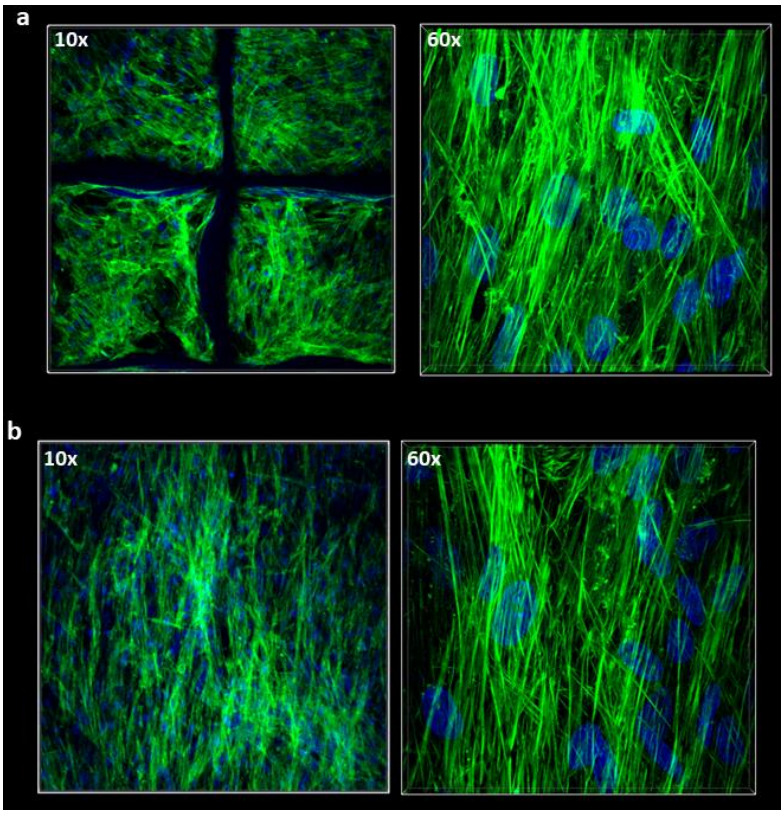

Figure 5-9: Expansion of fibroblasts from healthy and breast cancer patients on supported ecFn Fibroblasts obtained from either human breast cancer patients (a) or healthy patients undergoing breast reduction surgery (b) were expanded on supported ecFn. Future studies on the effect of stromal cells on tumor progression will consider use of these cell types. Blue channel marks the cell nucleus, green channel indicates actin. *Credits:* All cells generously donated by the Wicha Lab at the University of Michigan.

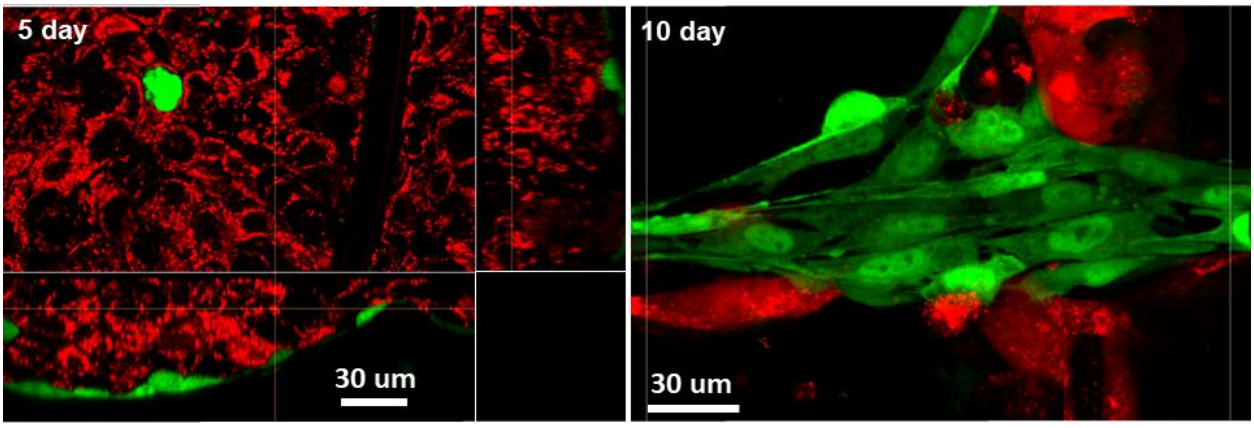

Figure 5-10: Segregation of cell types in co-culture of T47D human breast cancer cells with mouse NIH-3T3 fibroblasts on supported ecFn Five and ten day timepoint of a co-culture of human breast cancer cells of the T47D cell line with mCherry (red) with mouse GFP-NIH-3T3 fibroblasts (green) at a seeding ratio of 4:1. The segregation of the two cell types is evidenced in these live culture images of a cross sectional view *(left)* and volume view *(right)*. Scale bars 30 µm.

Appendices

Appendix A: Decellularization Protocol

Decellularization *(adapted from Lu et. al. [122])*

For the gentle removal of cells adhered to a substrate or protein matrix

1. Prepare 50 mM Tris buffer

2. Use the 50 mM Tris buffer as your solvent to prepare a 1.5 M KCl solution

3. Prepare 0.1% Triton X-100 (TX100) solution using the 1.5 M KCl solution you prepared in step 2 as your solvent. You should now have a solution of 0.1% TX100 with 1.5 M KCl in 50 mM Tris buffer.

4. Starting with live cells on the substrate, wash with PBS, then DI water

5. Immerse the sample in the 0.1% TX100 with 1.5 M KCl in 50 mM Tris buffer solution at 4ºC on a slow moving shaker. The original protocol suggested 6 hours for this step, but I have used 2 hours for cells cultured on glass. The thicker the sample, the longer the time needed immersed in solution.

6. Wash in 10 mM Tris buffer for 1 hour. This step can go for up to 3 hours if needed.

7. Wash in DI water for 1 hour. This step can go for up to 3 hours if needed.

Cells are now removed. The remaining protein matrix can be used for subsequent culture, or fixed and visualized directly.

Appendices

Appendix B: Dehydration Protocol

Dehydration of cell or protein based samples for imaging under vacuum

1. Rinse sample in PBS and fix (typically in formalin)

2. Wash 3x with PBS

3. Soak in ethanol solutions for 20 minutes in each solution:

30%, 50%, 70%, 90% 95%, 100%, 100% (percentage of ethanol, the rest is DI water)

4. Put sample into a microcentrifuge tube with enough tertbutanol to cover it.

(Tertbutanol may have to be warmed in order to flow as liquid. Immerse the bottle in warm to hot water for a couple of minutes.)

5. Close the microcentrifuge tube and submerge in liquid nitrogen for 2 minutes.

6. Open the tube, and immediately put in the lyophilizer overnight or until ready to image.

Appendices

Appendix C: Preparation of supported protein networks

Fibronectin

Materials

- Corning, Fibronectin, Human, 5mg (356008)
  https://catalog2.corning.com/LifeSciences/en-US/Shopping/ProductDetails.aspx?categoryname=&productid=356008(Lifesciences)
- Gibco DPBS, Calcium and Magnesium free
- N45 Neodymium 1/4"x1/8"x1/16" Rare Earth Magnets
  http://www.magnet4sale.com/n45-neodymium-magnets-1-4x1-8x1-16-rare-earth-magnets/
- Rubber bands: Neon Latex Orthodontic Elastics - 4.5 oz 1/8" - Medium Pull
  http://www.dentalcorp.com/elastomerics/latex-orthodontic-elastics.html
- Biotix Microcentrifuge Tube: VWR Microcentrifuge Tube with X-Resin™ 2 mL Clear Nonsterile 89511-266
  https://us.vwr.com/store/catalog/product.jsp?catalog_number=89511-266
- Incubator and rotisserie rotator for microcentrifuge tubes that fits inside incubator
- Rough or porous support (referred to as “support”)
- Metal Frames washed in soap and bleach after custom fabrication by Microphoto, Inc (Roseville, MI) depicted below:

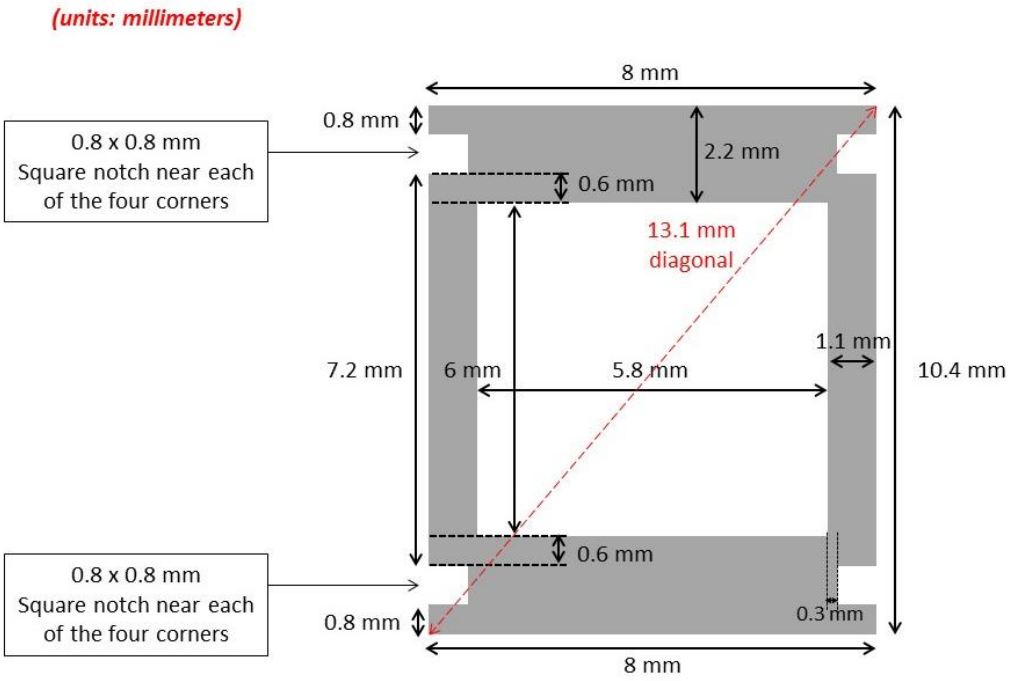

Figure C-1: Dimensions of metal frame used to secure polymer support in 2-mL tube during hydrodynamically induced fibrillogenesis or cell culture in 24-well plates.

Method

Aliquot

1. Chill DPBS until cold and keep on ice for aliquotting.
2. On ice, add DPBS to fibronectin bottle as commercially obtained to achieve a concentration of 1 mg/mL. Gently rotate commercially obtained bottle until all protein is dissolved.
3. Aliquot 100 uL of protein solution into non-fouling 2 mL microcentrifuge tube. Keep all solutions on ice for duration of aliquotting.
4. Store aliquots at -20°C.

Mount Supports into Frames

1. Sterilize frames by spraying with ethanol. Holding support with fine tip tweezer, lightly spray support with 70% ethanol on both sides to sterilize. The support is easier to mount in frames when support and frames are damp. Each support requires two frames (so that support is sandwiched in between).
2. Lay one frame down on sterile surface. Place support, while damp, onto frame such that support is aligned with open square area. Using fine tip tweezer, place second frame on top to evenly sandwich support in between.
3. To secure support between frames, place rubber band within grooves on the two ends of the frames. Fine tip tweezers are helpful, but there are various ways to achieve this mount. Be sure that the support does not shift as you are placing the rubber bands. Also, do not apply too much pressure on the frames while the support is in between as this may cut the support or sever the fibers.

Process: Forming Protein Network on Supports

1. Thaw one 100 uL aliquot at 4°C for 10-15 minutes or until thawed. Each support requires one aliquot.
2. Add 800 uL of DPBS (Calcium and Magnesium free) to each thawed aliquot without allowing the pipette tip to touch the fibronectin. Do not pipette up and down. You don't want to lose protein through adsorption to the inside of the pipette tip.
3. Gently rock the tube and rotate the tube by hand to ensure the solution is freely flowing under rotation in all directions. Be sure that all surfaces within the microcentrifuge tube are able to be wetted by protein solution. When tilting the tube in any direction, the solution must flow from one end to the other. Flicking the tube may also be helpful. Avoid bubbles as much as possible.
4. Place framed support (previously mounted in frame in earlier steps) into protein solution and close tube. Make sure the support and frame has completely air dried of ethanol. Flick tube to remove any bubbles that form within support pores. Again, avoid bubbles as much as possible.
5. Place magnet onto side of tube. Holding the tube vertically, slide the magnet up and down the outer side of the tube until the middle of the support frame is aligned with air-water interface. Turn tube on its side, and make sure that the support frame is level and at the center of the tube. Secure magnets with tape to hold support frame in this position.
6. Mount tubes onto rotator such that the tube tumbles end-over-end at 8 full rotations (360° of rotation) per minute. See image for detailed illustration on support orientation with respect to the tube and rotator. Green circles indicate proper position. Red cross-outs show incorrect position.
7. Tumble supports on rotator for 2 hours at 30°C.
8. Remove protein solution. Rinse three times with DPBS. Store protein supports in DPBS in microcentrifuge tube at 4°C. Use within 1 week.

Troubleshooting

- If the cFn network is not uniform, the support was not level
- If the support tears, too much pressure was applied when support was placed in between the frames
- If little or no cFn fibrils form, the support was not at the air water interface

Laminin

Materials

- Same as supplies listed for fibronectin, now with laminin instead of fibronectin:
  Mouse Laminin: Life Technologies 23017-015 (comes as a liquid)
  https://www.thermofisher.com/order/catalog/product/23017015
- Locite super glue (liquid, not gel): Super Glue Longneck Bottle from Loctite Adhesives
  http://www.loctiteproducts.com/p/4/2/sg_bottle/overview/Loctite-Super-Glue-Longneck-Bottle.htm
- Deionized Water (DI Water)

Method

Aliquot

1. Aliquot 300 uL of laminin solution into non-fouling 2 mL microcentrifuge tube. Keep all solutions on ice for duration of aliquotting.

2. Store aliquots at -20°C.

Mount Supports into Frames

1. Sterilize frames by spraying with ethanol. Holding support with fine tip tweezer, lightly spray support with 70% ethanol on both sides to sterilize. The support is easier to mount in frames when support and frames are damp. Each support requires two frames (so that support is sandwiched in between).
2. Lay one frame down on sterile surface. Run a line of Locite super glue around the outer edge of the square opening of the frame. Place support onto the frame such that support is aligned with open square area. Make sure the edges of the support are well wetted in the line of super glue. Using fine tip tweezer, place second frame on top to evenly sandwich support in between.
3. Allow super glue to cure for 30 minutes, fixing the support in between the frames. Do not apply too much pressure on the frames while the support is in between as this may cut the support or sever the fibers.
4. Rinse the mounted support three times for 10 minutes each in DI water.

Process: Forming Protein Network on Supports

Same as steps listed in Procedure for fibronectin except in steps 1-2 add 700 uL of DI water (not DPBS) to the 300 uL aliquot. Also, in steps 7 and 8, incubate for 2 hours at 26°C (rather than 30°C). After incubation, wash three times with DI water rather than DPBS. Store laminin meshes in DI water at room temperature rather than at 4°C since colder temperatures cause the laminin to resolubilize.

Troubleshooting

Same as steps listed in Procedure for fibronectin.

Collagen I

Materials

- Same as supplies listed for fibronectin, now with collagen I extracted from the tail of a rat
- 33 mM Acetic Acid
- 0.34 N NaOH
- DMEM (as purchased, without additives such as serum)

Method

Prepare Collagen Stock Solution and Aliquot

1. Weigh a clean 50 mL falcon tube
2. Add lyophilized Rat Collagen Type I to tube
3. Re-weigh the tube that now contains the Collagen
4. Add 33 mM acetic acid to collagen for a final collagen concentration of 2.7 mg/mL
5. Stir at 4°C until fully dissolved (2-7days). Store at 4°C until use.
6. Use directly from this stock, or create 900 uL aliquots in microcentrifuge tubes.
7. Store stock solution or aliquots at 4°C.

Mount Supports into Frames

Same as steps listed in Procedure for fibronectin.

Process: Forming Protein Network on Supports

Same as steps listed in Procedure for fibronectin except instead of steps 1 and 2, use 1-3 below:

1. Place DMEM and 0.34 N NaOH on ice
2. If not aliquotted, add 900 uL of the 2.7 mg/mL stock solution to microcentrifuge tube on ice.
3. On ice, add 100 uL of DMEM. The solution should be yellow in color. On ice still, add 140 uL of 0.34 N NaOH to microcentrifuge tube. The solution should now turn pink with the addition of base. (DMEM helps to mediate ionic strength of final solution, acts as a pH indicator, and helps achieve a more uniform protein mesh.)

Also, instead of step 7, tumble for 4 hours at 27°C.

Troubleshooting

Same as steps listed in Procedure for fibronectin.

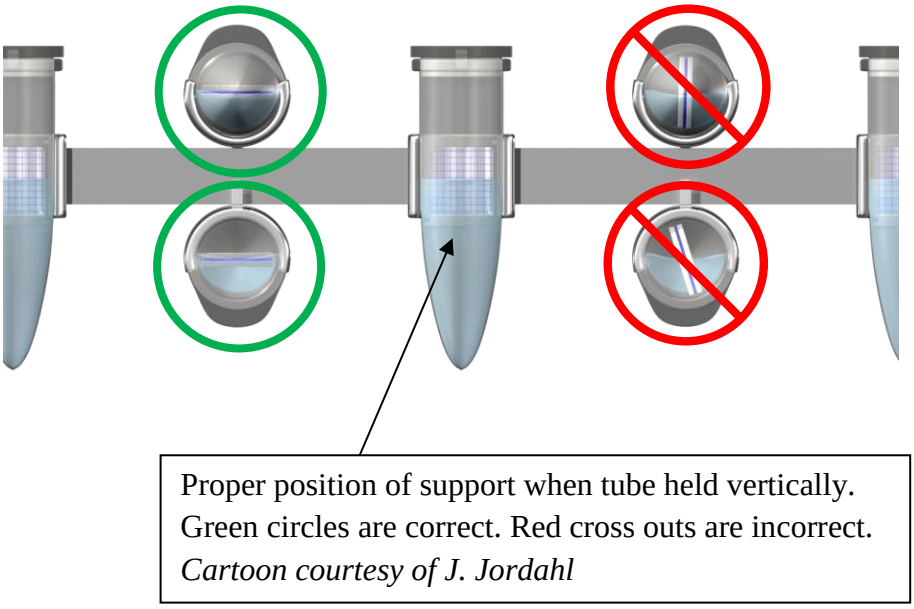

Proper position of support when tube held vertically. Green circles are correct. Red cross outs are incorrect. *Cartoon courtesy of J. Jordahl*

Figure C-2: Proper positioning of 2-mL tube containing mounted polymer support and protein solution on tumbling rotator.

References

1. Lutolf, M.P. & Hubbell, J.A. Synthetic biomaterials as instructive extracellular microenvironments for morphogenesis in tissue engineering. *Nature Biotechnology* **23**, 47-55 (2005).

2. Bhaskar, S. & Lahann, J. Microstructured materials based on multicompartmental fibers. *Journal of American Chemical Society* **131**, 6650-6651 (2009).

3. Leiss, M., Beckmann, K., Giros, A., Costell, M. & Fassler, R. The role of integrin binding sites in fibronectin matrix assembly in vivo. *Curr Opin Cell Biol* **20**, 502-507 (2008).

4. Mao, Y. & Schwarzbauer, J.E. Fibronectin fibrillogenesis, a cell-mediated matrix assembly process. *Matrix Biology* **24** (2005).

5. Fenner, J. et al. Macroscopic stiffness of breast tumors predicts metastasis. *Scientific reports* **4**, 5512 (2014).

6. Boontheekul, T. & Mooney, D.J. Protein-based signaling systems in tissue engineering. *Current Opinion in Biotechnology* **14**, 559-556 (2003).

7. Ruoslahti, E. & Pierschbacher, M.D. New Perspectives in Cell Adhesion: RGD and Integrins. *Science* **238**, 491-497 (1987).

8. Kim, J.B. Three-dimensional tissue culture models in cancer biology. *Semin Cancer Biol* **15**, 365-377 (2005).

9. Chiquet-Ehrismann, R., Kalla, P., Pearson, C.A., Beck, K. & Chiquet, M. Tenascin interferes with fibronectin action. *Cell* **53**, 383-390 (1988).

10. Cseh, B. et al. Autocrine fibronectin directs matrix assembly and crosstalk between cell-matrix and cell-cell adhesion in vascular endothelial cells. *J Cell Sci* **123**, 3989-3999 (2010).

11. To, W.S. & Midwood, K.S. Plasma and cellular fibronectin: distinct and independent functions during tissue repair. *Fibrogenesis & tissue repair* **4**, 21 (2011).

12. Little, W.C., Smith, M.L. & Vogel, V. Assay to mechanically tune and optically probe fibrillar fibronectin conformations from fully relaxed to breakage. *Matrix Biology* **27**, 451-461 (2008).

13. Ulmer, J., Geiger, B. & Spatz, J.P. Force-induced fibronectin fibrillogenesis *in vitro*. *Soft Matter* **4**, 1998-2007 (2008).

14. Mitsi, M. et al. The ultrastructure of fibronectin fibers pulled from a protein monolayer at the air-liquid interface and the mechanism of the sheet-to-fiber transition. *Biomaterials* **36**, 66-79 (2015).

15. Frantz, C., Stewart, K.M. & Weaver, V.M. The extracellular matrix at a glance. *J Cell Sci* **123**, 4195-4200 (2010).

16. Reticker-Flynn, N.E. et al. A combinatorial extracellular matrix platform identifies cell-extracellular matrix interactions that correlate with metastasis. *Nat Commun* **3**, 1122 (2012).

17. Zhou, Z. et al. MRI detection of breast cancer micrometastases with a fibronectin-targeting contrast agent. *Nat Commun* **6**, 7984 (2015).

18. Hakanson, M., Textor, M. & Charnley, M. Engineered 3D environments to elucidate the effect of environmental parameters on drug response in cancer. *Integrative biology : quantitative biosciences from nano to macro* **3**, 31-38 (2011).

19. Lee, J., Cuddihy, M.J. & Kotov, N.A. Three-Dimensional Cell Culture Matrices: State of the Art. *Tissue Engineering: Part B* **14**, 61-86 (2008).

20. Greiner, A. & Wendorff, J.H. Electrospinning: A fascinating method for the preparation of ultrathin fibers. *Angewandte Chemie* **46**, 5670-5703 (2007).

21. Pham, Q.P., Sharma, U. & Mikos, A.G. Electrospinning of polymeric nanofibers for tissue engineering applications: A review. *Tissue Engineering* **12**, 1197-1211 (2006).

22. Evangelatov, A. & Pankov, R. Regenerative Medicine and Tissue Engineering. (2013).

23. Keselowsky, B.G., Collard, D.M. & Garcia, A.J. Integrin binding specificity regulates biomaterial surface chemistry effects on cell differentiation. *Proceedings of the National Academy of Sciences of the United States of America* **102**, 5953-5957 (2005).

24. Fischbach, C. et al. Engineering tumors with 3D scaffolds. *Nature Methods* **4** (2007).

25. Li, M.L. et al. Influence of a reconstituted basement membrane and its components on casein gene expression and secretion in mouse mammary epithelial cells. *Proceedings of the National Academy of Sciences of the United States of America* **84**, 136-140 (1987).

26. Paget, S. The Distribution of Secondary Growths in Cancer of the Breast. *The Lancet* **133**, 571-573 (1889).

27. Hanahan, D. & Weinberg, R.A. Hallmarks of Cancer: The Next Generation. *Cell* **144** (2011).

28. Erez, N. Cancer: Opening LOX to metastasis. *Nature* **522**, 41-42 (2015).

29. Benton, G., Crooke, E. & George, J. Laminin-1 induces E-cadherin expression in 3-dimensional cultured breast cancer cells by inhibiting DNA methyltransferase 1 and reversing promoter methylation status. *FASEB journal : official publication of the Federation of American Societies for Experimental Biology* **23**, 3884-3895 (2009).

30. Mueller, M.M. & Fusenig, N.E. Friends or foes - bipolar effects of the tumour stroma in cancer. *Nature reviews. Cancer* **4**, 839-849 (2004).

31. Sceneay, J., Smyth, M.J. & Moller, A. The pre-metastatic niche: finding common ground. *Cancer metastasis reviews* **32**, 449-464 (2013).

32. Fischbach, C. et al. Cancer cell angiogenic capability is regulated by 3D culture and integrin engagement. *Proceedings of the National Academy of Sciences of the United States of America* **106**, 399-404 (2009).

33. Ma, J. et al. Concise review: cell-based strategies in bone tissue engineering and regenerative medicine. *Stem cells translational medicine* **3**, 98-107 (2014).

34. Fong, E.L. et al. Modeling Ewing sarcoma tumors in vitro with 3D scaffolds. *Proceedings of the National Academy of Sciences of the United States of America* **110**, 6500-6505 (2013).

35. Giovanni, V., Flaimb, C., Ahluwaliaa, A. & Sangeeta, B. Fabrication of PLGA scaffolds using soft lithography and microsyringe deposition. *Biomaterials* **24**, 2533-2540 (2003).

36. Mehta, G., Hsiao, A.Y., Ingram, M., Luker, G.D. & Takayama, S. Opportunities and challenges for use of tumor spheroids as models to test drug delivery and efficacy. *Journal of Controlled Release* **164**, 192-204 (2012).

37. Tse, J.R. & Engler, A.J. Preparation of Hydrogel Substrates with Tunable Mechanical Properties. *Current Protocols in Cell Biology* (2010).

38. Hoffman, A.S. Hydrogels for biomedical applications. *Advanced Drug Delivery Reviews* **64**, 18-23 (2012).

39. Villa-Diaz, L.G. et al. Synthetic polymer coatings for long-term growth of human embryonic stem cells. *Nat Biotechnol* **28**, 581-583 (2010).

40. Billiet, T., Vandenhaute, M., Schelfhout, J., Vlierberghe, S.V. & Dubruel, P. A review of trends and limitations in hydrogel-rapid prototyping for tissue engineering *Biomaterials* **33**, 6020-6041 (2012).

41. Lee, J., Abdeen, A.A., Wycislo, K.L., Fan, T.M. & Kilian, K.A. Interfacial geometry dictates cancer cell tumorigenicity. *Nat Mater* **15**, 856-862 (2016).

42. Wan, A.M. et al. Fibronectin conformation regulates the proangiogenic capability of tumor-associated adipogenic stromal cells. *Biochimica et biophysica acta* **1830**, 4314-4320 (2013).

43. Deravi, L.F. et al. Differential contributions of conformation extension and domain unfolding to properties of fibronectin nanotextiles. *Nano Letters* **12**, 5587-5592 (2012).

44. Greiner, J., Kaltschmidt, B., Kaltschmidt, C. & Widera, D. Going 3D – Cell Culture Approaches for Stem Cell Research and Therapy. *Current Tissue Engineering* **2**, 8-19 (2013).

45. Jones, D.L. & Wagers, A.J. No place like home: anatomy and function of the stem cell niche. *Nature Reviews Molecular Cell Biology* **9**, 11-21 (2008).

46. Rehfeldt, F., Engler, A.J., Eckhardt, A., Ahmed, F. & Discher, D.E. Cell responses to the mechanochemical microenvironment - Implications for regenerative medicine and drug delivery. *Advanced Drug Delivery Reviews* **59**, 1329-1339 (2007).

47. Choi, N.W. et al. Microfluidic scaffolds for tissue engineering. *Nature Materials* **6**, 908-915 (2007).

48. Jordahl, J.H. et al. 3D Jet Writing: Functional microtissues based on tessellated scaffold architectures. *Submitted* (2017).

49. Kolewe, M.E. et al. 3D Structural Patterns in Scalable, Elastomeric Scaffolds Guide Engineered Tissue Architecture. *Advanced Materials* **25**, 4459-4465 (2013).

50. Collins, G., Federici, J., Imura, Y. & Catalani, L.H. Charge generation, charge transport, and residual charge in the electrospinning of polymers: A review of issues and complications. *J. Appl. Phys.* **111** (2012).

51. Zeleny, J. Instability of electrified liquid surfaces. *The Physical Review* **X** (1917).

52. I., H., A., B. & F., T.T. Investigations into the Mechanism of Electrohydrodynamic Spraying of Liquids. *J Colloid Interface Sci* **117**, 222-230 (1986).

53. Taylor, G.I. Studies in Electrohydrodynamics. I. The Circulation Produced in a Drop by Electrical Field. *Proc. R. Soc. Lond. A* **291**, 159-166 (1966).

54. Taylor, G.I. Electrically Driven Jets. *Proc. R. Soc. Lond. A* **313**, 453-475 (1969).

55. Lahann, J. Recent Progress in nano-biotechnology: Compartmentalized Micro- and Nanoparticles via Electrohydrodynamic Co-jetting. *Small* **X**, 1-8 (2011).

56. M.M., H., M., S., G., R. & M.P., B. Electrospinning and electrically forced jets. I. Stability Theory. *Physics of Fluids* **13**, 2201-2220 (2001).

57. Vaquette, C. & Cooper-White, J. The use of an electrostatic lens to enhance the efficiency of the electrospinning process. *Cell and tissue research* **347**, 815-826 (2012).

58. Kim, G.H. Electrospun PCL nanofibers with anisotropic mechanical properties as a biomedical scaffold. *Biomed Mater* **3**, 025010 (2008).

59. Gentile, P., Chiono, V., Carmagnola, I. & Hatton, P.V. An overview of poly(lactic-co-glycolic) acid (PLGA)-based biomaterials for bone tissue engineering. *International journal of molecular sciences* **15**, 3640-3659 (2014).

60. East, E., Golding, J.P. & Phillips, J.B. A versatile 3D culture model facilitates monitoring of astrocytes undergoing reactive gliosis. *J Tissue Eng Regen Med* **3**, 634-646 (2009).

61. DeMali, K.A., Wennerberg, K. & Burridge, K. Integrin signaling to the actin cytoskeleton. *Curr Opin Cell Biol* **15**, 572-582 (2003).

62. Mandal, S., Bhaskar, S. & Lahann, J. Micropatterned Fiber Scaffolds for Spatially Controlled Cell Adhesion. *Macromolecular Rapid Communications* **30**, 1638-1644 (2009).

63. Rahmani, S., Park, T., Dishman, A.F. & Lahann, J. Multimodal delivery of irinotecan from microparticles with two distinct compartments. *Journal of Controlled Release* **172**, 239-245 (2013).

64. Esfahani, R.R., Jun, H., Rahmani, S., Miller, A. & Lahann, J. Microencapsulation of Live Cells in Synthetic Polymer Capsules. *ACS Omega* **2**, 2839-2847 (2017).

65. Yoon, J., Eyster, T.W., Misra, A.C. & Lahann, J. Cardiomyocyte-Driven Actuation in Biohybrid Microcylinders. *Adv Mater* (2015).

66. Wang, L., Zhang, Z., Chen, H., Zhang, S. & Xiong, C. Preparation and characterization of biodegradable thermoplastic Elastomers (PLCA/PLGA blends). *J Polym Res*, 77-82 (2010).

67. Jeong, S.I. et al. In vivo biocompatibilty and degradation behavior of elastic poly(L-lactide-co-epsilon-caprolactone) scaffolds. *Biomaterials* **25**, 5939-5946 (2004).

68. Fuerstman, M.J. et al. The pressure drop along rectangular microchannels containing bubbles. *Lab Chip* **7**, 1479-1489 (2007).

69. B.J., A. & S.S., V. Pressure drops for droplet flows in microfluidic channels. *Journal of Micromechanics and Microengineering* **16**, 1504-1510 (2006).

70. A., P. & C.H., A. Self-aligning microfluidic interconnects for glass- and plastic-based microfluidic systems. *Journal of Micromechanics and Microengineering* **12**, 35-40 (2002).

71. Rolland, J.P., Van Dam, R.M., Schorzman, D.A., Quake, S.R. & DeSimone, J.M. Solvent-resistant photocurable liquid fluoropolymers for microfluidic device fabrication [corrected]. *J Am Chem Soc* **126**, 2322-2323 (2004).

72. Kim, B., Hong, L., Chung, Y., Kim, D. & Lee, C. Solvent-Resistant PDMS Microfluidic Devices with Hybrid Inorganic/Organic Polymer Coatings. *Adv. Funct. Mater.* **19**, 3796-3803 (2009).

73. Abate, A.R. et al. Photoreactive coating for high-contrast spatial patterning of microfluidic device wettability. *Lab Chip* **8**, 2157-2160 (2008).

74. Paszek, M.J. et al. Tensional homeostasis and the malignant phenotype. *Cancer Cell* **8**, 241-254 (2005).

75. Yoo, I., Song, S., Yoon, B. & Kim, J. Size-Controlled Fabrication of Polydiacetylene-Embedded Microfibers on a Microfluidic Chip. *Macromolecular Rapid Communications* **33**, 1256-1261 (2012).

76. Cantini, M., Rico, P. & Salmeron-Sanchez, M. in Biomimetic Approaches for Biomaterials Development, Edn. 1. (ed. J.F. Mano) 189-212 (Wiley-VCH Verlag GmbH & Co. KGaA., 2012).

77. Wierzbicka-Patynowski, I. & Schwarzbauer, J.E. The ins and outs of fibronectin matrix assembly. *Journal of Cell Science* **116**, 3269-3276 (2003).

78. Chastain, S.R., Kundu, A.K., Dhar, S., Calvert, J.W. & Putnam, A.J. Adhesion of mesenchymal stem cells to polymer scaffolds occurs via distinct ECM ligands and controls their osteogenic differentiation. *Journal of Biomedical Materials Research Part A*, 73-85 (2006).

79. Tija, J.S., Aneskievich, B.J. & Moghe, P.V. Substrate-adsorbed collagen and cell secreted fibronectin concertedly induce cell migration on poly(lactide-glycolide) substrates. *Biomaterials* **20**, 2223-2233 (1999).

80. Orgel, J.P., San Antonio, J.D. & Antipova, O. Molecular and structural mapping of collagen fibril interactions. *Connective tissue research* **52**, 2-17 (2011).

81. Martino, M.M. et al. Controlling integrin specificity and stem cell differentiation in 2D and 3D environments through regulation of fibronectin domain stability. *Biomaterials* **30**, 1089-1097 (2009).

82. Martino, M.M. & Hubbell, J.A. The 12th-14th type III repeats of fibronectin function as a highly promiscuous growth factor-binding domain. *FASEB journal : official publication of the Federation of American Societies for Experimental Biology* **24**, 4711-4721 (2010).

83. Leahy, D.J., Aukhil, I. & Erickson, H.P. 2.0 A crystal structure of a four-domain segment of human fibronectin encompassing the RGD loop and synergy region. *Cell* **84**, 155-164 (1996).

84. Oberdorfer, Y., Fuchs, H. & Janshoff, A. Conformational analysis of native fibronectin by means of force spectroscopy. *Langmuir* **16**, 9955-9958 (2000).

85. Wang, K., Seo, B.R., Fischbach, C. & Gourdon, D. Fibronectin Mechanobiology Regulates Tumorigenesis. *Cellular and molecular bioengineering* **9**, 1-11 (2016).

86. Wang, K. et al. Stiffening and unfolding of early deposited-fibronectin increase proangiogenic factor secretion by breast cancer-associated stromal cells. *Biomaterials* **54**, 63-71 (2015).

87. Leight, J.L., Wozniak, M.A., Chen, S., Lynch, M.L. & Chen, C.S. Matrix rigidity regulates a switch between TGF-β1–induced apoptosis and epithelial–mesenchymal transition. *Mol. Biol. Cell* **23**, 781-791 (2012).

88. Akiyama, S.K., Yamada, K.M. & Hayashi, M. The structure of fibronectin and its role in cellular adhesion. *Journal of supramolecular structure and cellular biochemistry* **16**, 345-348 (1981).

89. Vakonakis, I., Staunton, D., Rooney, L.M. & Campbell, I.D. Interdomain association in fibronectin: insight into cryptic sites and fibrillogenesis. *The EMBO journal* **26**, 2575-2583 (2007).

90. Pankov, R. & Yamada, K.M. Fibronectin at a glance. *J Cell Sci* **115**, 3861-3863 (2002).

91. McKeown-Longo, P.J. & Etzler, C.A. Induction of fibronectin matrix assembly in human fibrosarcoma cells by dexamethasone. *The Journal of cell biology* **104**, 601-610 (1987).

92. Langenbach, K.J. & Sottile, J. Identification of protein-disulfide isomerase activity in fibronectin. *The Journal of biological chemistry* **274**, 7032-7038 (1999).

93. McKeown-Longo, P.J. & Mosher, D.F. Mechanism of formation of disulfide-bonded multimers of plasma fibronectin in cell layers of cultured human fibroblasts. *The Journal of biological chemistry* **259**, 12210-12215 (1984).

94. Mosher, D.F., Fogerty, F.J., Chernousov, M.A. & Barry, E.L.R. Assembly of Fibronectin into Extracellular Matrix. *Ann. N. Y. Acad. Sci.*, 167-180 (1991).

95. Chen, H. & Mosher, D.F. Formation of sodium dodecyl sulfate-stable fibronectin multimers. Failure to detect products of thiol-disulfide exchange in cyanogen bromide or limited acid digests of stabilized matrix fibronectin. *The Journal of biological chemistry* **271**, 9084-9089 (1996).

96. Litvinovich, S.V. et al. Formation of amyloid-like fibrils by self-association of a partially unfolded fibronectin type III module. *Journal of molecular biology* **280**, 245-258 (1998).

97. Ni, H. et al. Plasma fibronectin promotes thrombus growth and stability in injured arterioles. *Proceedings of the National Academy of Sciences of the United States of America* **100**, 2415-2419 (2003).

98. Cho, J. & Mosher, D.F. Role of fibronectin assembly in platelet thrombus formation. *Journal of thrombosis and haemostasis : JTH* **4**, 1461-1469 (2006).

99. Johnson, K.J., Sage, H., Briscoe, G. & Erickson, H.P. The compact conformation of fibronectin is determined by intramolecular ionic interactions. *The Journal of biological chemistry* **274**, 15473-15479 (1999).

100. Moretti, F.A. et al. A major fraction of fibronectin present in the extracellular matrix of tissues is plasma-derived. *The Journal of biological chemistry* **282**, 28057-28062 (2007).

101. Erickson, H.P., Carrell, N. & McDonagh, J. Fibronectin molecule visualized in electron microscopy: a long, thin, flexible strand. *The Journal of cell biology* **91**, 673-678 (1981).

102. Singh, P., Carraher, C. & Schwarzbauer, J.E. Assembly of fibronectin extracellular matrix. *Annual review of cell and developmental biology* **26**, 397-419 (2010).

103. Dzamba, B.J. & Peters, D.M. Arrangement of cellular fibronectin in noncollagenous fibrils in human fibroblast cultures. *J Cell Sci* **100 (Pt 3)**, 605-612 (1991).

104. Sottile, J. & Hocking, D.C. Fibronectin polymerization regulates the composition and stability of extracellular matrix fibrils and cell-matrix adhesions. *Mol Biol Cell* **13**, 3546-3559 (2002).

105. Huber, A.H., Wang, Y.M., Bieber, A.J. & Bjorkman, P.J. Crystal structure of tandem type III fibronectin domains from Drosophila neuroglian at 2.0 A. *Neuron* **12**, 717-731 (1994).

106. Erickson, H.P. Reversible unfolding of fibronectin type III and immunoglobulin domains provides the structural basis for stretch and elasticity of titin and fibronectin. *Proceedings of the National Academy of Sciences of the United States of America* **91**, 10114-10118 (1994).

107. Schwarzbauer, J.E. Identification of the fibronectin sequences required for assembly of a fibrillar matrix. *The Journal of cell biology* **113**, 1463-1473 (1991).

108. Sechler, J.L. et al. A novel fibronectin binding site required for fibronectin fibril growth during matrix assembly. *The Journal of cell biology* **154**, 1081-1088 (2001).

109. Shimoda, Y. & Watanabe, K. Contactins: emerging key roles in the development and function of the nervous system. *Cell adhesion & migration* **3**, 64-70 (2009).

110. Kielty, C.M., Sherratt, M.J. & Shuttleworth, C.A. Elastic fibres. *J Cell Sci* **115**, 2817-2828 (2002).

111. Rowe, S.L. & Stegemann, J.P. Interpenetrating collagen-fibrin composite matrices with varying protein contents and ratios. *Biomacromolecules* **7**, 2942-2948 (2006).

112. Ricard-Blum, S. & Ruggiero, F. The collagen superfamily: from the extracellular matrix to the cell membrane. *Pathologie-biologie* **53**, 430-442 (2005).

113. Xu, L. & Siedlecki, C.A. Effects of surface wettability and contact time on protein adhesion to biomaterial surfaces. *Biomaterials* **28**, 3273-3283 (2007).

114. Roach, P., Farrar, D. & Perry, C.C. Interpretation of Protein Adsorption: Surface-Induced Conformational Changes. *Journal of the American Chemical Society* **127**, 8168-8173 (2005).

115. Nakanishi, K., Sakiyama, T. & Imamura, K. On the Adsorption of Proteins on Solid Surfaces, a Common but Very Complicated Phenomenon. *Journal of Bioscience and Bioengineering* **91**, 233-244 (2001).

116. Wang, K., Changchun, Z., Hong, Y. & Zhang, X. A review of protein adsorption on bioceramics. *Interface Focus* **2**, 259-277 (2012).

117. Pernodet, N. et al. Fibronectin fibrillogenesis on sulfonated polystyrene surfaces. *Journal of biomedical materials research. Part A* **64**, 684-692 (2003).

118. Vuento, M., Vartio, T., Saraste, M., von Bonsdorff, C.H. & Vaheri, A. Spontaneous and polyamine-induced formation of filamentous polymers from soluble fibronectin. *European journal of biochemistry* **105**, 33-42 (1980).

119. Peters, D.M.P., Chen, Y., Zardi, L. & Brummel, S. Conformation of Fibronectin Fibrils Varies: Discrete Globular Domains of Type III Repeats Detected. *Microscopy and Microanalysis* **4**, 385-396 (1998).

120. Ejim, O.S., Blunn, G.W. & Brown, R.A. Production of artificial-orientated mats and strands from plasma fibronectin: a morphological study. *Biomaterials* **14**, 743–748 (1993).

121. Klotzsch, E. et al. Fibronectin forms the most extensible biological fibers displaying switchable force-exposed cryptic binding sites. *PNAS* **106**, 18267-18272 (2009).

122. Lu, H., Hoshiba, T., Kawazoe, N. & Chen, G. Comparison of decellularization techniques for preparation of extracellular matrix scaffolds derived from three-dimensional cell culture. *Journal of biomedical materials research. Part A* **100**, 2507-2516 (2012).

123. Huang, C.P. et al. Engineering microscale cellular niches for three-dimensional multicellular co-cultures. *Lab on a Chip* **9**, 1740-1748 (2009).

124. McKeown-Longo, P.J. & Mosher, D.F. Binding of plasma fibronectin to cell layers of human skin fibroblasts. *The Journal of cell biology* **97**, 466-472 (1983).

125. Carter, W.G. & Hakomori, S. A new cell surface, detergent-insoluble glycoprotein matrix of human and hamster fibroblasts. The role of disulfide bonds in stabilization of the matrix. *The Journal of biological chemistry* **256**, 6953-6960 (1981).

126. Erickson, H.P. Stretching fibronectin. *Journal of muscle research and cell motility* **23**, 575-580 (2002).

127. Keen, J., Chang, S.E. & Taylor-Papadimitriou, J. Monoclonal antibodies that distinguish between human cellular and plasma fibronectin. *Molecular biology & medicine* **2**, 15-27 (1984).

128. Gugutkov, D., Gonzalez-Garcia, C., Rodriguez Hernandez, J.C., Altankov, G. & Salmeron-Sanchez, M. Biological activity of the substrate-induced fibronectin network: insight into the third dimension through electrospun fibers. *Langmuir* **25**, 10893-10900 (2009).

129. Seo, B.R. et al. Obesity-dependent changes in interstitial ECM mechanics promote breast tumorigenesis. *Science translational medicine* **7**, 301ra130 (2015).

130. Kii, I. et al. Incorporation of tenascin-C into the extracellular matrix by periostin underlies an extracellular meshwork architecture. *The Journal of biological chemistry* **285**, 2028-2039 (2010).

131. Orend, G. Potential oncogenic action of tenascin-C in tumorigenesis. *The international journal of biochemistry & cell biology* **37**, 1066-1083 (2005).

132. Oskarsson, T. et al. Breast cancer cells produce tenascin C as a metastatic niche component to colonize the lungs. *Nat Med* **17**, 867-874 (2011).

133. Lowy, C.M. & Oskarsson, T. Tenascin C in metastasis: A view from the invasive front. *Cell adhesion & migration* **9**, 112-124 (2015).

134. Watanabe, G. et al. Induction of tenascin-C by tumor-specific EWS-ETS fusion genes. *Genes, chromosomes & cancer* **36**, 224-232 (2003).

135. Pedersen, E.A., Scannell, C.A., Menon, R. & Lawlor, E.R. Tenascin C is a canonical Wnt target gene in Ewing sarcoma and its expression is potentiated by R-spondin. [abstract]. *Proceedings of the 105th Annual Meeting of the American Association for Cancer Research* (2014).

136. Machado, I. et al. Epithelial cell adhesion molecules and epithelial mesenchymal transition (EMT) markers in Ewing's sarcoma family of tumors (ESFTs). Do they offer any prognostic significance? *Virchows Archiv : an international journal of pathology* **461**, 333-337 (2012).

137. Khan, Z.A. et al. EDB fibronectin and angiogenesis -- a novel mechanistic pathway. *Angiogenesis* **8**, 183-196 (2005).

138. Zhou, X. et al. Fibronectin fibrillogenesis regulates three-dimensional neovessel formation. *Genes & development* **22**, 1231-1243 (2008).

139. Kaczmarek, J. et al. Distribution of oncofetal fibronectin isoforms in normal, hyperplastic and neoplastic human breast tissues. *International journal of cancer* **59**, 11-16 (1994).

140. Zajac, A.L. & Discher, D.E. Cell differentiation through tissue elasticity-coupled, myosin-driven remodeling. *Current Opinion in Cell Biology* **20**, 609-615 (2008).

141. Ingham, K.C., Brew, S.A., Huff, S. & Litvinovich, S.V. Cryptic self-association sites in type III modules of fibronectin. *The Journal of biological chemistry* **272**, 1718-1724 (1997).

142. Schwarzbauer, J.E. & Scechler, J.L. Fibronectin fibrillogenesis: a paradigm for extracellular matrix assembly. *Current Opinion in Cell Biology* **11**, 622-627 (1999).

143. Fleischmajer, R. et al. Initiation of skin basement membrane formation at the epidermo-dermal interface involves assembly of laminins through binding to cell membrane receptors. *J Cell Sci* **111 (Pt 14)**, 1929-1940 (1998).

144. Henry, M.D. & Campbell, K.P. A role for dystroglycan in basement membrane assembly. *Cell* **95**, 859-870 (1998).

145. Stephens, L.E. et al. Deletion of beta 1 integrins in mice results in inner cell mass failure and peri-implantation lethality. *Genes & development* **9**, 1883-1895 (1995).

146. Sasaki, T. et al. Deficiency of beta 1 integrins in teratoma interferes with basement membrane assembly and laminin-1 expression. *Experimental cell research* **238**, 70-81 (1998).

147. Wu, P.H., Giri, A., Sun, S.X. & Wirtz, D. Three-dimensional cell migration does not follow a random walk. *Proceedings of the National Academy of Sciences of the United States of America* **111**, 3949-3954 (2014).

148. Lamouille, S., Xu, J. & Derynck, R. Molecular mechanisms of epithelial-mesenchymal transition. *Nature Reviews Molecular Cell Biology* **15**, 178-196 (2014).

149. Cho, S.H. et al. CD44 enhances the epithelial-mesenchymal transition in association with colon cancer invasion. *International journal of oncology* **41**, 211-218 (2012).

150. Liu, S. et al. Breast Cancer Stem Cells Transition between Epithelial and Mesenchymal States Reflective of their Normal Counterpar ts. *Stem Cell Reports* **2**, 78-91 (2014).

151. Xie, G. et al. IL-6-induced epithelial-mesenchymal transition promotes the generation of breast cancer stem-like cells analogous to mammosphere cultures. *International journal of oncology* **40**, 1171-1179 (2012).

152. Ginestier, C. et al. ALDH1 Is a Marker of Normal and Malignant Human Mammary Stem Cells and a Predictor of Poor Clinical Outcome. *Cell Stem Cell* **1**, 555-557 (2007).

153. Blick, T. et al. Epithelial mesenchymal transition traits in human breast cancer cell lines. *Clinical & experimental metastasis* **25**, 629-642 (2008).

154. Kim, Y. et al. Integrin alpha3beta1-dependent beta-catenin phosphorylation links epithelial Smad signaling to cell contacts. *The Journal of cell biology* **184**, 309-322 (2009).

155. Charafe-Jauffret, E. et al. Breast Cancer Cell Lines Contain Functional Cancer Stem Cells with Metastatic Capacity and a Distinct Molecular Signature. *Cancer Research* **69**, 1302-1313 (2009).

156. Croker, A.K. et al. High aldehyde dehydrogenase and expression of cancer stem cell markers selects for breast cancer cells with enhanced malignant and metastatic ability. *Journal of Cellular and Molecular Medicine* **13**, 2236-2252 (2009).

157. Al-Hajj, M., Wicha, M.S., Benito-Hernandez, A., Morrison, S.J. & Clarke, M.F. Prospective identification of tumorigenic breast cancer cells. *Proceedings of the National Academy of Sciences of the United States of America* **100**, 3983-3988 (2003).

158. Hirsch, H.A., Iliopoulos, D., Tsichlis, P.N. & Struhl, K. Metformin Selectively Targets Cancer Stem Cells, and Acts Together with Chemotherapy to Block Tumor Growth and Prolong Remission. *Cancer Research* **69** (2009).

159. Tanei, T. et al. Association of Breast Cancer Stem Cells Identified by Aldehyde Dehydrogenase 1 Expression with Resistance to Sequential Paclitaxel and Epirubicin-Based Chemotherapy for Breast Cancers. *Clinical Cancer Research* **15** (2009).

160. Pan, Q. et al. Concise Review: Targeting Cancer Stem Cells Using Immunologic Approaches. *Stem Cells* **33**, 2085-2092 (2015).

161. Jabbari, E. in Handbook of Biomimetics and Bioinspiration, Vol. 9. (eds. E. Jabbari, D. Kim, L.P. Lee, A. Ghaemmaghami & A. Khademhosseini) (World Scientific Publishing Co. Pte. Ltd., Singapore; 2014).

162. Mani, S.A. et al. The epithelial-mesenchymal transition generates cells with properties of stem cells. *Cell* **133**, 704-715 (2008).

163. Aboussekhra, A. Role of cancer-associated fibroblasts in breast cancer development and prognosis. *The International Journal of Developmental Biology* **55**, 841-849 (2011).

164. Kim, J.B. Three-dimensional tissue culture models in cancer biology. *Seminars in Cancer Biology* **15**, 365-377 (2005).

165. DeRose, Y.S. et al. Tumor grafts derived from women with breast cancer authentically reflect tumor pathology, growth, metastasis and disease outcomes. *Nature Medicine* **17**, 1514-1520 (2011).

166. Zhang, X. et al. A Renewable Tissue Resource of Phenotypically Stable, Biologically and Ethnically Diverse, Patient-Derived Human Breast Cancer Xenograft Models. *Cancer Research* **73**, 4885-4897 (2013).

167. Weigelt, B. & Bissell, M.J. Unraveling the microenvironmental influences on the normal mammary gland and breast cancer. *Semin Cancer Biol* **18**, 311-321 (2008).

168. Vargo-Gogola, T. & Rosen, J.M. Modelling breast cancer: one size does not fit all. *Nature reviews. Cancer* **7**, 659-672 (2007).

169. Marangoni, E. et al. A New Model of Patient Tumor-Derived Breast Cancer Xenografts for Preclinical Assays. *Clinical Cancer Research* **13**, 3989-3998 (2007).

170. Kabos, P. et al. Patient-derived luminal breast cancer xenografts retain hormone receptor heterogeneity and help define unique estrogen-dependent gene signatures. *Breast Cancer Research and Treatment* **135**, 415-432 (2012).

171. Kaplan, R.N. et al. VEGFR1-positive haematopoietic bone marrow progenitors initiate the pre-metastatic niche. *Nature* **438**, 820-827 (2005).

172. Fernandez-Garcia, B. et al. Expression and prognostic significance of fibronectin and matrix metalloproteases in breast cancer metastasis. *Histopathology* **64**, 512-522 (2014).

173. Godier-Furnemont, A.F. et al. Composite scaffold provides a cell delivery platform for cardiovascular repair. *Proceedings of the National Academy of Sciences of the United States of America* **108**, 7974-7979 (2011).

174. Simpson, D., Liu, H., Fan, T.H., Nerem, R. & Dudley, S.C., Jr. A tissue engineering approach to progenitor cell delivery results in significant cell engraftment and improved myocardial remodeling. *Stem Cells* **25**, 2350-2357 (2007).

175. Wang, C., Varshney, R.R. & Wang, D.A. Therapeutic cell delivery and fate control in hydrogels and hydrogel hybrids. *Adv Drug Deliv Rev* **62**, 699-710 (2010).

176. Badylak, S.F. The extracellular matrix as a scaffold for tissue reconstruction. *Semin Cell Dev Biol* **13**, 377-383 (2002).

177. Solorio, L.D., Vieregge, E.L., Dhami, C.D., Dang, P.N. & Alsberg, E. Engineered cartilage via self-assembled hMSC sheets with incorporated biodegradable gelatin microspheres releasing transforming growth factor-beta1. *J Control Release* **158**, 224-232 (2012).

178. Zhang, M. et al. Identification of tumor-initiating cells in a p53-null mouse model of breast cancer. *Cancer Res* **68**, 4674-4682 (2008).

179. Malanchi, I. et al. Interactions between cancer stem cells and their niche govern metastatic colonization. *Nature* **481** (2012).

180. Cho, R.W. et al. Isolation and Molecular Characterization of Cancer Stem Cells in MMTV-Wnt-1 Murine Breast Tumors. *Stem Cells* **26**, 364-371 (2008).

181. Zhang, M. et al. Identification of Tumor-Initiating Cells in a p53-Null Mouse Model of Breast Cancer. *Cancer Research* **68** (2008).

182. Lobba, A.R., Forni, M.F., Carreira, A.C. & Sogayar, M.C. Differential expression of CD90 and CD14 stem cell markers in malignant breast cancer cell lines. *Cytometry. Part A : the journal of the International Society for Analytical Cytology* **81**, 1084-1091 (2012).

183. Sheridan, C. et al. CD44+/CD24- breast cancer cells exhibit enhanced invasive properties: an early step necessary for metastasis. *Breast Cancer Research* **8** (2006).

184. Jovanovic, B. et al. Transforming growth factor beta receptor type III is a tumor promoter in mesenchymal-stem like triple negative breast cancer. *Breast cancer research : BCR* **16**, R69 (2014).

185. Grigoriadis, A. et al. Molecular characterisation of cell line models for triple-negative breast cancers. *BMC genomics* **13**, 619 (2012).

186. Blanpain, C., Lowry, W.E., Geoghegan, A., Polak, L. & Fuchs, E. Self-renewal, multipotency, and the existence of two cell populations within an epithelial stem cell niche. *Cell* **118**, 635-648 (2004).

187. Chen, Y.T. et al. A testicular antigen aberrantly expressed in human cancers detected by autologous antibody screening. *Proceedings of the National Academy of Sciences of the United States of America* **94**, 1914-1918 (1997).

188. Yen, B.L. et al. Isolation of multipotent cells from human term placenta. *Stem Cells* **23**, 3-9 (2005).

189. Potter, S.M. & DeMarse, T.B. A new approach to neural cell culture for long-term studies. *Journal of neuroscience methods* **110**, 17-24 (2001).

190. Biddle, A. & Mackenzie, I.C. Cancer stem cells and EMT in carcinoma. *Cancer metastasis reviews* (2012).

191. Prendergast, G.C. & Jaffee, E.M. Cancer immunologists and cancer biologists: why we didn't talk then but need to now. *Cancer Res* **67**, 3500-3504 (2007).

192. Ponta, H., Sherman, L. & Herrlich, P.A. CD44: from adhesion molecules to signalling regulators. *Nature reviews. Molecular cell biology* **4**, 33-45 (2003).

193. Baumann, P. et al. CD24 expression causes the acquisition of multiple cellular properties associated with tumor growth and metastasis. *Cancer Res* **65**, 10783-10793 (2005).

194. Leight, J.L., Wozniak, M.A., Chen, S., Lynch, M.L. & Chen, C.S. Matrix rigidity regulates a switch between TGF-β1–induced apoptosis and epithelial–mesenchymal transition. *Molecular Biology of the Cell* **23**, 781-791 (2012).

195. Yamada, K.M. & Cukierman, E. Modeling Tissue Morphogenesis and Cancer in 3D. *Cell* **130**, 601-610 (2007).

196. Ioachim, E. et al. Immunohistochemical expression of extracellular matrix components tenascin, fibronectin, collagen type IV and laminin in breast cancer: their prognostic value and role in tumour invasion and progression. *European Journal of Cancer* **38**, 2362-2370 (2002).

197. Reticker-Flynn, N.E. et al. A combinatorial extracellular matrix platform identifies cell-extracellular matrix interactions that correlate with metastasis. *Nature Communications* **3**, 1-12 (2012).

198. Wendt, M.K., Cooper, A.N. & Dwinell, M.B. Epigenetic silencing of CXCL12 increases the metastatic potential of mamary carcinoma cells. *Oncogene* **27**, 1461-1471 (2008).

199. Muller, A. et al. Involvement of chemokine receptors in breast cancer metastasis. *Nature Biotechnology* **410**, 50-56 (2001).

200. Griffith, L.G. & Swartz, M.A. Capturing complex 3D tissue physiology in vitro. *Nature reviews. Molecular cell biology* **7**, 211-224 (2006).

201. Rahmani, S., Park, T.H., Dishman, A.F. & Lahann, J. Multimodal delivery of irinotecan from microparticles with two distinct compartments. *Journal of controlled release : official journal of the Controlled Release Society* **172**, 239-245 (2013).

202. Baneyx, G., Baugh, L. & Vogel, V. Fibronectin extension and unfolding within cell mtarix fibrils controlled by cytoskeletal tension. *PNAS* **99**, 5139-5143 (2002).

203. Smith, M.L. et al. Force-Induced Unfolding of Fibronectin in the Extracellular Matrix of Living Cells. *PLoS Biol* **5** (2007).

204. Asakawa, N. et al. Pre-vascularization of in vitro three-dimensional tissues created by cell sheet engineering. *Biomaterials* **31**, 3903-3909 (2010).

205. Sasagawa, T. et al. Design of prevascularized three-dimensional cell-dense tissues using a cell sheet stacking manipulation technology. *Biomaterials* **31**, 1646-1654 (2010).

206. Nishiguchi, A., Matsusaki, M., Asano, Y., Shimoda, H. & Akashi, M. Effects of angiogenic factors and 3D-microenvironments on vascularization within sandwich cultures. *Biomaterials* **35**, 4739-4748 (2014).

207. Nishiguchi, A., Yoshida, H., Matsusaki, M. & Akashi, M. Rapid construction of three-dimensional multilayered tissues with endothelial tube networks by the cell-accumulation technique. *Adv Mater* **23**, 3506-3510 (2011).

208. Matsusaki, M. et al. Morphological and histological evaluations of 3D-layered blood vessel constructs prepared by hierarchical cell manipulation. *Journal of biomaterials science. Polymer edition* **23**, 63-79 (2012).

209. Laib, A.M. et al. Spheroid-based human endothelial cell microvessel formation in vivo. *Nature protocols* **4**, 1202-1215 (2009).

210. Shekhar, M.P., Werdell, J., Santner, S.J., Pauley, R.J. & Tait, L. Breast stroma plays a dominant regulatory role in breast epithelial growth and differentiation: implications for tumor development and progression. *Cancer Res* **61**, 1320-1326 (2001).

211. Bischel, L.L., Beebe, D.J. & Sung, K.E. Microfluidic model of ductal carcinoma in situ with 3D, organotypic structure. *BMC cancer* **15**, 12 (2015).